DIMENSIONAL ANALYSIS BASED CFD MODELLING FOR POWER TRANSFORMERS

A thesis submitted to The University of Manchester for the degree of Doctor of Philosophy
in the Faculty of Science and Engineering

2017

Xiang Zhang

School of Electrical and Electronic Engineering

Blank page

Contents

Word count: 53,451

Blank page

List of Figures

List of Tables

Blank page

Nomenclature

A	Cross sectional area of the vertical duct (m^2)
D_h	Hydraulic diameter (m) ($4A/P$)
$\bar{c}_p$	Mean specific heat of the oil ($J/(\mathrm{kg}\cdot\mathrm{K})$)
c_{pc}	Copper specific heat at constant pressure ($J/(\mathrm{kg}\cdot\mathrm{K})$)
C_{pd}	Pressure drop coefficient over the winding passes
c_{pp}	Paper specific heat at constant pressure ($J/(\mathrm{kg}\cdot\mathrm{K})$)
g	Gravitational acceleration (m/s^2)
g'	Local temperature gradient ($T_{bulk}-T_{to}$) (K)
g_{ave}	Average temperature gradient ($T_{aw}-(T_{to}+T_{bo})/2$) (K)
Gr	The Grashof number ($g\beta_T(T_{aw}-(T_{bo}+T_{to})/2)D_h^3/\nu^2$)
Gr/Re^2	The ratio of Gr to Re^2 ($g\beta_T(T_{aw}-(T_{bo}+T_{to})/2)D_h/u_m^2$)
h	Heat transfer coefficient at the hot-spot ($W/(m^2\cdot K)$)
h'	Heat transfer coefficient of the winding ($\mathrm{W}/(\mathrm{m}^2\cdot\mathrm{K})$)
H	The hot-spot factor ($(T_{hs}-T_{to})/(T_{aw}-(T_{to}+T_{bo})/2)$)
H_{disc}	Disc vertical (axial) height (m)
H_{duct}	Horizontal (radial) duct height (m)
H_{plate}	Plate vertical height (m)
k	Oil thermal conductivity ($W/(m\cdot K)$)
k_p	Paper thermal conductivity ($W/(m\cdot K)$)
k_c	Copper thermal conductivity ($W/(m\cdot K)$)
LDP	Laser Doppler Velocimetry
lpm	liters per minute
$\dot{m}$	Mass flow rate in the pass (kg/s)
n_1	Number of passes in the winding
n_2	Number of discs per pass
N_{de}	Number of domain mesh elements
Nu	The Nusselt number ($h\cdot D_h/k$)

OD	Oil forced and directed
ON	Oil natural
p	Static pressure (Pa)
P	Perimeter of the vertical duct (m)
P_{fi}	Volumetric flow proportion in horizontal duct i
p_{to}	Top oil static pressure (Pa)
Pr	The Prandtl number ($\mu \times c_p / k$)
ΔP	Static pressure drop (Pa)
q''	Local heat flux at the hot-spot (W / m^2)
$q''_{\max}$	Maximum local heat flux (W / m^2)
$\bar{q}''$	Average heat flux on all winding discs (W / m^2)
Q	Nonuniformity of power loss distribution ($q''_{\max} / \bar{q}''$)
Q'	Ratio of hot-spot heat flux to average flux ($q''/\bar{q}''$)
r	Rounding radius of the strand (m)
Ra	The Rayleigh number ($Gr \cdot \Pr$)
R_{inn}	Winding inner radius (m)
Re	The Reynolds number at the pass inlet ($\rho \cdot \bar{v}_{in} \cdot 2W_{duct} / \mu$)
S	Nonuniformity of oil flow distribution
T	Temperature in Kelvin (K)
T_{aw}	Average winding temperature (K)
T_{bo}	Bottom oil temperature (K)
T_{bulk}	Bulk oil temperature surrounding the hot-spot (K)
T_{hs}	The hot-spot temperature on the copper (K)
T'_{hs}	The hot-spot temperature in the fluid domain (K)
T_{to}	Top oil temperature (K)
ΔT	Temperature gradient across the paper insulation (K)
T_{b1}	Oil bulk temperature at the inlet of pass 1 (K)
T_{b3}	Oil bulk temperature at the inlet of pass 3 (K)
$\bar{v}_i$	Average oil velocity at the entrance of duct i (m / s)

$\overline{v}_{in}$	Average pass inlet oil velocity (m/s)
u_m	Average oil velocity at winding pass inlet (m/s)
u_r	Radial velocity component (m/s)
u_z	Axial velocity component (m/s)
W_{disc}	Disc horizontal (radial) width (m)
W_{duct}	Vertical (axial) duct width (m)
W_{inn}	Inner vertical duct width (m)
W_{out}	Outer vertical duct width (m)
W_{plate}	Plate horizontal width (m)
Δx	The thickness of the paper insulation (m)
z	Coordinate in axial direction (m)
α	Dimensionless horizontal duct height (H_{duct}/W_{duct})
β	Dimensionless disc axial height (H_{disc}/W_{duct})
β_T	Oil volumetric thermal expansion coefficient ($1/K$)
γ	Dimensionless disc radial width (W_{disc}/W_{duct})
ρ	Oil density (kg/m^3)
ρ_p	Paper density (kg/m^3)
ρ_c	Copper density (kg/m^3)
μ	Oil dynamic viscosity ($Pa \cdot s$)
ν	Kinematic viscosity (m^2/s)

Blank page

Dimensionless Groups

Group	Definition	Interpretation
Grashof number (Gr_L)	$\frac{g\beta_T(T_s - T_\infty)L^3}{\nu^2}$	Measure of the ratio of buoyancy forces to viscous forces
Nusselt number (Nu_L)	$\frac{hL}{k_f}$	Ratio of convection to pure conduction heat transfer
Prandtl number (Pr)	$\frac{c_p\mu}{k} = \frac{\nu}{\alpha}$	Ratio of the momentum to thermal diffusivities
Reynolds number (Re_L)	$\frac{VL}{\nu}$	Ratio of the inertia to viscous forces

Blank page

Abstract

Reliable thermal modelling approaches are crucial to transformer thermal design and operation. The highest temperature in the winding, usually referred to as the hot-spot temperature, is of the greatest interest because the insulation paper at the hot-spot undergoes the severest thermal ageing, and determines the life expectancy of the transformer insulation. Therefore, the primary objective of transformer thermal design is to control the hot-spot temperature rise over the ambient temperature within certain limit.

For liquid-immersed power transformers, the hot-spot temperature rise over the ambient temperature is controlled by the winding geometry, power loss distribution, liquid flow rate and liquid properties. In order to obtain universally applicable thermal modelling results, dimensional analysis is adopted in this PhD thesis to guide computational fluid dynamics (CFD) simulations for disc-type transformer windings in steady state and their experimental verification. The modelling work is split into two parts on oil forced and directed (OD) cooling modes and oil natural (ON) cooling modes. COMSOL software is used for the CFD simulation work

For OD cooling modes, volumetric oil flow proportion in each horizontal cooling duct (P_{fi}) and pressure drop coefficient over the winding (C_{pd}) are found mainly controlled by the Reynolds number at the winding pass inlet (Re) and the ratio of horizontal duct height to vertical duct width (α). The correlations for P_{fi} and C_{pd} with the dimensionless controlling parameters are derived from CFD parametric sweeps and verified by experimental tests. The effects of different liquid types on the flow distribution and pressure drop are investigated using the correlations derived. Reverse flows at the bottom part of winding passes are shown by both CFD simulations and experimental measurements. The hot-spot factor, H, is interpreted as a dimensionless temperature at the hot-spot and the effects of operational conditions e.g. ambient temperature and loading level on H are analysed.

For ON cooling modes, the flow is driven by buoyancy forces and hot-streak dynamics play a vital role in determining fluid flow and temperature distributions. The dimensionless liquid flow and temperature distributions and H are all found to be controlled by Re, Pr and Gr/Re^2. An optimal design and operational regime in terms of obtaining the minimum H, is identified from CFD parametric sweeps, where the effects of buoyancy forces are balanced by the effects of inertial forces. Reverse flows are found at the top part of winding passes, opposite to the OD results. The total liquid flow rates of different liquids for the same winding geometry with the same power loss distribution in an ON cooling mode are determined and with these determined total liquid flow rates, the effects of different liquids on fluid flow and temperature distributions are investigated by CFD simulations.

The CFD modelling work on disc-type transformer windings in steady state present in this PhD thesis is based on the dimensional analyses on the fluid flow and heat transfer in the windings. Therefore, the results obtained are universally applicable and of the simplest form as well. In addition, the dimensional analyses have provided insight into how the flow and temperature distribution patterns are controlled by the dimensionless controlling parameters, regardless of the transformer operational conditions and the coolant liquid types used.

Bland page

Declaration

No portion of the work referred to in this thesis has been submitted in support of an application for another degree of qualification of this or any other university, or other institution of learning.

Blank page

Copyright Statement

Blank page

Acknowledgement

PhD is an adventure! It is filled with struggles and delights as well. This thesis itself, I believe, has made it all worthwhile. I could not have made it through to this point without the help and support from people connected to me.

First, I would like to thank Professor Yang Xu who recommended me to The University of Manchester to start this adventure. I would also like to thank all the colleagues in our transformer research group who have made my 3-and-a-half-year PhD study seem not so long because of all the activities we had for work and for fun. To my colleague Muhammad Daghrah, I appreciate your work on the experimental aspect of the research topic we share. I believe both of our research work has become stronger through our cooperation.

Great thanks are also given to industrial sponsors of the Transformer Research Consortium Phase 3 at The University of Manchester. The financial and technical support is crucial to my PhD study. In addition, the 12 presentations I made in the project meetings during my PhD study have been of great help to improve my presentation skills and more importantly my understanding of how to communicate and cooperate properly with industrial partners.

To my supervisor Professor Zhongdong Wang and my co-supervisor Doctor Qiang Liu, I owe my academic achievements made during the PhD study to you two. You set the example to me of how to behave as an academic. Your dedication to work inspired me. Most of all, you provided me with all the guidance and support I needed and the freedom to wander in my research field and to find my own path eventually.

Last but not least, I wish to give my heartfelt gratitude to my family—my brother, my parents and most of all my wife Mrs Xuemei Cai and my lovely son Yiyi. Your support and love has accompanied me all the way and all the time. You are the source of my strength!

Blank page

The Author

The author has a BSc degree in Electrical and Electronic Engineering from Xi'an Jiaotong University, Xi'an, P.R. China. The research work during the undergraduate study was on the electrical treeing phenomenon in cross-linked polyethylene (XLPE) insulation in high voltage power cables, which is an electrical degradation process under divergent electric field and forms tree-shaped degradation traces.

The PhD study on transformer thermal modelling started in January 2014 at The University of Manchester. The author had been through a steep learning curve to master the basics of fluid mechanics and heat transfer during the first year of the PhD study. The most eye-opening and thought-provoking concept the author encountered during the catch-up period is the method of dimensional analysis. The method is so powerful that the author cannot stop using it to look at the physical world in a brand new viewpoint. In this PhD thesis, the author makes an attempt to apply dimensional analysis to the topic of transformer thermal modelling and hopes to promote this method to the community of transformer thermal modelling research, in which many electrical engineers are engaged.

Blank page

Chapter 1 Introduction

1.1 Background

The first transformer was built and patented by three Hungarian engineers—Károly Zipernowsky, Ottó Bláthy and Miksa Déri—in 1885 to transfer electrical energy between 2 different AC voltages, consisting of two induction coils combined with a closed magnetic circuit [1]. With the rapid technological progress and widespread use of transformers throughout the world shortly thereafter, this invention has been one of the fundamental engineering bases to develop effective electric power transmission and distribution systems. A typical contemporary UK electricity supply network is shown in Figure 1-1 [2].

Nowadays it is hard to imagine that a modern society performs economic activities and leads a normal life without electric power. On the other hand, losing supply from a power station can be resulted from cascaded failures of transformers, which could even endanger the interconnected power network [3]. Therefore, stringent reliability requirements are placed on both transformer design and operation.

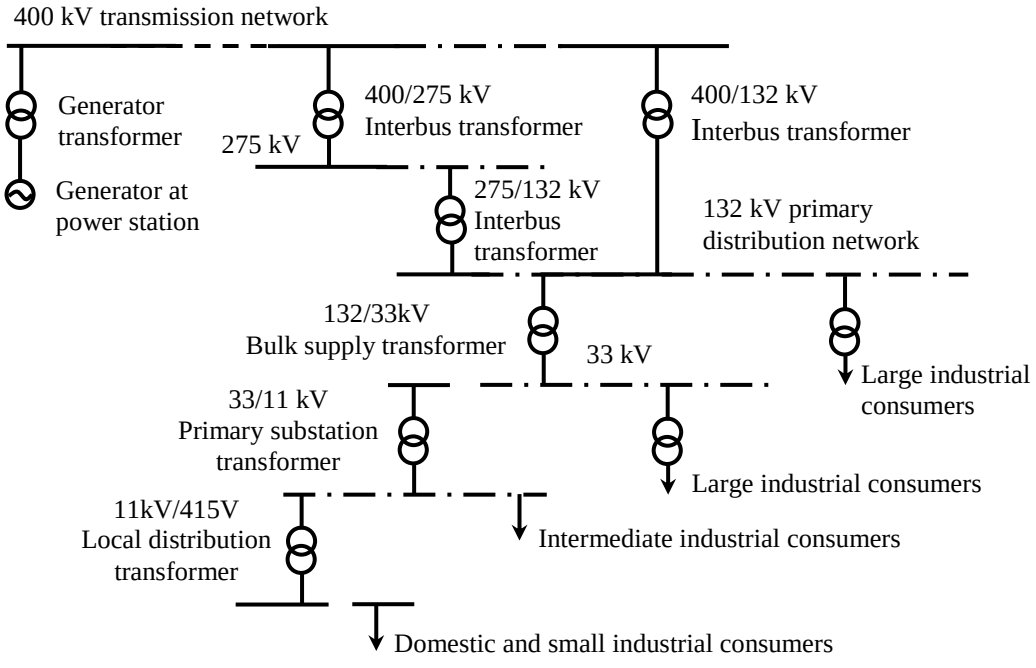

Figure 1-1. Typical UK public electricity supply network [2].

1.1.1 Transformer Reliability Survey

An international transformer reliability survey was conducted by CIGRE Working Group A2.37. The survey collected 964 major transformer failures that occurred between 1996 to 2010, contributed by 56 utilities from 21 countries [4]. The overall failure rates of different investigated transformer groups from the survey, defined as the ratio of the number of major failures to the total number of transformer-years, were found to be generally smaller than 1% [4].

Failure locations, failure causes and failure modes were analysed for the 964 failures. Failures locations were mainly in the windings (47.7%), tap changers (23.2%) and bushings (14.4%) [4]. Failure causes were mainly design and manufacturing (19.92%), ageing (12.34%) and external short-circuit (11.62%) related [4]. For the failure cause statistics, it is worth mentioning that the causes of 29.05% of the failures were classified as unknown [4]. Failure modes were mainly dielectric (36.62%), followed by mechanical (20.02%), electrical (16.49%) and thermal (10.89%) failure modes [4]. For different transformer groups, the compositions of the failure modes were different: substation transformers tended to have failures related to dielectric (38.30%) and mechanical (22.15%) issues with thermal failure percentage being 6.51%; whereas generator step-up (GSU) transformer failures were mainly thermal ageing (32.12%) and dielectric behaviour (28.48%) related [4]. The prominent difference between thermal failure percentages of substation and GSU transformers can be explained by the constantly higher loading conditions of GSU units than their substation counterparts.

The major failures of large generator and transmission transformers (>100 MVA) in the UK between 2003 and 2009 was compiled and reported in the survey [4]. The statistics from the review is shown in Table 1-1. There were 32 major failures recorded, among which approximately 1/3 was removed from service before failure thanks to the condition assessment related to the increasing main tank gas levels; and the majority of the remainder, i.e. the in-service failures, were caused by inter-turn failures [4].

Most of the 1004 UK transformers in the survey were 40 or more years old and the majority of failures occurred in the 36-40 years age band [4]. However, no increased failure rate with age was identified due to a proactive condition based replacement programme [4, 5]. This means statistical analysis of failure rate is not helpful in transformer lifetime modelling. On the other hand, experience and thermal modelling of transformer indicates that, apart from premature failure due to fault, transformer lifetime expectancy is mainly dictated by the thermal ageing of the transformer.

Table 1-1. Major UK transformer failures between 2003 and 2009 [4].

Transformer type	Subgroup	Population	Number of failures	Failure rate, %
GSU	G1	62	11	2.5
	G2	28	3	1.5
	G3	114	4	0.5
Transmission	T	800	14	0.3

G1 refers to the group of three phase GSU units of 340 to 735 MVA; G2 refers to single phase banks of 800 MVA; G3 refers to younger three phase GSUs built after privatisation.

1.1.2 Thermal Ageing and Hot-spot Temperature

For liquid-immersed power transformers, apart from the dielectric coolant liquid, the electrical insulation mainly involves paper and pressboard insulation [6]. The ageing or deterioration of the insulation is a time function of temperature, moisture content, oxygen content and acid content [7, 8]. By treating temperature as a controlling parameter, the relative ageing rates, *V*, for non-thermally upgraded paper and thermally upgraded paper are reduced to equation (1.1) and (1.2), respectively: [7]

$$V = 2^{(\theta_h - 98)/6} \tag{1.1}$$

$$V = e^{\left(\frac{15000}{110+273} - \frac{15000}{\theta_h+273}\right)} \tag{1.2}$$

where θ_h refers to the highest temperature in ºC.

The temperature distribution in the winding is not uniform, and the part under the highest temperature, usually referred to as the hot-spot temperature, normally undergoes the greatest deterioration. Therefore, the relative ageing rate is referred to the one at the hot-spot temperature. For non-thermally upgraded paper, the benchmark hot-spot temperature used in IEC 60076-7 (2005) is 98 ºC, and every increase of 6 ºC doubles the relative ageing rate and vice versa [7]. For thermally upgraded paper, the benchmark hot-spot temperature according to both IEC 60076-7 (2005) and IEEE Std C57.91 (2011) is 110 ºC, and every increase of approximately 7 ºC doubles the relative ageing rate and vice versa [7, 8].

Apart from the long-term ageing effect, uncontrolled hot-spot temperature, resulted from poor thermal design or overloading of the transformer, can give rise to the hazard of gas bubble generation in the insulation. When the hot-spot temperature exceeds 140 ºC for a transformer with a winding insulation moisture content of about 2% immersed in mineral oil, gas bubbles are likely to occur [7]. In addition, this critical temperature will decrease as the moisture concentration increases [7]. The presence of gas bubbles in the insulation can seriously jeopardize the dielectric strength of the insulation. The reduction of dielectric strength in a region of high electrical stress, i.e. the windings and the leads, can lead to a catastrophic failure of the transformer.

1.2 **Research Scope**

This PhD thesis is on the thermal modelling of liquid-immersed power transformers using computational fluid dynamics (CFD) models implemented by COMSOL Multiphysics, which is a finite element method (FEM) based simulation software. The validity of the CFD models used in this thesis is verified by experimental tests on a disc-type winding model for some typical isothermal flow conditions. Transformer thermal modelling mainly involves the determination of power losses in the windings, fluid flow and heat transfer in both the windings and the radiators. Two facts about the power losses and the cooling function of the radiators in relation to fluid flow and heat transfer in the winding need to be noted. First, the power losses in the winding, consisting of resistive losses in the copper wires and eddy current losses due to leakage magnetic flux, are in a quasi-unidirectional coupling

with the fluid flow and heat transfer in the windings, that is, the power losses as the heat source can affect the fluid flow and heat transfer, whereas the fluid flow and heat transfer has weak impact on the power losses. Second, the cooling function of the radiator provides boundary conditions to the fluid flow and heat transfer in the windings, and these boundary conditions can be derived from the temperature rise test results [9]. Based on these two facts and time constraint of PhD research, the focus of this PhD thesis is placed on the fluid flow and heat transfer in the winding with given power loss distribution and boundary conditions.

1.2.1 Classification of Transformer Thermal Modelling

There are mainly four aspects of the fluid flow and heat transfer in the winding and each aspect has two major contents, as detailed below and shown in Figure 1-2. The contents investigated in this PhD thesis are designated by bright purple blocks.

The first aspect is the operational condition of the transformer. In normal operation, the transformer is in a dynamic process with varying loading and changing ambient temperature. At the end of the temperature rise test, however, the transformer is in a quasi-steady state after being loaded constantly with an equivalent rated load for a period of time.

The second aspect is the cooling mode of the transformer. When a pump is used to deliver oil from the radiator to the bottom of the windings and oil directing washers are installed in the windings, it is referred to as an oil directed (OD) cooling mode [7]. When there is no pump used and thermal syphon forces are responsible for the oil circulation between the winding and the radiator, it is referred to as an oil natural (ON) cooling mode [7].

The third aspect is the power loss distribution in the winding. In reality, the power loss distribution in the winding is non-uniform with quasi-uniform resistive losses along the winding and eddy current losses concentrating on the top and bottom part of the winding. For the resistive power losses, for example, if the minimum winding temperature is 70 °C and the maximum is 100 °C, then the ratio of the maximum resistivity or resistive power loss to the minimum one is approximately 1.1. For the

eddy current power losses, when the leakage magnetic flux is properly controlled by using flux shunt for example to reduce its radial component, the eddy current losses in the winding can generally be reduced to less than 30% of the resistive losses, to the best of the author's knowledge.

The fourth aspect is the geometry of the winding. Generally, layer-type windings are adopted for distribution transformers and disc-type windings are adopted for high voltage transmission transformers.

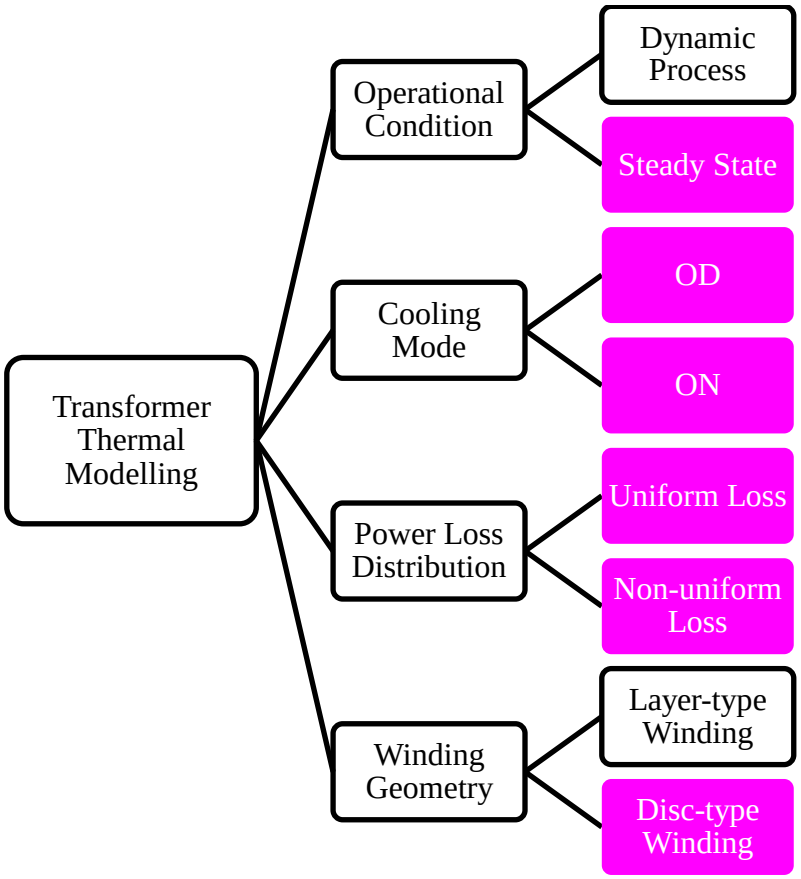

Figure 1-2. Possible classification of transformer thermal modelling. The contents investigated in this PhD thesis are designed by bright purple blocks

1.2.2 Winding Geometry and Parameter Ranges

The geometry of a disc-type transformer winding consists of paper-insulated winding discs, which are separated from one another by radial dovetailed spacers to form horizontal (radial) cooling ducts. Axial dovetailed strips are inserted between the discs and the synthetic-resin-bonded-paper (s.r.b.p) cylinders, onto which the winding is wound, to form vertical (axial) cooling ducts. In addition, oil directing

washers are usually used, which split the winding into several passes and force oil to enter a pass via one vertical duct and exiting via the other, leading to a zigzag flow pattern among passes. The winding has an angular periodicity dictated by the number of spacers present along the circumference of the disc. The geometry of a disc type winding and a segment of one pass with 6 discs are shown in Figure 1-3 (a) and (b), respectively. Since the width of the horizontal cooling duct is much larger than its height, the 3D geometry can be reduced to axisymmetric 2D geometry, of which a 3-pass winding is shown in Figure 1-3 (c) with flow direction indicated.

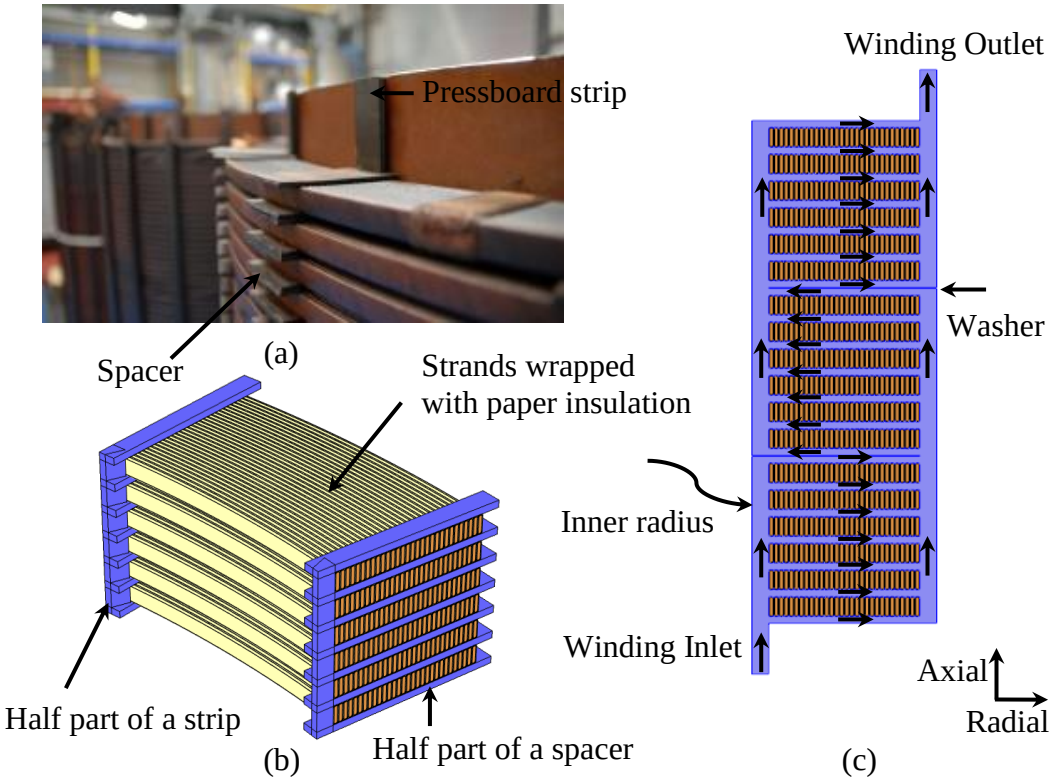

Figure 1-3. Disc-type winding geometry. (a) 3D winding geometry. (b) A segment of a pass between two adjoining sets of spacers. (c) 2D axisymmetric geometry of a 3-pass case.

In the CFD modelling, for realistic case studies the winding inlet liquid velocity is controlled below 0.5 m/s, which is a commonly adopted velocity limit to avoid generation of static electricity from liquid flow. Winding inlet liquid temperature is set to be in the range from 20 °C to 60 °C. Three liquids—a mineral oil, a gas-to-liquid (GTL) oil and a synthetic ester—are investigated. The liquid properties as functions of temperature are obtained from curve fittings of the measured data provided by the liquid manufacturers. The properties of density, dynamic viscosity,

thermal conductivity and specific heat of the three liquids are shown in Figure 1-4, Figure 1-5, Figure 1-6 and Figure 1-7, respectively.

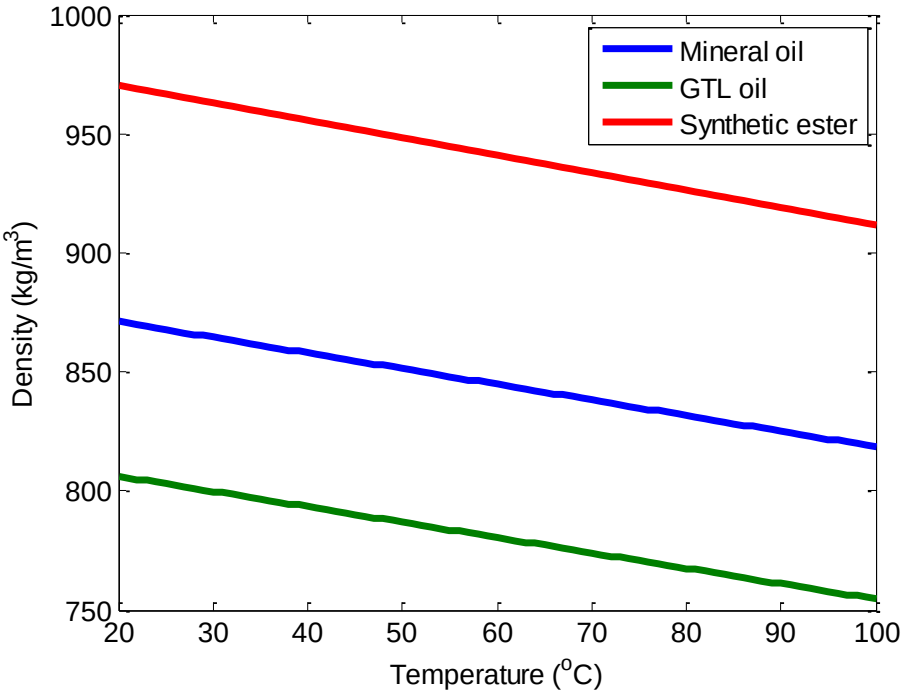

Figure 1-4.Temperature dependant density.

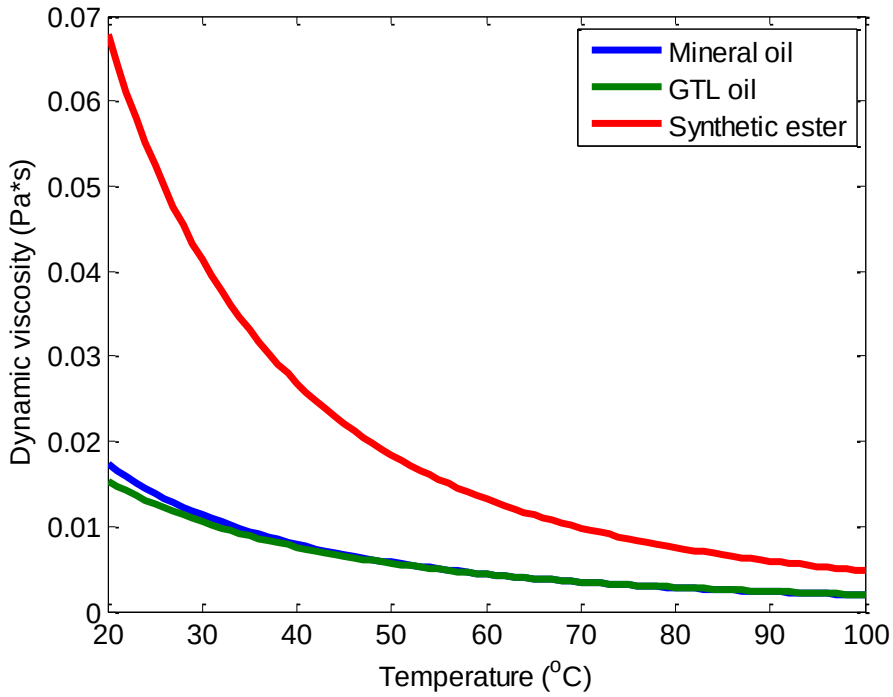

Figure 1-5. Temperature dependant dynamic viscosity.

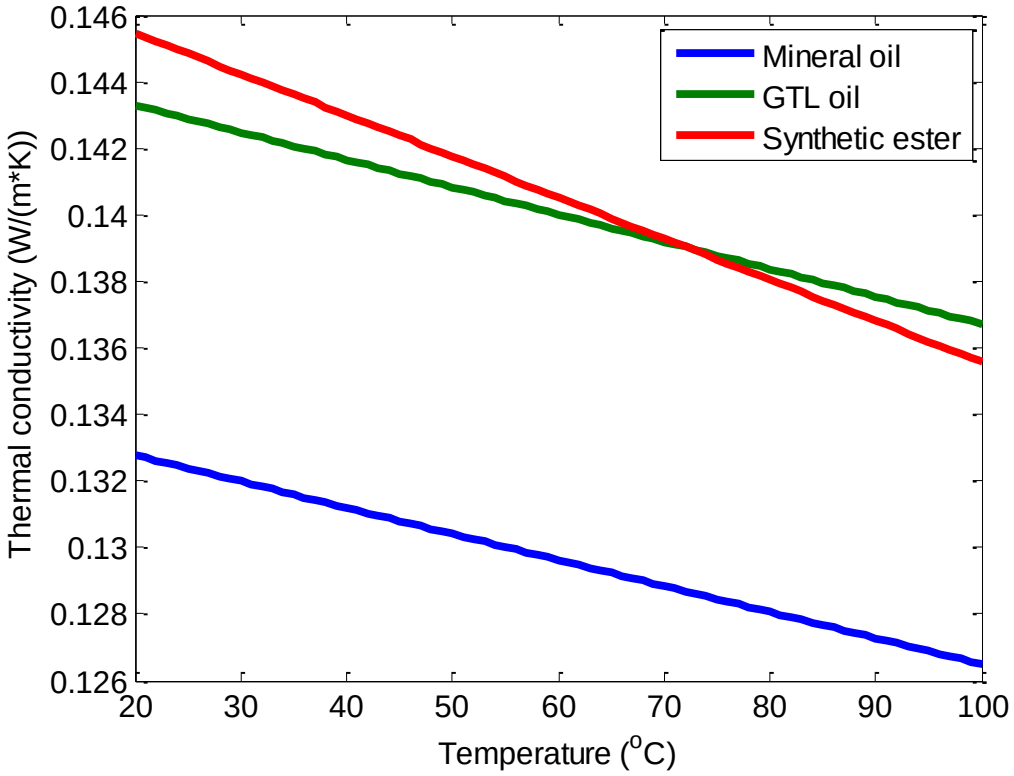

Figure 1-6. Temperature dependant thermal conductivity.

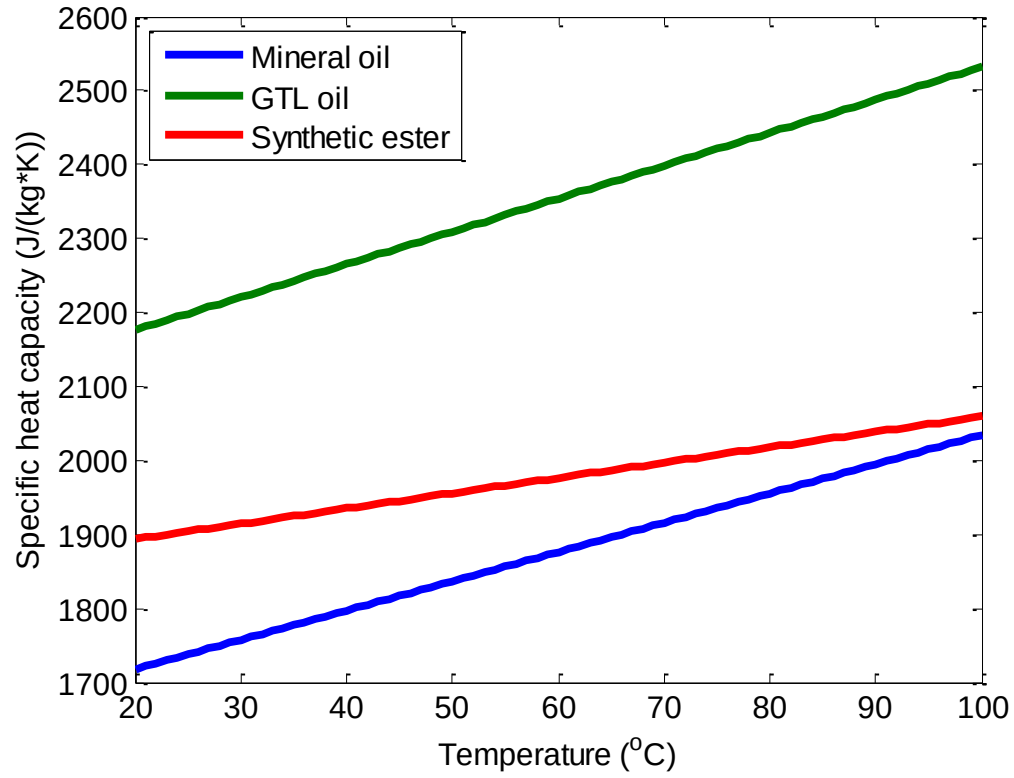

Figure 1-7. Temperature dependant specific heat.

1.3 Aims and Objectives

The aims of this PhD programme are to help determine the location and the magnitude of the hot-spot temperature in the winding and optimize transformer design and operation. In order to achieve these aims and to get universally applicable results, dimensional analysis is adopted. Based on dimensional analyses on the liquid flow and heat transfer, the relationships of liquid flow distribution and temperature distribution with their controlling parameters can be simplified, which would make parametric sweeps much more manageable. In addition, the dimensional analyses can provide insights into the liquid flow and heat transfer processes. The detailed technical objectives set in this PhD study are as follows:

1. To differentiate ON cooling modes and OD cooling modes in terms of their different governing equations, and different liquid flow and heat transfer behaviours.

2. To quantify the effects of different liquid types, liquid flow rates, and winding geometries on flow distribution in and static pressure drop over disc-type windings.

3. To analyse the effects of flow distribution on temperature distribution.

4. To identify the controlling parameters of the hot-spot temperature and the uniformity of temperature distribution.

5. To optimize transformer design and operation to achieve a more uniform temperature distribution and a lower hot-spot temperature.

1.4 Original Contributions

In summary, this PhD thesis focuses on CFD thermal modelling of disc-type transformer windings in steady state with both uniform and non-uniform power loss distributions in OD and ON cooling modes. Dimensional analysis is adopted to analyse pressure drop over, flow distribution and temperature distribution in disc-

type transformer windings, which provides one with simplicity, insight and universally applicable results. The original contributions of this thesis are seen as follows:

1. For OD cooling modes, liquid average velocity in a horizontal cooling duct and pressure drop over the winding are transformed by dimensional analysis into liquid flow proportion in that horizontal cooling duct and pressure drop coefficient over the winding, respectively. The controlling parameters of the flow proportion and pressure drop coefficient are found to be the Reynolds number (*Re*) at the winding inlet and dimensionless geometric parameters. Comprehensive CFD parametric sweeps are conducted and the CFD results of flow proportion and pressure drop coefficient are correlated with the controlling dimensionless parameters by adopting a multi-layer fitting strategy. The validity of the correlations is verified by numerical and experimental tests. The practical implications of the correlations are fully exploited, including the identification of the criteria for the occurrence of reverse flow in the winding and the feasible approach to control maldistribution factor, which quantifies the uniformity of the flow distribution in the winding.

2. The effects of three different liquids—a mineral oil, a gas-to-liquid (GTL) oil and a synthetic ester—on flow distribution in and pressure drop over the winding in OD cooling modes are compared and their different flow and pressure drop features are identified.

3. The hot-spot factor, *H*, which has been used for decades in transformer industry to derive the hot-spot temperature from temperature rise test results, is interpreted as a dimensionless temperature at the hot-spot. For a given loss distribution and winding geometry, the relationships between *H* and its controlling dimensionless groups are identified: For OD cooling modes, *H* is a function of *Re* and the Prandtl number (*Pr*). For ON cooling modes, *H* is a function of *Re*, *Pr* and the ratio of the Grashof number (*Gr*) to Re^2. A linear relationship between *H* and the non-uniformity of power loss at the hot-spot, defined as the ratio of power loss at the hot-spot to the average power loss in the

whole winding, is identified. This linear relationship is coupled with the non-linear relationship between H and the other controlling dimensionless groups.

4. For ON cooling modes, a relationship is established between the total liquid flow rate in the winding and the controlling parameters: liquid properties, the total power loss in the winding and the height difference between the centre point of the radiator and the centre point of the winding, ΔH. This relationship obtained is in line with the experimental results reported in literature [10]. Based on this relationship, different total flow rates are determined for the three liquids (a mineral oil, a GTL oil and a synthetic ester) under the identical conditions of total power loss in the winding and ΔH. Different liquid flow and temperature distribution features of the three liquids are identified and compared.

1.5 **Outline of Thesis**

This thesis is structured in a journal format because the quantity and quality of the papers produced from the research work is identified by the supervisor as sufficient to do so. The remainder of this thesis is organized as follows:

Chapter 2: Literature Review

This chapter presents a literature survey on the subject of transformer steady state thermal modelling. The temperature rise test and the thermal diagram are introduced first, and the review of the two commonly adopted thermal modelling methods: thermal-hydraulic network models and CFD models are reviewed. A special attention is paid to review the experimental tests, which are used to verify the proposed models.

Chapter 3: OD Cooling Modes

This chapter consists of 4 papers related to the topic of thermal modelling of disc-type transformer windings at steady state in OD cooling modes. These 4 papers describe a thorough research attempt to investigate the liquid flow and heat transfer

in the winding and conclude on how they are controlled by the liquid properties, liquid flow rate and the geometry of the winding.

The first paper, "Prediction of Pressure Drop and Flow Distribution in Disc Type Transformer Windings in an OD Cooling Mode", is published in IEEE Transactions on Power Delivery. The first author of this paper is the author of this thesis and the second and third authors are his supervisor and co-supervisor, respectively. This paper presents dimensional analyses on flow distribution in and pressure drop over disc-type transformer windings. The relationship between flow rate in each horizontal cooling duct, or static pressure drop over the winding mode, and the controlling parameters related to liquid properties, liquid flow rate and geometric dimensions, is simplified by conducting dimensional analysis. Computational tests are conducted to verify the validity of dimensional analysis and CFD parametric sweeps are followed to quantify the relationships obtained from the dimensional analysis. The verification of the correlations obtained from the parametric sweeps and the practical implications of these correlations are then presented.

The second paper, "Experimental Verification of Dimensional Analysis Results on Flow Distribution and Pressure Drop for Disc Type Windings in OD Cooling Modes", has been accepted by IEEE Transactions on Power Delivery. The first author of this paper is the author of this thesis who did 50% of the work by conducting theoretical analysis and CFD parametric sweeps on a wide range of conditions related to the experimentally tested winding models and wrote the majority of the paper. The second author is another PhD student who did the other 50% of the work by designing the test strategy in conjunction with the first author and conducting experimental tests. The third and fourth authors are the supervisor and co-supervisor of the two PhD students. The fifth and sixth authors are some of the industrial partners who provided the technical support. This paper satisfactorily verifies the conclusions drawn in the first paper, including the conclusion that heat transfer in OD cooling modes has negligible effects on fluid flow, by conducting flow rate measurement in horizontal cooling ducts using a particle image velocimetry (PIV) system and pressure drop measurement over the winding models using a differential pressure instrument.

The third paper, "Numerical Investigation of Influence of Coolant Types on Flow Distribution and Pressure Drop in Disc Type Transformer Windings", is published in the proceedings of the International Conference on Condition Monitoring and Diagnosis (CMD), Xi'an, P.R. China, 2016. The first author of this paper is the author of this thesis. The second and third authors are the supervisor and co-supervisor, respectively. The fourth, fifth and sixth authors are some of the industrial partners who provided the technical support. This paper follows the technical points present in the first two papers and investigates the influence of liquid types on flow distribution and pressure drop by using the correlations obtained in the first paper.

The fourth paper, "Interpretation of Hot Spot Factor for Transformers in OD Cooling Modes", has been accepted by IEEE Transactions on Power Delivery. The first author of this paper is the author of this thesis. The second and third authors are the supervisor and co-supervisor, respectively. This paper follows the investigation on fluid flow and heat transfer in the previous papers and interprets the hot-spot factor as a dimensionless temperature at the hot-spot according to the dimensional analyses on liquid flow and heat transfer in the winding. For uniform power loss distribution conditions, the relationship between the hot-spot factor and the controlling dimensionless groups, *Re* and *Pr*, is quantified by CFD parametric sweeps and the effects of operational conditions on the hot-spot factor are analysed. For non-uniform power loss distribution conditions, the linear relationship between the hot-spot factor and the non-uniformity of power loss at the hot-spot, defined as the ratio of the power loss at the hot-spot to the average power loss in the winding, is identified.

Chapter 4: ON Cooling Modes

This chapter comprises 2 papers and investigates the liquid flow distribution and temperature distribution in disc-type transformer windings at steady state in ON cooling modes. In ON cooling modes, fluid flow and heat transfer are strongly coupled and therefore need to be considered simultaneously.

The first paper, "Numerical Investigation of Oil Flow Distribution and Temperature Distribution for ON Transformer Windings", is to be submitted to Applied Thermal Engineering. The first author of this paper is the author of this thesis. The second and

third authors are the supervisor and co-supervisor, respectively. The fourth and fifth authors are some of the industrial partners who provided the technical support. This paper conducts dimensional analysis on fluid flow and heat transfer by non-dimensionalising the governing differential equations with the adoption of the Boussinesq approximation. It is found that dimensionless flow and temperature distributions are controlled by *Re*, *Pr*, Gr/Re^2. In addition, Gr/Re^2 governs the flow and temperature distributions, and *Re* is more influential than *Pr*. According to the controlling dimensionless groups derived, CFD parametric sweeps are then conducted. The optimal design and operational regime in terms of achieving a minimum hot-spot factor is identified from the parametric sweep results.

The second paper, "Numerical Investigation of Influence of Liquid Types on Flow Distribution and Temperature Distribution in Disc Type ON Transformers", is accepted by the International Conference on Dielectric Liquids (ICDL), Manchester, UK, 2017. The first author of this paper is the author of this thesis. The second and third authors are the supervisor and co-supervisor, respectively. The fourth, fifth and sixth authors are some of the industrial partners who provided the technical support. This paper investigates the influence of liquid types on flow and temperature distributions in an ON transformer winding. It follows the principles laid down by the former paper and conducts further study to determine the total liquid flow rate in the winding in ON cooling modes. According to the total liquid flow rates determined for the three investigated liquids (a mineral oil, a GTL oil and a synthetic ester), the comparisons of flow and temperature distributions for the three liquids in the winding are then performed.

Chapter 5: Conclusion and Future Work

This chapter summarises the major conclusions of this PhD study and provides recommendations for further study. Ideas for further experimental verification and dynamic thermal modelling are particularly mentioned.

Blank page

Chapter 2 Literature Review

2.1 Introduction

A primary objective of transformer thermal design is to control the hot-spot temperature rise over ambient temperature within specification at rated load in steady state. If not otherwise agreed between manufacturer and purchaser, a hot-spot temperature rise limit of 78 K at rated load in steady state is usually specified for both Kraft and thermally upgraded paper in IEC standards [7, 11]. In practice, the fulfilment of the objective is checked by the factory temperature rise tests. The results of the temperature rise tests are interpreted by an empirical thermal diagram, which has been used for decades, to derive the hot-spot temperature rise [7, 11].

In the transformer design phase, the determination of temperature distribution in the winding is typically based on either empirical formulae or thermal models, including thermal-hydraulic network models and CFD models [12]. With the ever-increasing voltage level and power rating, power transformers are becoming increasingly larger and more complicated. The design engineers have to take the transportation limits into consideration and design compact transformers with reduced internal clearances based on computer aided design techniques, e.g. thermal modelling techniques [4]. However, a reliable thermal modelling tool with reasonable computational requirements is at a premium.

The validity of the thermal diagram or any thermal models needs to be checked by experimental tests on either real transformers or transformer models. Experimental tests reported in literature has been lacking because of the great effort required to conduct such tests.

In this chapter, temperature rise tests and the concept of hot-spot factor are introduced first, and then the methods of thermal hydraulic network modelling and CFD modelling are compared. The incremental work of the calibrations of network models using CFD results is also introduced. Finally, detailed CFD modelling strategies and results, and experimental test results in the literature are reviewed.

2.2 Temperature Rise Test and Hot-spot Factor

Generally, the temperature rise test results are interpreted by a thermal diagram from which the hot-spot temperature can be derived [7, 11]. The hot-spot factor is a crucial parameter in the thermal diagram, which determines the accuracy of the hot-spot temperature derived.

2.2.1 Temperature Rise Test

The factory temperature rise test should be performed with the cooling air temperature being in the range between 10 ºC and the maximum ambient temperature for which the transformer is designed, and if cooling water is used, the water temperature should be in the range between 5 ºC and the maximum water temperature for which the transformer is designed [11]. The temperature rise over the ambient temperature limits are set to 60/65 K, where 60 K for top liquid temperature rise and 65 K for average winding temperature rise [7, 8, 11].

The method of short-circuit test for the determination of temperature rises in the winding and coolant liquid is recommended in IEC 60076-2: 2011 [11]. The short-circuit test consists of two steps: the total power loss injection step and the rated current injection step. In the short-circuit test, the rated voltage cannot be reached and therefore a higher current above the rated one corresponding to the total losses is injected at the total loss injection step. This step ends when the rate of change of the top-liquid temperature rise over ambient temperature is within 1 K/h and has remained there for at least 3 hours [11]. The rated current injection step follows the first step without a break with the current reduced to the rated one. This step is maintained for 1 hour with all temperature measurements being taken at a 5-minute interval [11]. Immediately after this 1-hour test, the resistance values of the windings are measured to derive the average winding temperatures at the instant of shutdown.

Generally, the ambient temperature, the bottom liquid temperature, the top liquid temperature and the average winding temperature are measured or derived in the temperature rise test. It is worth mentioning that the top liquid temperature is conventionally measured by temperature sensors immersed in the liquid at the top of the tank or, in pockets in the cover or even at the inlet of the cooling equipment if

agreed between the manufacturer and the purchaser. Similarly, the bottom liquid temperature is, in practice, measured at the outlet of the cooling equipment. The average liquid temperature is set to be the average of the top and bottom liquid temperature. The hot-spot winding temperature is usually not measured in the temperature rise test—unless the measurement is agreed between the manufacturer and the purchaser or the transformer is a strategic asset or operates in specific conditions (e.g., nuclear power plant) [11]. Generally, the measurement of the hot-spot temperature is done by installing fibre optical temperature sensors in the transformer manufacturing stage based on thermal modelling results.

2.2.2 Hot-spot Factor

The hot-spot winding temperature is usually derived from the temperature rise test results by using a thermal diagram, as shown in Figure 2-1.

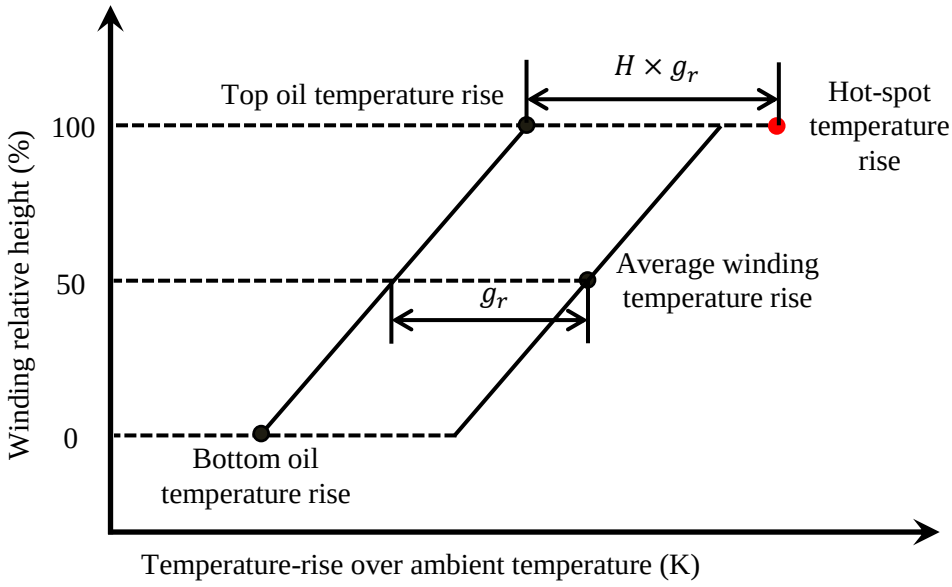

Figure 2-1. Thermal diagram for temperature rises in the winding [7, 11]. *H* is the hot-spot factor and g_r is the average temperature gradient between the winding and the oil at rated load.

In the thermal diagram, it is assumed that both the oil temperature and the winding temperature rise linearly with height. In addition, the temperature gradient between the winding and the oil is assumed to be constant. In order to compensate the error introduced by these assumptions, the temperature gradient between the hot-spot and the top oil is set to be the product of the average temperature gradient (g_r) and a

dimensionless parameter referred to as the hot-spot factor (*H*). In so doing, the difficulty in determining the hot-spot temperature has been shifted to the determination of *H*. The hot-spot factor is an indicator of the uniformity of the temperature distribution in the winding: The larger *H* is, the more uneven the temperature distribution will be. A close-to-unity *H* is desired for transformer thermal design to avoid localized overheating, which require reasonably uniform flow distribution and power loss distribution.

An experimental investigation of *H* for power transformers was carried out by CIGRE working group 12.09 [13, 14]. In the investigation, wide ranges of cooling modes, voltage levels and power ratings were covered. The statistics of *H* obtained is shown in Table 2-1. As can be seen from Table 2-1, *H* ranged from 0.51 to 2.06. The inverse accumulative distribution of the *H* is shown in Figure 2-2 [13, 14]. It can be seen that a number of *H's* derived were smaller than 1. These *H's* smaller than 1 are most probably erroneous due to improper temperature sensor installation or wrong sensor installation locations, etc. The widespread *H's* obtained indicate that the traditional assumptions that *H* is 1.1 for distribution transformers and 1.3 for transmission transformers are too simplistic.

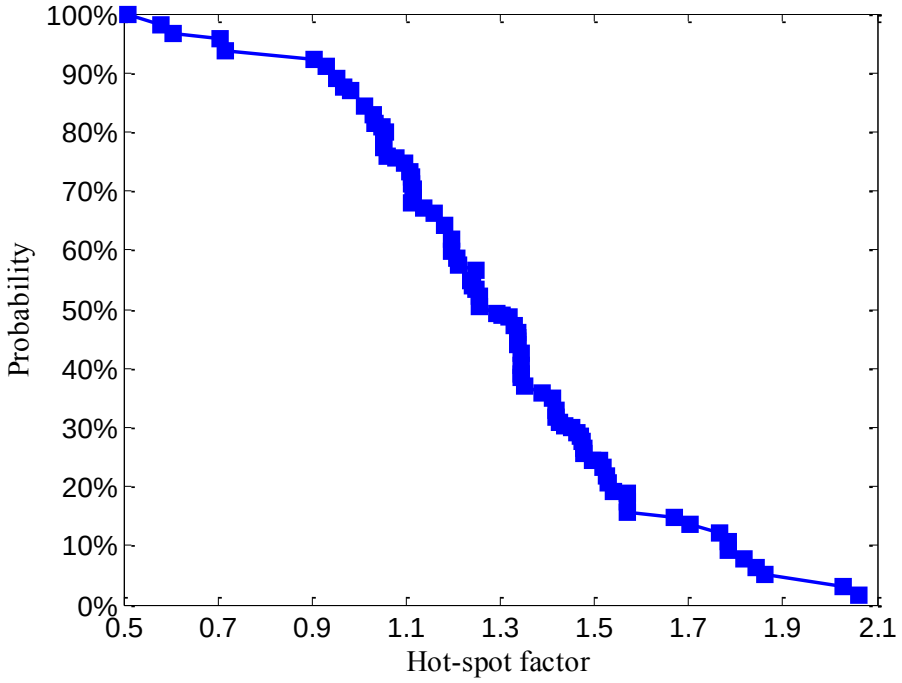

Figure 2-2. Inverse accumulative distribution of the hot-spot factor [13, 14].

Table 2-1. Statistical data of the measured hot-spot factor [13, 14].

Cooling	ONAN			ON			OF			OD		
Winding	HV	LV	HV+LV	HV	LV	HV+LV	HV	LV	HV+LV	HV	LV	HV+LV
Number of tests	9	10	19	6	9	15	2	4	6	14	13	27
Minimum	0.72	1.05	0.72	0.61	0.91	0.61	1.29	1.11	1.11	0.51	0.58	0.51
Maximum	2.06	1.78	2.06	1.57	1.68	1.68	1.82	1.78	1.82	1.83	1.52	1.83
Average	1.42	1.36	1.39	1.14	1.32	1.25	1.55	1.59	1.58	1.22	1.13	1.18
Standard deviation	0.48	0.22	0.36	0.33	0.25	0.29	0.38	0.32	0.30	0.35	0.22	0.29

The hot-spot factor is affected by both the local power losses and local cooling efficiency at the hot-spot. Based on this fact, the IEC 60076-2: 2011 standard prescribes the relationship between *H* and *Q* and *S* as below:

$$H = Q \times S \tag{2.1}$$

where "*factor Q relates to the additional loss*" and "*factor S relates to the efficiency of liquid cooling circuits inside the winding*" [11].

Equation (2.1) is purely empirical because the relationship is not derived from rigorous physical reasoning. The relationship does not withstand rigorous experimental tests as shown in [15] or numerical tests as shown in [16] because the *Q* factor and the *S* factor are found to be interdependent and the location with the highest power loss does not always coincide with the location with the poorest cooling efficiency.

Revised definitions of the *Q* factor and the *S* factor are proposed in [12]. The *Q* factor is defined as a distributed parameter in each part of the winding:

$$Q = Q(r, z, \varphi, T) / Q_{ave} \tag{2.2}$$

where $Q(r, z, \varphi, T)$ is a local power loss with r, z and φ referring to coordinates and T referring to the local temperature; Q_{ave} is the average power loss in the winding at average winding temperature [12].

The *S* factor is defined as the ratio of *H* to *Q*:

$$S = H / Q \tag{2.3}$$

The definition of the *Q* factor in equation (2.2) requires the information of detailed power loss distribution and temperature distribution in the winding. This requirement detracts from the value of *H* because if detailed power loss distribution and temperature distribution are already known, then *H* is no longer of interest. The definition of the *S* factor in equation (2.3) requires *H* as an input and this violates the original objective of determining *H* as a function of the *Q* factor and the *S* factor.

An effective hot-spot factor is proposed in [17]. This effective hot-spot factor is not determined based on heat transfer analysis in the winding; it is reversely derived from a model that incorporates paper ageing mechanism and moisture accumulation effect into the IEC thermal model and based on the degree of polymerization (DP) value of paper samples from scrapped transformers [17]. The key parameters which are used in the reverse derivation are the load level and the ambient temperature a transformer has experienced over its operating lifetime and the thermal "characteristics" indicated by its heat run test report. Hence their accuracy may affect the values of effective hot-pot factors and renders sensitivity studies. It is found that the median of the effective hot-spot factors of 35 scrapped transformers taken from the UK transmission system is 2.95 [17].

Specifying *H* to be 1.1 and 1.3 for distribution and transmission transformers turns out to be over-simplified. In addition, decomposing *H* into *S* and *Q* is not helpful because the relationship of $H=S\times Q$ is not derived from rigorous physical reasoning and therefore introduces further confusion to the concept of *H*. On the other hand, *H* is such an important parameter for guiding transformer thermal design and transformer operation that a sound interpretation of *H* based on fundamental, physical reasoning is needed. In this thesis, attempts have been done to interpret *H* based on dimensional analysis on the liquid flow and heat transfer processes in the winding for both OD and ON cooling modes.

2.3 Network Modelling and CFD Modelling Comparisons

The determination of the liquid flow distribution and the temperature distribution in transformer windings in steady state is mainly done by performing thermal-hydraulic network modelling [18-24] or CFD modelling using commercial software [25-29].

Heat transfer in transformer windings consists of thermal conduction in the solid domain (copper conductor and insulation paper) and thermal convection in the liquid domain. The conduction, which is relatively easy to simulate, is governed by Fourier's law of conduction. The convection, which is the challenging part, involves the conservation of mass, momentum and energy.

The network models and CFD models share the same physical principles of thermal conduction and convection [12]. However, they simulate the physical processes in different manners: Network models are lumped-parameter models that adopt correlations to describe the liquid flow and heat transfer in rather coarse networks. CFD models, on the other hand, are distributed-parameter models that solve the governing differential equations directly with fine discretization. More accurate and detailed liquid flow and temperature distribution results are obtained from CFD models compared to those obtained from network models at the cost of a higher computational requirement. The details of thermal hydraulic network models and CFD models are shown in the following subsections.

2.3.1 Thermal Hydraulic Network Models

The thermal hydraulic network model, as suggested by its name, is composed of a hydraulic network model and a thermal network model. The hydraulic network and the thermal network are coupled. For OD cooling modes it is a weak coupling, whereas it is a strong coupling for ON cooling modes.

2.3.1.1 Hydraulic Network

The determination of liquid flow distribution in the winding requires the consideration of mass conservation and pressure equilibrium in each closed flow loop as shown below:

$$\sum_{i=1}^{N_m} \dot{m}_i = 0 \tag{2.4}$$

$$\sum_{j=1}^{N_p} \Delta P_j = 0 \tag{2.5}$$

where N_m is the number of flows entering or leaving a junction and N_p is the number of elements composing a closed flow loop. $\dot{m}_i$ is a mass flow rate entering or leaving the junction. ΔP_j refers to a pressure drop in the loop due to friction pressure losses, or losses related to flow splitting, flow combining or flow at elbows. The term ΔP_j can also refer to pressure gain due to buoyancy forces in ON cooling modes.

Equation (2.4) and (2.5) are interlinked as the pressure drop in each element is related to the mass flow rate or even heat transfer processes as for ON cooling modes. A typical hydraulic network of a disc-type winding is shown in Figure 2-3 [19].

In this hydraulic network, R_f stands for hydraulic resistance due to friction, R_C for resistance due to flow at elbow, $\rho g \Delta H$ for pressure gain due to buoyancy force and R_1 for resistance due to flow splitting and R_2 for combining. The correlations—used in the hydraulic network to correlate the hydraulic resistance to the liquid flow rate, liquid properties and the geometry—are usually taken from literature pertaining to circular pipe flows [30], which are not always representative of flows in the cooling ducts in transformer windings. The accuracy of the hydraulic network model depends crucially on the correlations adopted and these correlations are susceptible of improvement [31, 32].

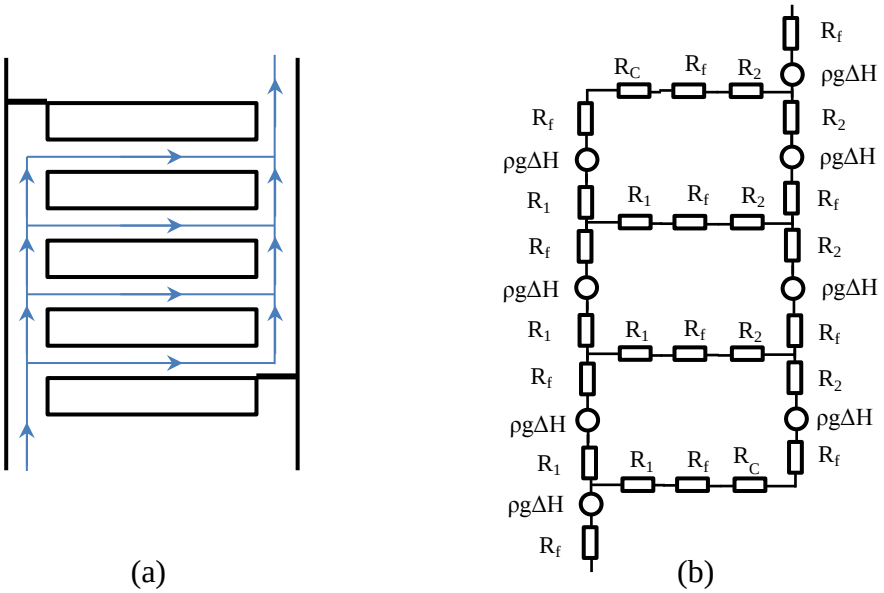

Figure 2-3. Hydraulic network representation [19]. (a) Illustration of one winding pass with barriers. (b) Hydraulic network with simplified symbols representing different types of hydraulic resistance: R_f for friction resistance, R_c for corner resistance, R_1 for splitting resistance, R_2 for combining resistance.

2.3.1.2 Thermal Network

In the thermal network, conservation of thermal energy is applied to each node in the network and heat transfer equation is applied to each path. A simplified thermal network of a disc-type transformer winding is shown in Figure 2-4.

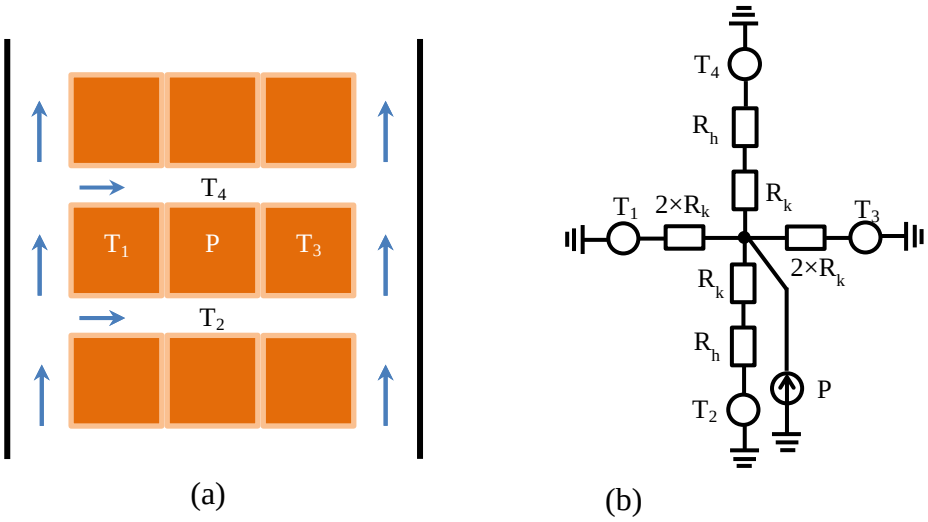

Figure 2-4. Simplified thermal network of one disc of disc type windings. (a) Illustration of winding discs. (b) Thermal network of one strand. P stands for power generated in the strand, T_1 for left strand temperature, T_3 for right strand temperature, T_2 for below oil temperature, T_4 for above oil temperature, R_k for conduction thermal resistance, R_h for convection thermal resistance.

In this thermal network, temperatures are treated as voltage sources and power losses treated as current sources; the effects of conduction and convection are lumped into thermal resistance. The thermal resistance related to conduction in a thermal network (R_k) are determined by paper thermal conductivity (k_p) and its thickness (δ) and surface area (A) with the thermal resistance of the copper conductors ignored ($R_k = \frac{1}{k_p}\frac{\delta}{A}$). The thermal resistance related to convection (R_h) are determined from the local heat transfer coefficient and surface area ($R_k = \frac{1}{hA}$). In order to determine the local heat transfer coefficient universally, it is nondimensionalised into the Nusselt number (Nu). The correlation between Nu and the liquid flow rate, liquid thermal properties and the cooling duct geometry, is usually taken from literature pertaining to simpler experimental tests [33, 34], and used in the thermal network for transformer windings. Similarly, the correlation for Nu is susceptible of improvement [35, 36].

2.3.2 CFD Models

CFD models use numerical methods, e.g. finite element method, finite volume method, finite difference method, etc. to solve the governing differential equations for fluid flow and heat transfer. The governing equations for CFD models in steady state are [37-39]

$$\nabla \cdot (\rho \boldsymbol{u}) = 0 \tag{2.6}$$

$$\rho \boldsymbol{u} \cdot \nabla \boldsymbol{u} = -\nabla p + \nabla \cdot (\mu(\nabla \boldsymbol{u} + (\nabla \boldsymbol{u})^T) - \frac{2\mu}{3}(\nabla \cdot \boldsymbol{u})\boldsymbol{I}) + \rho \boldsymbol{g} \tag{2.7}$$

$$\nabla \cdot (\rho c_p \boldsymbol{u} T) = \nabla \cdot (k \nabla T) + S_E \tag{2.8}$$

where ρ is the density (kg/m^3); $\boldsymbol{u}$ is the velocity vector (m/s); p is pressure (Pa); $\boldsymbol{I}$ is an identity matrix; μ is the dynamic viscosity (Pa·s); $\boldsymbol{g}$ is the gravitational acceleration vector (m/s^2); c_p is the specific heat at constant pressure (J/(kg·K)); T is temperature (K); k is the thermal conductivity (W/(m·K)); S_E is the energy source term (W/m^3).

Equation (2.6) is the continuity equation for mass conservation. Equation (2.7) is the Navier-Stokes equation set for momentum conservation. The left-hand side term in equation (2.7) represents the momentum flux variation and the right-hand side terms represent the variation of forces causing the variation of momentum: the first term on the right is the pressure variation; the second term is the viscous stress variation acting on the control volume; the third term is the body force due to gravity. The Navier-Stokes equations are greatly simplified when applied to the condition of incompressible flow with constant viscosity, which is approximately the case for transformers in OD cooling modes and ON cooling modes when the adoption of the Boussinesq approximation is suitable. Equation (2.8) is for energy conservation where the left-hand side term represents convection and the right-hand side terms represent conduction and energy source, respectively.

2.4 Calibration of Network Modelling

As mentioned in section 2.3.1, the accuracy of the network models depends crucially on the correlations adopted and the off-the-shelf correlations obtained from literature are susceptible of improvement, either by experimentation or CFD simulations. Experimentation on flows in disc-type transformer windings is rare to find partly because it is difficult to perform due to the narrow horizontal cooling ducts, of which the height is just several millimetres. The calibration of the correlations has therefore usually been performed by CFD simulations [31, 32, 35, 36, 40, 41].

The calibration for the thermal network or, more precisely, the calibration for the correlation of *Nu* is relatively easier to perform because it is only related to fluid flow and heat transfer in a single horizontal cooling duct [35, 36]. In addition, the off-the-shelf correlation from literature, when properly chosen, turns out to be accurate enough [36] (shown in Apendix 3).

The calibration for the hydraulic network, especially the calibration of the correlations for the so-called minor pressure losses due to flows in corners, in dividing and combining T-junctions, turns out to be challenging. Great improvements of the correlations for the "minor losses" in elbows and T-junctions were achieved by conducting dimensional analysis and performing CFD parametric sweeps based on the dimensional analysis [32]. The CFD results were then correlated to the dimensionless groups identified in the dimensional analysis by a multilayer fitting strategy [32]. It is worth mentioning that these correlations for "minor losses" are derived from a simple geometry of one vertical duct and one horizontal duct. In practice, however, multiple horizontal ducts are connected to the vertical duct and the horizontal ducts interact with one another. The duct-by-duct consideration in [32] will lose some accuracy in determining pressure drop and flow distribution in the winding.

The comparisons of mass flow distribution for a disc-type winding with the same input conditions (the same pass inlet oil temperature and inlet velocity of 0.485 *m/s* leading to *Re* being 1001 [32]) obtained from network models with different the so-called minor loss correlations [30-32, 42] and a CFD model are shown in Figure 2-5

(b) [32]. The prominent feature of the 2D winding geometry, shown in Figure 2-5 (a), is that the height of the top horizontal cooling duct is 2 mm and the heights of the other horizontal cooling ducts are 4 mm. The CFD mass flow distribution results are the most reliable results and are therefore treated as the benchmark to compare with. It can be seen from Figure 2-5 (b) that the flow distribution obtained from [32] is the closest to the CFD results, while the other network models give flow distributions significantly different from the CFD results. The comparisons of static pressure drop over the one-pass winding model and the maldistribution, κ, defined as the ratio of the maximum horizontal duct flow rate to the minimum horizontal duct flow rate, from different models are shown in Table 2-2. It can be seen from Table 2-2 that the total pressure loss from [32] is also the closest to CFD results. The high κ value from the CFD simulation indicates that the inlet velocity of 0.485 *m/s* for the winding is too high for a reasonably uniform flow distribution. The still noticeable discrepancies between the CFD results and those from [32] are mainly due to the error in the correlations for minor pressure losses introduced by the duct-by-duct consideration, indicating a pass-by-pass consideration is required to further improve the network prediction on flow distribution.

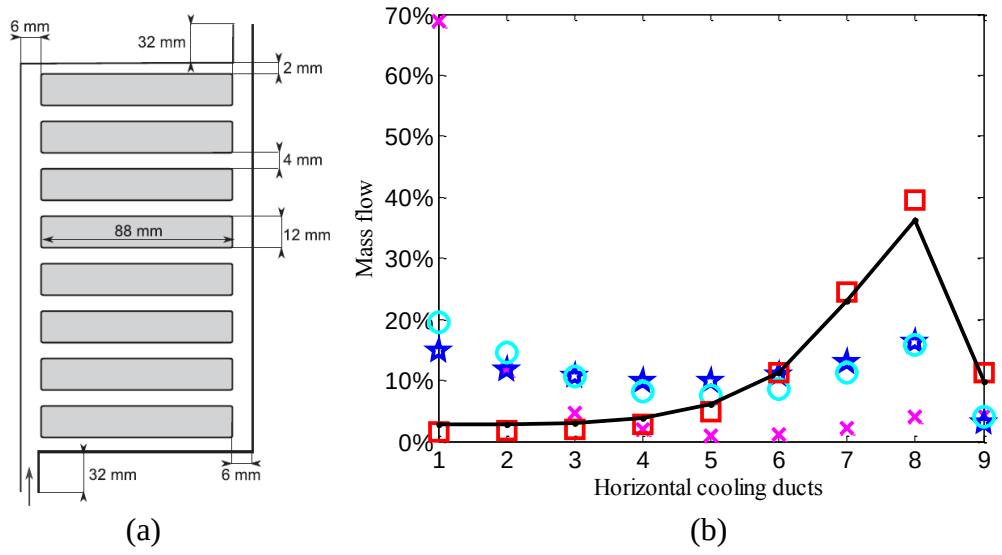

Figure 2-5. Comparisons of mass flow distributions from different numerical models with the same input conditions [32]. (a) Geometry of a disc-type one-pass winding model. (b) Comparisons of mass flow distributions obtained from different models: × from [30], ★ from [31], O from [42], □ from [32], ▬ from CFD [32].

Table 2-2. Comparisons of maldistribution and pressure drop over a one-pass winding [32].

correlation	κ	ΔP_{pass} (Pa)
From [30]	61.87	2143.3
From [31]	4.78	230.89
From [42]	4.88	163.00
From [32]	23.75	263.56
CFD	12.64	275.35

It is worth emphasizing that although susceptible of improvement by proper CFD calibrations, network models have the intrinsic drawback of low spatial resolution and therefore cannot capture detailed phenomena, e.g. hot-streak dynamics which arises from the high Prandtl number (*Pr*) of the coolant liquid and plays a crucial role in determining liquid flow and temperature distribution in ON cooling modes [26].

2.5 **CFD Modelling**

CFD modelling is the most reliable modelling method among all the modelling methods available, which comes at a cost of higher computational requirement. In this section, literature pertaining to CFD modelling strategies and results is reviewed.

2.5.1 CFD Modelling Strategies

The strategies employed in CFD modelling have direct impacts on the reliability and accuracy of the simulation results. The strategies mainly involve the type of model to choose (laminar or turbulent) and the approximations employed in the CFD model. Once the CFD simulations have been properly conducted, important flow and temperature distribution features can be revealed, which are hot-streak dynamics and reverse flows for both OD and ON cooling modes.

2.5.1.1 Laminar model and turbulence model

For OD cooling modes, a laminar model is usually adopted in CFD modelling due to the low *Re* at the winding inlet (usually much smaller than 2000). In ON cooling

modes, the Rayleigh number (*Ra*) could be high enough to bring about transition to turbulence in certain places [26]. A turbulence simulation for the LV winding of an ON transformer was conducted with the low-*Re* κ-ε Launder-Sharma model in [43]. A laminar solution was obtained from the turbulence simulation, indicating that the flow is laminar [26]. It is suggested in [26] that certain transformer operational conditions and winding geometries may necessitate the inclusion of a turbulence model for ON cooling modes.

2.5.1.2 CFD Approximations

Approximations are inevitable in CFD modelling. However, the degree of approximation should be controlled to guarantee the reliability and accuracy of the model. The major approximations that could be adopted in CFD modelling are the approximation of the winding discs, the exclusion of buoyancy forces and the approximation from 3D winding geometry to axisymmetric 2D winding geometry. The effects of these approximations are assessed in detail in literature.

The approximations of the stranded winding disc to a bare copper block, or prescribing a constant equivalent heat flux on the surface of the disc to represent its presence have all been found to be inadequate. This is particularly the case for ON cooling modes because these approximations will affect the heat transfer in the winding discs and therefore affect the hot-streak dynamics, which play crucial roles in determining fluid flow and heat transfer in the winding [26, 27].

For ON and OF (oil forced but not directed) cooling modes, the exclusion of buoyancy forces in CFD modelling is found not acceptable because buoyancy forces are the principal driving forces [25, 27]. For OD cooling modes, however, the conclusion made in [25] that buoyancy forces have a significant effect on both flow distribution and temperature distribution, needs close inspection because of the conditions adopted in the simulation.

In the simulation setting for the OD cooling mode in [25], the power loss density is set to be 1,375,324 W/m^3 with an inlet velocity of 0.2 m/s [25]. This power density

prescription is not representative of an OD transformer because of the following reasoning. Current density, j, in a transformer winding is usually in the range of 2 to 4 A/mm^2 [2] and copper resistivity, ρ_Ω, at 80 °C is $2.06\times10^{-8}\ \Omega{\cdot}m$ with resistivity at 20 °C being $1.68\times10^{-8}\ \Omega{\cdot}$m and the temperature coefficient being 0.0038 K^{-1}. Therefore, the power density, $\rho_\Omega \cdot j^2$, in the winding would have a range from 82,400 to 329,600 W/m^3, which is much lower than 1,375,324 W/m^3 prescribed in [25]. Therefore, the unrealistically high power loss density used in [25] undermines the conclusion drawn. In fact, the relative effects of buoyancy forces depend on both the total liquid flow rate and the total power losses in the winding. Based on dimensional analysis, the relative effect of buoyancy forces depends on the ratio of the Grashof number (Gr) to Re^2 (Gr/Re^2): only when the ratio is much smaller than unity is the effect of buoyancy forces negligible [38, 44]. For OD cooling modes, the ratio of Gr/Re^2 is generally much smaller than unity; therefore the effects of buoyancy forces are negligible.

The approximation of 3D geometry to axisymmetric 2D geometry is commonly adopted in CFD modelling [25-27, 32, 45]. The 2D approximation reduces the computational requirement significantly at the cost of losing detailed liquid flow and heat transfer phenomena in the vicinity of winding spacers and some potential 3D liquid flow and heat transfer features [28]. However, the axisymmetric 2D CFD results are found to be representative to their 3D CFD counterparts by matching Gr/Re^2 [28]. The hot-spot temperature in a 3D CFD simulation can also be derived from the corresponding axisymmetric 2D CFD results by adopting correction factors to take into account of effects of radial spacers with respect to both the proportion of disc surface area being covered and the change of liquid flow rate due to the presence of the spacers [28]. It is worth mentioning that in the 2D and 3D comparison in [28], if both Re and Gr/Re^2 can be matched, then the dimensionless flow distribution and temperature distribution would have an even better match between the 2D and 3D results.

2.5.2 CFD Flow and Temperature Distribution Features

Hot-streaks are found in CFD modelling [25-28]. This phenomenon is because of the large Pr of the coolant liquid (typically larger than 50), which means the momentum

diffusivity of the liquid is much larger than its thermal diffusivity. Large *Pr* results in the hot liquid layers forming on the surfaces of winding discs to stay constantly hotter than its surrounding liquid layers when transported to the vertical cooling duct, as shown in Figure 2-6 [27].

For OD cooling modes, the effect of buoyancy forces is usually minor and therefore the hot-streaks have little effect on liquid flow distribution in the winding. When convected into downstream horizontal cooling ducts, however, the hot-streaks can affect the heat transfer in the horizontal cooling ducts [25].

Reverse flows, which are liquid flows from the pass outlet vertical duct to the inlet vertical duct, are found to occur at the bottom of winding passes in OD cooling modes at the condition of high total liquid flow rates or high liquid temperatures [45, 46]. The occurrence of reverse flows usually results in small transverse flow rates or even flow stagnation and can therefore seriously jeopardize the cooling performance of the winding, causing localized overheating.

For ON cooling modes, the persistent hot-streaks generated in one pass can be convected into the downstream passes and affect the liquid flow distribution and the temperature distribution in these downstream passes, resulting in a strong coupling among the winding passes [26]. This hot-streak dynamics can lead to complicated liquid flow and temperature distribution patterns. Reverse flows at the top part of the winding passes, in contrast to the bottom part for OD cooling modes, are observed as shown in Figure 2-7. Hot plumes resulted from bidirectional flows in horizontal cooling ducts are also observed, as shown in Figure 2-7 [26]. The reverse flows and hot-plumes disappear when the buoyancy force term is removed [26].

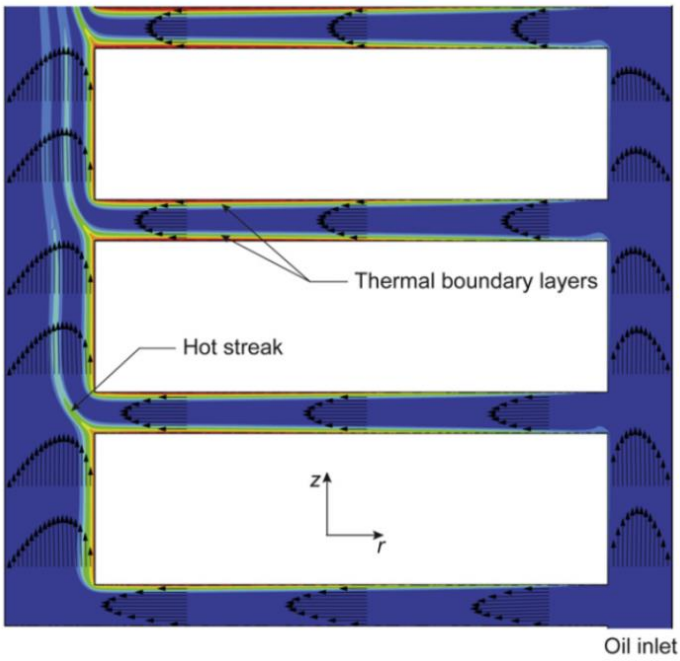

Figure 2-6. Thermal (contours) and momentum (vectors) boundary layers in the cooling ducts of a disc-type winding [27].

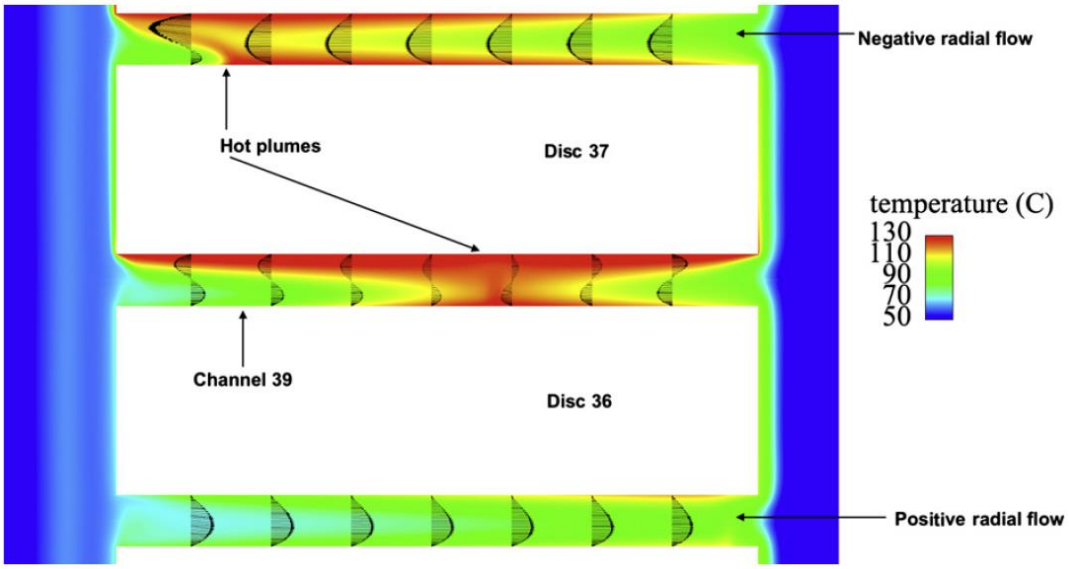

Figure 2-7. Reverse flow and hot plumes at the top part of a winding pass in an ON transformer [26].

2.6 **Experimental Tests**

Experimental tests designed to verify transformer thermal models mainly involve the measurements of liquid flow distribution and temperature distribution in winding models. In addition, static pressure drops over transformer winding models are sometimes also measured. It is rare to find these types of measurements in literature

due to the great effort required to perform such measurements, especially the measurements of liquid flow rate in horizontal cooling ducts, of which the height is usually just 3-6 mm [23]. The available experimental tests and their conclusions in literature are reviewed as below.

Temperature measurements in disc-type transformer winding models were conducted with ON flow rates to calibrate the correlations for local *Nu* in horizontal cooling ducts in [47]. It is found from the tests that the copper conductor temperature gradients in the circumferential direction are negligible, indicating the validity of performing 2D axisymmetric modelling [47]. The experimentally derived correlations for local *Nu's* under both one-side heating and both-side heating conditions are reported to be more accurate than those obtained from literature [47]. Unfortunately, the experimentally derived correlations are not shared in [47].

Static pressure drop measurements in a disc-type winding model in OD cooling modes were conducted to verify the CFD model and network model used in [45, 48]. The consistency between the measured pressure drops and those derived from the hydraulic network model and the CFD model is regarded sufficient to verify the models in [45]. This conclusion, however, should be treated with caution because a close pressure drop match does not necessarily ensure a reasonable match for liquid flow distribution, as shown in Table 2-2 and Figure 2-5.

Liquid flow distribution and temperature distribution in a unique disc-type winding model with two stacks of discs (three vertical ducts) and no flow directing washers were measured by a Laser Doppler Velocimetry (LDV) system and thermocouples, respectively [49, 50]. Complicated flow pattern in the horizontal cooling ducts were found due to a lack of flow control in the winding [49].

Liquid flow distribution in a disc-type winding model was measured in [51] in isothermal conditions using a hot wire anemometry system to investigate the flow pattern in OD transformer windings. The results were described by the authors of [51] as preliminary. In addition, the vertical duct width for most of the test cases was set to be 4 mm, which is out of the range of 6-12 mm in modern transformer design practice [23]. It was found in these measurements that higher flow proportions occur

in horizontal ducts at the top and bottom part of the winding pass with the horizontal ducts in the middle suffering from liquid flow deficit [51]. Two derived velocities in the horizontal cooling ducts were obtained from the measurements: the velocity difference between the maximum velocity and the minimum one, ΔV, and the mean velocity in all the horizontal cooling ducts, V_m . A rough linear relationship was found between $\Delta V / V_m$ and the number of discs in the pass [51].

The total liquid flow rates in an ON transformer model—consisting of a disc-type winding model, a radiator and the pipework connecting the winding and the radiator—were measured using a LDV system to investigate the effects of different controlling parameters on the total liquid flow rate in the winding. The effects of different total power injections in the winding model ranging from 100 W to 6,000 W and different height differences between the centre point of the radiator and the centre point of the winding model, ΔH, of 392 mm and 643 mm were tested [10]. It was found that the total liquid flow rate was roughly proportional to the square root of the amount of heat generated in the winding and the square root of ΔH [10].

Fluid flow distribution in and static pressure drop over a disc-type winding model of a gas-filled OD transformer were measured to investigate the effects of different winding geometries on the fluid flow distribution and pressure drop. In the winding model tests, water was used to substitute the gas used in the transformer (SF_6) in such a way that the Reynolds numbers for the water tested in the model and the gas used in reality were matched [52]. A particle image velocimetry (PIV) system was used to measure the liquid flow rate in the horizontal cooling ducts. It was found that with the increase of the number of discs in the winding pass the flow distribution got less uniform, and when the number of discs exceeds 6 reverse flows at the bottom part of the winding pass started to occur [52]. The smallest flow proportion was found at the bottom horizontal cooling duct and this flow proportion decreased monotonically with the increase of the ratio of horizontal duct height to vertical duct width [52]. In addition, the static pressure drop over the winding model was found to decrease monotonically with the increase of the ratio of horizontal duct height to vertical duct width [52].

2.7 **Summary**

In this chapter, methods to determine the hot-spot temperature in a transformer winding in a steady state are reviewed. The empirical method is based on the results of the temperature rise test in the factory, after a transformer is designed and built. The temperature rise test results are interpreted by the thermal diagram, in which the hot-spot factor is a crucial parameter that determines the accuracy of the hot-spot temperature derived. The physics-based methods are the thermal hydraulic network modelling and CFD modelling, normally used for prediction before the construction of the transformer. These two modelling methods share the same physical principles. CFD methods are more reliable and accurate than network methods at the cost of a much higher computational requirement.

Network models are susceptible of improvement by adopting CFD calibrated correlations for pressure losses and heat transfer in the winding. However, the low spatial resolution prevents network models from capturing detailed phenomena, such as hot-streak dynamics, which play a crucial role in determining liquid flow distribution and temperature distribution in ON transformers.

CFD results reveal the existence of hot streaks and reverse flow in disc-type transformer windings, which is confirmed by experimental tests. The validity of detailed CFD modelling results still needs to be verified by experimental tests. However, experimental test results have been found lacking in literature due to the great effort required to perform such tests. More reliable CFD modelling and experimental tests are therefore required to advance the understanding of the thermal behaviour of transformer windings.

Chapter 3 OD Cooling Modes

3.1 Introduction

In an OD cooling mode, oil is pumped from the radiators and delivered to the bottom of the windings. In the windings, oil directing washers are installed in a way to form connected passes and zigzag flow patterns among the passes. In each pass, the total liquid flow rate and the flow distribution have a direct impact on the heat transfer, especially convection heat transfer in the pass. A relatively more uniform flow distribution is always desired to avoid potential localized overheating. In addition, the pressure drop over a winding in relation to the total oil flow rate through the winding is important mainly because it determines oil split among windings connected hydraulically in parallel, e.g. LV winding and HV winding in the same phase of the transformer.

Transformer thermal modelling for OD cooling modes mainly involves the determination of the pressure drop over, flow distribution in and heat transfer in the windings. These are controlled by the winding geometry (number of passes in the winding, number of discs per pass, vertical duct width, horizontal duct height, disc radial width and disc axial height), oil properties (density, dynamic viscosity, thermal conductivity and specific heat) and the total oil flow rate in the winding. With so many parameters to consider, how can one perform the thermal modelling with a manageable investigation strategy and extract a big picture out of it? Investigation on a case-by-case basis is overwhelming in terms of workload and data processing. Dimensional analysis, which has been widely adopted in fluid mechanics and heat transfer, can simplify the problem prior to obtaining a quantitative answer and therefore should be adopted in the field of transformer thermal modelling as well.

In this chapter, dimensional analysis is adopted to tackle the problem of transformer thermal modelling in OD cooling modes to obtain simplicity, insight and universally applicable results, by both dimensional consideration (Buckingham's Pi Theorem) and functional consideration, i.e. nondimensionalizing the governing differential equations. Four papers are presented to demonstrate the application of dimensional

analysis on OD transformer thermal modelling. Paper 1 deals with the topic of pressure drop and flow distribution by theoretical analysis and CFD simulations. Paper 2 verifies experimentally the conclusions made in paper 1. Paper 3 applies the results from paper 1 to investigate the influence of different liquids used on flow distribution in and pressure drop over the winding. Paper 4 advances the investigation to heat transfer in the winding and interprets the hot-spot factor, which is a concept widely used in the transformer industry, as a dimensionless temperature at the hot-spot.

In the study of OD cooling modes, it is found that the liquid flow distribution for fixed winding pass geometry is governed by *Re* at the pass inlet. With the increase of *Re* flow distribution becomes increasingly more distorted. When *Re* is smaller than 300, the flow distribution is relatively uniform with a U-shaped flow distribution and a maldistribution factor (the ratio of the maximum duct velocity to the minimum duct velocity in the same pass) being smaller than approximately 3. However, when *Re* exceeds 300, the flow distribution becomes J-shaped leading to an increasing maldistribution factor, and with a further increase of *Re* reverse flows occur at the bottom part of the pass.

The relationship between the flow distribution and *Re* is mainly related to the flow separation at the entrances of the horizontal cooling ducts at the bottom of the pass, as shown in an example case in Figure 3-1. In this case, a 3-pass winding model is simulated using the COMSOL Multiphysics CFD module. The liquid flow in the first bottom duct in pass 3 is shown with streamline representations. As can be seen from Figure 3-1, when *Re* is 50, flow separation is not obvious at the entrance of the duct and a significant proportion of the total flow enters the bottom duct. With the increase of *Re* flow separation becomes more obvious, which makes the effective horizontal duct height increasingly smaller and this results in less liquid flowing into the bottom duct. When Re reaches 1000, the flow proportion in the bottom duct is hardly noticeable.

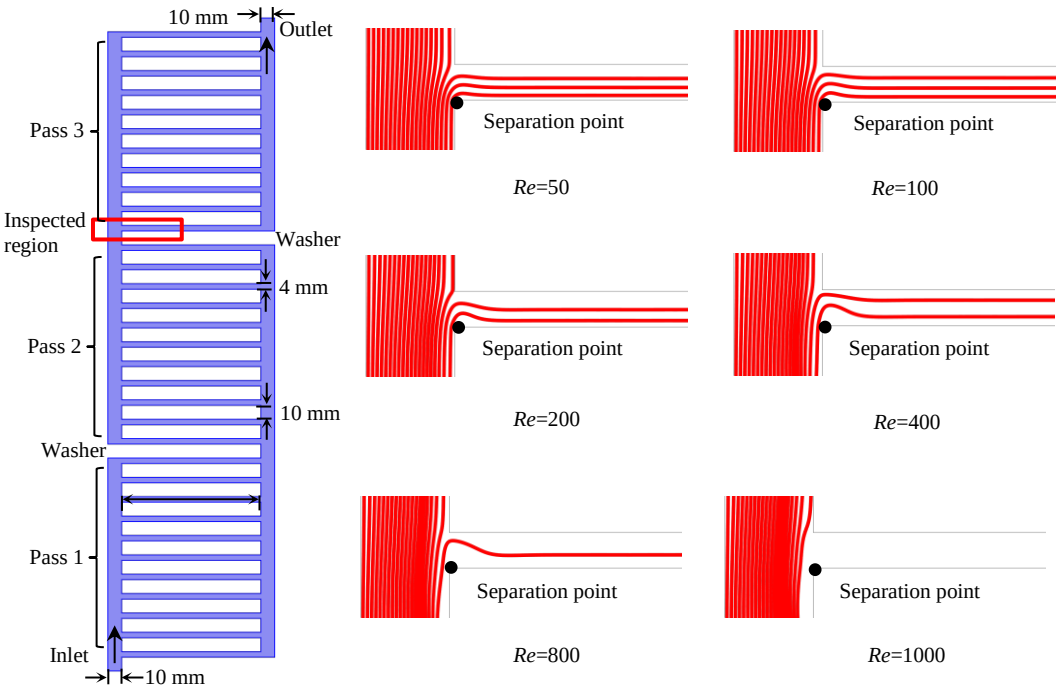

Figure 3-1. Flow separation at the entrance of the bottom duct in pass 3 with different *Re's* shown by streamline representations.

3.2 **Paper 1**

Prediction of Pressure Drop and Flow Distribution in Disc Type Transformer Windings in an OD Cooling Mode

Xiang Zhang, Zhongdong Wang and Qiang Liu

2017

IEEE Transactions on Power Delivery

Published (Volume: 32, Issue: 4, Aug. 2017, Pages: 1655 - 1664)

Prediction of Pressure Drop and Flow Distribution in Disc Type Transformer Windings in an OD Cooling Mode

Xiang Zhang, Zhongdong Wang, Member, IEEE, and Qiang Liu, Member, IEEE

***Abstract*— In this paper, a method for predicting pressure drop and flow distribution in disc-type transformer windings in an oil forced and directed (OD) cooling mode is proposed. First, dimensional analyses are conducted to identify the independent dimensionless variables that affect pressure drop over and flow distribution in the winding. Next, parametric sweeps are performed with computational fluid dynamics (CFD) simulations under isothermal flow conditions. Finally, pressure drop and flow distribution results obtained from the simulations are correlated with the previously identified dimensionless variables to derive correlation equations. These equations have been verified over a range of different isothermal and non-isothermal flow cases and applied to identify the criteria for the occurrence of reverse flow resulting from a combination of pass inlet flow rate and winding geometry. In addition, the method provides an insight into the controlling parameters for determining the minimum oil velocity in horizontal cooling ducts.**

***Index Terms*— Dimensional analysis, disc type winding, flow distribution, OD cooling mode, pressure drop, transformer**

NOMENCLATURE

$\bar{c}_p$	Mean specific heat of the oil ($J/(\mathrm{kg}\cdot\mathrm{K})$)
C_{pd}	Pressure drop coefficient over the winding passes
H_{disc}	Disc vertical (axial) height (m)
H_{duct}	Horizontal (radial) duct height (m)
$\dot{m}$	Mass flow rate in the pass (kg/s)
n_1	Number of passes in the winding
n_2	Number of discs per pass
N_{de}	Number of domain mesh elements
P_{fi}	Volumetric flow proportion in horizontal duct i
ΔP	Static pressure drop (Pa)
Q	Total power loss in pass 1 and pass 2 (W)
r	Rounding radius of the strand (m)
R_{inn}	Winding inner radius (m)
Re	Reynolds number at the pass inlet ($\rho\cdot\bar{v}_{in}\cdot 2W_{duct}/\mu$)
T	Temperature in Kelvin (K)
T_{b1}	Oil bulk temperature at the inlet of pass 1 (K)
T_{b3}	Oil bulk temperature at the inlet of pass 3 (K)
$\bar{v}_i$	Average oil velocity at the entrance of duct i (m/s)
$\bar{v}_{in}$	Average pass inlet oil velocity (m/s)
W_{disc}	Disc horizontal (radial) width (m)
W_{duct}	Vertical (axial) duct width (m)
α	Dimensionless horizontal duct height (H_{duct}/W_{duct})
β	Dimensionless disc axial height (H_{disc}/W_{duct})
γ	Dimensionless disc radial width (W_{disc}/W_{duct})
ρ	Oil density (kg/m^3)
μ	Oil dynamic viscosity ($Pa\cdot s$)

I. Introduction

Transformer life expectancy is generally determined (with the exception of premature failure due to faults) by the temperature of the hottest point in the winding, which is referred to as *hot spot* [1]. The primary objective of transformer thermal design is to control the hot spot temperature within certain limitations, as specified in standards e.g. IEC 60076-2 and IEEE C57.91 [2, 3].

Heat generation and dissipation in the winding are the critical factors that determine the hot spot temperature. Heat generation in the winding is the result of resistive and eddy current losses. Heat dissipation is usually facilitated by oil circulation between the winding and the cooler/radiator. In disc-type transformer windings, flow distribution in the horizontal (radial) cooling ducts should ideally match the loss distribution [4].

Various thermo-hydraulic network models have been proposed to determine the oil flow and heat transfer processes in the winding [5-7]. The performance of these network models depends crucially on the coefficient correlation equations adopted. These correlation equations are for pressure losses (mainly minor losses) to determine flow distribution in the winding, and for the Nusselt numbers to determine the heat transfer coefficients in the horizontal cooling ducts. They are usually obtained from literature pertaining to circular pipe flow and 2D duct heat transfer processes. The applicability of these traditional correlation equations proved to be unsatisfactory when compared with the performance of newly established correlation equations derived from computational fluid dynamics (CFD) models [8-10]. It is probably worth mentioning that the correlation equations proposed in [9] were partially verified by measuring the pressure drop over one pass of a test rig; however flow distributions obtained from the calibrated network model were significantly different from those obtained from 2D CFD simulations, especially for the cases of high oil flow rates [11].

The correlation equations for minor pressure losses of flow over elbows, in dividing, and merging T-junctions have been greatly improved in [10]. However, the discrepancy between flow distributions in a winding pass from a CFD simulation and a network model with the newly developed minor loss correlation equations is still not negligible (figure 8 in [10]). This could be because flows in the adjoining horizontal ducts interact with one another, whereas a single horizontal duct was employed in [10] in the procedure for deriving the minor pressure drop correlation equations. Therefore, consideration of a whole pass is necessary to capture the complete characteristics of pressure drop and flow distribution in disc-type transformer windings.

In addition to CFD calibrations for the correlation equations, experiments were conducted to calibrate the Nusselt numbers in horizontal ducts [12]. Isothermal flow experiments were also conducted to determine the flow

distribution and total pressure drop in a disc-type winding [13]. The influences of the number of discs per pass, ratio of horizontal duct height to vertical (axial) duct width and the effect of the elevation of the cooling system were investigated experimentally as well as via network modelling and CFD simulations using a finite difference method [13, 14].

Fluid flow and heat transfer in transformer windings are coupled. This is self-evident for a natural cooling mode (ON) where buoyancy is the only driving force. For ON cooling mode, the temperature profile at the inlet of a pass and the subsequent hot-streak dynamics can significantly affect the flow distribution in the pass [15, 16]. For oil forced and directed (OD) cooling mode, pressure generated by the pump dominates the flow pattern and therefore the effects of hot-streak dynamics and buoyancy force are much less influential.

In this paper, parameters that affect pressure drop and flow distribution in an OD cooling mode under isothermal flow conditions are identified and grouped into dimensionless groups in section II. The influence of these dimensionless parameters on pressure drop and flow distribution is then quantified by conducting 640 sets of parametric sweeps with CFD simulations in section III. Correlation equations for pressure drop over and flow distribution in the winding with winding geometry and oil flow rate are developed in section IV and verified in section V. The practical implications of these correlation equations are presented in section VI, followed by discussion and conclusion in section VII and VIII.

II. Dimensional Analyses on Pressure Drop and Flow Distribution in Disc-Type Transformer Winding Pass

Any physically significant equation must be dimensionally homogeneous, and this is the premise for dimensional analysis. Dimensional analysis can reduce the number of independent variables and simplify the procedure for analyzing physical problems enormously [17, 18].

A. Winding Geometry of Interest

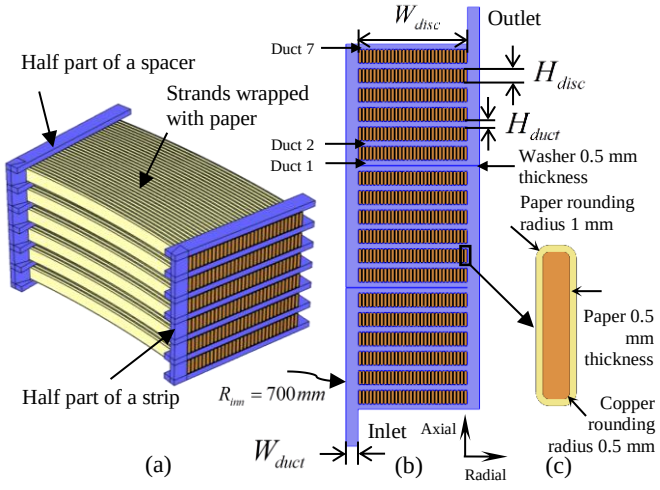

Fig. 1. Disc-type winding geometry. (a) 3D geometry of a segment of one pass between two adjoining sets of spacers. (b) 2D axisymmetric geometry of a 3-pass case. (c) Geometric details of the cross section of a strand. The annotations are added to facilitate dimensional analyses in section II part B and part C. The geometric dimensions are for baseline cases in section III part B and part D.

A disc-type winding possesses an angular periodicity dictated by the number of spacers present along the circumference of the disc. A segment of one pass between two adjoining sets of spacers is shown in Fig. 1(a). Since oil flow in the winding segment is a quasi-2D flow, the winding geometry can be further reduced to an axisymmetric 2D approximation, omitting the details in the vicinity of spacers and strips. The 2D approximation would lead to larger cross section area compared to the real situation with spacers and strips and therefore lower oil velocities for the same oil mass flow rate. This limitation can be partially compensated by applying an area correction coefficient, as indicated in [19]. The 2D geometry of a 3-pass winding with 6 discs per pass is shown in Fig. 1(b), where the details of the cross section of a strand are illustrated in Fig. 1(c).

B. Dimensional Analysis on Pressure Drop

The following expression is deemed sufficient to determine the static pressure drop over the winding (ΔP):

$$\Delta P = f(n_1, n_2, \bar{v}_{in}, \rho, \mu, H_{duct}, H_{disc}, W_{disc}, W_{duct}, R_{inn}, r) \tag{1}$$

Repeating parameters are set to be $\bar{v}_{in}$, ρ , and W_{duct} , which are combined with the remaining parameters to transform (1) into the dimensionless form:

$$\frac{\Delta P}{\rho \bar{v}_{in}^2/2} = C_{pd} = g(n_1, n_2, \frac{\rho \bar{v}_{in}(2W_{duct})}{\mu}, \frac{H_{duct}}{W_{duct}}, \frac{H_{disc}}{W_{duct}}, \frac{W_{disc}}{W_{duct}}, \frac{R_{inn}}{W_{duct}}, \frac{r}{W_{duct}}) \tag{2}$$

where $\rho \cdot \bar{v}_{in}^2 / 2$ is the dynamic pressure at the pass inlet; $2W_{duct}$ is the hydraulic diameter of the vertical cooling duct.

C. Dimensional Analysis on Flow Distribution

Flow distribution in a pass for inlet at inner vertical duct differs slightly from that of inlet at outer vertical duct. In this analysis we focus on the case of flow inlet at the inner vertical duct, as is the case in the third pass in Fig. 1(b).

The average oil velocity in horizontal cooling duct i , which can be any duct in the pass, is expressed in the form of:

$$\bar{v}_i = f_i(n_2, \bar{v}_{in}, \rho, \mu, H_{duct}, H_{disc}, W_{disc}, W_{duct}, R_{inn}, r) \tag{3}$$

Similarly, $\bar{v}_{in}$, ρ , and W_{duct} are chosen to be repeating parameters, resulting in the dimensionless form of:

$$\frac{\bar{v}_i}{\bar{v}_{in}} = g_i(n_2, \frac{\rho \bar{v}_{in} 2 \cdot W_{duct}}{\mu}, \frac{H_{duct}}{W_{duct}}, \frac{H_{disc}}{W_{duct}}, \frac{W_{disc}}{W_{duct}}, \frac{R_{inn}}{W_{duct}}, \frac{r}{W_{duct}}) \tag{4}$$

As the functional form of g_i has not been determined yet, it is permissible to modify these dimensionless groups. The $\bar{v}_i / \bar{v}_{in}$ is replaced by the product of itself and H_{duct} / W_{duct} , which is actually the volumetric flow proportion in duct i .

$$\frac{\bar{v}_i}{\bar{v}_{in}} \cdot \frac{H_{duct}}{W_{duct}} = P_{fi} = g_i'(n_2, \frac{\rho \bar{v}_{in}(2W_{duct})}{\mu}, \frac{H_{duct}}{W_{duct}}, \frac{H_{disc}}{W_{duct}}, \frac{W_{disc}}{W_{duct}}, \frac{R_{inn}}{W_{duct}}, \frac{r}{W_{duct}}) \tag{5}$$

where $\bar{v}_i \cdot H_{duct}$ represents oil flow rate in horizontal duct i, $\bar{v}_{in} \cdot W_{duct}$ represents oil flow rate at the pass inlet.

D. Determination of Functional forms

According to the dimensional analyses, pressure drop coefficient (C_{pd}) and flow proportion in duct i (P_{fi}) can be determined by (2) and (5), respectively. However, the functional forms of (2) and (5) are not specified by the analyses themselves, but need to be obtained either by experimentation or theoretical calculations.

In this paper, CFD simulations are conducted. The results for C_{pd} and P_{fi} are extracted from the simulations and then correlated with the dimensionless parameters via curve fitting to obtain the functional forms.

III. Parametric Sweeps

Before performing parametric sweeps, a set of test cases were conducted to check the validity of the foregoing dimensional analyses and to provide some insight into the effects of the dimensionless groups.

A. CFD Simulations

COMSOL Multiphysics is employed to implement the theoretical calculations for which the Navier-stokes equations and the continuity equation are solved directly using a finite element method. Because the Reynolds number (Re) at the pass inlet is smaller than the criterion value for transition to turbulence, no turbulence model is included.

In all CFD simulations, the meshes consist of layers of thin rectangles for the flow boundary layers and triangles for the main flow domains. Mesh refinement studies are conducted to guarantee mesh-independent solutions. It is found that the number of rectangle layers has negligible influence on the results of flow distribution and pressure drop. Therefore, 2 layers of thin rectangles are used in all the meshes. For a typical CFD case, such as the benchmark case to be shown in section III part B, the mesh consists of 1,159,948 triangular domain elements and 48,048 rectangular boundary elements. The number of degrees of freedom is 2,143,368. The meshing time is 24 minutes and the calculation time is 9 minutes. The results of mesh refinement study of the benchmark case are shown in Table I. The tracking parameters at each mesh size or number of domain elements (N_{de}) are pressure drop over the three passes (ΔP) and the average oil velocity in the bottom duct of pass 3 ($\bar{v}_1$). According to the varying trend of the tracking parameters with the number of domain elements shown in Table I, the mesh strategy corresponding to mesh 4 is adopted for all the CFD simulations.

TABLE I
MESH REFINEMENT STUDY RESULTS OF THE BENCHMARK CASE

Strategy	mesh 1	mesh 2	mesh 3	mesh 4	mesh 5
N_{de}	390,862	568,428	966,554	1,159,948	2,866,688
ΔP (Pa)	445.42	473.85	493.46	495.19	495.54
$\bar{v}_1$ (mm/s)	46.760	46.539	46.672	46.607	46.617

B. Computational Tests of Dimensional Analyses

The geometries of the test cases resemble those of HV windings for transmission transformers. In the tests, n_1 is fixed to be 3, n_2 6, R_{inn} 700 mm, r 1 mm, washer thickness 0.5 mm. The radial width of the strand is fixed to be 3 mm, whereas the axial height of the strand is adjustable. A mineral oil is used as the coolant whose temperature (in Kelvin) dependent density and viscosity are

$$\rho = -0.65110 \times T + 1067.0 \tag{6}$$

$$\mu = 5.9622 \times 10^{-5} \times \exp\left(\frac{707.64}{T - 165.20}\right) \tag{7}$$

Under these test conditions, we presume that C_{pd} and P_{fi} are dominated by Re at the pass inlet, dimensionless horizontal duct height (α), dimensionless disc axial height (β), and dimensionless disc radial width (γ).

1) Test cases

Five test cases are performed with *Re*, α, β, and γ being kept identical in all the cases. Case 1 is set as a benchmark where the vertical duct width (W_{duct}) is 10 mm, horizontal duct height (H_{duct}) 4 mm ($\alpha = 0.4$), disc axial height (H_{disc}) 12 mm ($\beta = 1.2$), disc radial width (W_{disc}) 90 mm ($\gamma = 9$), the average pass inlet velocity 0.3 m/s, oil density 876 kg/m^3 and dynamic viscosity 0.01506 $Pa \cdot s$, being the values at 293.15 K (20 $^{\circ}C$) based on (6) and (7), respectively. Therefore, Re at the pass inlet is calculated as equal to 349. Case 2 is the same as case 1, except that pass inlet velocity is changed to 0.5 m/s, and μ is changed accordingly to keep Re remaining constant at 349. Similarly, in case 3 the pass inlet velocity is changed to 0.4 m/s, whereas ρ is changed to keep Re identical. In case 4, W_{duct} is changed to 8 mm and the other parameters are changed accordingly to maintain the constant values of *Re*, α, β and γ. Case 5 is the same as case 4 except that W_{duct} is changed to 12 mm.

2) Comparison of Results

The results of the C_{pd} of each case for 1 pass, 2, and 3 passes are shown in Table II. The differences in C_{pd}'s among the five cases for the same number of passes are negligible, as shown by each row. In addition, C_{pd} rise approximately linearly with the number of passes, as shown by each column.

Average oil velocity of each horizontal duct was extracted at the same radial position. The volumetric oil flow proportion in one duct was then calculated by dividing its average velocity by the sum of all the average velocities in that pass.

The results of P_{fi} in the second and third passes of each case are compared in Fig. 2. As can be seen, flow distributions for the same pass are similar to one another in all cases with negligible differences. In addition, there are only slight differences in flow distributions between pass 2 and pass 3, for which the flow directions are opposite.

The consistency of these test results with the forgoing dimensional analyses indicates that the analyses in section II are reliable. It is worth noticing that in the test cases R_{inn} and r are fixed, whereas W_{duct} for case 1 (10 mm), case 4 (8 mm) and case 5 (12 mm) are different. Therefore, R_{inn}/W_{duct} and r/W_{duct} are different with the ratio of their maximum value to the minimum value being 1.5. However, the results of C_{pd} and P_{fi} in these cases are so close that we conclude that these two dimensionless parameters are negligible in the investigated range when compared with *Re*, α, β, and γ.

From these test results, we conclude that it is reasonable to confine the study to investigate the influence of *Re*, α, β, and γ on C_{pd} for 3 passes and P_{fi} in the third pass. The number of discs per pass is fixed to be 6. The investigated winding geometry is shown schematically in Fig. 1(b). The values of the investigated parameters, apart from *Re*, α, β, and γ, are the same as those specified in the test cases and shown in Fig. 1(b) and Fig. 1(c).

TABLE II
PRESSURE DROP COEFFICIENTS OF THE FIVE TEST CASES

Pass No.	Case 1	Case 2	Case 3	Case 4	Case 5
Pass 3	3.8218	3.8259	3.8226	3.8693	3.7712
Pass 2, 3	8.0770	8.0852	8.0786	8.0947	8.0454
Pass 1, 2, 3	11.643	11.656	11.646	11.712	11.557

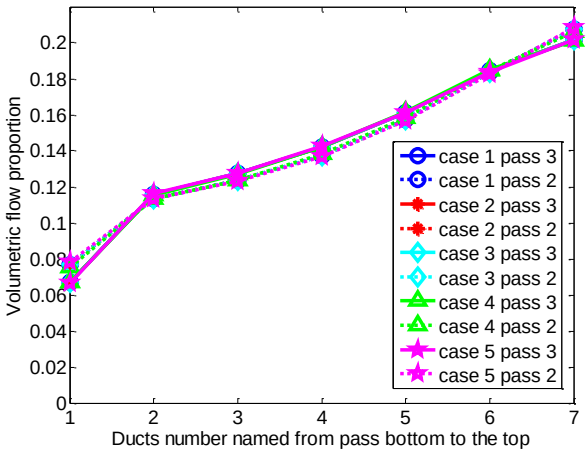

Fig. 2. Flow distribution in pass 2 and pass 3 of the five test cases.

C. *Ranges of Parameters of Interest*

The ranges of geometric parameters of interest taken from [20] are shown in Table III. For the OD cooling mode, Re at the pass inlet is set to range from 50 to 1200, as shown in table IV. The ranges of the dimensionless geometric parameters (α, β, γ) are determined based on the data range in Table III, and are selected to keep the resultant winding geometry practical.

D. *CFD Simulation Strategies*

The parametric sweep of Re is relatively easy as when the winding geometry is fixed, mesh only needs to be done once. The required Re can be accommodated by adjusting fluid properties. This is permissible, as is indicated by the test cases. However, to accommodate all of the 80 combinations of α, β, and γ, which represent 80 winding geometries, each geometry would need a separate CFD model and meshing process.

It is chosen to relate the vertical duct width to β as illustrated in Table IV, where the vertical duct width in mm is the denominator of each β value. For example, when $\beta = 10/10$, the vertical duct width is set to be 10 mm, and the actual winding geometries can be determined by combining all the different α's and γ's, as demonstrated in Table V.

TABLE III
RANGES OF SELECTED GEOMETRIC PARAMETERS [20]

W_{duct} (mm)	H_{duct} (mm)	H_{disc} (mm)	W_{disc} (mm)
6-12	3-6	7-20	40-170

TABLE IV
RANGES OF THE SWEPT DIMENSIONLESS PARAMETERS

Re	50, 100, 200, 400, 600, 800, 1000, 1200
α	0.25, 0.3, 0.4, 0.5, 0.6
β	8/12, 10/10, 16/8, 18/6
γ	6, 9, 12, 15

TABLE V
ACTUAL WINDING DIMENSIONS FOR $\beta = 10/10$ ($W_{duct}, H_{duct}, H_{disc}, W_{disc}$)

(10,2.5,10,60)	(10,2.5,10,90)	(10,2.5,10,120)	(10,2.5,10,150)
(10,3.0,10,60)	(10,3.0,10,90)	(10,3.0,10,120)	(10,3.0,10,150)
(10,4.0,10,60)	(10,4.0,10,90)	(10,4.0,10,120)	(10,4.0,10,150)
(10,5.0,10,60)	(10,5.0,10,90)	(10,5.0,10,120)	(10,5.0,10,150)
(10,6.0,10,60)	(10,6.0,10,90)	(10,6.0,10,120)	(10,6.0,10,150)

All the geometric dimensions are in mm.
In this table, α varies with row number ranging from 0.25 to 0.6; γ varies with column number ranging from 6 to 15.

IV. Correlation Equations

In total, 640 CFD simulations are conducted for the parametric sweeps, from which C_{pd} for three passes and P_{fi} of the third pass are computed based on the simulation results. C_{pd} and P_{fi} are then correlated with *Re*, α, β, and γ.

A. *Correlation equations for pressure drop coefficient*

The results of C_{pd} against Re can be plotted on a log-log scale. The relationship for several exemplary geometries are illustrated in Fig. 3. The other geometries lead to similar varying trend. The C_{pd}'s for a particular geometry fall on a curve that is straight at the beginning and then levels off at the end, indicating a power law as well as an exponentially decreasing dependence of the C_{pd} on the increasing *Re*. This varying trend is similar to that of the drag coefficient of a smooth sphere immersed in a uniform stream [18].

The fitting method of correlating C_{pd} to *Re*, α, β, and γ closely follows the strategy adopted in [10]. The functional forms are

$$\begin{cases} C_{pd} = a_1 \dfrac{1000}{\mathrm{Re}} e^{a_2 \mathrm{Re}/1000} \\ a_i = b_{i1}(4\alpha)^{b_{i2}} e^{4\alpha b_{i3}}; \quad i = \{1, 2\} \\ b_{ij} = c_{ij1}\beta^{c_{ij2}} e^{c_{ij3}\beta}; \quad j = \{1, 2, 3\} \\ c_{ijk} = d_{ijk1}\gamma^3 + d_{ijk2}\gamma^2 + d_{ijk3}\gamma + d_{ijk4}; \; k = \{1, 2, 3\} \end{cases} \tag{8}$$

where a_i, b_{ij}, c_{ijk} are dummy parameters, and 72 parameter $d's$ are generated, shown in Appendix 1.

In each fitting layer, least-squares curve fittings are adopted using MATLAB curve fitting tool *lsqcurvefit*. The final fitting results are $R^2 = 0.99994$, the maximum absolute error 1.4998, and the maximum relative error 17.115 %.

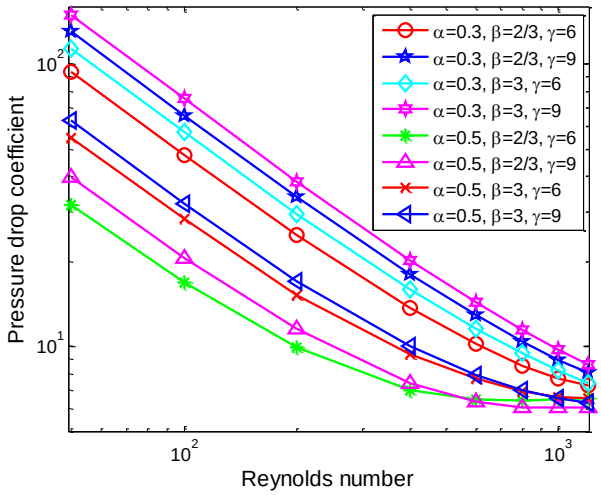

Fig. 3. Varying trends of pressure drop coefficients against the Reynolds numbers for several exemplary geometries.

B. Correlation equations for flow distribution

The same fitting strategy is adopted to correlate P_{fi} in the third pass to *Re*, α, β, and γ. The consistency of the correlation equations is tested subsequently.

1) Correlation equations of the flow proportions

The functional forms of the correlations are:

$$\begin{cases} P_{fi} = \dfrac{a_{i1}}{\mathrm{Re}^{1/3}} + a_{i2} \ln \mathrm{Re} + a_{i3} \mathrm{Re}^{1/3} + a_{i4}; i = \{1, 2, 3, 4, 5, 6, 7\} \\ a_{ij} = b_{ij1}\alpha^3 + \mathrm{b}_{ij2}\alpha^2 + \mathrm{b}_{ij3}\alpha + \mathrm{b}_{ij4}; \quad j = \{1, 2, 3, 4\} \\ b_{ijk} = c_{ijk1}\beta^3 + \mathrm{c}_{ijk2}\beta^2 + \mathrm{c}_{ijk3}\beta + \mathrm{c}_{ijk4}; \quad k = \{1, 2, 3, 4\} \\ c_{ijkm} = d_{ijkm1}\gamma^3 + d_{ijkm2}\gamma^2 + d_{ijkm3}\gamma + d_{ijkm4}; \; m = \{1, 2, 3, 4\} \end{cases} \tag{9}$$

where a_{ij}, b_{ijk}, c_{ijkm} are dummy parameters, and 256 parameter $d's$ are generated for each P_{fi}, shown in Appendix 1.

Similarly, least-squares fittings are adopted for each fitting layer. The fitting results for each duct of the third pass are shown in Table VI. The reason why maximum relative errors are huge for duct 1-4 compared with those for duct 5-7 is that reverse flow or stagnant flow, which results in extremely small flow proportion values, occurs in the bottom ducts under certain conditions in the investigated parameter ranges. Because the maximum errors for all the ducts are negligible, the huge relative errors have no significant impact on the accuracy of the fitting.

2) Consistency Test of correlation equations

Flow proportion in each duct is correlated independently. The consistency of these correlation equations means that the sum of all the horizontal duct flow proportions in the third pass should be approximately 1, i.e.

$$\sum_{i=1}^{7} P_{fi} \approx 1 \tag{10}$$

This consistency requirement should be obeyed by the 640 simulated data points as well as by the points in their vicinity. The ranges of the parameters for the consistency test are shown in Table VII. The consistency has been tested outside the range for which the formulae have been set up. In total, 43,200 cases have been tested based on the correlation equations. The minimum sum of all duct flow proportions in the third pass is 0.99983, and the maximum is 1.0001, indicating an excellent consistency of the correlation equation sets.

TABLE VI
FITTING RESULTS FOR EACH DUCT IN THIRD PASS

Duct number	R^2	Maximum absolute error	Maximum relative error (%)
1	0.99852	0.0081035	263.16
2	0.99112	0.020949	1497.4
3	0.98843	0.024869	354.62
4	0.97816	0.021017	1223.5
5	0.99780	0.0052281	3.0054
6	0.99952	0.0073791	2.9525
7	0.99946	0.010038	2.9733

TABLE VII
RANGES OF TESTED PARAMETERS

Parameter	Minimum	Maximum	Interval	No. of values
Re	50	1600	50	32
α	0.1	0.8	0.05	15
β	0.6	3.0	0.3	9
γ	6	15	1	10

V. Verifications and Predictions

The aim of performing dimensional analyses, conducting parametric sweeps, and correlating the results of C_{pd} and P_{fi} to the dimensionless parameters is to use the correlation equations to predict pressure drops and flow distributions in various OD cooling conditions. To validate the correlating strategies adopted in section IV, comparing the results from the correlation equations and the CFD simulations for new cases must be conducted. Because the correlation equations are derived from isothermal flow conditions, its suitability to be applied for prediction under non-isothermal flow conditions is also demonstrated in this section.

A. Predictions of isothermal flow cases

The new winding geometry for the isothermal flow prediction cases is the same as those in the parametric

sweeps, except that $W_{duct}=7mm$, $H_{duct}=3mm$ ($\alpha=3/7$), $H_{disc}=12mm$ ($\beta=12/7$), and $W_{disc}=90mm$ ($\gamma=90/7$). The oil temperature is set to be 40 ^oC. The first pass inlet velocity is set to range from 0.1 m/s to 0.5 m/s with an interval of 0.1 m/s, resulting in corresponding Reynolds number of 170.14, 340.28, 510.42, 680.56, and 850.70.

The correlation equations from section IV are used directly to obtain C_{pd} for three passes and P_{fi} in the third pass. These pressure drops and flow distributions are also obtained from new CFD simulations for comparison purpose.

1) Comparisons of pressure drops for isothermal flows

The pressure drops obtained from the correlation equation set and the new CFD simulations are shown in Fig. 4. Compared with the CFD results, the maximum absolute and relative errors of the correlation equation set are approximately 17 Pa and 4.5 %, respectively.

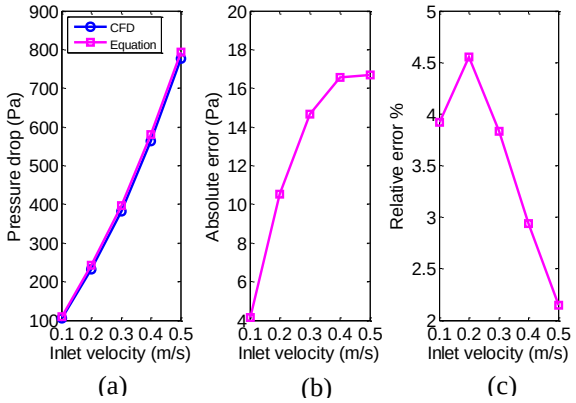

Fig. 4. Pressure drop under isothermal flow conditions. (a) Comparison of pressure drops from the correlation equation set and the CFD simulations. (b) Absolute errors. (c) Relative errors.

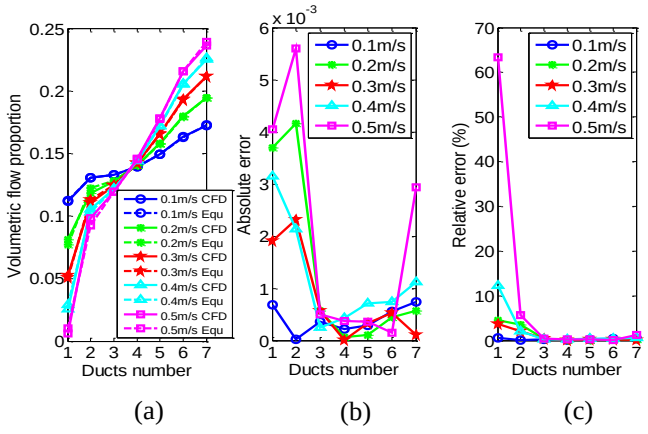

Fig. 5. Flow distribution under isothermal flow conditions for different pass inlet velocities with horizontal ducts numbered from the pass bottom to the top. (a) Comparison of flow distributions obtained from correlation equations and CFD simulations. (b) Absolute errors. (c) Relative errors.

2) Comparisons of flow distribution for isothermal flows

Flow distributions obtained from the correlation equations and the new CFD simulations are shown in Fig. 5. Results from these two methods are close to each other with the maximum absolute error being smaller than 0.6 % of the total volumetric flow rate. The large relative errors for duct 1 at the pass inlet velocities of 0.5 m/s and 0.4 m/s are because of the small flow proportions in these two cases. The relative errors for the other cases are smaller than 5 %.

B. Predictions of non-isothermal flow cases

The winding geometry and flow conditions for non-isothermal flow cases are the same as those for the isothermal flow cases. Since the hot-spot temperature is not the purpose of the tests, a uniform loss distribution is imposed to all winding discs. An average heat flux of 1248 W/m^2 is prescribed to the copper surface of each strand, as shown in Fig. 1(c), which corresponds to an average heat flux of 3505.8 W/m^2 on the surface of each disc. The oil inlet temperature of the first pass is set to be 40 ^oC. Conjugate Heat Transfer (CHT) simulations are performed which couple the fluid flow and heat transfer processes completely without adopting the Boussinesq approximation to obtain the pressure drops and flow distributions. These CHT results are set as benchmarks to be compared with prediction results from the correlation equations.

For non-isothermal flow, oil bulk temperature at the inlet of the third pass is different from that of the first pass and therefore needs to be calculated to modify the Reynolds number. Energy conservation is adopted to calculate the oil bulk temperature at the inlet of the third pass:

$$T_{b3}=T_{b1}+\frac{Q}{\dot{m}\bar{c}_p} \tag{11}$$

Iterative procedure is needed so as to determine the mean specific heat at the mean temperature of T_{b1} and T_{b3}.

1) Comparisons of pressure drops for non-isothermal flows

The pressure drops over the three passes obtained from the correlation equation set with modified Reynolds numbers and those from the CHT simulations are shown in Fig. 6. The discrepancies in the pressure drops are quite similar to those in Fig. 5, indicating that the effects of non-isothermal flow have negligible influence on the pressure drop over the winding pass.

2) Comparisons of flow distribution for non-isothermal flows

The flow distributions obtained from the correlation equations with modified Reynolds numbers and the CHT simulations are shown in Fig. 7. Compared with Fig. 5, the absolute and relative errors are larger, especially in the top duct (duct 7) and for the case of the winding pass inlet velocity being 0.1 m/s which corresponds to an average horizontal duct velocity of 0.033 m/s. These discrepancies are due to the impact of hot-streak dynamics and buoyancy force, which are more influential in the case of a lower flow rate. However, for a higher flow rate it is less influential, as in the cases of pass inlet velocities larger than 0.1 m/s where the maximum absolute error of flow proportion in each duct is smaller than approximately 1 % of the total volumetric flow rate. The huge relative errors for duct 1 at pass inlet velocities being 0.5 m/s and 0.4 m/s are also because of the

small flow proportions in these two cases. The relative errors for the other cases are within 15 %.

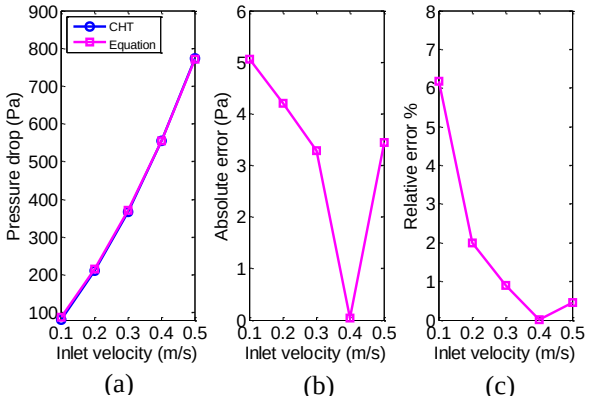

Fig. 6. Pressure drop under non-isothermal flow condition. (a) Comparison of pressure drop over three passes from CHT simulations and the correlation equation set. (b) Absolute errors. (c) Relative errors.

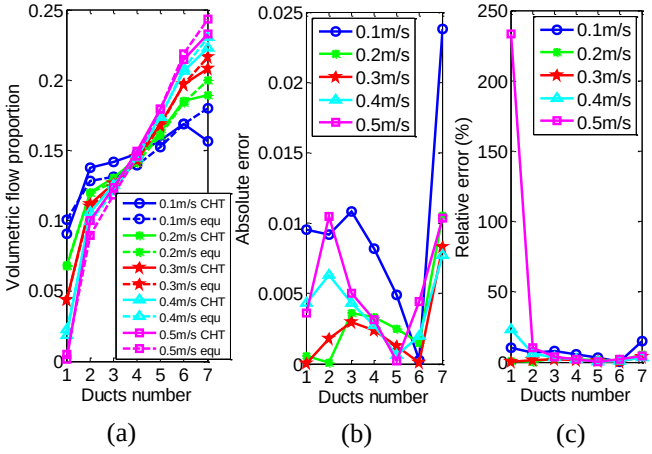

Fig. 7. Flow distribution under non-isothermal flow condition for different pass inlet velocities with ducts numbered from the pass bottom to the top. (a) Comparison of flow distributions from CHT simulations and correlation equations. (b) Absolute errors. (c) Relative errors.

VI. Practical Implications

By using these correlation equations, the pressure drop and flow distribution of a disc-type transformer winding in an OD cooling mode can be easily investigated.

A. Predicting the occurrence of reverse flow in a pass

Reverse flow can occur in the winding in an OD cooling mode, as indicated by the experimental work in [13] and the computational work in [21]. Once reverse flow occurs it can jeopardize the cooling performance because the reverse flow usually leads to a low flow rate, and some horizontal cooling ducts may even suffer from stagnant flows.

Since the reverse flow happens initially in the bottom duct of a pass, the correlation equation for flow proportion in duct 1 can be applied to investigate the criterion for the occurrence of reverse flow in the winding.

Previous study demonstrated that flow proportion in a duct is a function of Re at the pass inlet and the geometric parameters (α, β, and γ), more importantly, it is mainly controlled by Re and the ratio of horizontal duct height to vertical duct width (α). To show the variation of the flow proportion in duct 1 with different combinations of Re and α, β is fixed to be 1 and γ to be 10.

The variation of flow proportion in duct 1 with *Re* and α is shown in Fig. 8. There are two distinct regions in Fig. 8, where region 1 is a reversal-free region and region 2 would experience reverse flow.

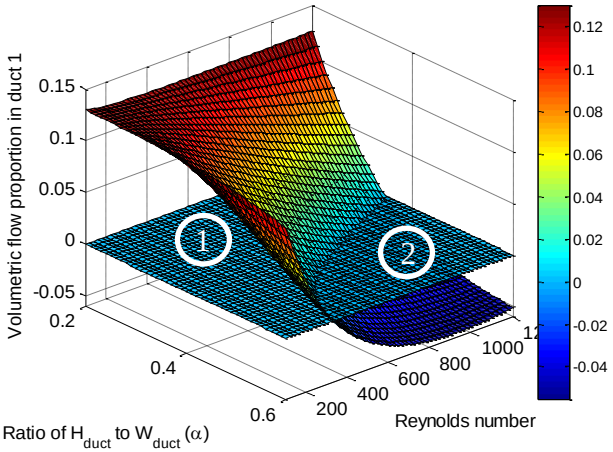

Fig. 8. Volumetric flow proportion in duct 1 for different combinations of Re and α. Two regions are identified with region 1 being reversal-free and region 2 experiencing reverse flow.

B. Improving the cooling performance

Flow distribution in the winding pass changes with the pass inlet flow rate, and a higher flow rate does not necessarily result in a better cooling performance. In fact, a too high flow rate can result in reverse flow in the pass bottom duct, as illustrated in Fig. 8.

In an OD cooling mode, flow proportion rises with duct number in a pass, numbered from the pass bottom to the top, as can be seen in Fig. 5 and Fig. 7. For a relative uniform loss distribution, the overall cooling performance is therefore determined by the velocity in the bottom horizontal duct, which is dictated by both the pass inlet flow rate and flow proportion in the bottom duct. Such an observation helps to systematically adjust and optimize the combination of design parameters including winding geometric parameters and pass inlet flow rate.

A demonstration case is given here, where H_{duct} is fixed at 4 mm, the oil temperature at 40 ^{o}C, and the other parameters being the same as those in section VI part A. The average oil velocity at the entrance of duct 1 is:

$$\bar{v}_1 = \frac{\bar{v}_{in} P_{f1}}{\alpha} \tag{12}$$

In order to obtain P_{fi}, Re is determined from:

$$\mathrm{Re} = \frac{\bar{v}_{in}\rho(2W_{duct})}{\mu} = \frac{\bar{v}_{in}\rho(2\,\mathrm{H}_{duct})}{\mu\alpha} \tag{13}$$

where ρ and μ are calculated from (6) and (7), respectively.

Finally, the variation of $\bar{v}_1$ with α and $\bar{v}_{in}$, as shown in Fig. 9, is obtained by applying the correlation equation for P_{fi}. As can be seen, the maximum value of average oil

velocity in duct 1 ($\bar{v}_1$) is not achieved at the maximum average pass inlet velocity ($\bar{v}_{in}$). For example, when the ratio of horizontal duct height to vertical duct width is 0.25 ($\alpha = 0.25$), the maximum $\bar{v}_1$ is achieved at $\bar{v}_{in} \approx 0.3 m/s$. In addition, when α increases, $\bar{v}_{in}$ needs to decrease to achieve the corresponding maximum $\bar{v}_1$. For example, when $\alpha = 0.6$, the maximum $\bar{v}_1$ is achieved at $\bar{v}_{in} = 0.1 m/s$ which is the lowest pass inlet velocity in the study.

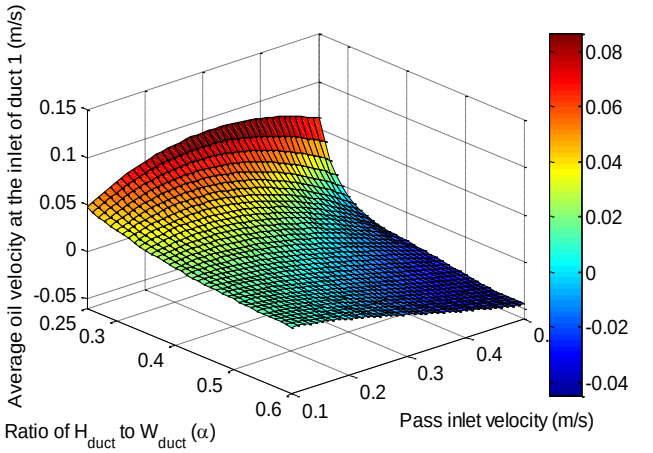

Fig. 9. Variation of average velocity in bottom horizontal duct with α and pass inlet velocity.

VII. Discussion

Coolant flow distribution in a disc-type transformer winding has a direct impact on the temperature distribution in the winding. Pressure drop over the winding is also an important parameter for selecting pumps and determining the split of coolant flow among different windings connected hydraulically in parallel. Flow distribution in and pressure drop over the winding can be modelled by using network models or CFD simulations. However, even with the modelling solutions, one could still be baffled as to how flow distribution and pressure drop are controlled by the variables of winding geometries, fluid properties and coolant flow rate because of the large number of the possible combinations of all these variables.

Dimensional analysis, which has been widely adopted in fluid mechanics, provides a method of simplifying the relationship among the variables without losing accuracy. After performing dimensional analysis, we may find that variables that seem to be unrelated are grouped into a dimensionless parameter and different combinations of these variables can possibly lead to identical effect in a dimensionless sense. In addition, the decrease of the number of variables by transforming them into dimensionless groups makes parametric sweeps much more manageable. CFD simulations have the advantage of accuracy over network models, though they require much higher computational effort. With the help of CFD simulations, parametric sweeps of the identified dimensionless parameters are performed. The dimensionless CFD results are then correlated with the identified dimensionless parameters to form predictive correlation equations.

Results in section V demonstrate that the correlation equations are capable of predicting pressure drop and flow distribution for both isothermal flow and non-isothermal flow conditions in an OD cooling mode with acceptable accuracy. This is because firstly and fundamentally the pressure drop over and flow distribution in the winding do not change their varying trends drastically when the dimensionless parameters are altered, and secondly the correlation equations can preserve the accuracy of the CFD simulations as long as the parametric sweeps have appropriate intervals within the selected ranges of the controlling dimensionless parameters and the curve fitting procedures are sufficiently accurate.

By applying the correlation equations, we are able to identify the criteria for the occurrence of reverse flow and the conditions of achieving the maximum value of the lowest duct oil velocity in the pass.

It is worth emphasizing that the method presented in this paper can be considered to be not constrained to the number of passes of the winding. The number of passes in the winding does not affect flow distribution within a pass for isothermal flow conditions. Even opposite flow directions would just lead to negligible effect on flow distribution, as shown in Fig. 2. For non-isothermal flow conditions, which are the practical situations, the effect of buoyancy force, hot-streak dynamics and the increase of oil temperature with the elevation along the winding would affect the flow distribution. The effect of temperature increase can be accounted for by modifying the Reynolds number at the pass inlet, as shown in (11). By modifying the Reynolds number reasonable flow distribution approximation for the non-isothermal flow condition can be obtained, as shown in Fig. 7. Pressure drop over the winding can be reasonably considered as proportional to the number of passes, as shown in Table II. Isothermal flow and non-isothermal flow have almost the same pressure drop characteristics, as shown by Fig. 4 and Fig. 6. Therefore, a 3-pass winding would be representative for the simulations with pass 2 and pass 3 showing the effect of opposite flow directions and pass 1 acting as a buffer zone to eliminate the effect of prescribing velocity profile at the inlet of pass 1.

In addition, these correlation equations for pressure drop and flow distribution may be used to replace the hydraulic part of network model to improve the performance of network modelling. In order to cover all the possible disc-type winding geometries, additional parametric sweeps and correlations need to be performed for the cases of:

1. Different numbers of discs per pass.
2. Different inner and outer vertical duct width. This would generate another dimensionless parameter of the ratio of outer vertical duct width to inner vertical duct width.
3. Non-uniform horizontal duct heights which follow a certain pattern or rule, for example, the case of alternately varied horizontal duct height.
4. Different schemes of positioning washers and the case of zigzag winding created with seals next to the discs, etc.

Eventually, a library that can accommodate all the cases could be established.

Furthermore, this method is performed on a pass-by-pass basis. Therefore, the results of pressure drop and flow distribution would be applicable to windings consisting of passes with different numbers of discs, provided that the

generalization of the method for new cases presented above has been accomplished.

VIII. Conclusion

Dimensional analyses were conducted to identify the independent dimensionless variables that affect the pressure drop over disc-type transformer windings and the oil flow distribution in the windings in an OD cooling mode.

Parametric sweeps for a 3-pass winding with 6 discs per pass were performed, using CFD simulations under isothermal flow conditions. The pressure drop coefficient (C_{pd}) for the three passes and flow proportion in duct i (P_{fi}) for the third pass were extracted from the simulations and correlated to the dimensionless parameters to form predictive correlation equations. The correlation equations were then verified over a range of different isothermal and non-isothermal flow cases.

The correlation equation for the flow proportion in the pass bottom duct was applied to identify the criteria for the occurrence of reverse flow, an important phenomenon in an OD cooling mode, resulting from a combination of pass inlet flow rate and winding geometry, and resulting in lower oil flow rate and therefore higher hot-spot temperature than expected. In addition, the method provides an insight into the controlling parameters for determining the minimum oil velocity in horizontal cooling ducts. These two applications indicate that higher pass inlet flow rate does not necessarily mean better cooling performance and an appropriate combination of winding geometry and pass inlet flow rate can optimize the cooling performance.

Acknowledgment

The authors would like to express their gratitude to M&I Materials, National Grid, Scottish Power, Shell, TJ|H2b Analytical Services, UK Power Networks and Weidmann Electrical Technology for their financial and technical contributions to the Transformer Research Consortium at The University of Manchester.

References

[1] M. Heathcote, *J & P transformer book (page 158),* Thirteenth ed.: Newnes, 2007.

[2] Temperature rise for liquid-immersed transformers, IEC standard 60076-2, 2011.

[3] IEEE Guide for Loading Mineral-Oil-Immersed Transformers and Step-Voltage Regulators, IEEE standard C57.91, 2011.

[4] J. Zhang, and X. Li, "Oil cooling for disk-type transformer windings-Part II: Parametric studies of design parameters," *IEEE Trans. Power Del.*, vol. 21, no. 3, pp. 1326-1332, 2006.

[5] A. J. Oliver, "Estimation of transformer winding temperatures and coolant flows using a general network method," *Proc. Inst. Elect. Eng.*, vol. 127, pp. 395-405, 1980.

[6] Z. R. Radakovic, and M. S. Sorgic, "Basics of detailed thermal-hydraulic model for thermal design of oil power transformers," *IEEE Trans. Power Del.*, vol. 25, no. 2, pp. 790-802, 2010.

[7] J. Zhang, and X. Li, "Oil cooling for disk-type transformer windings-part 1: theory and model development," *IEEE Trans. Power Del.*, vol. 21, no. 3, pp. 1318-1325, 2006.

[8] W. Wu, Z.D. Wang, A. Revell, P. Jarman, "Computational fluid dynamics calibration for network modelling of transformer cooling oil flows-part I heat transfer in oil ducts," *IET Electric Power Applications,* vol. 6, no. 1, pp. 19-27, 2012.

[9] W. Wu, Z.D. Wang, A. Revell, P. Jarman, "Computational fluid dynamics calibration for network modelling of transformer cooling flows–Part II: pressure loss at junction nodes," *IET electric power applications,* vol. 6, no. 1, pp. 28-34, 2012.

[10] J. Coddé, W. Van der Veken, and M. Baelmans, "Assessment of a hydraulic network model for zig–zag cooled power transformer windings," *Appl. Therm. Eng.*, vol. 80, pp. 220-228, 2015.

[11] A. Weinläder, W. Wu, S. Tenbohlen, Z.D. Wang, "Prediction of the oil flow distribution in oil-immersed transformer windings by network modelling and computational fluid dynamics," IET electric power applications, vol. 6, no. 2, pp. 82-90, 2012.

[12] J. Zhang, X. Li, and M. Vance, "Experiments and modeling of heat transfer in oil transformer winding with zigzag cooling ducts," *Appl. Therm. Eng.*, vol. 28, no. 1, pp. 36-48, 2008.

[13] M. Nakadate, K. Toda, K. Sato, D. Biswas, C. Nakagawa, T. Yanari, "Gas cooling performance in disc winding of large-capacity gas-insulated transformer," *IEEE Trans. Power Del.*, vol. 11, no. 2, pp. 903-908, 1996.

[14] E. Rahimpour, M. Barati, M. Schafer, "An investigation of parameters affecting the temperature rise in windings with zigzag cooling flow path", *Appl. Therm. Eng.*, vol. 27, no. 11-12, pp. 1923-1930, 2007.

[15] F. Torriano, M. Chaaban, and P. Picher, "Numerical study of parameters affecting the temperature distribution in a disc-type transformer winding," *Appl. Therm. Eng.*, vol. 30, no. 14, pp. 2034-2044, 2010.

[16] A. Skillen, A. Revell, H. Iacovides, W. Wu, "Numerical prediction of local hot-spot phenomena in transformer windings," *Applied Thermal Engineering*, vol. 36, pp. 96-105, 2012.

[17] Ain A. Sonin. (2001) *Dimensional Analysis* (2nd ed. *page 34-49,) [Onl*ine] :http://web.mit.edu/2.25/www/pdf/DA_unified.pdf

[18] R. W. Fox, A. T. McDonald, and P. J. Pritchard, *Fluid Mechanics*, (page 290-301 and 296), New York: John Wiley & Sons, 2012.

[19] F. Torriano, P. Picher, M. Chaaban, "Numerical investigation of 3D flow and thermal effects in a disc-type transformer winding", *Appl. Therm. Eng.*, vol. 40, pp. 121-131, 2012.

[20] J. Zhang, X. Li, "Coolant flow distribution and pressure loss in ONAN transformer windings. Part II: Optimization of design parameters," *IEEE Trans. Power Del.*, vol. 19, pp. 194-199, 2004.

[21] A. Weinläder, and S. Tenbohlen, "Thermal-hydraulic investigation of transformer windings by CFD-modelling and measurements." Paper D-22, Proc.16th ISH, South Africa, 2009.

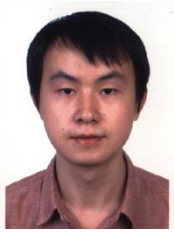

Xiang Zhang received the B.Eng. degree in Electrical and Electronic Engineering (2012) from Xi'an Jiaotong University, Xi'an, China. He is pursuing the PhD degree at the Electrical Energy and Power Systems Group of the School of Electrical and Electronic Engineering at The University of Manchester, Manchester, UK. His research programme is on transformer thermal modelling.

Zhongdong Wang received the BSc and the MSc degrees in high voltage engineering from Tsinghua University in 1991 and 1993 and the PhD degree in electrical engineering from UMIST in 1999. Currently she is a Professor of High Voltage Engineering of the School of Electrical and Electronic Engineering at The University of Manchester. Her research interests focus on power transformers covering all aspects of modelling and simulation, materials & systems, and asset management policies.

Qiang Liu (S'08-M'12) obtained the B.Eng. degree in electrical engineering (2005) and the M.Eng. degree in high voltage and electrical insulation (2008) from Xi'an Jiaotong University in China, and the Ph.D. degree in electrical power engineering (2011) from The University of Manchester in the UK. Currently he is a Senior Lecturer of the School of Electrical and Electronic Engineering at The University of Manchester. His

research interests are on pre-breakdown and breakdown phenomena in liquids, ester transformer liquids, streaming electrification, ageing of insulating materials, transformer asset management and high voltage testing.

3.3 Paper 2

Experimental Verification of Dimensional Analysis Results on Flow Distribution and Pressure Drop for Disc Type Windings in OD Cooling Modes

Xiang Zhang, Muhammad Daghrah, Zhongdong Wang, Qiang Liu, Paul Jarman and Massimo Negro

2017

IEEE Transactions on Power Delivery

Accepted

Blank page

Experimental Verification of Dimensional Analysis Results on Flow Distribution and Pressure Drop for Disc Type Windings in OD Cooling Modes

Xiang Zhang, Muhammad Daghrah, Zhongdong Wang, *Member*, IEEE, Qiang Liu, *Member,* IEEE, Paul Jarman, Massimo Negro

***Abstract*—Oil flow distribution in the winding has a direct impact on the cooling performance. In addition, static pressure drop over the winding determines oil split among windings connected hydraulically in parallel. In this paper, experimental verifications are provided to support computational fluid dynamics (CFD) simulations for disc-type windings in oil forced and directed (OD) cooling modes. Oil flow distribution in and pressure drop over disc-type winding models are measured using a particle image velocimetry (PIV) system and a differential pressure instrument, respectively. Dimensional analysis is adopted to analyze the relationship between flow distribution, or pressure drop, and the controlling parameters. CFD parametric sweeps of the dimensionless parameters obtained from the dimensional analysis are conducted and the CFD results are then correlated with the dimensionless parameters. The comparisons between measured results and the corresponding results obtained from the correlations demonstrate constant consistency, proving the validity of both the method of dimensional analysis and the correlations. Finally, comparisons of experimental results from isothermal and nonisothermal conditions in OD cooling modes are executed, which show that the isothermal conclusions can be extended to nonisothermal cases because the effects of buoyancy force and hot-streak dynamics are proved to be negligible.**

***Index Terms*—CFD, dimensional analysis, disc-type winding, flow distribution, OD, PIV, pressure drop, transformer**

NOMENCLATURE

A	Cross sectional area of the vertical duct (m^2)
C_{pd}	Pressure drop coefficient over the winding model
D_h	Hydraulic diameter (m) ($4A/P$)
H_{plate}	Plate vertical height (m)
H_{duct}	Horizontal duct height (m)
Gr	*The* Grashof number ($g\beta_T(T_{out}-T_{in})D_h^3/\nu^2$)
lpm	liters per minute
n_1	Number of passes in the winding model
n_2	Number of discs per pass
P	Perimeter of the vertical duct (m)
P_{fi}	Volumetric flow proportion in horizontal duct i
ΔP	Static pressure drop (Pa)
Re	The Reynolds number ($\rho\cdot\bar{v}_{in}\cdot D_h/\mu$)
T	Temperature in Kelvin (K)
T_{in}	Temperature at pass 3 inlet in Kelvin (K)
T_{out}	Temperature at pass 3 outlet in Kelvin (K)
$\bar{v}_i$	Average oil velocity in duct i (m/s)
$\bar{v}_{in}$	Average pass-inlet oil velocity (m/s)
W_{plate}	Plate horizontal width (m)
W_{duct}	Vertical duct width (m)
α	Dimensionless horizontal duct height (H_{duct}/W_{duct})
β	Dimensionless plate axial height (H_{plate}/W_{duct})
β_T	Volumetric thermal expansion coefficient
γ	Dimensionless plate radial width (W_{plate}/W_{duct})
ρ	Oil density (kg/m^3)
μ	Oil dynamic viscosity ($Pa\cdot s$)

I. Introduction

THE oil flow distribution in a disc-type transformer winding has a direct impact on the cooling performance which, in conjunction with power loss distribution, determines the position and magnitude of the hot-spot temperature in the winding. In addition, the static pressure drop over a disc-type transformer winding determines the selection of pump for oil forced and directed (OD) cooling modes and more importantly oil split among windings connected hydraulically in parallel, for example LV winding and HV winding in the same phase.

Different models have been developed to predict oil flow distribution in and pressure drop over disc type transformer windings. These models can be grouped into two categories: network models [1-4] and computational fluid dynamics (CFD) models [5-7]. These two types of model share the same physical principles of conservation of mass, momentum and energy. Endeavors of combining the merits of both methods have been made by using CFD results to calibrate the correlation equations used in network models [8-10]. CFD modelling is usually conducted in axisymmetric 2D geometries to reduce computational requirements. Compared to 3D CFD simulations, 2D simulations cannot capture detailed fluid flow and heat transfer phenomena in the vicinity of the spacers. However, for an ON cooling mode, comparisons of fluid flow and temperature distributions between 2D axisymmetric and 3D CFD models show that 2D results are representative of the 3D results as long as the governing dimensionless parameters (Gr/Re^2) are matched [7]. In addition, key 3D results, e.g. top oil temperature and hot-spot temperature, can be derived from 2D CFD results based on the improvement strategies in [7].

Only a few experimental studies were reported to record flow rates within horizontal cooling ducts to verify simulation models. Hot wire anemometry was used in [11] to record flow distribution within an isothermal winding model. It was observed that the lowest flow rate occurred in the central ducts of the tested pass of the winding model and more uniform flow distribution was achieved with wider inlet vertical cooling duct. A CCD camera was used in [12] to track the movements of tracer particles within a zig-zag disc type winding model under isothermal conditions. Pressure drops were measured along winding vertical ducts. It was observed in [12] that flow distribution is more uniform for lower number of discs per pass at the cost of higher pressure losses over the winding model. Reverse flow

was observed in the first horizontal cooling duct under higher number of discs per pass. It was also reported in [12] that wider vertical ducts would produce more uniform flow distribution in and lower pressure drop over the winding. Laser doppler velocimetry was used to measure flow velocities within vertical cooling ducts in [13] to verify a proposed numerical model on a non-directed winding under nonisothermal conditions. Pressure drop over one pass of a winding model was measured in [14] to verify a 2D CFD model and a network model with calibrated correlation equations from [9].

Systematic simulation studies of oil flow distribution in and pressure drop over disc-type transformer windings were conducted by adopting dimensional analyses in [15]. From dimensional analyses, oil flow distribution and pressure drop were transformed to dimensionless parameters of flow proportion in each horizontal cooling duct and pressure drop coefficient over the winding, respectively. The controlling parameters were transformed to the Reynolds number at the winding pass inlet and dimensionless geometric parameters (α, β, γ in [15]). The quantitative relationships between flow proportion, or pressure drop coefficient, and the dimensionless controlling parameters were obtained by conducting CFD parametric sweeps and correlating the CFD results with the controlling dimensionless parameters.

In this paper, experiments are designed to verify the method of dimensional analysis and the correlations obtained from CFD parametric sweeps. The experimental set-up and the implementation of the measurements of flow distribution and pressure drop are illustrated in section II. Theoretical analyses and numerical modeling of the flow distribution in and pressure drop over the winding model are presented in section III. In section IV, experimental verification of the modeling results are presented. Finally, the comparisons of isothermal and nonisothermal measurements are shown in section V, followed by discussion and conclusion in sections VI and VII, respectively.

II. Experimental set-up

Experimental setup is shown in Fig. 1. It consists of a winding model resembling a disc-type winding structure as shown in Fig. 2, a radiator to cool oil down, a pump to circulate oil and a flow meter to record flow rates. An external heating unit is used to heat up and control winding inlet oil temperature. The experimental setup is described as follows:

A. Winding Model

The rectangular winding model consists of 3 passes. Each pass is fitted with 10 disc segments. The disc segments are modeled as rectangular aluminum plates with geometric dimensions of 100 mm × 104 mm × 10 mm. Each plate sits on 3 mm grooves of the side walls of the winding model making the actual depth of horizontal cooling ducts 94 mm. The winding model walls are made of lexan* 9030 polycarbonate sheets. Washers are made of acrylic material with geometric dimensions of 100 mm × (104 + vertical duct width) mm × 10 mm. Table I provides a summary of the geometric dimensions of the winding models. Inner and outer vertical duct width are made equal and two vertical duct widths, 10 mm and 12 mm, are tested. The heights of horizontal ducts are uniform being 4 mm or 6 mm. Thermocouples are fitted at the inlet and outlet of the winding model to record winding inlet and outlet oil temperatures, respectively. Accuracy of the thermocouples used is $\pm 1\ ^{\circ}C$.

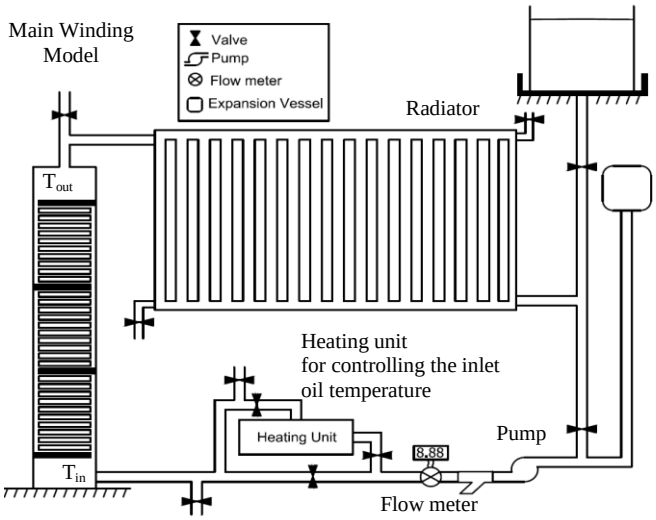

Fig. 1. Schematic diagram of the experimental setup.

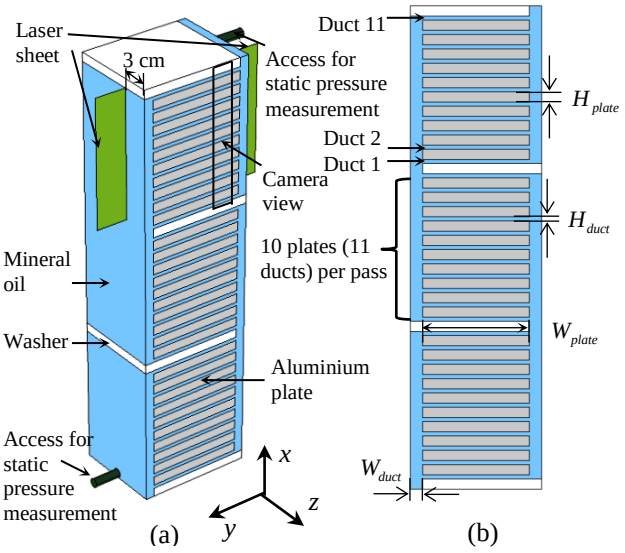

Fig. 2. Geometry of the winding model. (a) 3D geometry; (b) 2D geometry

TABLE I
WIDING MODEL GEOMETRIC PARAMETERS

Horizontal Duct depth	Horizontal duct height (H_{duct})	Vertical duct width (W_{duct})	Aluminum plates	
			Height (H_{plate})	Width (W_{plate})
94 mm	4 mm, 6 mm	10 mm, 12 mm	10 mm	104 mm

The oil flow in the winding model is directed into a zig-zag fashion using washers. Washers are placed at the entrance and exit of each pass. A washer blocks a vertical duct from one side and allows the oil to flow into or out of a pass from the opposite side. To guarantee complete oil blockage, silicone sealant is applied between a washer and the winding model wall at the location where the oil is

desired to be blocked. It is intended that all plates and washers are perfectly aligned. However, during winding model assembly minimal geometric deviations still occur, e.g. a plate is either slightly inward or outward. It was observed, after conducting the tests, that this slight geometric deviation gives a signature, or a footprint, to the flow distribution within the pass as will be highlighted later. More details of the winding model can be found in [16].

B. Pressure Measurement

Two pressure ports, as shown in Fig. 2, were used to record static pressure drop over the 3-pass winding model with a differential pressure instrument. The pressure instrument has an accuracy of ± 0.2% of the full scale of 10 kPa or equivalently the accuracy is ± 20 Pa and a repeatability of ± 10 Pa in this range. Each pressure measurement was taken 10 times. Since the pressure readings were stable, the average of the 10 measurements was used as a representative value.

C. Flow Measurement

Total oil flow rate is measured using a positive displacement flow meter, as it is less affected by viscosity variations, with accuracy of 0.5% of its reading. Within horizontal cooling ducts, a Particle Image Velocimetry (PIV) system is used to record oil flow rates. The PIV system consists of a laser source, light sheet optics and a camera. A synchronizer is used to synchronize the laser, the camera and the acquisition computer in order to obtain the velocity profile.

The accuracy of PIV measurements depends on the quality of raw images which is affected by both the density of seeding particles and their distribution within the duct. Silver coated hollow glass spheres with 9-14 micrometer diameter were used as seeding particles. In all PIV measurements, the laser sheet plane was aligned with the flow direction and perpendicular to the winding plate in each duct and was fixed only at one plane that is 3 cm from the winding model wall close to the camera as shown in Fig. 2. The camera field of view was focused on the 2 cm of the horizontal duct towards its exit as indicated in Fig. 2. All PIV measurements were taken in steady state and in a hydraulically developed region in horizontal ducts. Twenty raw images were taken for each measurement and the statistical average of these images was used to extract the final result. The reason for using 20 raw images instead of using more is that a sweep of the number of raw images processed —1, 5, 10, 20, 30, 40, 50—shows that the case using 20 raw images gives results that are as accurate as those obtained from cases of a larger number of images. Finally, the accuracy of PIV measurements was checked by comparing the total flow rate obtained from all the PIV measurements in pass 3 to that recorded by the flow meter. Discrepancies between the PIV results and the flow meter readings were within 7%.

Flow distribution in a pass is hardly affected by the number of passes in the winding [15]. Therefore, only the flow rates within the horizontal cooling ducts of the third pass were measured using the PIV system. Fig. 3 shows the results of experiments repeated 3 times in 3 different days, under the same operating conditions, to confirm the repeatability of the PIV measurements. The total flow rate, recorded by the flow meter, was 12.0 litres per minute (lpm) while the inlet oil temperature was maintained within the range of 46 $^{\circ}C$ to 48 $^{\circ}C$. It can be seen from Fig. 3 that the total flow rates derived from the PIV measurements are constantly slightly higher than that from the flow meter. This is partially because only one plane in the horizontal duct is measured and the end-wall effects are neglected.

D. Oil Properties

The tested oil is a mineral oil of which the variations of density and dynamic viscosity with temperature in Kelvin are shown in (1) and (2). These equations are from least-square curve fittings of the measured data provided by the oil manufacturer.

$$\rho = -0.65683 \times T + 1063.6 \tag{1}$$

$$\mu = 7.8630 \times 10^{-5} \times \exp\left(\frac{631.96}{T - 176.03}\right) \tag{2}$$

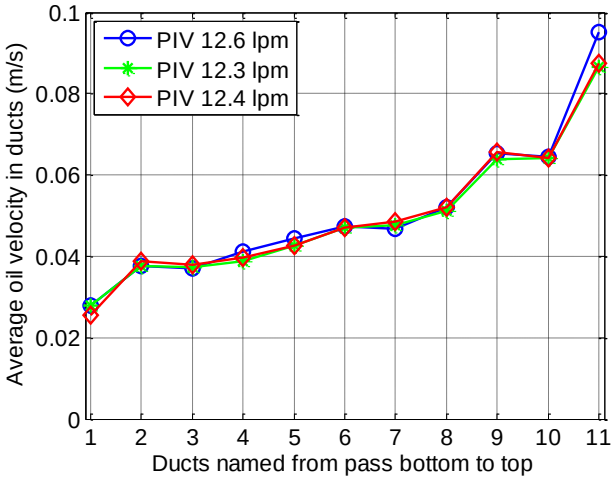

Fig. 3. Repeatability tests of the PIV system. In each test, total oil flow rate is controlled to be 12 lpm according to the reading of the flow meter and the sum of flow rate in each duct from PIV differs slightly from 12 lpm.

III. Analytical Analyses on Flow Distribution and Pressure Drop for the Winding model

The methodology of conducting dimensional analyses, performing CFD parametric sweeps and correlating the CFD results with the identified dimensionless parameters was detailed in our previous publication [15]. This paper follows the same methodology for the winding model tested.

A. Dimensional Analyses on Pressure Drop over and Flow Distribution in the Winding Model

In dimensional forms, the average oil velocity in a horizontal cooling duct *i* ($\bar{v}_i$) and the pressure drop over the 3-pass winding model (ΔP) can be expressed as functions shown in (3) and (4):

$$\bar{v}_i = f_i(n_2, \bar{v}_{in}, \rho, \mu, H_{duct}, H_{\text{plate}}, W_{plate}, W_{duct}) \tag{3}$$

$$\Delta P = g(n_1, n_2, \bar{v}_{in}, \rho, \mu, H_{duct}, H_{\text{plate}}, W_{plate}, W_{duct}) \tag{4}$$

These dimensional forms can be transformed to their dimensionless forms by choosing pass inlet velocity ($\bar{v}_{in}$), oil density (ρ), and vertical duct width (W_{duct}) as the

repeating parameters. The dimensionless forms are (5) and (6):

$$\frac{\bar{v}_i}{\bar{v}_{in}} \cdot \frac{H_{duct}}{W_{duct}} = P_{fi} = f_i'(n_2, \mathrm{Re}, \alpha, \beta, \gamma) \tag{5}$$

$$\frac{\Delta P}{\rho \bar{v}_{in}^2/2} = C_{pd} = g'(n_1, n_2, \mathrm{Re}, \alpha, \beta, \gamma) \tag{6}$$

B. Parametric Sweeps

In the winding model, the number of discs per pass and the number of passes are 10 and 3, respectively, as shown in Fig. 2. In such a case, flow proportion in a duct i (P_{fi}) and pressure drop coefficient over the 3-pass winding model (C_{pd}) are functions of four dimensionless parameters: *Re*, α, β and γ.

According to the practical ranges of the total oil flow rate and the geometric dimensions of disc-type transformer windings [15, 17], the four dimensionless parameters are set to be in the ranges shown in Table II. All the combinations of these discrete parameters were simulated by CFD simulations using COMSOL Multiphysics 5.2. In total, 720 CFD simulations were conducted involving 80 winding geometries which is the number of combinations of α, β and γ. Mesh refinement studies were conducted to guarantee mesh-independent results following the same procedures as presented in [15].

TABLE II
RANGES OF THE SWEPT DIMENSIONLESS PARAMETERS

Symbol	Discrete parameter value
Re	20, 50, 100, 200, 400, 600, 800, 1000, 1200
α	0.25, 0.3, 0.4, 0.5, 0.6
β	0.67, 1, 2, 3
γ	6, 10, 12, 15

Discrete values are used to cover the practical range of each parameter.

C. Correlations

The results of flow proportion in the third pass and pressure drop coefficient over the 3-pass winding model were extracted and correlated with the four dimensionless controlling parameters by a multi-layer least square curve fitting strategy.

1) Correlation of Flow Distribution

The volumetric flow proportion in duct i in the third pass (P_{fi}) were correlated with *Re*, α, β and γ by equation set (7):

$$\begin{cases} P_{fi} = \dfrac{a_{i1}}{\mathrm{Re}^{1/3}} + a_{i2}\ln \mathrm{Re} + a_{i3}\mathrm{Re}^{1/3} + a_{i4}; i = \{1, 2, \cdots, 11\} \\ a_{ij} = b_{ij1}\alpha^3 + \mathrm{b}_{ij2}\alpha^2 + \mathrm{b}_{ij3}\alpha + \mathrm{b}_{ij4}; \quad j = \{1, 2, 3, 4\} \\ b_{ijk} = c_{ijk1}\beta^3 + \mathrm{c}_{ijk2}\beta^2 + \mathrm{c}_{ijk3}\beta + \mathrm{c}_{ijk4}; \quad k = \{1, 2, 3, 4\} \\ c_{ijkm} = d_{ijkm1}\gamma^3 + d_{ijkm2}\gamma^2 + d_{ijkm3}\gamma + d_{ijkm4}; \; m = \{1, 2, 3, 4\} \end{cases} \tag{7}$$

where a_{ij}, b_{ijk}, c_{ijkm} are dummy correlation coefficients, which are determined from α, β, γ and the 256 coefficient $d's$ from the last equation in (7), shown in Appendix 2.

2) Correlation of Pressure Drop Coefficient

The pressure drop coefficient over the 3-pass winding model (C_{pd}) were correlated with *Re*, α, β and γ by equation set (8):

$$\begin{cases} C_{pd} = a_1 \dfrac{1000}{\mathrm{Re}} e^{a_2 \mathrm{Re}/1000} \\ a_i = b_{i1}(4\alpha)^{b_{i2}} e^{4\alpha b_{i3}}; \quad i = \{1, 2\} \\ b_{ij} = c_{ij1}\beta^{c_{ij2}} e^{c_{ij3}\beta}; \quad j = \{1, 2, 3\} \\ c_{ijk} = d_{ijk1}\gamma^3 + d_{ijk2}\gamma^2 + d_{ijk3}\gamma + d_{ijk4}; \; k = \{1, 2, 3\} \end{cases} \tag{8}$$

where a_i, b_{ij}, c_{ijk} are dummy correlation coefficients, which are determined from α, β, γ and the 72 coefficient $d's$ from the last equation in (8), shown in Appendix 2.

The aforementioned dimensional analyses offer ways to reduce the relationships between flow distribution, or pressure drop, and the controlling parameters to the simplest forms as expressed by (5) and (6). The CFD parametric sweeps and the subsequent correlations of the CFD results quantify the relationships as shown in (7) and (8).

IV. Experimental Verification of Dimensional Analyses and CFD Correlations

From the dimensional analyses presented in section III, oil flow proportion in a duct and pressure drop coefficient over the 3-pass winding model are functions of the Reynolds number at the winding inlet, α, β and γ. To validate the method of dimensional analysis and the correlations obtained, measurements of flow distribution in and pressure drop over the winding model were implemented and compared with the theoretical predictions from (7) and (8).

The experimental tests of the winding model were designed to fulfil two objectives:

1. To verify that P_{fi} and C_{pd} are controlled by *Re* itself instead of the components it is composed of.
2. To verify that results from the correlation equation sets (7) and (8) fit well with measurements in the practical range of *Re* for two chosen winding geometries: vertical duct width 10 mm and vertical duct width 12 mm.

Since vertical duct width is the denominator of the three dimensionless geometric parameters, even the other geometric dimensions keep unchanged each vertical duct width would lead to a new set of α, β and γ.

A. Verification of Objective 1

Since the hydraulic diameter is defined as D_h=4*A*/*P*, for a given oil type, the Reynolds number at the winding pass inlet is mainly controlled by the total oil flow rate and the oil temperature. The tested three cases with similar *Re* for two vertical duct widths 10 mm and 12 mm are shown in Table III.

1) Flow Distribution

For the winding model of vertical duct width 10 mm, the comparisons of average oil velocities and flow proportions in the third pass from PIV measurements are shown in Fig. 4 (a) and (b), respectively. The comparisons for vertical duct

width 12 mm are shown in Fig. 5. It can be seen from both Fig. 4 and Fig. 5 that although the average velocities for the three cases are different, the flow distributions in terms of volumetric flow proportion in each duct are almost identical.

TABLE III
THREE CASES WITH SIMILAR RE

	Case 1	Case 2	Case 3
Pass inlet oil flow rate (lpm)	6	12	18
Oil temperature (^{o}C)	77	48	36
Re (W_{duct}=10 mm)	541	536	547
Re (W_{duct}=12 mm)	531	526	537

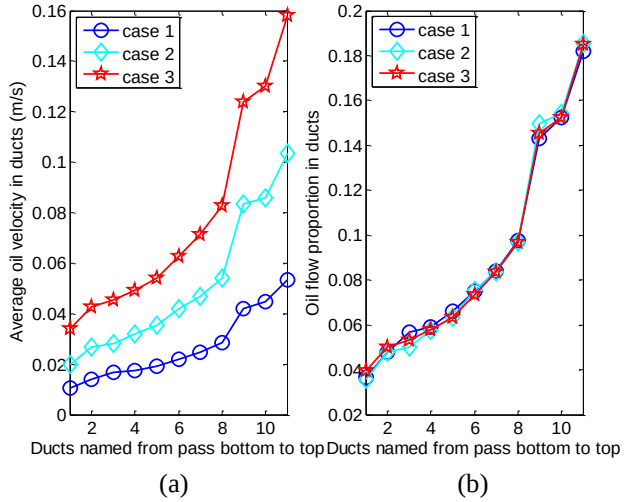

Fig. 4. Comparison of flow distribution for the three cases in Table III with similar Re and vertical duct width of 10 mm. (a) Average velocity. (b) Flow proportion where the total oil flow rate is regarded as one unit.

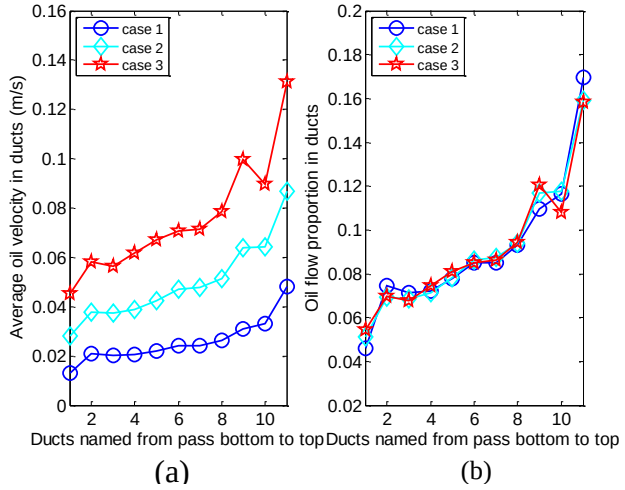

Fig. 5. Comparison of flow distribution for the three cases in Table III with similar Re and vertical duct width of 12 mm. (a) Average velocity. (b) Flow proportion where the total oil flow rate is regarded as one unit.

2) Pressure Drop Coefficient

The comparisons of pressure drops and pressure drop coefficients over the 3-pass winding model for vertical duct width 10 mm and 12 mm are shown in Table IV. For each geometry, the absolute static pressure drops are very different but the corresponding pressure drop coefficients are similar.

TABLE IV
COMPARISON OF PRESSURE DROP AND PRESSURE DROP COEFFICIENT

		Case 1	Case 2	Case 3
10 mm	ΔP (pa)	43	200	466
	C_{pd}	9.1	10.4	10.6
12 mm	ΔP (pa)	37	148	303
	C_{pd}	11.29	11.04	9.96

From these comparisons for flow distributions and pressure drop coefficients from cases with similar *Re*, objective 1 is acceptably achieved.

B Verification of Objective 2

1) Flow Distribution

To verify that the flow distribution correlation equation set (7) holds valid in the practical range of *Re*, flow distributions of two more cases were tested for both geometries. The tested cases are shown in Table V.

TABLE V
THREE CASES TO COVER THE PRACTICAL RANGE OF RE

	Case 4	Case 2	Case 5
Pass inlet oil flow rate (lpm)	6	12	18
Oil temperature (^{o}C)	20	48	70
Re (W_{duct}=10 mm)	97	536	1402
Re (W_{duct}=12 mm)	95	526	1375

For the geometry of vertical duct width 10 mm, the comparisons of average oil velocities and flow proportions obtained from PIV measurements and (7) are shown in Fig. 6 (a) and (b), respectively. The comparisons for vertical duct width 12 mm are shown in Fig. 7. As can be seen from both Fig. 6 and Fig. 7, results from both methods share the same varying trends. With the increase of *Re*, flow distribution gets less uniform.

For case 4 and case 2, flow distribution curves from the equation set (7) follow closely the PIV results for both geometries. For case 5, the flow distribution curves from the two methods deviate more from each other.

For case 5 of the 10 mm vertical duct width geometry, both PIV measurement and the flow correlation equation set (7) show the occurrence of reverse flow at the bottom of the pass; for the geometry of vertical duct width 12 mm, the correlation shows a nearly stagnated flow in the horizontal duct at the bottom of the pass, while the PIV measurement shows an average velocity of 18 mm/s. Apart from the difference in total oil flow rate obtained from PIV measurements and that from the flow meter, which is the input for (7), and the geometric deviations of the winding model as is mentioned in section II part A, another reason for the increased discrepancy could be that *Re* for case 5 (around 1400) is beyond the upper boundary of Re (Re=1200) in the CFD parametric sweeps from which the correlation equation sets were derived. It is worth mentioning that case 5 should be avoided in real transformers because the occurrence of reverse flow can seriously jeopardize the cooling performance.

Comparing Fig. 6 and Fig. 7, we can see that with the increase of vertical duct width (mainly due to the decrease of α) oil flow distribution gets relatively more uniform. To further verify the point that the decrease of α brings a relatively more uniform flow distribution, a comparison between two cases with different horizontal duct heights is executed. The geometries of the two cases are shown in Table VI and the comparison of flow distribution is shown in Fig. 8. As can be seen from Fig. 8, the flow distribution for the case of α being 0.4 is more uniform than the case of α being 0.6. In fact, reverse flow occurs for the case of α being 0.6. In addition, the predicted results obtained from (7) follow the measured results closely. The velocity profiles in the bottom ducts of case 6 and case 7 are shown in Fig. 9, where the velocity of reverse flow in case 7 is designated as negative velocities.

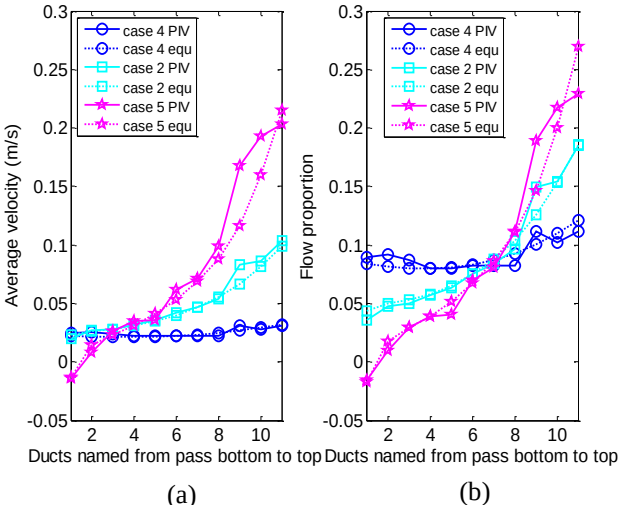

(a) (b)

Fig. 6. Comparison of flow distribution for Re in the range in Table V with vertical duct width being 10 mm. (a) Average velocity in each duct of pass 3. (b) Flow proportion in each duct of pass 3 where the total oil flow rate is regarded as one unit. The legend 'equ' refers to correlation equation (7).

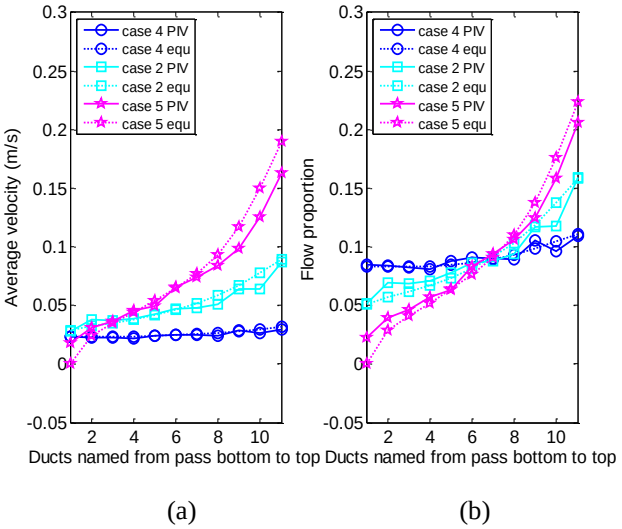

(a) (b)

Fig. 7. Comparison of flow distribution for Re in the range in Table V with vertical duct width of 12 mm. (a) Average velocity in each duct of pass 3. (b) Flow proportion in each duct of pass 3 where the total oil flow rate is regarded as one unit. The legend 'equ' refers to correlation equation (7).

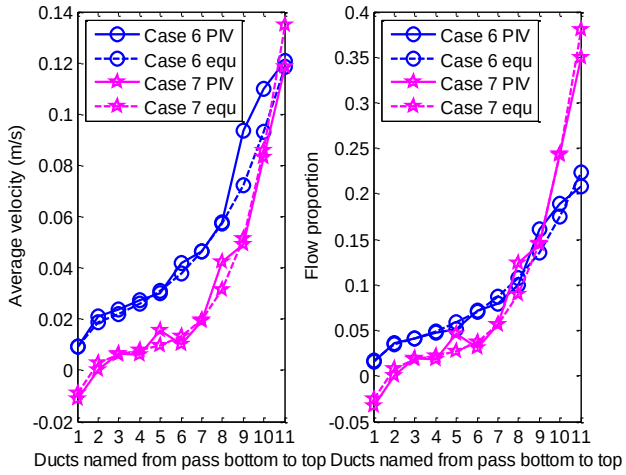

(a) (b)

Fig. 8. Comparison of flow distribution for two horizontal duct heights in Table VI. (a) Average velocity in each duct of pass 3 where the total oil flow rate is regarded as one unit. (b) Flow proportion in each duct of pass 3. The legend 'equ' refers to correlation equation (7).

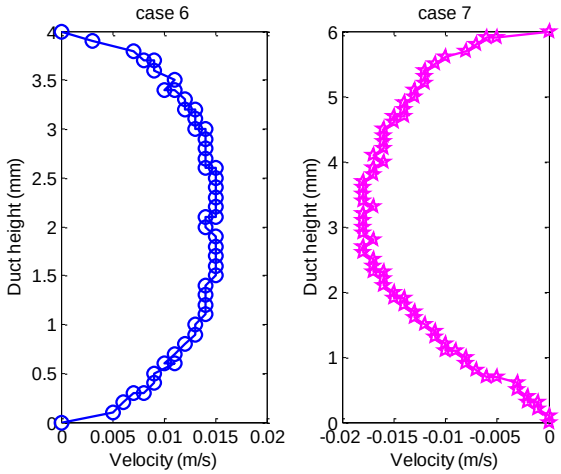

Fig. 9. Velocity profiles in the first ducts of case 6 and case 7 from PIV measurements.

TABLE VI
THREE CASES TO COVER THE PRACTICAL RANGE OF RE

	Case 6	Case 7
Pass inlet oil flow rate (lpm)	12	12
Oil temperature (^oC)	70	70
Vertical duct width (mm)	10	10
Horizontal duct height (mm)	4	6
α	0.4	0.6
Re	878	878

2) Pressure Drop Coefficient

To verify that the pressure drop coefficient correlation equation set (8) holds valid in the practical range of *Re*, more pressure measurements were implemented. In these measurements, oil temperature was set to be 20 *ºC*, 35 *ºC*, 50 *ºC*, and 77 *ºC*, while the total oil flow rates ranges from 6 lpm to 18 lpm for the vertical duct width 10 mm geometry and 6 lpm to 21 lpm for the geometry of vertical duct width

12 mm. For the geometry of vertical duct width 10 mm, the comparisons of pressure drops and pressure drop coefficients obtained from the measurements and (8) are shown in Fig. 10 (a) and (b), respectively. The comparisons for vertical duct width 12 mm are shown in Fig. 11. As can be seen from both Fig. 10 and Fig. 11, the pressure drops from measurements and those derived from (8) are consistent with maximum relative error being 16.9%. From the prediction of (8), the variation of pressure drop coefficient against *Re* for both geometries in log-log scale is a straight line at the beginning and then levels off in the region of high *Re*. When the measured pressure points are transformed to pressure drop coefficients, they fall close to the predicted curves from (8) and in the same way with maximum relative error being 16.9%.

From the comparisons for flow distributions and pressure drops from cases covering the practical range of *Re*, objective 2 is acceptably achieved.

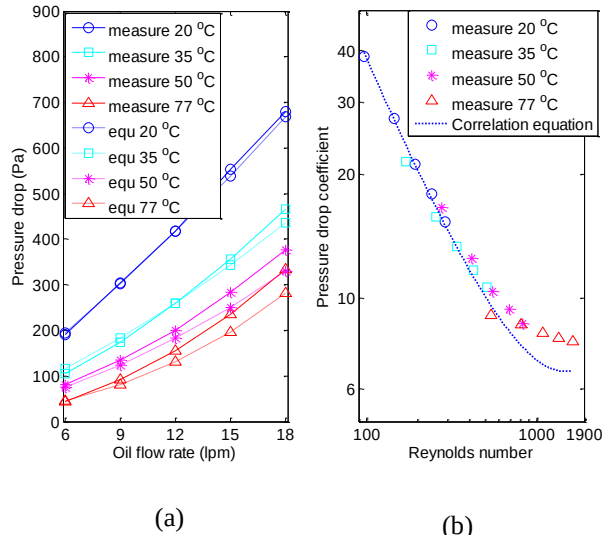

Fig. 10. Comparison of static pressure drops for the geometry of vertical duct width being 10 mm. (a) absolute pressure drop; (b) pressure drop coefficient.

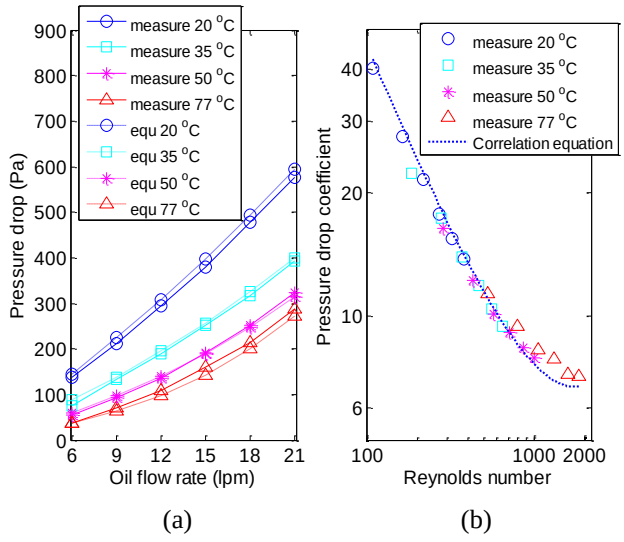

Fig. 11. Comparison of static pressure drops for the geometry of vertical duct width of 12 mm. (a) absolute pressure drop; (b) pressure drop coefficient

V. Comparison of Isothermal and Nonisothermal Cases

In practice, buoyancy force and hot-streak dynamics are involved in determining flow distribution in and pressure drop over the winding, especially for oil natural (ON) cooling modes [5-7]. To verify that for OD cooling modes the influence of buoyancy force and hot-streak dynamics are negligible and therefore the foregoing isothermal results hold valid for practical cases, comparison between isothermal and nonisothermal cases are shown in this section.

A Power Injection in Each Plate

The current density in the copper conductor of a disc-type power transformer is in the range of 2-4 A/mm^2 [18]. Assuming the plates in the winding model were made of copper and a current density of 4 A/mm^2 ran through each plate with copper resistance at 85 ^oC, then the resistive power generated in each plate would be approximately 35 W. To account stray losses and eddy current losses in the winding and to provide some margin, a power injection of 50 W per plate was selected which was delivered by two cartridge heaters embedded in each plate as detailed in [16].

B Comparisons of Flow Distribution and Pressure Drop

The comparisons of flow distribution and pressure drop between isothermal and nonisothermal conditions were implemented on the winding geometry of vertical duct width 10 mm. For an OD cooling mode, typical oil velocity in horizontal ducts range from 0.075 m/s to 0.15 m/s [17]. Therefore, oil velocity at the winding pass inlet would be larger than 0.1 m/s corresponding to a total oil flow rate of approximately 6 lpm. In the nonisothermal tests, two flow rates of 6 lpm and 12 lpm are tested, of which the related parameters are shown in Table VII. For comparison purposes, two isothermal flow cases of 6 lpm, 45 ^oC and 12 lpm, 47 ^oC were conducted.

The comparisons of flow distributions in pass 3 from PIV measurements are shown in Fig. 12. As can be seen, flow distributions from isothermal and nonisothermal conditions are almost identical. The comparisons of pressure drops for these isothermal and nonisothermal cases are shown in Table VIII. The discrepancies on pressure drop between the isothermal and nonisothermal cases are negligible. The negligible Gr/Re^2 for case 6 and case 7 (much smaller than 1) shown in Table VII is responsible for the negligible differences in flow and pressure drop results between the isothermal and nonisothermal cases.

It can be concluded that for OD cooling modes, the influence of buoyancy force and hot-streak dynamics is negligible. Therefore, the aforementioned results obtained from isothermal flow conditions are valid for OD cooling modes.

TABLE VII
PARAMETERS RELATED TO NONISOTHERMAL TESTS

	6 lpm	12 lpm
Pass 3 inlet temperature (°C)	45	47
Pass 3 outlet temperature (°C)	48	48.5
Gr/Re^2	0.046	0.006

In calculating Gr/Re^2, the thermal expansion coefficient is 7.8×10^{-4} (1/K) and the temperature gradients are taken as the differences between the pass 3 outlet temperatures and the pass 3 inlet temperatures.

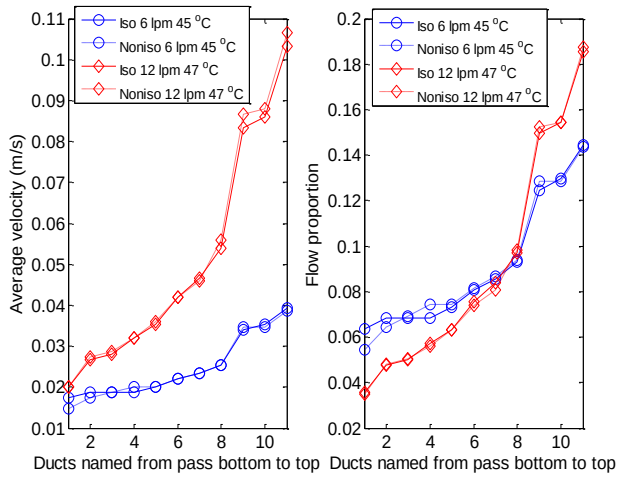

(a) (b)

Fig. 12. Comparison of flow distribution for isothermal and nonisothermal flow conditions with vertical duct width being 10 mm. (a) average velocity in each duct; (b) flow proportion in each duct where the total oil flow rate is regarded as one unit.

TABLE VIII
COMPARISON OF PRESSURE DROP AND PRESSURE DROP COEFFICIENT

		6 lpm 45 ^oC	12 lpm 47 ^oC
Isothermal	ΔP (pa)	91	223
Nonisothermal	ΔP (pa)	90	215

Each pressure drop result is the average of ten repeated tests.

VI. Discussion

The method of dimensional analysis, which can simplify a physical problem to its simplest form prior to obtaining a quantitative relationship, has been widely used in fluid mechanics. However, it has not yet become the common practice for transformer thermal modeling.

In this paper, the methodology presented in [15] was verified experimentally on a disc-type transformer winding model. It is worth mentioning that none of the experimental scenarios were simulated directly by CFD, yet the experimental results are in line with the results generated from the correlation equation sets obtained from 2D CFD parametric sweeps. Therefore the 2D modeling, the method of dimensional analysis, the CFD simulations, and the correlations of the CFD results are all verified to be valid for the investigation of flow distribution and pressure drop.

Since the correlation equation sets have been verified experimentally, some insight into oil flow distribution in and pressure drop over the winding model can be obtained conveniently from the correlation equation sets. It was found that the geometric parameter α is more influential than the other two geometric parameters β and γ [15].

The uniformity of oil flow distribution in a pass can be represented by a parameter called maldistribution defined as the ratio of the maximum to the minimum flow rate in the ducts of a pass [10]. For the 3-pass winding model with 10 plates per pass (11 ducts), with the help of the flow correlation equation set (7), the variation of maldistribution with the two influential parameters, *Re* and α, can be obtained conveniently with β set to be 1 (vertical duct width equals disc axial height) and γ to be 10 (disc radial width is 10 times vertical duct width), as shown in Fig. 13. It can be seen that maldistribution increases monotonically with increasing *Re* and α. The higher the total oil flow rate and the larger the ratio of horizontal duct height to vertical duct width, the more uneven the flow distribution would be. For design purpose, if maldistribution is desired to be smaller than 5, then region 1 indicates the feasible combinations of *Re* and α, as shown in Fig. 13.

It was observed in the experiments that geometric deviations lead to non-smooth flow distribution which could cause some horizontal cooling ducts suffering from smaller flow rate than expected. Although the trend of flow distribution will not change significantly, the reduction of flow rate in some specific ducts may still cause noticeable winding temperature rise. Geometric deviations during the transformer manufacturing process are difficult to avoid and therefore the effects of some typical geometric deviations are worth further investigation.

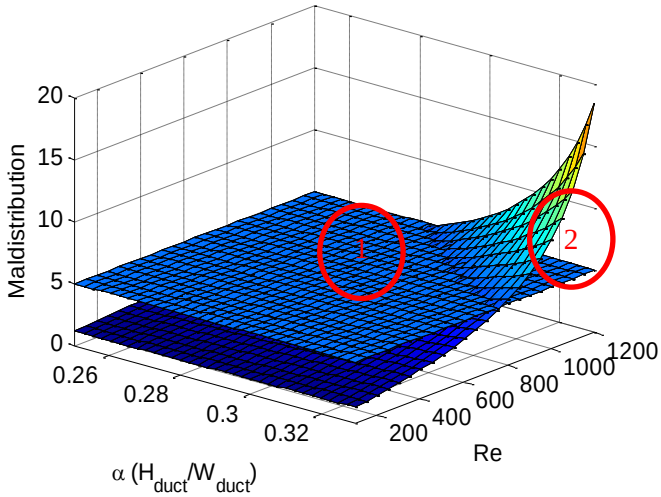

Fig. 13. Variation of maldistribution with *Re* and α. In region 1, maldistribution is smaller than 5, whereas in region 2 maldistribution is larger than 5.

VII. Conclusion

Dimensional analyses were conducted to simplify the physical problems of oil flow distribution in and pressure drop over a winding model to the simplest forms. CFD parametric sweeps of the identified dimensionless controlling parameters were performed and then the CFD results obtained were correlated to form predictive correlation equation sets.

Measurements of flow distribution in pass 3 using a PIV system and recording of pressure drop over the 3-pass winding model were implemented to verify the method of dimensional analysis and the correlation equation sets obtained from CFD parametric sweeps. The fact that it is the Reynolds number itself instead of its components that controls oil flow distribution and pressure drop coefficient, was verified experimentally for fixed winding geometries in OD cooling modes.

It was also satisfactorily verified that the correlation equation sets can generate results that are in line with the measurements in the practical range of *Re*. Therefore, the 2D CFD simulations and the strategies of correlating the CFD results to form predictive correlation equation sets are also valid.

The conclusions obtained based on isothermal conditions can be extended to nonisothermal conditions, as the experiments on nonisothermal conditions confirmed that buoyancy force and hot-streak dynamics are negligible for OD cooling modes.

Acknowledgment

The authors would like to express their gratitude to M&I Materials, National Grid, Scottish Power, Shell, TJ|H2b Analytical Services, UK Power Networks and Weidmann Electrical Technology AG for their financial and technical contributions to the Transformer Research Consortium at The University of Manchester.

References

[1] A. J. Oliver, "Estimation of transformer winding temperatures and coolant flows using a general network method," *Proc. Inst. Elect. Eng.*, vol. 127, pp. 395-405, 1980.

[2] Z. R. Radakovic, and M. S. Sorgic, "Basics of detailed thermal-hydraulic model for thermal design of oil power transformers," *IEEE Trans. Power Del., vol. 25*, no. 2, pp. 790-802, 2010.

[3] E. Rahimpour, M. Barati, and M. Schäfer, "An investigation of parameters affecting the temperature rise in windings with zigzag cooling flow path," *Appl. Therm. Eng., vol. 27*, no. 11, pp. 1923-1930, 2007.

[4] J. Zhang, and X. Li, "Coolant flow distribution and pressure loss in ONAN transformer windings. Part I: Theory and model development," *IEEE Trans. Power Del.,,* vol. 19, no. 1, pp. 186-193, 2004.

[5] F. Torriano, M. Chaaban, and P. Picher, "Numerical study of parameters affecting the temperature distribution in a disc-type transformer winding," *Appl. Therm. Eng.*, vol. 30, no. 14, pp. 2034-2044, 2010.

[6] A. Skillen, A. Revell, H. Iacovides, W, Wu, "Numerical prediction of local hot-spot phenomena in transformer windings," *Applied Thermal Engineering*, vol. 36, pp. 96-105, 2012.

[7] F. Torriano, P. Picher, and M. Chaaban, "Numerical investigation of 3D flow and thermal effects in a disc-type transformer winding," *Appl. Therm. Eng.*, vol. 40, pp. 121-131, 2012.

[8] W. Wu, Z.D. Wang, A. Revell, H. Iacovides, P. Jarman, "Computational fluid dynamics calibration for network modelling of transformer cooling oil flows-part I heat transfer in oil ducts," *IET Electric Power Applications*, vol. 6, no. 1, pp. 19-27, 2012.

[9] W. Wu, Z.D. Wang, A. Revell, P. Jarman., "Computational fluid dynamics calibration for network modelling of transformer cooling flows–Part II: pressure loss at junction nodes," *IET electric power applications*, vol. 6, no. 1, pp. 28-34, 2012.

[10] J. Coddé, W. Van der Veken, and M. Baelmans, "Assessment of a hydraulic network model for zig–zag cooled power transformer windings," *Appl. Therm. Eng.*, vol. 80, pp. 220-228, 2015.

[11] P. Allen, O. Szpiro, and E. Campero, "Thermal analysis of power transformer windings," *Electric Manchines and Electromechanics*, vol. 6, no. 1, pp. 1-11, 1981.

[12] M. Nakadate, K. Toda, K. Sato, D. Biswas, C. Nakagawa, T. Yanari, "Gas cooling performance in disc winding of large-capacity gas-insulated transformer," *IEEE Trans. Power Del.*, vol. 11, no. 2, pp. 903-908, 1996.

[13] J.-M. Mufuta, "Comparison of experimental values and numerical simulation on a set-up simulating the cross-section of a disc-type transformer," *International journal of thermal sciences*, vol. 38, no. 5, pp. 424-435, 1999.

[14] A. Weinläder, W. Wu, S. Tenbohlen, Z.D. Wang, "Prediction of the oil flow distribution in oil-immersed transformer windings by network modelling and computational fluid dynamics," *IET electric power applications*, vol. 6, no. 2, pp. 82-90, 2012.

[15] X. Zhang, Z.D. Wang, and Q. Liu, "Prediction of Pressure drop and flow distribution in disc type transformer windings in an OD cooling mode," *IEEE Trans. Power Del*., 2016, DOI (identifier) 10.1109/TPWRD.2016.2557490.

[16] M. Daghrah, Z.D. Wang, Q. Liu, D. Walker, P.W.R. Smith, P. Mavrommatis, "Design of Experimental Setup to Study Factors Affecting Hot Spot Temperature in Disc Type Winding Transformers," *in The IET International Conference of Resilience of Transmission and Distribution Networks*, 2015.

[17] J. Zhang, and X. Li, "Coolant flow distribution and pressure loss in ONAN transformer windings. Part II: Optimization of design parameters," *IEEE Trans. Power Del.*, vol. 19, no. 1, pp. 194-199, 2004.

[18] M. Heathcote, *J & P transformer book*, Thirteenth ed.: Newnes, 2007.

Blank page

3.4 **Paper 3**

Numerical Investigation of Influence of Coolant Types on Flow Distribution and Pressure Drop in Disc Type Transformer Windings

Xiang Zhang, Zhongdong Wang, Qiang Liu, Paul Jarman, Attila Gyore and Paul Dyer

2016

The 19th International Conference on Diagnosis and Monitoring (CMD), Xi'an, P.R. China

Published

Blank page

Numerical Investigation of Influence of Coolant Types on Flow Distribution and Pressure Drop in Disc Type Transformer Windings

Xiang Zhang[1], Zhongdong Wang[1*], Qiang Liu[1], Paul Jarman[2], Attila Gyore[3], Paul Dyer[4]
[1]School of Electrical and Electronic Engineering, The University of Manchester, UK
[2]National Grid, Warwick, UK
[3]M&I Materials, Manchester, UK
[4]UK Power Networks, Crawley, UK
*zhongdong.wang@manchester.ac.uk

***Abstract*—In this paper dimensional analyses of flow distribution in and pressure drop over disc-type transformer windings in an oil forced and directed (OD) cooling mode are presented. Computational fluid dynamics (CFD) parametric sweeps were conducted to quantify the dimensionless relationships obtained from the dimensional analyses to form predictive correlation equation sets. With the help of the correlation equation sets, the influence of coolant types including a mineral oil, a gas-to-liquid (GTL) oil and a synthetic ester on flow distribution in and pressure drop over a winding model was investigated. It was found that the synthetic ester, which has a higher viscosity than the others, could be advantageous in terms of suppressing reverse flow and getting a relatively more uniform flow distribution at the cost of a higher static pressure drop.**

Keywords— Transformer; Disc-type winding; dimensinal analysis; flow distribution; pressure drop; coolant types.

I. Introduction

The hot-spot in transformer windings determines the thermal ageing rate of the insulation. The primary objective of transformer thermal design is to limit hot-spot temperature in operation below certain limitations defined by international standards, e.g. IEC 60076-7 [1] and IEEE C57.91 [2].

Power transformers are often of disc-type winding cooled by oil circulation between the winding and the cooler/radiator. Pumps are usually used to facilitate the oil circulation. Oil flow distribution in the disc-type winding has a direct impact on the cooling performance. In addition, pressure drop over the winding determines the selection of pump and more importantly the oil split between windings connected hydraulically in parallel.

Two major methods have been developed to investigate oil flow distribution in and pressure drop over disc-type transformer windings: network models [3-5] and computational fluid dynamics (CFD) models [6, 7]. These two methods share the same physical principles: conservations of mass, momentum and energy. Disc-type transformer windings are usually reduced to a 2D axisymmetric geometry. Network models are lumped-parameter models that approximate the 2D geometry into a network of nodes representing critical parts and junctions in the winding geometry. Correlations for fluid flow and heat transfer processes are adopted in network models and the correlation results are processed to obey the three conservation laws. CFD models, on the other hand, solve the governing differential equations directed with high spatial resolution and accuracy at the cost of much higher computational effort. CFD models have the advantage of accuracy over network models and therefore can provide network models with correlations for the processes of fluid flow and heat transfer [8-10].

The difficulty one may face is that even with the modelling solutions one could still be baffled as to how oil flow distribution in and pressure drop over the winding are influenced by winding geometric dimensions, fluid properties and coolant flow rate. This is because of the sheer number of possible combinations of the variations of all the controlling parameters.

Dimensional analysis, which has been widely adopted in fluid mechanics, was used to simplify the relationship between flow distribution, or pressure drop, and the controlling parameters for a winding model [11]. The simplification without losing accuracy was achieved by transforming the controlling parameters to their dimensionless forms. With the help of CFD simulations, the relationships were quantified to form predictive correlation equation sets.

The quantified relationships for flow distribution in and pressure drop over the winding model are universal for different types of coolants. In this paper, the characteristics of flow distribution and pressure drop for a mineral oil, a gas-to-liquid (GTL) oil and a synthetic ester are investigated using the correlation equation sets obtained.

II. Winding Geometry

A disc-type transformer winding possesses an angular periodicity dictated by the number of spacers present along the circumference of the winding disc. A segment of one pass between two adjoining sets of spacers of a winding model is shown in Fig. 1 (a). Since oil flow in the winding segment is a quasi-2D flow, the winding geometry can be further reduced to an axisymmetric 2D approximation, omitting the details in the vicinity of spacers and strips. The 2D geometry of a 3-pass winding model with 6 discs per pass is shown in Fig. 1 (b), where the details of the cross section of a strand are illustrated in Fig. 1 (c).

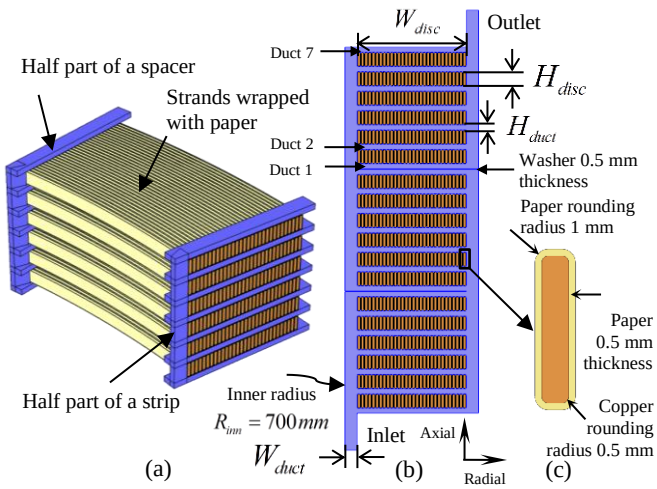

Fig. 1. Disc-type winding geometry. (a) 3D geometry of a segment of one pass between two adjoining sets of spacers. (b) 2D axisymmetric geometry of a 3-pass winding. (c) Geometric details of the cross section of a strand.

III. Dimensional Analyses

A. Coolant Flow Distribution

In oil forced and directed (OD) cooling modes, coolant flow distributions in different passes are similar and the influence of hot-streak dynamics and buoyancy forces is negligible [11]. Therefore, coolant flow distribution in pass 3 of the winding model is representative. The average coolant velocity in duct i ($\bar{v}_i$) in pass 3 can be expressed as a function of the controlling parameters:

$$\bar{v}_i = f_i(\bar{v}_{in}, \rho, \mu, H_{duct}, H_{disc}, W_{disc}, W_{duct}) \quad (1)$$

where the subscript i is for duct number in pass 3 named from the bottom to the top of the pass, $\bar{v}_{in}$ is for average coolant velocity at pass 3 inlet, ρ is for coolant density, μ is for coolant dynamic viscosity, H_{duct} is for horizontal duct height, H_{disc} is for winding disc height, W_{duct} is for vertical duct width, W_{disc} is for disc radial width.

In dimensional analysis, $\bar{v}_{in}$, ρ, and W_{duct} are chosen to be repeating parameters. After mathematical processing, the dimensionless relationship is reached:

$$\frac{\bar{v}_i}{\bar{v}_{in}} \cdot \frac{H_{duct}}{W_{duct}} = P_{fi} = g_i(\mathrm{Re}, \alpha, \beta, \gamma) \quad (2)$$

where P_{fi} represents volumetric coolant flow proportion in duct i, $\rho \bar{v}_{in} 2W_{duct}/\mu$ is the Reynolds number (Re) at the inlet of pass 3, H_{duct}/W_{duct} is referred to as α, H_{disc}/W_{duct} is referred to as β and W_{disc}/W_{duct} is referred to as γ.

B. Pressure Drop over the Winding

Static pressure drop over the winding is proportional to the number of passes [11]. Therefore the pressure drop over the three-pass winding model is investigated. Pressure drop over the 3-pass winding model can be expressed as a function of the controlling parameters:

$$\Delta P = f(\bar{v}_{in}, \rho, \mu, H_{duct}, H_{disc}, W_{disc}, W_{duct}) \quad (3)$$

Similarly, by choosing, $\bar{v}_{in}$, ρ, and W_{duct} as repeating parameters, the dimensionless forms of pressure drop can be obtained:

$$\frac{\Delta P}{\rho \bar{v}_{in}^2/2} = C_{pd} = g(\mathrm{Re}, \alpha, \beta, \gamma) \quad (4)$$

where C_{pd} is pressure drop coefficient for the three-pass winding model.

IV. CFD Parametric Sweeps and Correlations

The ways how coolant flow distribution and pressure drop are controlled by the geometric dimensions, coolant properties and total coolant flow rate are simplified into (2) and (4) by conducting dimensional analyses prior to obtaining the quantified relationships. There are two methods to quantify the relationships: experimentation and theoretical calculations. In this paper, the theoretical calculations are presented.

A. CFD Parametric Sweeps

Theoretical calculations were implemented by performing CFD parametric sweeps with COMSOL Multiphysics 5.1. The practical ranges of winding geometric dimensions from [12] are presented in Table I.

TABLE I
RANGES OF PRACTICAL GEOMETRIC PARAMETERS [12]

W_{duct} (mm)	H_{duct} (mm)	H_{disc} (mm)	W_{disc} (mm)
6-12	3-6	7-20	40-170

From the practical ranges of the geometric dimensions, the ranges of the dimensionless parameters can be obtained. Re is set to range from 50 to 1200. The swept discrete dimensionless parameters were shown in Table II.

TABLE II
RANGES OF THE SWEPT DIMENSIONLESS PARAMETERS

Re	50, 100, 200, 400, 600, 800, 1000, 1200
α	0.25, 0.3, 0.4, 0.5, 0.6
β	0.67, 1, 2, 3
γ	6, 9, 12, 15

All the combinations of *Re*, α, β and γ were simulated by CFD simulations. Mesh refinement study was conducted to guarantee mesh independent solutions.

B. Correlations

The results of flow distribution in pass 3 and pressure drop over the 3-pass winding model were extracted from the CFD simulations and they were correlated with the identified dimensionless parameters.

1) Correlations for Flow Distribution

The flow proportion in duct i of the third pass (P_{fi}) were correlated with *Re*, α, β and γ by equation set (5):

$$\begin{cases} P_{fi} = \dfrac{a_{i1}}{\mathrm{Re}^{1/3}} + a_{i2}\ln \mathrm{Re} + a_{i3}\,\mathrm{Re}^{1/3} + a_{i4}; i = \{1,2,\cdots,7\} \\ a_{ij} = b_{ij1}\alpha^3 + \mathrm{b}_{ij2}\,\alpha^2 + \mathrm{b}_{ij3}\,\alpha + \mathrm{b}_{ij4}; \quad j = \{1,2,3,4\} \\ b_{ijk} = c_{ijk1}\beta^3 + \mathrm{c}_{ijk2}\,\beta^2 + \mathrm{c}_{ijk3}\,\beta + \mathrm{c}_{ijk4}; \quad k = \{1,2,3,4\} \\ c_{ijkm} = d_{ijkm1}\gamma^3 + d_{ijkm2}\gamma^2 + d_{ijkm3}\gamma + d_{ijkm4}; \; m = \{1,2,3,4\} \end{cases} \tag{5}$$

where a_{ij}, b_{ijk}, c_{ijkm} are dummy correlation coefficients, and 256 correlation coefficient d's are generated for each P_{fi}.

2) Correlations for Pressure Drop

The pressure drop coefficient over the 3-pass winding model (C_{pd}) were correlated with *Re*, α, β and γ by equation set (6):

$$\begin{cases} C_{pd} = a_1 \dfrac{1000}{\mathrm{Re}} e^{a_2 \mathrm{Re}/1000} \\ a_i = b_{i1}(4\alpha)^{b_{i2}} e^{4\alpha b_{i3}}; \;\; i = \{1,2\} \\ b_{ij} = c_{ij1}\beta^{c_{ij2}} e^{c_{ij3}\beta}; \;\; j = \{1,2,3\} \\ c_{ijk} = d_{ijk1}\gamma^3 + d_{ijk2}\gamma^2 + d_{ijk3}\gamma + d_{ijk4}; \; k = \{1,2,3\} \end{cases} \tag{6}$$

where a_i, b_{ij}, c_{ijk} are dummy correlation coefficients, and 72 correlation coefficient d's are generated for pressure drop coefficient.

The accuracy of equation sets (5) and (6) has been verified by comparing results from new CFD simulations with those from the two equation sets [11].

V. Comparisons for Different Types of Coolant

The correlation equation sets (5) and (6) are universal for any type of coolant. The flow distributions and pressure drops for different types of coolant can therefore be investigated conveniently using the correlation equation sets.

A. Coolant Properties

The coolant properties of three coolants, a mineral oil Gemini X, a GTL oil Diala S4 ZX-I and a synthetic ester MIDEL 7131 are shown by the following equations and Fig. 2.

$$\begin{cases} \rho_1 = \text{-}0.6568 \times \mathrm{T} + 1064 \\ \mu_1 = 7.863 \times 10^{-5} \times \exp(632.0/(\mathrm{T}\text{-}176.0)) \\ \rho_2 = \text{-}0.6455 \times \mathrm{T} + 995.5 \\ \mu_2 = 6.133 \times 10^{-5} \times \exp(749.8/(\mathrm{T}\text{-}157.4)) \\ \rho_3 = \text{-}0.7327 \times \mathrm{T} + 1185 \\ \mu_3 = 6.239 \times 10^{-5} \times \exp(914.1/(\mathrm{T}\text{-}162.4)) \end{cases} \tag{7}$$

where the subscript 1 is for the mineral oil, 2 for the GTL, 3 for the synthetic ester, *T* is for temperature in Kelvin.

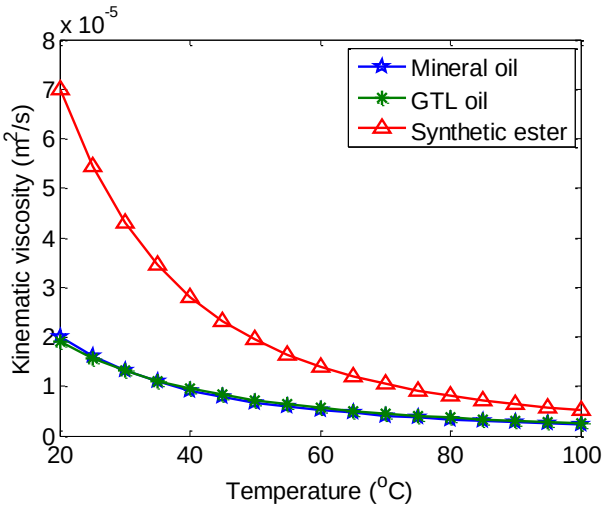

Fig. 2. Temperature dependant kinematic viscosities.

B. Flow Distribution and Pressure Drop

The forgoing dimensional analyses show that flow distribution and pressure drop coefficient are controlled by the Reynolds number at the pass inlet and the dimensionless geometric parameters, α, β and γ. The Reynolds number is mainly controlled by coolant properties and total coolant flow rate. Therefore, the effect of geometric dimensions can be segregated from the effects of coolant properties and total coolant flow rate. It was found that for a fixed winding geometry flow distribution gets less uniform with the increase of Re [11].

The influence of different coolant types on flow distribution and pressure drop is focused on in this paper. The winding geometry is fixed to be vertical duct width of 10 mm, horizontal duct height of 4 mm ($\alpha = 0.4$), disc axial height of 10 mm ($\beta = 1$) and disc radial width of 100 mm ($\gamma = 10$). Coolant temperatures are fixed to be 333.15 K (60 ℃).

1) A Fixed Total Volumetric Flow Rate

When the pass inlet coolant velocity is fixed to be 0.3 m/s, the Reynolds numbers for the mineral oil, the GTL oil and the synthetic ester are 1155, 1071 and 428, respectively. The coolant velocity (flow proportion) distributions in pass 3 for the three coolants can then be obtained by using (5). The flow distributions are shown in Fig. 3.

It can be seen from Fig. 3 that flow distributions for the mineral oil and the GTL oil are similar but they are different from that of the synthetic ester. Reverse flow occurs for the mineral oil and the GTL oil at the bottom of the pass. This is because the mineral oil and the GTL oil share similar kinematic viscosity and they are less viscous than the synthetic ester. The more viscous liquid

leads to smaller *Re* and a relatively more uniform flow distribution as shown in [11].

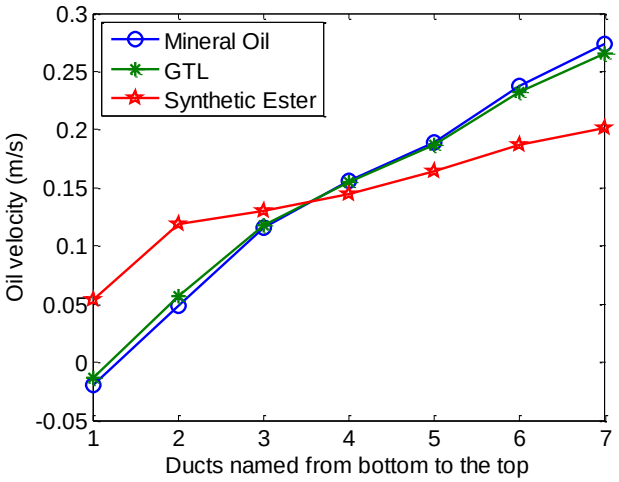

Fig. 3. Coolant velocity distributions in pass 3 for the three coolants with the same total coolant flow rate.

The pressure drop coefficient can be obtained by using (6) and the pressure drop over the 3-pass winding model can then be obtained, as shown in Table III.

TABLE III
PRESSURE DROPS FOR THREE COOLANTS

	Mineral Oil	GTL	Synthetic Ester
Pressure drop (Pa)	228	217	446

As it can be seen from Table III, the synthetic ester experiences a higher pressure drop, which is the penalty of a more uniform flow distribution.

2) A Fixed Pressure Drop

If the static pressure drop over the 3-pass winding model is fixed to be 446 Pa, the pass inlet coolant velocity and *Re*, according to (6), are shown in Table IV. The flow distribution for the three coolants can then be obtained by using (5), as shown in Fig. 4.

TABLE IV
VELOCITY AND RE FOR THREE COOLANTS

	Mineral Oil	GTL	Synthetic Ester
Velocity (m/s)	0.43	0.45	0.3
Re	1665	1606	428

It can be seen from Fig.4 that flow distributions of the mineral oil and the GTL oil are more uneven. Because reverse flow occurs, oil velocity in duct 2 is close to zero, which could cause localized overheating and therefore jeopardize the cooling performance. The synthetic ester does not experience reverse flow under this condition because of higher viscosity. Therefore, ester liquids, which are more viscous, can be advantageous in terms of suppressing reverse flow and getting a relatively more uniform flow distribution.

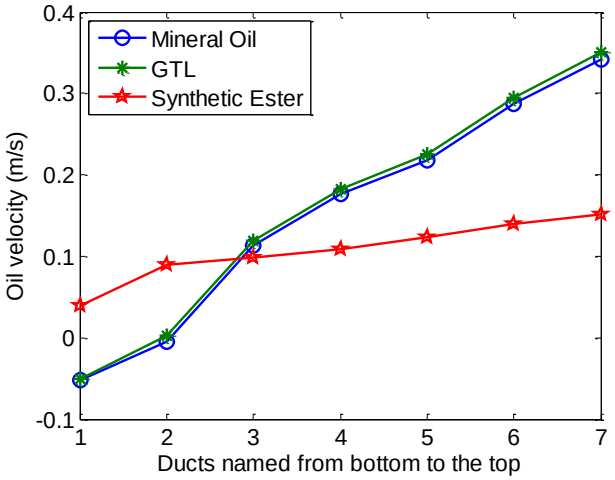

Fig. 4. Coolant velocity distribution in pass 3 for the three coolants with the same static pressure drop over the winding model.

VI. Conclusion

Dimensional analyses of flow distribution in and pressure drop over disc-type transformer windings in OD cooling modes were performed to identify the dimensionless controlling parameters. CFD parametric sweeps were conducted to quantify the relationships and to generate predictive correlation equation sets. With the help of the correlation equation sets, the influence of different coolant types, a mineral oil, a GTL oil and a synthetic ester on flow distribution in and pressure drop over a winding model was investigated. It was found that the synthetic ester, which is the most viscous of the three, could be advantageous in terms of suppressing reverse flow and getting a relatively more uniform flow distribution at the cost of a higher pressure drop. Different design strategy should be adopted for different liquids.

Acknowledgment

The authors would like to express their gratitude to M&I Materials, National Grid, Scottish Power, Shell, TJ|H2b Analytical Services, UK Power Networks and Weidmann Electrical Technology for their financial and technical contributions to the Transformer Research Consortium at The University of Manchester.

References

[1] Loading guide for oil-immersed power transformers, IEC standard IEC 60076-7, 2005.

[2] IEEE Guide for Loading Mineral-Oil-Immersed Transformers and Step-Voltage Regulators, IEEE standard C57.91, 2011.

[3] A. J. Oliver, "Estimation of transformer winding temperatures and coolant flows using a general network method," Proc. Inst. Elect. Eng., vol. 127, pp. 395-405, 1980.

[4] J. Zhang, and X. Li, "Coolant flow distribution and pressure loss in ONAN transformer windings. Part I: Theory and model development," IEEE Transactions on Power Delivery, vol. 19, no. 1, pp. 186-193, 2004.

[5] Z. R. Radakovic, and M. S. Sorgic, "Basics of detailed thermal-hydraulic model for thermal design of oil power transformers,"

IEEE Transactions on Power Delivery, vol. 25, no. 2, pp. 790-802, 2010.

[6] F. Torriano, M. Chaaban, and P. Picher, "Numerical study of parameters affecting the temperature distribution in a disc-type transformer winding," Applied Thermal Engineering, vol. 30, no. 14, pp. 2034-2044, 2010.

[7] A. Skillen, A. Revell, H. Iacovides, W. Wu, "Numerical prediction of local hot-spot phenomena in transformer windings," Applied Thermal Engineering, vol. 36, pp. 96-105, 2012.

[8] W. Wu, Z. Wang, A. Revell, H. Iacovides, P. Jarman, "Computational fluid dynamics calibration for network modelling of transformer cooling oil flows-part I heat transfer in oil ducts," IET Electric Power Applications, vol. 6, no. 1, pp. 19-27, 2012.

[9] W. Wu, Z. Wang, A. Revell, P. Jarman, "Computational fluid dynamics calibration for network modelling of transformer cooling flows–Part II: pressure loss at junction nodes," IET electric power applications, vol. 6, no. 1, pp. 28-34, 2012.

[10] J. Coddé, W. Van der Veken, and M. Baelmans, "Assessment of a hydraulic network model for zig–zag cooled power transformer windings," Applied Thermal Engineering, vol. 80, pp. 220-228, 2015.

[11] X. Zhang, Z. Wang, and Q. Liu, "Prediction of Pressure Drop and Flow Distribution in Disc Type Transformer Windings in an OD Cooling Mode," IEEE Transactions on Power Delivery, under review.

[12] J. Zhang, and X. Li, "Coolant flow distribution and pressure loss in ONAN transformer windings. Part II: Optimization of design parameters," IEEE Transactions on Power Delivery, vol. 19, no. 1, pp. 194-199, 2004.

3.5 **Paper 4**

Interpretation of Hot Spot Factor for Transformers in OD Cooling Modes

Xiang Zhang, Zhongdong Wang and Qiang Liu

2017

IEEE Transactions on Power Delivery

Accepted

Interpretation of Hot Spot Factor for Transformers in OD Cooling Modes

Xiang Zhang, Zhongdong Wang, *Member*, IEEE, and Qiang Liu, *Member*, IEEE

***Abstract*— The hot-spot factor (*H*) is a crucial component of the thermal diagram in IEC 60076-2 to derive the hot-spot temperature from the test data. In this paper, *H* is expressed as the sum of two separable components, one relating to convection in the fluid domain and the other relating to conduction in the solid domain. Dimensional analyses on fluid flow and heat transfer show that both components are functions of dimensionless winding geometry, loss distribution, *Re* and *Pr*. The relationship between *H* and *Re* and *Pr* for a fixed winding geometry with uniform loss distribution is obtained by conducting computational fluid dynamics (CFD) parametric sweeps and multilayer least-square based correlation. The correlation obtained is verified by the consistency between *H* from new CFD simulations and those from the correlation. For nonuniform loss distribution, when the hot-spot is at the location of the highest power loss, *H* is in a linear relationship with *Q* and this linear relationship is coupled with a nonlinear relationship between *H* and *Re* and *Pr*.**

***Index Terms*—CFD, Dimensional analysis, disc winding, fluid flow, heat transfer, hot-spot factor, OD cooling mode, transformer.**

NOMENCLATURE

c_p	Oil specific heat at constant pressure ($J/(kg \cdot K)$)
c_{pp}	Paper specific heat at constant pressure ($J/(kg \cdot K)$)
c_{pc}	Copper specific heat at constant pressure ($J/(kg \cdot K)$)
D_h	Hydraulic diameter at the pass inlet ($2\times W_{duct}$) (m)
ΔT	Temperature gradient across the paper insulation (K)
Δx	The thickness of the paper insulation (m)
g	Average temperature gradient ($T_{aw}-(T_{to}+T_{bo})/2$) (K)
g'	Local temperature gradient ($T_{bulk}-T_{to}$) (K)
h	Heat transfer coefficient at the hot-spot ($W/(m^2 \cdot K)$)
h'	Heat transfer coefficient of the winding ($W/(m^2 \cdot K)$)
H	The hot-spot factor
H_{du}	The conductive component of H
H_{ve}	The convective component of H
k	Oil thermal conductivity ($W/(m \cdot K)$)
k_p	Paper thermal conductivity ($W/(m \cdot K)$)
k_c	Copper thermal conductivity ($W/(m \cdot K)$)
N_{de}	Number of domain elements
Nu	The Nusselt number ($h \cdot D_h/k$)
p	Static pressure (Pa)
Pr	The Prandtl number ($\mu \times c_p / k$)
q''	Local heat flux at the hot-spot (W/m^2)
$q''_{\max}$	Maximum local heat flux (W/m^2)
$\bar{q}''$	Average heat flux on all winding discs (W/m^2)
Q	Nonuniformity of power loss distribution ($q''_{\max} / \bar{q}''$)
Q'	Ratio of hot-spot heat flux to average flux ($q''/\bar{q}''$)
r	Coordinate in radial direction
Re	The Reynolds number ($u_m \times \rho \times D_h / \mu$)
S	Nonuniformity of oil flow distribution
T	Temperature (K)
T_{aw}	Average winding temperature (K)
T_{bo}	Bottom oil temperature (K)
T_{bulk}	Bulk oil temperature surrounding the hot-spot (K)
T_{hs}	The hot-spot temperature on the copper (K)
T'_{hs}	The hot-spot temperature in the fluid domain (K)
T_{to}	Top oil temperature (K)
u_m	Average oil velocity at winding pass inlet (m/s)
u_r	Radial velocity component (m/s)
u_z	Axial velocity component (m/s)
W_{duct}	Vertical duct width (m)
z	Coordinate in axial direction
ρ	Oil density (kg/m^3)
ρ_p	Paper density (kg/m^3)
ρ_c	Copper density (kg/m^3)
μ	Dynamic viscosity ($Pa \cdot s$)

I. INTRODUCTION

THE hottest point in a transformer winding, usually referred to as the hot-spot, determines the loadability and lifetime of the transformer [1, 2]. The hot-spot temperature could be measured directly using fiber-optic temperature sensors embedded in the windings during the manufacturing process [3-5]. It is shown that the hot-spot temperature may not be located in the topmost disc/turn, but in disc 2 or 3 from the topmost [4]. An accurate thermal modelling of transformers is therefore required to support the positioning of fiber-optic temperature sensors [5].

The fiber optic temperature sensors have not yet been widely installed for in-service transformers. The standard procedure for determining temperature distribution in a transformer is the temperature rise test, which, however, does not provide the hot-spot temperature directly. In the temperature rise test the top oil and bottom oil temperatures are measured either directly or indirectly, and the average winding temperature is derived from the winding resistance measurement. The hot-spot temperature can then be derived according to a thermal diagram, which has been used for decades [1, 6]. In the thermal diagram, it is assumed that the oil temperature inside the winding increases linearly from the bottom to the top and there is a constant temperature

gradient (g) between the winding and the surrounding oil. The hot-spot is assumed to be located at the top of the winding. In order to compensate the error due to the linearity assumptions, the temperature gradient between the hot-spot and the top oil is made equal to $H \times g$, where H is referred to as the hot-spot factor and is generally regarded as larger than unity. In so doing, the difficulty in determining the hot-spot temperature in transformer windings has been shifted to the determination of H. The inaccuracy in determining H results in the uncertainty of the hot-spot temperature derived. In general, H of 1.1 and 1.3 is used for distribution and transmission transformers when no specific information about the transformers is available.

H is related to the oil flow distribution and power loss distribution in the winding. Therefore, H is decomposed into factor S, describing the nonuniformity of the cooling, and factor Q, describing the nonuniformity of the power loss in IEC 60076-2:2011 [7]. However, how the S and Q factors should be quantified and how they should be formulated to characterize the variation of H based on fundamental physical reasoning remains to be open questions.

A study of the decomposition of H as the product of S and Q by using a detailed thermal-hydraulic network model showed that the S factor and Q factor as defined were interdependent [8]. Experimental determination of H using fiber-optic temperature sensors for transformers of a wide range of power rating and cooling modes was conducted in [9]. It was found that H obtained from 60 different load tests scattered from 0.51 to 2.06 [9]. A concept of effective hot-spot factor was raised in [10]. The effective hot-spot factor was reversely derived from a model that incorporates paper ageing mechanism and moisture accumulation effect into IEC thermal model [1]. It was found that the median of the effective hot-spot factors obtained from 35 scrapped power transformers was as high as 2.95.

In this paper, analytical and numerical investigations of H for transformers in OD cooling modes (pump-driven and directed oil flow) are presented. An interpretation of H based on fundamental heat transfer and fluid flow analyses in the winding with the aid of dimensional analysis rather than the thermal diagram is provided in section II. Numerical investigation of H using computational fluid dynamics (CFD) modelling is presented in section III, followed by discussion and conclusion in section IV and V, respectively.

II. Interpretation of the Hot-Spot Factor

A. Winding Geometry under Investigation

Disc-type transformer windings are investigated in this paper. Since the disc-type winding has an angular periodicity dictated by the number of radial spacers present along the circumference of the disc, the annular three-dimensional (3D) winding geometry can be reduced to the sector region between two sets of adjoining spacers. The fluid flow and heat transfer in the sector region is quasi two-dimensional (2D). Therefore, the winding geometry is further approximated into an axisymmetric 2D geometry in which the detailed phenomena in the vicinity of the spacers and strips are neglected. The differences in oil flow pattern and hot-spot temperature between 2D and 3D models can be alleviated by matching the governing dimensionless parameters, e.g. the ratio of the Grashof number to the Reynolds number square for oil natural (ON) cooling modes [11].

The investigated axisymmetric 2D winding model is shown in Fig. 1, where the detailed geometric dimensions are presented. The winding model consists of 3 passes with 6 discs per pass and uniform horizontal duct height. The rounding radii of each strand are neglected to facilitate the meshing process, which will be detailed in section III part A.

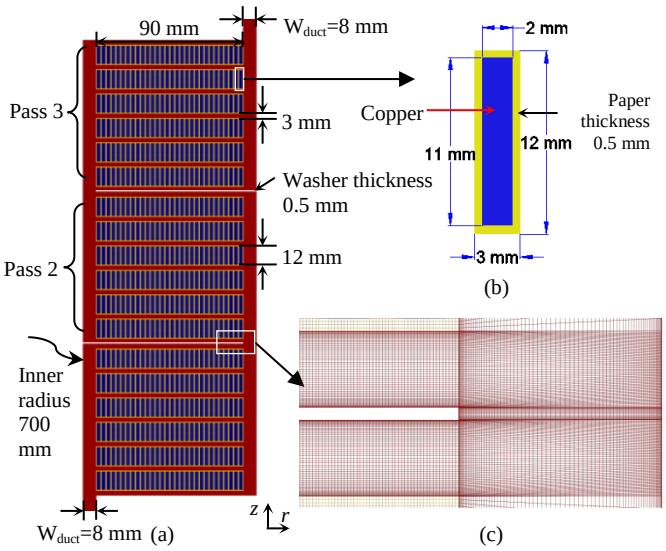

Fig. 1. Axisymmetric 2D winding model. (a) A three-pass winding model with 6 discs per pass. (b) Geometric details of the cross section of a strand. (c) Mesh details near a washer to be discussed in section III part A.

B. Fluid Flow and Heat Transfer in the Winding

Heat is generated in copper strands due to resistive losses and eddy current losses once the transformer is energized. The loss distribution in the winding can be obtained independently by considering the winding geometry, loading level and leakage flux distribution, etc. In this paper, we focus on the fluid flow and heat transfer processes in the winding with given loss distributions.

The thermal conduction within each copper strand is negligible due to the high thermal conductivity and the small size of the copper strand. The conduction through the paper insulation is governed by Fourier's law of conduction:

$$q'' = \bar{q}'' \cdot Q' = k_p \frac{\Delta T}{\Delta x} \tag{1}$$

where the Q' factor is the ratio of power loss at the hot-spot to the average power loss in the winding. The thermal convection in the fluid domain, which is the challenging part of the thermal analysis, is governed by the conservation laws of mass, momentum and energy.

The hot-spot temperature (T_{hs}) in the winding can be regarded as the sum of the highest temperature in the fluid domain (T'_{hs}) and the temperature gradient across the paper insulation (ΔT).

$$T_{hs} = T'_{hs} + \Delta T \tag{2}$$

It is worth emphasizing that (2) is one way to express the hot-spot temperature, which will facilitate the following theoretical analyses. Equation (2) implicitly represents the fluid flow and heat transfer processes in the vicinity of the hot-spot because the determination of T'_{hs} involves both the conduction in the solid domain and the convection in the fluid domain.

Based on (2), H can be rewritten as:

$$H = \frac{T_{hs} - T_{to}}{T_{aw} - (\mathrm{T}_{to} + \mathrm{T}_{bo})/2} = \frac{\Delta T}{g} + \frac{T'_{hs} - T_{to}}{g} = H_{du} + H_{ve} \quad (3)$$

The conductive component of H, $\Delta T/g$, is related to conduction in the paper insulation, referred to as H_{du}. The convective component of H, $(T'_{hs}\text{-}T_{to})/g$, is related to convection in the fluid domain, referred to as H_{ve}.

1) Conductive Component of the Hot-Spot Factor

Combining the conductive component, $\Delta T/g$, with (1) and noticing that the term $\bar{q}''/g$ can be interpreted as the overall heat transfer coefficient for the whole winding, h', we have:

$$H_{du} = \frac{\Delta T}{g} = \frac{\bar{q}'' \cdot \Delta x}{g \cdot k_p} Q' = \frac{h' \cdot \Delta x}{k_p} Q' \quad (4)$$

Since Δx can be linearly related to a characteristic length in the fluid domain and k_p can also be linearly related to oil thermal conductivity, the term $h' \cdot \Delta x/k_p$ is proportional to the Nusselt number associated with the overall heat transfer coefficient in the fluid domain. The Nusselt number for OD cooling modes is a function of the Reynolds number (Re) and the Prandtl number (Pr) [12, 13]. Therefore, for a fixed winding geometry and a fixed power loss distribution in dimensionless senses, H_{du} would only be a function of Re and *Pr* [12, 13].

2) Convective Component of the Hot-Spot Factor

The highest temperature in the fluid domain can be obtained according to Newton's law of cooling:

$$q'' = \bar{q}'' \cdot Q' = h(\mathrm{T}'_{hs} - \mathrm{T}_{bulk}) \quad (5)$$

where T_{bulk} refers to oil bulk temperature surrounding the hot-spot and h refers to the local heat transfer coefficient at the hot-spot in the fluid domain.

Combining the convective component, $(\mathrm{T}'_{hs}\text{-}\mathrm{T}_{to})/g$, with (5), we have:

$$H_{ve} = \frac{T'_{hs} - T_{to}}{g} = \frac{\bar{q}''}{g \cdot h} Q' + \frac{T_{bulk} - T_{to}}{g} = \frac{h'}{h} Q' + \frac{g'}{g} \quad (6)$$

For a fixed winding geometry and a fixed power loss distribution in dimensionless senses, the ratio of the overall heat transfer coefficient, h', to the local heat transfer coefficient, h, and the ratio of the local oil temperature gradient, g', to the overall temperature gradient, g, are all functions of *Re* and *Pr*. This conclusion can be proved by conducting dimensional analyses on fluid flow and heat transfer in the fluid domain.

C. Dimensional analyses on fluid flow and heat transfer

1) Governing Equations in the Fluid Domain

For OD cooling modes, the influence of buoyancy force is negligible as shown in [14]. Therefore, the conservation equations of mass, momentum and energy for steady, 2D flow of an imcompressible fluid with constant properties in cylindrical coordinates can be expressed by (7), (8), and (9), respectively [13].

$$\frac{1}{r}\frac{\partial(\mathrm{r}u_r)}{\partial r} + \frac{\partial u_z}{\partial z} = 0 \quad (7)$$

$$\begin{cases} \rho(\mathrm{u}_r \dfrac{\partial u_r}{\partial r} + \mathrm{u}_z \dfrac{\partial u_r}{\partial z}) = -\dfrac{\partial p}{\partial r} + \mu(\dfrac{\partial}{\partial r}(\dfrac{1}{r}\dfrac{\partial(\mathrm{r}u_r)}{\partial r}) + \dfrac{\partial^2 u_r}{\partial z^2}) \\ \rho(\mathrm{u}_r \dfrac{\partial u_z}{\partial r} + \mathrm{u}_z \dfrac{\partial u_z}{\partial z}) = -\dfrac{\partial p}{\partial z} + \mu(\dfrac{1}{r}\dfrac{\partial}{\partial r}(\mathrm{r}\dfrac{\partial u_z}{\partial r}) + \dfrac{\partial^2 u_z}{\partial z^2}) \end{cases} \quad (8)$$

$$u_r \frac{\partial T}{\partial r} + u_z \frac{\partial T}{\partial z} = \frac{k}{\rho c_p}(\frac{1}{r}\frac{\partial}{\partial r}(\mathrm{r}\frac{\partial T}{\partial r}) + \frac{\partial^2 T}{\partial z^2}) \quad (9)$$

Note that the viscous dissipation term for energy conservation is neglected because the oil velocity is small and therefore the viscous dissipation is negligible relative to advection and conduction.

2) Nondimensionalization

The dimensionless independent variables are defined as:

$$r^* = \frac{r}{D_h} \quad \text{and} \quad z^* = \frac{z}{D_h} \quad (10)$$

$$u_r^* = \frac{u_r}{u_m} \quad \text{and} \quad u_z^* = \frac{u_z}{u_m} \quad (11)$$

$$p^* = \frac{p}{\rho u_m^2} \quad \text{and} \quad T^* = \frac{T - T_{to}}{T_{aw} - (\mathrm{T}_{to} + \mathrm{T}_{bo})/2} = \frac{T - T_{to}}{g} \quad (12)$$

Substituting (10)-(12) into (7)-(9) and noticing that the hydraulic diameter (D_h), the average oil velocity at the pass inlet (u_m), and the lumped temperatures (T_{aw}, T_{to}, T_{bo}) are not functions of the coordinates, we can get the dimensionless forms of the governing equations as:

$$\frac{1}{r^*}\frac{\partial(\mathrm{r}^* \mathrm{u}_r^*)}{\partial r^*} + \frac{\partial u_z^*}{\partial z^*} = 0 \quad (13)$$

$$\begin{cases} \mathrm{u}_r^* \dfrac{\partial u_r^*}{\partial r^*} + \mathrm{u}_z^* \dfrac{\partial u_r^*}{\partial z^*} = -\dfrac{\partial p^*}{\partial r^*} + \dfrac{1}{\mathrm{Re}}(\dfrac{\partial}{\partial r^*}(\dfrac{1}{r^*}\dfrac{\partial(\mathrm{r}^* \mathrm{u}_r^*)}{\partial r^*}) + \dfrac{\partial^2 u_r^*}{\partial z^{*2}}) \\ \mathrm{u}_r^* \dfrac{\partial u_z^*}{\partial r^*} + \mathrm{u}_z^* \dfrac{\partial u_z^*}{\partial z^*} = -\dfrac{\partial p^*}{\partial z^*} + \dfrac{1}{\mathrm{Re}}(\dfrac{1}{r^*}\dfrac{\partial}{\partial r^*}(\mathrm{r}^* \dfrac{\partial u_z^*}{\partial r^*}) + \dfrac{\partial^2 u_z^*}{\partial z^{*2}}) \end{cases} \quad (14)$$

$$u_r^* \frac{\partial T^*}{\partial r^*} + u_z^* \frac{\partial T^*}{\partial z^*} = \frac{1}{\mathrm{Re} \cdot \mathrm{Pr}}(\frac{1}{r^*}\frac{\partial}{\partial r^*}(\mathrm{r}^* \frac{\partial T^*}{\partial r^*}) + \frac{\partial^2 T^*}{\partial z^{*2}}) \quad (15)$$

3) Flow and Temperature in the Fluid Domain

For OD cooling modes, coolant flow determines heat transfer process, whereas the heat transfer has negligible influence on coolant flow distribution [14]. Therefore, fluid flow and heat transfer can be decoupled with fluid flow being determined first followed by the determination of the corresponding heat transfer.

From (13) and (14), it can be seen that for a fixed winding geometry, which is in a dimensionless sense with all the geometric dimensions normalized against D_h, the dimensionless static pressure (p^*) and the dimensionless velocities (u_r^*, u_z^*) are functions of the dimensionless coordinates (r^*, z^*) and the Reynolds number at the pass inlet. Here *Re* is the coefficient in the dimensionless flow differential equations. The static pressure drop coefficient over the winding model is related to p^* at the inlet and outlet of the winding and the oil flow proportion in a particular horizontal duct is related to u_r^* and u_z^* in that duct. Since the locations for pressure drop and duct flow proportion are fixed, the pressure drop coefficient flow proportion in a duct are only functions of *Re* at the winding pass inlet. It is detailed in [14] about the ways how pressure drop coefficient and flow distribution are controlled by *Re* and dimensionless geometric parameters.

From (15), it can be seen that for a fixed winding geometry and a fixed power loss distribution in dimensionless senses, the dimensionless temperature (T^*) is a function of the dimensionless coordinates (r^*, z^*), *Re* and *Pr*. The dimensionless temperature at the hot-spot in the fluid domain, of which there can be only one location, is actually the convective component of the hot-spot factor (H_{ve}). Therefore, H_{ve} is only a function of *Re* and *Pr*.

D. Determination of the Hot-Spot Factor

From the aforementioned dimensional analyses, it can be concluded that for a fixed winding geometry and a fixed loss distribution in dimensionless senses both the conductive and convective components of *H* are functions of *Re* and *Pr*. The power loss distribution in the winding or the Q' factor will affect *H* directly. The magnitude of the power loss will affect *H* only through its influence on *Re* and *Pr*. Combining (3), (4) and (6), we have:

$$H = \left(\frac{h'}{h} + \frac{h' \cdot \Delta x}{k_p}\right) \cdot Q' + \frac{g'}{g} \tag{16}$$

The ratios of h'/h, $h' \cdot \Delta x/k_p$ and g'/g, are all functions of *Re* and *Pr*, following similar analyses presented in section II part C. It can be seen from (16), *H* is in a linear relationship with Q' and this linear relationship is coupled with the nonlinear relationship between *H* and *Re* and *Pr*. The quantitative relationship between *H* and Q', *Re* and *Pr* can be determined by either experimentation or theoretical calculations.

III. Theoretical Determination of Hot Spot Factor

In this paper, theoretical approach based on CFD simulations and a subsequent correlation exercise is adopted to quantify the relationship between *H* and Q', *Re* and *Pr*.

A. CFD Simulations

CFD models are established using commercial software COMSOL Multiphysics 5.2.

1) Numerical models

In the CFD models, conduction heat transfer is modeled in the solid domain (copper and paper), with copper and paper properties treated as temperature independent in the investigated temperature range [11, 16]:

$$k_c = 401\,(\mathrm{W/(m\cdot K)})$$
$$k_p = 0.19\,(\mathrm{W/(m\cdot K)})$$
$$\rho_c = 8933\,(\mathrm{kg/m^3})$$
$$\rho_p = 930\,(\mathrm{kg/m^3})$$
$$\mathrm{c}_{pc} = 385\,(\mathrm{J/(kg\cdot K)})$$
$$\mathrm{c}_{pp} = 1340\,(\mathrm{J/(kg\cdot K)})$$

For the convection heat transfer in the fluid domain, since the Reynolds numbers for practical winding cooling situation are smaller than the transition criterion to turbulence, no turbulence model is included in the CFD models. The continuity equation, Navier-stokes equations and the energy equation are solved directly, taking into account buoyancy force and without adopting the Boussinesq approximation. It is worth mentioning that the use of the Boussinesq approximation to take into account buoyancy forces brings negligible differences in flow distribution and temperature distribution as compared to a fluid flow and heat transfer fully coupled model [16]. These equations solved in the CFD models differ from (7)-(9) in the way that the properties of the fluid, a mineral oil, are treated as functions of temperature. The oil properties are obtained from least-square curve fittings of the data provided by the oil manufacturer, given as follows:

$$\rho = -0.6568 \times \mathrm{T} + 1064 \tag{17}$$
$$\mu = 7.863 \times 10^{-5} \times \exp(632.0/(\mathrm{T}-176.0)) \tag{18}$$
$$k = -7.837 \times 10^{-5} \times T + 0.1557 \tag{19}$$
$$c_p = 3.950 \times T + 560.2 \tag{20}$$

where the temperatures are in Kelvin.

In this paper, conjugate heat transfer modeling as specified in [16] is adopted for the numerical investigation.

2) Mesh Refinement Study

In the CFD models, the meshes consist of rectangular layers, as illustrated in Fig. 1(c). The rounding radii of the strands are omitted because the practical range of the rounding radii of the strands have negligible influence on oil flow distribution in the winding pass [14], whereas omitting the rounding radii can facilitate mesh control significantly. In the meshes, 4 elements are present to discretize the 0.5 mm paper thickness, as recommended in [11], and 256 elements are present to discretize each copper strand. In the fluid domain, the rectangular layers are structured in such a way that more elements are present close to the duct wall to capture the thermal and hydraulic boundary layers. Mesh refinement study of the fluid domain for the case of *Re* being 200 and *Pr* being 150 is performed. The tracking parameter for each mesh size or number of fluid domain

elements (N_{de}) is H. The mesh refinement study results are shown in Table I.

As can be seen from Table I, the differences in H obtained from the four mesh strategies are negligible. Nevertheless, a finer mesh size can better capture the hot-streak dynamics. Therefore, the mesh strategy corresponding to mesh 4, which discretizes the 3 mm horizontal duct height with 60 elements and the 8 mm vertical duct width with 80 elements, is adopted for all the CFD models.

TABLE I
MESH REFINEMENT STUDY RESULTS

Strategy	mesh 1	mesh 2	mesh 3	mesh 4
N_{de}	389,480	596,800	766,320	1,087,040
H	1.1924	1.1869	1.1867	1.1869
Computational time	18 minutes	36 minutes	50 minutes	68 minutes

B. Uniform Power Loss Distribution Cases

Power losses in the winding conductor consist of resistive losses and eddy current losses. For a fixed winding geometry, the resistive losses are dictated by the current density and copper temperature and the eddy current losses are dictated by the leakage magnetic flux distribution and copper temperature. For power transformers, the current density in the copper wire ranges from 2-4 A/mm^2 [15], and the average winding temperature rise over ambient temperature is required to be not higher than 65 K. For uniform-loss cases that account only the resistive losses, volumetric heat source of 3.397×10^5 W/m^3, corresponding to the condition of current density being 4 A/mm^2 and copper resistance at 85 ℃, is prescribed to each copper strand. The study of uniform loss cases is to investigate the effect of flow distribution on the hot-spot factor.

1) Parametric Sweeps and Correlations

For the fixed winding geometry shown in Fig. 1 with a uniform loss distribution (Q=Q'=1), the hot-spot factor is a function of Re and Pr, which are defined at the average temperature of the top oil and bottom oil temperatures. The bottom oil temperature is a given condition and the top oil temperature can be calculated according to energy conservation, as shown in [14] section V part B. The quantitative relationship between H and Re and Pr can be obtained by conducting CFD parametric sweeps and correlating the H results from CFD with Re and Pr.

a. Parametric sweeps

For OD cooling modes, Re is set to range from 200 to 1200. For the mineral oil whose properties as functions of temperature are shown in (17)-(20), when average oil temperature increases from 30 ℃ to 80 ℃, Pr decreases from 151 to 43. Therefore, in the parametric sweeps, Pr ranges from 60 to 150. The discrete Re and Pr swept are shown in Table II.

TABLE II
RANGES OF THE SWEPT DIMENSIONLESS PARAMETERS

Re	200, 300, 400, 500, 600, 700, 800, 900, 1000, 1100, 1200
Pr	60, 100, 150

All the combinations of Re and Pr in Table II, in total 33 cases, are simulated to quantify the relationship between H and Re and Pr. It is worth emphasizing that according to the principle of dimensional analysis it is Re and Pr themselves rather than their components that determines H [14].

It is concluded in [14] that with the increase of Re, oil flow distribution in the winding pass gets less uniform with more oil flowing through the top horizontal ducts in a pass and hence bottom ducts suffering from oil starvation. Therefore, the temperature distribution could become less uniform with the increase of Re. Figure 2 shows an example, where Pr of both cases is fixed to be 100. When Re is 200, temperature distribution in the winding is rather uniform as a result of rather uniform flow distribution. For the case of Re being 1200, temperature distribution gets uneven because oil starvation in the bottom ducts of each pass causes localized overheating. The flow distributions in the top pass for the two cases are shown in Fig. 3. Furthermore, reverse flow at the bottom of the pass can occur with a further increase of Re [14].

The variations of H with Re and Pr from the CFD parametric sweeps are shown in Fig. 4. Because the loss distribution is uniform, the hot-spot temperature is determined by oil flow distribution. As can be seen in Fig. 4, when Re<600, H fluctuates slightly as the hot-spot temperature shifts from the middle to the bottom of pass 3 with the increase of Re. When Re>600, H increases with increasing Re due to more uneven flow distribution. The fact that H is 1.2 at low Re is due to both uneven radial and axial temperature distribution in the winding. In addition, Pr in its practical range is much less influential than Re.

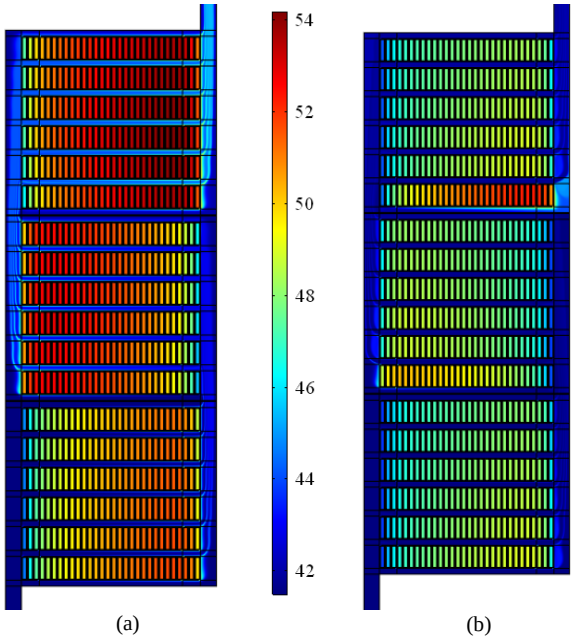

Fig. 2. Temperature distribution in the winding for Pr=100 in Celsius. (a) Re=200; (b) Re=1200. (a) and (b) share the same colorbar.

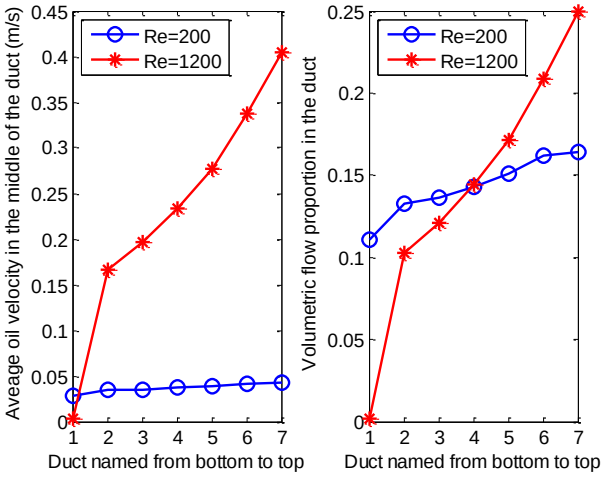

Fig. 3. Flow distribution in the winding model.

b. Correlations

The hot-spot factors obtained from the CFD parametric sweeps are correlated with *Re* and *Pr* by multilayer least-square curve fittings in the form of:

$$\begin{cases} H = \exp(a_1(\frac{\mathrm{Re}}{1000})^3 + a_2(\frac{\mathrm{Re}}{1000})^2 + a_3(\frac{\mathrm{Re}}{1000}) + a_4) \\ a_i = b_{i1}(\frac{\mathrm{Pr}}{100})^2 + b_{i2}(\frac{\mathrm{Pr}}{100}) + b_{i3} \qquad i = \{1,2,3,4\} \end{cases} \tag{21}$$

where the correlation coefficients a_1 to a_4 are dummy coefficients, which are dictated by *Pr* and the corresponding *b* coefficients. With all the *b* coefficients provided in Table III, *H* for any combination of *Re* and *Pr* can be obtained from (21). With the least-square curve fitting strategy, the maximum relative error between *H* obtained from (21) and that from the CFD simulations is 1.34%. It is worth mentioning the correlation coefficients in Table III are specific to the winding shown in Fig. 1 because the geometry of the winding defines boundary conditions for (13)-(15) and therefore results in different solutions.

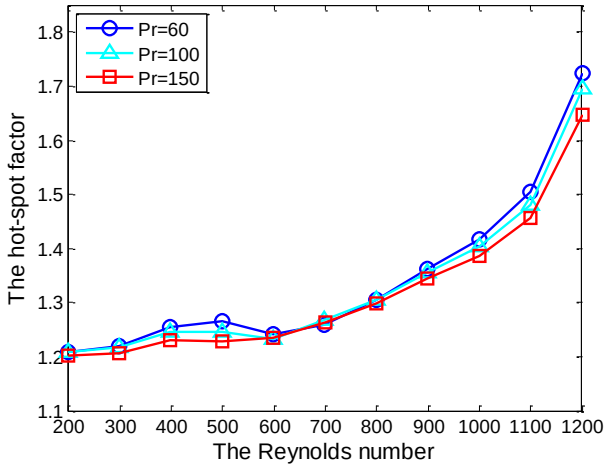

Fig. 4. Variation of H with *Re* and *Pr*.

TABLE III
CORRELATION COEFFICIENTS

b_{ij}	*j*=1	*j*=2	*j*=3
i=1	0.0217	-0.3199	1.0633
i=2	-0.0898	0.6795	-1.7344
i=3	0.0931	-0.4571	0.9839
i=4	-0.0300	0.0896	0.0408

2) Verifications and Predictions

In order to verify the correlation (21) obtained, new CFD simulations are performed for comparison purposes. For the new simulations, winding pass inlet oil temperature is fixed to be 40 ℃ and pass inlet average oil velocity is set to range from 0.2 m/s to 0.5 m/s with an interval of 0.1 m/s. Two uniform loss distributions are tested. One is of volumetric power density 3.397×10^5 W/m^3 corresponding to the current density of 4 A/mm^2 with copper resistance at 85 ℃. The other is of volumetric power density 7.643×10^5 W/m^3 corresponding to the current density of 6 A/mm^2 with copper resistance at 85 ℃. In all these CFD cases, the Prandtl numbers are approximately 100±7.

The comparisons of *H* obtained from the new CFD simulations and the prediction curve obtained from correlation (21) with *Pr* being 100 are shown in Fig. 5 (a). It can be seen that *H* from the CFD simulations with different power losses fall close to the prediction curve with maximum absolute error being 0.018 and maximum relative error being 1.39 %. It is worth mentioning that this maximum relative error of 1.39% is close to the maximum relative error of 1.34% when deriving the correlation (21) and this further verifies the applicability of the correlation and that *H* is determined by the loss distribution pattern rather than the magnitude of the losses.

The hot-spot temperature can be calculated from the definition of *H*. In the calculations, the top oil and average oil temperatures are derived from energy conservation and the average winding temperature is taken from the CFD simulations, which is permissible because in practice average winding temperature can be derived from winding resistance measurements. The comparisons of T_{hs} derived from the correlation of *H* and those from the new CFD simulations are shown in Fig. 5 (b). It can be seen that T_{hs} from both methods are almost identical for both power losses with maximum deviation being 0.2 ℃.

The hot-spot temperature shown in Fig. 5 (b) decreases at first with the increase of *Re*, which is proportional to total oil flow rate for a fixed winding geometry and a fixed oil type, then the hot-spot temperature starts to level off. In fact, with a further increase of *Re*, the hot-spot temperature tends to increase. This varying trend of T_{hs} with *Re* is caused by the variation of oil flow distribution in the winding pass. With a higher *Re*, i.e. a higher flow rate, the flow distribution gets more uneven and causes localized overheating and higher *H*. This influence of the flow distribution on T_{hs} is characterized by the variation of *H* illustrated in Fig. 4 and more specifically in Fig. 5 (a).

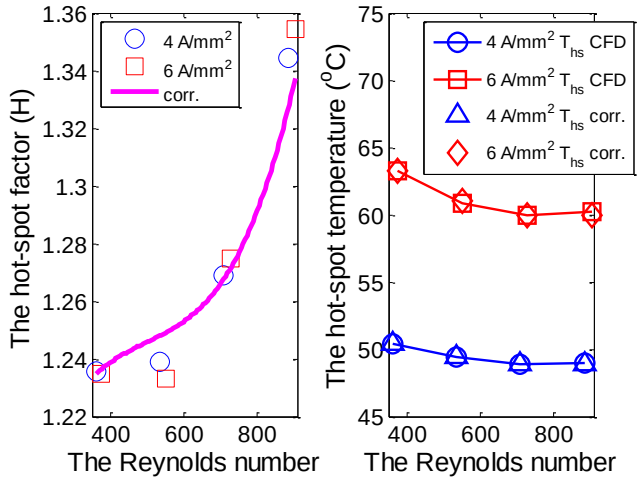

Fig. 5. Comparisons of H and the hot-spot temperatures obtained from theoretical calculations and new CFD simulations.

C. Nonuniform Power Loss Distribution Cases

In a transformer winding, the eddy current losses concentrate on the top and bottom of the winding. For the 3-pass winding model shown in Fig. 1, extra losses are prescribed to the top three discs to represent the presence of eddy current losses. The 3-pass winding model can therefore be regarded as the top 3 passes of a practical winding. All the discs except for the top three maintain the resistive loss of 3.397×10^5 W/m^3. The losses in the top three discs from the top of the winding are raised to the power ratios of n_1, n_2, n_3 relative to the resistive loss. Loss variation along the radial direction is ignored. Five sets of nonuniform loss cases shown in Fig. 6 are simulated by CFD simulations. The corresponding Q values are shown in Table IV

Since Pr is much less influential than Re, Pr is controlled to be 100 and Re ranges from 200 to 1000, which is a practical range of Re, with an interval of 200 in these simulations. The hot-spot temperatures of these cases locate at the top disc because of the highest extra losses at that disc. Therefore, Q equals Q' and H is a function of Re and Q. The variations of H and T_{hs} with Re and Q for these cases are shown in Fig. 7 (a) and (b), respectively. It can be seen that both H and T_{hs} decrease monotonically with the increase of Re, and increase monotonically with the increase of Q factor.

TABLE IV
NONUNIFORM-LOSS CASES

	Case 1	Case 2	Case 3	Case 4	Case 5
n_1	1.3	1.6	1.8	2.0	2.2
n_2	1.2	1.4	1.5	1.5	1.8
n_3	1.1	1.2	1.2	1.2	1.2
Q	1.27	1.54	1.71	1.89	2.05

n_1 refers to the ratio of power loss at the top disc to the average power loss, n_2 refers to the ratio for the second disc from the top, n_3 refers to the ratio for the third disc from the top.

The variations of H with Q for different Reynolds numbers are shown in Fig. 8. As can be seen, H increases linearly with increasing Q (Q'), verifying the linear relationship predicted in (16). In addition, the slops for different Reynolds numbers are almost identical, indicating that the term $h'/h + h'\cdot dx/k_p$ is quite constant for the five Reynolds numbers investigated.

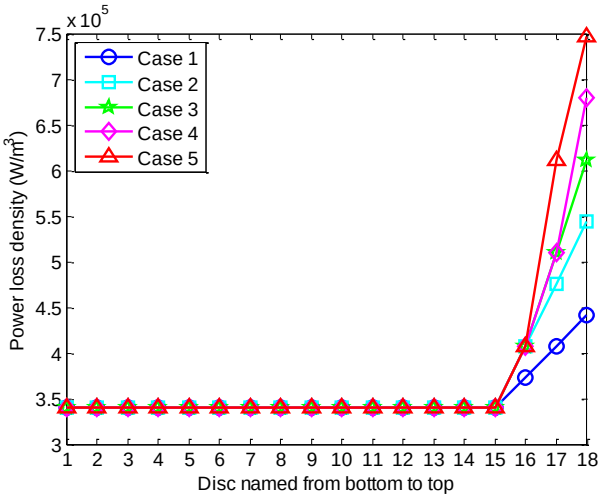

Fig. 6. Nonunifrom loss distribution in the winding model.

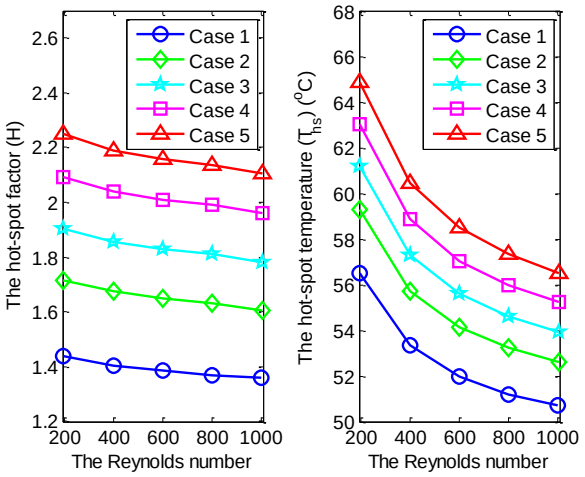

Fig. 7. The variations of H and T_{hs} with Re for nonuniform-loss cases.

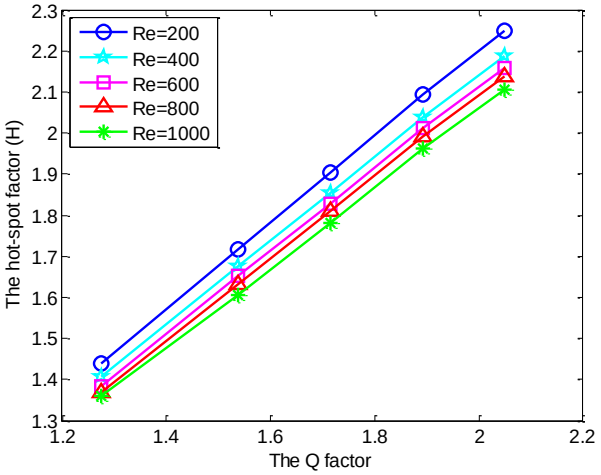

Fig. 8. The variation of H with the Q factor for different Reynolds numbers.

IV. Discussions

The hot-spot factor, *H*, is a crucial component of the thermal diagram for determining the hot-spot temperature from temperature rise test data. The linearity assumptions in the thermal diagram, however, make the concept of *H* more empirical than theoretical. Therefore, *H* is still open to better interpretation.

A. Interpretation of the Hot-Spot Factor

This paper presents a different interpretation of *H* based on dimensional analyses of the fluid flow and heat transfer processes in the winding, rather than the linearity assumptions in the thermal diagram.

According to the dimensional analysis shown in section II part *C*, *H* is interpreted as the dimensionless temperature at the hot-spot. The locations of the lumped temperatures ($T_{aw,}$ T_{to}, T_{bo}) in the definition of *H* do not affect the physical meaning of *H*, but will affect the magnitude of *H* derived. For example, wherever the location of the top oil temperature is defined, top of the winding or top of the tank, once the location is fixed the top oil temperature will no long be a function of the coordinates and therefore the same dimensionless governing equations will be applicable, giving *H* the same physical meaning.

B On the Experimentally Derived H from CIGRE Report

A statistic of *H* based on optical fibre measurements during heat run tests was previously provided in [9] when CIGRE conducted work on experimental determination of power transformer hot-spot factor. For OD transformers, 27 hot spot factors were obtained with the minimum being 0.51 and the maximum 1.83; statistically resulting in a mean of 1.18 with standard deviation of 0.29.

The hot spot factors less than 1 are likely due to the fact, apart from measurement errors, that the installation of fibre-optic temperature sensors in the radial spacers unintentionally allowed oil flowing into the sensor area which resulted in the temperature in the fluid domain being measured. Therefore, the hot-spot factors derived might be their convective components, H_{ve}, which was introduced previously in this paper and can be less than 1 due to the presence of the paper insulation in the winding. As an example, when *Re* is less than 1000, the convective hot-spot factors obtained for the uniform loss cases in section III part B are always less than 1. Another likely reason could be that the temperature measured was not the hot-spot temperature because the hot-spot can be located at the bottom of the top pass, as shown in Fig. 2 (b).

The maximum hot spot factor was 1.83 for the measured OD transformers in the CIGRE report, such a scenario could occur as the case demonstrated when *Re* is as high as 1200 for the winding studied shown in Fig. 1. The mean of the hot spot factors obtained being 1.18 in the report is close to the hot spot factors in Fig. 4 when *Re* is around 600, which should be regarded as an optimal operational regime.

It is worth emphasizing that Fig. 4 and the correlation coefficients in Table III for (21) are specific to the winding investigated under uniform loss distribution condition. However, the general trend of *H* variation with *Re* and *Pr* and the magnitude of *H* shown in Fig. 4 would be representative for all winding geometries. The reasoning is as follows: oil flow distribution in the winding tends to be reasonably uniform when *Re* is moderate corresponding to a moderate total oil flow rate and moderate oil temperature [14], which would lead to a reasonably uniform temperature distribution and a hot spot factor close to 1. On the other hand, with the increase of *Re*, which is usually due to an increase of total oil flow rate, flow distribution would start to get uneven [14]. Hence the effect of increasingly uneven flow distribution competes with the effect of increased total oil flow rate, and results in a slightly fluctuating or stable hot spot factor. However, when *Re* is increased too much, the flow distribution becomes severely uneven and reverse flow even occurs [14], and this can jeopardize the cooling performance, so high hot spot factors are observed. For OD cooling modes, it is not necessarily the higher the total oil flow rate the better the cooling performance. In a word, the influence of operational conditions, which can affect *Re* and *Pr*, has been investigated in this paper for a given winding geometry. If the influence of geometric parameters is to be taken into account for (21), CFD geometric parameter sweeps are needed, of which the method is shown in [14].

C. Influence of Operational Conditions on H

Heat transfer analysis decomposes *H* into two separable components: H_{du} and H_{ve}. Both components are related to dimensionless winding geometry, power loss distribution, *Re* and *Pr*. With this decomposition and the understanding of the two components, *H* for OD transformers can be better understood in terms of how it is controlled by the ambient temperature, the total oil flow rate, and the loading level.

1) Influence of ambient temperature

The ambient temperature affects *H* indirectly through changing oil properties to change *Re* and *Pr*. Therefore, the effect of ambient temperature on *H* depends on both the fluctuation range of ambient temperature, oil property sensitivity to temperature and transformer operational regime.

One of the cases in section III-B-2 can be taken as an example to demonstrate the influence of ambient temperature on *H*. The chosen case was shown in Fig. 5, where the winding inlet velocity is 0.4 m/s; the power loss density is 3.397×10^5 W/m^3 (equivalent to a current density of 4 A/mm^2); the average oil temperature is 40 ºC; *Re* and *Pr* are 700 and 107, respectively. To demonstrate the influence of ambient temperature on *H*, two reasonable assumptions are further made. First, the average oil temperature of 40 ºC corresponds to an ambient temperature of 20 ºC, i.e. average oil temperature rise over ambient is a constant of 20 K for the investigated winding model. Second, when the ambient temperature changes the total oil flow rate and power losses in the winding are kept unchanged. Therefore, the average oil temperature changes linearly with the ambient temperature, subsequently changing *Re* and *Pr*. The variation of *H* with ambient temperature for the case can then be obtained through (21) as shown in Fig. 9.

As can be seen in Fig. 9, the variation of ambient temperature can have either a negligible or profound influence on *H*. On one hand, *H* does not change significantly when the ambient temperature is lower than 20 ºC (this is corresponding to a regime when the transformer is

operated with *Re*<700 shown in Fig. 4), so variation of ambient temperature when lower than 20 ºC has a negligible influence on *H*. However, on the other hand when the ambient temperature is higher than 20 ºC the increase of ambient temperature can result in a profound influence on *H*, as this corresponds to a critical regime of *Re*>700 shown in Fig. 4, where a moderate increase of *Re* can result in an obvious increase of *H*.

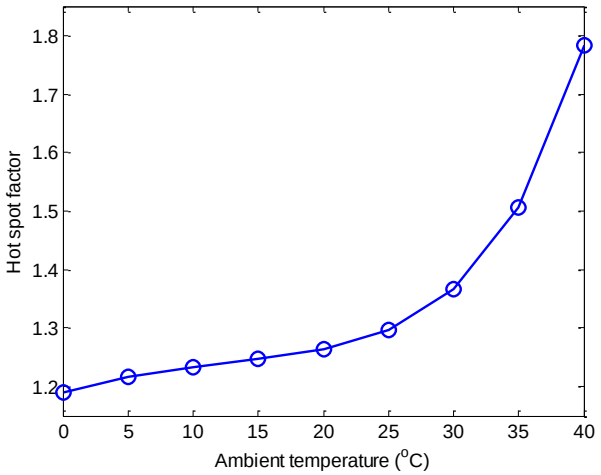

Fig. 9. Example of influence of ambient temperature on hot spot factor.

2) Influence of total oil flow rate

The total oil flow rate determines *Re* directly. Depending on flow distribution and loss distribution, the total oil flow rate can have a moderate influence on *H* if it is a uniform loss distribution with *Re*<600, as shown in Fig. 4, or have a significant influence if it is a uniform loss distribution with *Re*>600, or a uneven power loss distribution, as shown in Fig. 7 (a).

3) Influence of loading level

The influence of the loading level or the power loss distribution on *H* is from the *Q*' instead of the magnitude of the loss, i.e. *H* is not related to load factor, K, but *Q'*, as shown in Fig. 8.

In general, the hot-spot locates at the point of the highest power loss as shown in section III part C-unless the flow is so uneven that a serious local overheating is resulted, which anyway should be avoided. Therefore, *Q*' can be regarded to be the same as *Q* and by so doing the hot-spot temperature could be slightly over estimated.

For a fixed winding geometry, when the hot-spot is at the point of the highest power loss, *H* is in a linear relationship with *Q* and this linear relationship is coupled with the nonlinear relationship between *H* and *Re* and *Pr*. The Prandtl number is much less influential than *Re*. Therefore, according to (16) and the dimensional analyses on fluid flow and heat transfer, *H* can be expressed qualitatively as:

$$H = f_s(\mathrm{Re},\mathrm{Pr})\cdot Q + f_i(\mathrm{Re},\mathrm{Pr}) \approx f_s'(\mathrm{Re})\cdot Q + f_i'(\mathrm{Re}) \quad (22)$$

where $f_s(Re,Pr)$ and $f_s'(Re)$ represent the slope term $h'/h + h'\cdot dx/k_p$ and $f_i(Re,Pr)$ and $f_i'(Re)$ represent the intercept term g'/g.

For the investigated cases in section III part C, when *Re* ranges from 200 to 1000, the slope term ranges from 0.969 to 1.05 and the intercept term ranges from 0.100 to 0.122. The slope term and the intercept term are quite constant, indicating the importance of having a moderate *Q* factor because *Q* is almost directly added into *H*.

Compared to the formula in IEC 60076-2: 2011, $H=S\times Q$, (22) replaces the *S* factor with *Re* and *Pr* (or solely with *Re*) and changes the formula as well.

D. On Winding Temperature Indicator

The quantitative relationship between *H* and the dimensionless controlling parameters, *Q*, *Re* and *Pr* for a transformer can be obtained through experimental or numerical parametric sweeps. When the relationship is quantified, the real-time hot-spot factor can be determined according to real-time operational conditions and therefore the real-time hot-spot temperature can be obtained through a winding temperature indicator, which is widely used to control the operation of the pumps and fans.

V. Conclusion

The hot-spot factor, *H*, is interpreted as the dimensionless temperature at the hot-spot based on dimensional analyses of fluid flow and heat transfer. *H* is decomposed into the sum of two separable components: the conductive component, H_{du}, and the convective component, H_{ve}. For a fixed winding geometry with a fixed power loss distribution in dimensionless senses in OD cooling modes, no matter it is uniform or not, both components are functions of *Re* and *Pr*.

The relationship between *H* and *Re* and *Pr* for uniform-loss cases has been obtained by performing CFD parametric sweeps and correlating the hot-spot factors from CFD results with *Re* and *Pr*. The correlation has been verified by the consistency between the hot-spot factors obtained from new CFD simulations and the corresponding ones obtained from the correlation.

When the loss distribution is a variable, *H* is a function of the *Q* factor, *Re* and *Pr*. For the condition of the hot-spot at the location of the highest power loss, *H* is in a linear relationship with *Q* and this linear relationship is coupled with the nonlinear relationship between *H* and *Re* and *Pr*. Therefore, the overall relationship between *H* and *Q*, *Re* and *Pr* is nonlinear and experimental or numerical parametric sweeps are needed to quantify the relationship.

Acknowledgment

The authors would like to express their gratitude to M&I Materials, National Grid, Scottish Power, Shell, TJ|H2b Analytical Services, UK Power Networks and Weidmann Electrical Technology for their financial and technical contributions to the Transformer Research Consortium at The University of Manchester.

References

[1] Loading guide for oil-immersed power transformers, IEC standard IEC 60076-7, 2005.

[2] IEEE Guide for Loading Mineral-Oil-Immersed Transformers and Step-Voltage Regulators, IEEE standard C57.91, 2011.

[3] W. Lampe, L. Pettersson, C. Ovren, "Hot-spot measurements in power transformers," CIGRE, Pep. 12-20, 1984.

[4] H. Nordman, and M. Lahtinen, "Thermal overload tests on a 400-MVA power transformer with a special 2.5-pu short time loading capability," *IEEE Trans. Power Del.*, vol. 18, no. 1, pp. 107-112, 2003.

[5] P. Picher, F. Torriano, M. Chaaban, s. Gravel, C. Rajotte, B. Girard, "Optimization of transformer overload using advanced thermal modelling." CIGRE Pep. A2-305, 2010.

[6] A. J. Oliver, "Estimation of transformer winding temperatures and coolant flows using a general network method," *Proc. Inst. Elect. Eng.*, vol. 127, pp. 395-405, 1980.

[7] Temperature rise for liquid-immersed transformers, IEC standard 60076-2, 2011.

[8] Z. Radakovic, U. Radoman, and P. Kostic, "Decomposition of the Hot-Spot Factor," *IEEE Trans. Power del.*, vol. 30, pp. 403-411, 2015.

[9] "Experimental determination of power transformer hot-spot factor," CIGRE WG 12-09, Electra no. 161, August 1995.

[10] D. Feng, Z. Wang, and P. Jarman, "Evaluation of Power Transformers' Effective Hot-Spot Factors by Thermal Modeling of Scrapped Units," *IEEE Trans. Power Del.*, vol. 29, no. 5, pp. 2077-2085, 2014.

[11] F. Torriano, P. Picher, and M. Chaaban, "Numerical investigation of 3D flow and thermal effects in a disc-type transformer winding," *Appl. Therm. Eng.*, vol. 40, pp. 121-131, 2012.

[12] X. Zhang, Z. D. Wang, Q. Liu, A. Gyore, P. Jarman, P. Dyer, "Investigation of Convective Heat Transfer Efficiency in the Horizontal Cooling Duct of a Disc Type Transformer Winding," Paper ID 280, 19th ISH, Czech Republic, 2015.

[13] T. L. Bergman, F. P. Incropera, and A. S. Lavine, *Fundamentals of heat and mass transfer*: John Wiley & Sons, 2011.

[14] X. Zhang, Z. Wang, and Q. Liu, "Prediction of Pressure drop and flow distribution in disc type transformer windings in an OD cooling mode," *IEEE Trans. Power Del*., 2016, DOI (identifier) 10.1109/TPWRD.2016.2557490, In press.

[15] M. Heathcote, *J & P transformer book*, Thirteenth ed.: Newnes, 2007.

[16] F. Torriano, M. Chaaban, and P. Picher, "Numerical study of parameters affecting the temperature distribution in a disc-type transformer winding," *App. Therm. Eng.*, vol. 30, no. 14, pp. 2034-2044, 2010.

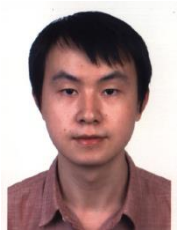

Xiang Zhang received the B.Eng. degree in Electrical and Electronic Engineering from Xi'an Jiaotong University, Xi'an, China, in 2012 and is currently pursuing the Ph.D. degree at power and energy division of the School of Electrical and Electronic Engineering at The University of Manchester, Manchester, UK. His research programme is on transformer thermal modelling.

Zhongdong Wang received the BSc and the MSc degrees in high voltage engineering from Tsinghua University in 1991 and 1993 and the PhD degree in electrical engineering from UMIST in 1999. Currently she is a Professor of High Voltage Engineering of the School of Electrical and Electronic Engineering at The University of Manchester. Her research interests focus on power transformers covering all aspects of modelling and simulation, materials & systems, and asset management policies.

Qiang Liu (S'08-M'12) obtained the B.Eng. degree in electrical engineering (2005) and the M.Eng. degree in high voltage and electrical insulation (2008) from Xi'an Jiaotong University in China, and the Ph.D. degree in electrical power engineering (2011) from The University of Manchester in the UK. Currently he is a Senior Lecturer of the School of Electrical and Electronic Engineering at The University of Manchester. His research interests are on pre-breakdown and breakdown phenomena in liquids, ester transformer liquids, streaming electrification, ageing of insulating materials, transformer asset management and high voltage testing.

Chapter 4 ON Cooling Modes

4.1 Introduction

Compared to an OD transformer, the total oil flow rate in an ON transformer arising from thermosiphon is usually one order of magnitude lower, causing the pressure drop over the winding to be about one or two orders of magnitude lower than its OD counterpart [23, 53]. In practice, the measurement of the static pressure drop over the winding in an ON cooling mode is not feasible due to its low magnitude. In addition, static pressure drop over the winding is not as dominant in determining oil split among windings as in OD cooling modes and a relatively uniform oil split is likely to be established for an ON transformer because of the following reasoning. A lower flow rate in a winding will cause higher temperature gradient and therefore higher buoyancy forces in that winding, which in turn will drive up the flow rate in that winding and eventually lead to a relatively uniform oil split among windings connected hydraulically in parallel. Therefore, pressure drops over ON transformer windings are not investigated in this chapter.

The study of fluid flow and heat transfer in an ON transformer winding is even more challenging than in an OD transformer winding because the hydraulic system and the thermal system are fully coupled and therefore cannot be considered separately. In this chapter, dimensional analysis is also adopted to provide guide to CFD simulations. Due to the fact that ON CFD simulations are much more difficult to converge and more time consuming than OD CFD simulations, only the influences of the total liquid flow rate in the winding, the total power loss in the winding and the fluid properties are investigated in this chapter. Paper 1 investigates the oil flow distribution and temperature distribution in an ON transformer winding. Paper 2 conducts case studies on three different liquids with a theoretical prediction of the total flow rates in the winding for the three liquids investigated.

4.2 **Paper 5**

Numerical Investigation of Oil Flow Distribution and Temperature Distribution for ON Transformer Windings

Xiang Zhang, Zhongdong Wang, Qiang Liu, Paul Jarman and Massimo Negro

2017

Applied Thermal Engineering

To Be Submitted

Numerical Investigation of Oil flow Distribution and Temperature Distribution for ON Transformer Windings

Xiang Zhang, Zhongdong Wang, Qiang Liu, Paul Jarman, Massimo Negro

***Abstract*—In this paper, numerical investigation of oil flow distribution and temperature distribution is performed for a disc-type transformer winding in oil natural (ON) cooling modes. First, dimensional analysis is performed based on the governing differential equations with the adoption of the Boussinesq approximation. *Re*, *Gr/Re*^{2} and *Pr* are found to be the governing dimensionless parameters in determining flow and temperature distribution. Then a CFD case study of the winding model is performed as a benchmark case, in which reverse flow and hot-plumes are observed. After the case study, CFD parametric sweeps of *Re* and *Gr/Re*^{2} are executed. It is found from the parametric sweeps that the minimum value of the hot-spot factor, which characterizes the thermal performance of the transformer, is achieved in a relatively narrow and fixed range of *Gr/Re*^{2} (from 0.4 to 0.6) regardless of the values of *Re* and *Pr* in their practical ranges. The relationship of an invariable minimum hot-spot factor with a fixed narrow range of *Gr/Re*^{2} makes the optimization of the transformer design and operation possible. Finally, a new CFD case study is performed based on the benchmark case to confirm the shifting of an uncontrolled operational regime to a quasi-optimal one by changing *Gr/Re*^{2} from 1.46 in the benchmark case to 0.6 in the new case.**

***Keywords*—Disc-type transformer, Dimensional analysis, CFD, hot-spot factor, optimal operational regime**

NOMENCLATURE

c_p	Oil specific heat at constant pressure ($J/(kg \cdot K)$)
c_{pp}	Paper specific heat at constant pressure ($J/(kg \cdot K)$)
c_{pc}	Copper specific heat at constant pressure ($J/(kg \cdot K)$)
D_h	Hydraulic diameter at the pass inlet ($2 \times W_{inn}$) (m)
g	Gravitational acceleration (m/s^2)
g_{ave}	Average temperature gradient (T_{aw}-(T_{to}+T_{bo})/2) (K)
Gr	The Grashof number ($g\beta(T_{aw}-(T_{to}+T_{bo})/2)D_h^3/\nu^2$)
Gr/Re^2	The ratio of Gr to Re^2 ($g\beta(T_{aw}-(T_{to}+T_{bo})/2)D_h/u_m^2$)
h	Heat transfer coefficient of the winding ($W/(m^2 \cdot K)$)
H	The hot-spot factor ($(T_{hs}-T_{to})/(T_{aw}-(T_{bo}+T_{to})/2)$)
k	Oil thermal conductivity ($W/(m \cdot K)$
k_p	Paper thermal conductivity ($W/(m \cdot K)$)
k_c	Copper thermal conductivity ($W/(m \cdot K)$)
Nu	The Nusselt number ($h \cdot D_h/k$)
p	Static pressure (Pa)
p_{to}	Top oil static pressure (Pa)
Pr	The Prandtl number ($\mu \times c_p / k$)
q"	Heat flux at the hot-spot (W/m^2)
r	Coordinate in radial direction (m)
Re	The Reynolds number ($u_m \times \rho \times D_h / \mu$)
Ra	The Rayleigh number ($Gr \cdot Pr$)
T	Temperature (K)
ΔT	Temperature gradient across the paper insulation (K)
T_{aw}	Average winding temperature (K)
T_{bo}	Oil temperature at the bottom of the winding (K)
T_{bulk}	Bulk oil temperature surrounding the hot-spot (K)
T_{hs}	The hot-spot temperature in the disc (K)
T_{hs}^*	Dimensionless highest temperature in fluid domain
T'_{hs}	The hot-spot temperature in the fluid domain (K)
T_{to}	Oil temperature at the top of the winding (K)
u_m	Average oil velocity at the winding inlet (m/s)
u_r	Radial velocity component (m/s)
u_z	Axial velocity component (m/s)
W_{inn}	Inner vertical duct width (m)
W_{out}	Outer vertical duct width (m)
Δx	The thickness of the paper insulation (m)
z	Coordinate in axial direction (m)
β_T	Oil volumetric thermal expansion coefficient ($1/K$)
ρ	Oil density (kg/m^3)
ρ_{to}	Top oil density (kg/m^3)
ρ_p	Paper density (kg/m^3)
ρ_c	Copper density (kg/m^3)
μ	Dynamic viscosity ($Pa \cdot s$)
ν	Kinematic viscosity (m^2/s)

I. Introduction

Power transformers connect electric power networks of different voltage levels and convert electric power efficiently. However, the power losses in the transformer can be problematic though it is a small fraction of the power conveyed by the transformer (around 1%). The power losses in the transformer cause temperature rises in transformer windings, which are usually wrapped with insulation paper. The thermal ageing of the insulation paper accelerates with the increase of temperature. It is generally taken that every increase of 6 ^oC will double the paper thermal ageing rate [1, 2]. The highest temperature in the winding, usually referred to as the hot-spot temperature, is therefore of great importance to guide transformer thermal design and transformer operation especially in overloading conditions.

The determination of the hot-spot temperature relies mainly on empirical methods, e.g. the thermal diagram [1, 3] and thermal modelling of the winding because direct measurements using fibre optic temperature sensors are not

yet readily available. In addition, the positioning of the sensors to measure the hot-spot temperature requires an accurate thermal modelling [4].

Transformer thermal modelling in steady state is done by either utilising thermal-hydraulic network models [5-7] or models that incorporate computational fluid dynamics (CFD) [8, 9]. These two methods share the same physical principles, i.e. conservation of mass, momentum and energy. Compared to CFD models, network models are computationally more economical, which employ correlations to simplify the fluid flow and heat transfer processes. To improve the performance of network models, CFD results can be employed to calibrate the correlations adopted in network models [10-12].

For transformers in oil natural (ON) cooling modes, CFD simulations have revealed important flow and temperature distribution features [13, 14]. A strong coupling of fluid flow and temperature distribution exists between different passes due to hot streak dynamics, which are also responsible for the occurrence of reverse flows in certain passes [13]. The comparisons of fluid flow and temperature distributions between 2D axisymmetric and 3D CFD models illustrate that 2D results can be representative as long as the governing dimensionless parameters (Gr/Re^2) are matched [14]. In addition, improvement strategies can be employed to derive key 3D results, e.g. hot-spot temperature from axisymmetric 2D simulations [14]. It is worth mentioning that the winding geometries in [13] and [14] are the same except that the winding pass inlets in the last 4 passes are on the opposite sides.

In order to generalize the CFD results and provide generally useful guidance on transformer thermal design and transformer operation, dimensional analysis can be adopted. For transformers in oil forced and directed (OD) cooling modes, dimensional analysis was adopted in [15, 16] to guide the CFD parametric sweeps to investigate fluid flow and temperature distribution in and pressure drop over disc-type transformer windings.

In the present study, both oil flow distribution and temperature distribution in an ON transformer winding are investigated. The winding geometry investigated is the same as that in [4, 9, 14]. Therefore, comparisons of flow distribution and temperature distribution in a one pass model with [9] act as a useful numerical verification of the numerical models employed in this paper. Dimensional analyses on the governing equations are performed with the adoption of the Boussinesq approximation to provide insight into the fluid flow and heat transfer behaviour as well as guidance on parametric sweeps. In so doing, the flow and temperature distribution results are generalized and the optimal operational regime for the investigated winding is identified and verified by a subsequent case study.

II. Winding Geometry under Investigation

The winding under investigation is a LV winding of a 66 MVA 225/26.4 kV ONAN/ONAF transmission transformer [4, 14]. This LV winding consists of 4 passes with pass 1 at the bottom being an anomaly, as shown in Fig. 1. There are 2 parts in pass 1. Part 1 is not representative of an ON transformer winding pass with 2 discs and three horizontal ducts. Part 2 is a typical ON winding pass and it is repeated to become the other 3 following passes with inlet alternating between inner and outer vertical ducts to form a zigzag flow pattern. Since the geometry of the last 3 passes repeats part 2 of pass 1, the geometry of the whole winding is not illustrated in Fig. 1.

For the investigated LV winding, each disc is composed of 18 strands individually wrapped with insulation paper of thickness 0.4 mm. Horizontal ducts are uniformly 4.1 mm. Inner vertical duct width is 8.9 mm and outer vertical duct width 6.4 mm. The thickness of the washer is 1 mm.

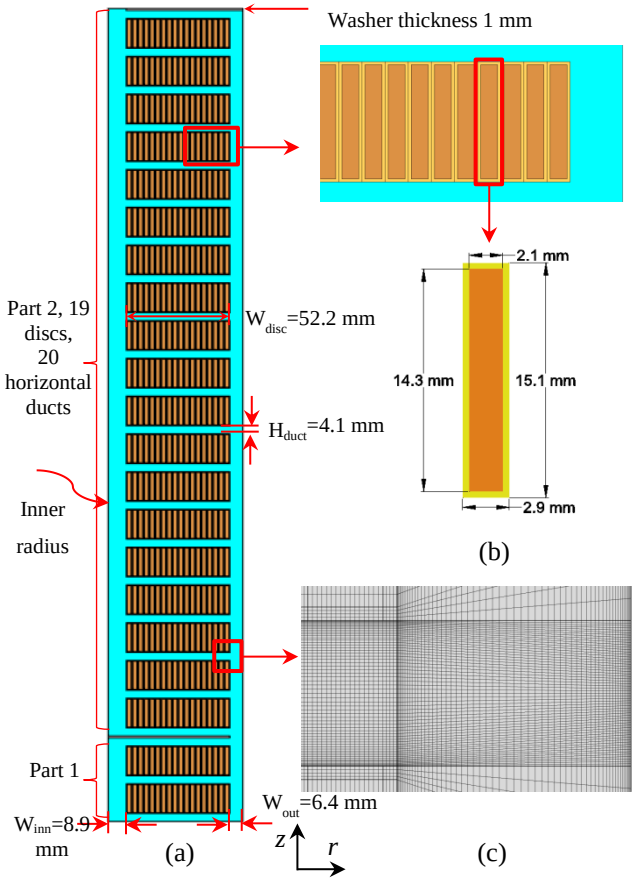

Fig. 1. Axisymmetric 2D geometry. (a) Winding geometry of pass 1at the bottom of the LV winding. (b) Geometric details of one strand. (c) Mesh at the junction of horizontal duct and vertical duct, to be explained in section 4.

III. Dimensional Analyses on Flow Distribution and Temperature Distribution

Heat transfer in the winding mainly consists of convection in the fluid domain (oil flow domain) and conduction in the solid domain (copper and paper domain). Conduction in the solid domain is governed by Fourier's law of conduction. Convection in the fluid domain, which is the challenging part, is governed by three conservation laws, i.e. conservations of mass, momentum and energy.

A. Boussinesq Approximation

According to the Boussinesq approximation all fluid properties are assumed constant except for density in the buoyancy force term (ρg). In cylindrical coordinates, the conservation equations of mass, momentum and energy for axisymmetric 2D flow can be expressed by (1), (2) and (3), respectively.

$$\frac{1}{r}\frac{\partial(\mathrm{r}u_r)}{\partial r}+\frac{\partial u_z}{\partial z}=0 \tag{1}$$

$$\begin{cases} \mathrm{u}_r\dfrac{\partial u_r}{\partial r}+\mathrm{u}_z\dfrac{\partial u_r}{\partial z}=-\dfrac{1}{\rho}\dfrac{\partial p}{\partial r}+\nu\left(\dfrac{\partial}{\partial r}\left(\dfrac{1}{r}\dfrac{\partial(\mathrm{r}u_r)}{\partial r}\right)+\dfrac{\partial^2 u_r}{\partial z^2}\right) \\ \mathrm{u}_r\dfrac{\partial u_z}{\partial r}+\mathrm{u}_z\dfrac{\partial u_z}{\partial z}=-\dfrac{1}{\rho}\dfrac{\partial p}{\partial z}-g+\nu\left(\dfrac{1}{r}\dfrac{\partial}{\partial r}\left(\mathrm{r}\dfrac{\partial u_z}{\partial r}\right)+\dfrac{\partial^2 u_z}{\partial z^2}\right) \end{cases} \tag{2}$$

$$u_r\frac{\partial T}{\partial r}+u_z\frac{\partial T}{\partial z}=\frac{k}{\rho c_p}\left(\frac{1}{r}\frac{\partial}{\partial r}\left(\mathrm{r}\frac{\partial T}{\partial r}\right)+\frac{\partial^2 T}{\partial z^2}\right) \tag{3}$$

In the energy equation the viscous dissipation term is neglected due to the small flow rates in transformer windings.

Apart from the Boussinesq approximation, it is also assumed that static pressure gradients in *z*-direction ($\partial p/\partial z$) are the same everywhere in the fluid domain and it equals to that at the centre of the winding outlet, where the *r*-velocity component (u_r) and the gradient of *z*-velocity component in both *r*-direction ($\partial u_z/\partial r$) and *z*-direction ($\partial u_z/\partial z$) are all zeros because this point corresponds to the top of the parabolic velocity profile. Therefore, the *z*-direction momentum conservation equation becomes:

$$\mathrm{u}_r\frac{\partial u_z}{\partial r}+\mathrm{u}_z\frac{\partial u_z}{\partial z}=-\frac{1}{\rho}\frac{\partial p_{to}}{\partial z}-g+\nu\left(\frac{1}{r}\frac{\partial}{\partial r}\left(\mathrm{r}\frac{\partial u_z}{\partial r}\right)+\frac{\partial^2 u_z}{\partial z^2}\right) \tag{4}$$

where p_{to} refers to the static pressure at the top of the winding, i.e. top oil pressure.

Applying (4) to the centre of the winding outlet, we have:

$$\frac{\partial p_{to}}{\partial z}=-\rho_{to}g \tag{5}$$

where ρ_{to} refers to oil density at the top of the winding, i.e. top oil density.

Substituting (5) into (4), we have:

$$\mathrm{u}_r\frac{\partial u_z}{\partial r}+\mathrm{u}_z\frac{\partial u_z}{\partial z}=g\frac{(\rho_{to}-\rho)}{\rho}+\nu\left(\frac{1}{r}\frac{\partial}{\partial r}\left(\mathrm{r}\frac{\partial u_z}{\partial r}\right)+\frac{\partial^2 u_z}{\partial z^2}\right) \tag{6}$$

Relating (6) to the volumetric thermal expansion coefficient, β_T, we have:

$$\mathrm{u}_r\frac{\partial u_z}{\partial r}+\mathrm{u}_z\frac{\partial u_z}{\partial z}=g\beta_T(T-T_{to})+\nu\left(\frac{1}{r}\frac{\partial}{\partial r}\left(\mathrm{r}\frac{\partial u_z}{\partial r}\right)+\frac{\partial^2 u_z}{\partial z^2}\right) \tag{7}$$

B. Nondimensionalization

To transfer the governing equations to their dimensionless forms, the dimensionless independent variables are defined as:

$$r^*=\frac{r}{D_h} \quad \text{and} \quad z^*=\frac{z}{D_h} \tag{8}$$

$$u_r^*=\frac{u_r}{u_m} \quad \text{and} \quad u_z^*=\frac{u_z}{u_m} \tag{9}$$

$$p^*=\frac{p}{\rho u_m^2} \quad \text{and} \quad T^*=\frac{T-T_{to}}{T_{aw}-(\mathrm{T}_{to}+\mathrm{T}_{bo})/2}=\frac{T-T_{to}}{g_{ave}} \tag{10}$$

Substituting (8), (9) and (10) into the governing equations and noticing that the reference parameters (D_h, T_{aw}, T_{to}, T_{bo}, u_m) are not functions of the coordinates, we have the dimensionless governing equations:

$$\frac{1}{r^*}\frac{\partial(\mathrm{r}^*\mathrm{u}_r^*)}{\partial r^*}+\frac{\partial u_z^*}{\partial z^*}=0 \tag{11}$$

$$\begin{cases} \mathrm{u}_r^*\dfrac{\partial u_r^*}{\partial r^*}+\mathrm{u}_z^*\dfrac{\partial u_r^*}{\partial z^*}=-\dfrac{\partial p^*}{\partial r^*}+\dfrac{1}{\mathrm{Re}}\left(\dfrac{\partial}{\partial r^*}\left(\dfrac{1}{r^*}\dfrac{\partial(\mathrm{r}^*\mathrm{u}_r^*)}{\partial r^*}\right)+\dfrac{\partial^2 u_r^*}{\partial z^{*2}}\right) \\ \mathrm{u}_r^*\dfrac{\partial u_z^*}{\partial r^*}+\mathrm{u}_z^*\dfrac{\partial u_z^*}{\partial z^*}=\dfrac{Gr}{\mathrm{Re}^2}T^*+\dfrac{1}{\mathrm{Re}}\left(\dfrac{1}{r^*}\dfrac{\partial}{\partial r^*}\left(\mathrm{r}^*\dfrac{\partial u_z^*}{\partial r^*}\right)+\dfrac{\partial^2 u_z^*}{\partial z^{*2}}\right) \end{cases} \tag{12}$$

$$u_r^*\frac{\partial T^*}{\partial r^*}+u_z^*\frac{\partial T^*}{\partial z^*}=\frac{1}{\mathrm{Re}\cdot\mathrm{Pr}}\left(\frac{1}{r^*}\frac{\partial}{\partial r^*}\left(\mathrm{r}^*\frac{\partial T^*}{\partial r^*}\right)+\frac{\partial^2 T^*}{\partial z^{*2}}\right) \tag{13}$$

where the definitions of *Re*, Gr/Re^2 and *Pr* are shown below:

$$Re=\frac{u_m D_h}{\nu} \tag{14}$$

$$\frac{Gr}{Re^2}=\frac{g\beta_T(T_{aw}-(T_{to}+T_{bo})/2)D_h}{u_m^2} \tag{15}$$

$$Pr=\frac{\mu c_p}{k} \tag{16}$$

C. Flow and Temperature Distribution in the Fluid Domain

For a fixed winding geometry with a fixed power loss distribution in dimensionless senses, which determine the boundary conditions of the dimensionless governing equations (11)-(13), both oil flow distribution (u_r^*, u_z^*) and temperature distribution (T^*) are determined by the coefficients, *Re*, Gr/Re^2 and *Pr*.

Pr plays the same role as *Re* in (13). In addition, *Re* in conjunction with Gr/Re^2 determines oil flow distribution in (12). For ON cooling modes, fluid flow and heat transfer are strongly coupled. Therefore, *Re* is more influential than *Pr* in determining fluid flow and temperature distribution. Gr/Re^2 must be influential because it is related to the buoyancy force which is the main driving force of the flow.

D. Determination of Hot-Spot Factor

The hot-spot factor, *H*, is a crucial component in the thermal diagram in IEC 60076-2: 2011 [3] to determine the hot-spot temperature, T_{hs}, in the winding from the heat run test results. The dimensionless temperature defined in (10) has the same formula as the hot-spot factor except that the temperature, *T*, in (10) refers to any temperature in the fluid domain while it is specifically T_{hs} in the definition of *H*.

The T_{hs} can be regarded as the sum of the highest temperature in the fluid domain, T'_{hs}, and the temperature gradient across the insulation paper, ΔT. Therefore, *H* can be expressed as:

$$H = \frac{T'_{hs} + \Delta T - T_{to}}{g_{ave}} = T^*_{hs} + \frac{\Delta T}{g_{ave}} \quad (17)$$

The dimensionless highest temperature in the fluid domain, T^*_{hs}, is controlled by *Re*, *Gr/Re*^{2} and *Pr*, as shown in section III part B and section III part C.

By relating ΔT to Fourier's law of conduction, $q'' = k_p \Delta T/\Delta x$, we have:

$$\frac{\Delta T}{g_{ave}} = \frac{q''\cdot \Delta x}{g_{ave}\cdot k_p} = \frac{h\cdot \Delta x}{k_p} \quad (18)$$

where q''/g_{ave} can be regarded as the overall heat transfer coefficient in the winding, *h*. Since Δx can be linearly related to a characteristic length in the fluid domain and k_p can be linearly related to oil thermal conductivity, *k*, the term $\Delta T/g_{ave}$ can therefore be linearly related to *Nu* associated with the overall heat transfer coefficient in the winding. For natural convection, *Nu* is a function of *Ra* [17]. For ON cooling modes, it is a combined natural and forced convection in the winding due to the effect of the radiator in the circulation loop. Therefore, the term $\Delta T/g_{ave}$ is related to *Re*, *Pr* and *Gr* (or *Gr/Re*^{2}).

To sum up, the hot-spot factor, *H*, in an ON transformer with a fixed power loss distribution in a dimensionless sense is determined by *Re*, *Gr/Re*^{2} and *Pr*.

IV. Numerical Model

Computations have been performed by using commercial finite element method software COMSOL Multiphysics. The continuity equation, Navier-Stokes equations and energy equation are solved directly without adopting the Boussinesq approximation in 2D axisymmetric models. Conjugate heat transfer modelling of the solid and fluid domain without including turbulence model is executed as specified in [9].

A. Solid and fluid properties

The properties of copper and paper are set to be temperature independent, as shown below:

$$k_c = 401\,(\mathrm{W/(m\cdot K)})$$
$$k_p = 0.19\,(\mathrm{W/(m\cdot K)})$$
$$\rho_c = 8933\,(\mathrm{kg/m^3})$$
$$\rho_p = 930\,(\mathrm{kg/m^3})$$
$$\mathrm{c}_{pc} = 385\,(\mathrm{J/(kg\cdot K)})$$
$$\mathrm{c}_{pp} = 1340\,(\mathrm{J/(kg\cdot K)})$$

The properties of a mineral oil as functions of temperature in Kelvin are obtained from least-square curve fittings of the data provided by the oil manufacturer, given as follows:

$$\rho = -0.6568\times \mathrm{T} + 1064 \quad (19)$$
$$\mu = 7.863\times 10^{-5}\times \exp(632.0/(\mathrm{T}-176.0)) \quad (20)$$
$$k = -7.837\times 10^{-5}\times T + 0.1557 \quad (21)$$
$$c_p = 3.950\times T + 560.2 \quad (22)$$

B. Boundary conditions and mesh

At the inlet of pass 1, uniform oil velocities are specified with fixed inlet oil temperature of 46.7 ºC for all the cases investigated in this paper. At the outlet of pass 4, zero pressure is specified. No-slip condition is specified for all the solid surfaces in contact with fluid. The inner and outer walls of the winding bounding the vertical ducts and the washers separating passes are set to be adiabatic. Uniform power losses are specified in each copper strand.

The mesh of both the solid and the fluid domains consists of rectangular elements. 4 elements are used to discretize the 0.4 mm paper thickness as recommended in [14]. 60 elements are present to discretize the width of vertical ducts and the height of horizontal ducts and 360 elements are used to discretize the width of the horizontal ducts. The mesh is organized in a way that a higher element density is present near the solid surface to better capture the thermal and hydraulic boundaries. For the whole winding model, 3,787,704 elements are generated, resulting in the number of degrees of freedom solved in the computation being 12,869,027. A mesh illustration at the junction of a horizontal duct and a vertical duct is shown in Fig. 1 (c). Mesh refinement study shows that an approximate 50% decrease or 10% increase of the mesh element number brings negligible effect on the fluid flow and temperature distribution.

C. Numerical model validation

To check the validity of the numerical models in this paper, comparisons of oil flow distribution and disc temperature distribution of a one-pass model for different total oil flow rates are performed against the data provided in [9].

The one-pass model has the same geometry as part 2 of pass 1 shown in Fig. 1. Uniform power losses of 676.9 W/disc and the same oil properties as shown in [9] are adopted for the comparison purposes. The total oil flow rate ranges from 0.78 kg/s to 4 kg/s. The comparisons of oil flow distribution and the distribution of disc average temperature rise over top oil energy-average temperature are shown in Fig. 2 and Fig. 3, respectively. As can be seen, the discrepancies for both flow distributions and temperature distributions are negligible, proving that the CFD models in the present study follow the same established computational principles as in [9].

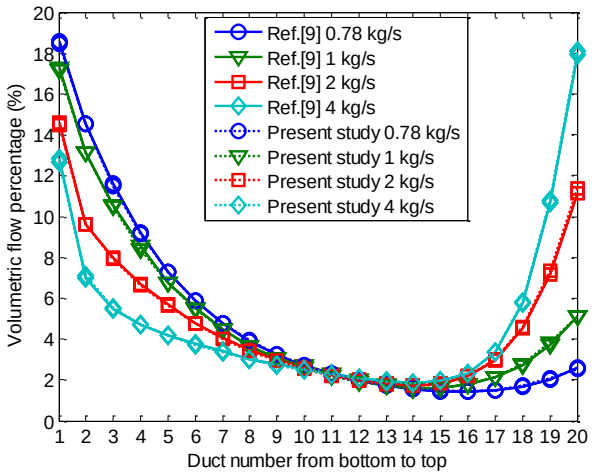

Fig. 2. Comparisons of oil flow distribution through horizontal ducts with data extracted from ref. [9].

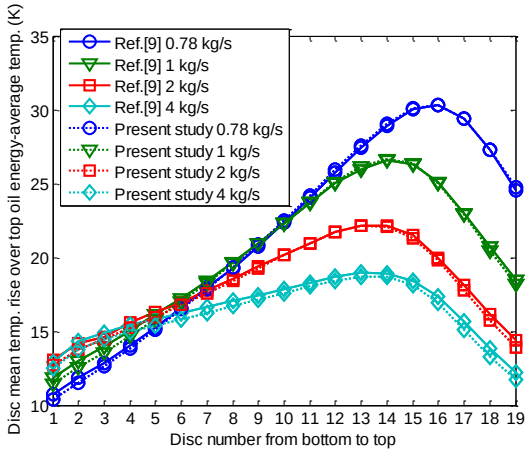

Fig. 3. Comparisons of disc average temperature rise over top oil energy-average temperature with data extracted from ref. [9].

V. Case Study of the Full Winding Model

In the full winding model, a uniform power loss of 677 W/disc is prescribed with a total mass flow rate of 0.78 kg/s and a winding inlet oil temperature of 46.7 ºC. These conditions are the same as those used in [9, 13, 14]. Since part 1 of pass 1 as shown in Fig. 1 is not representative of an ON transformer winding, the results of this part are not included in this paper.

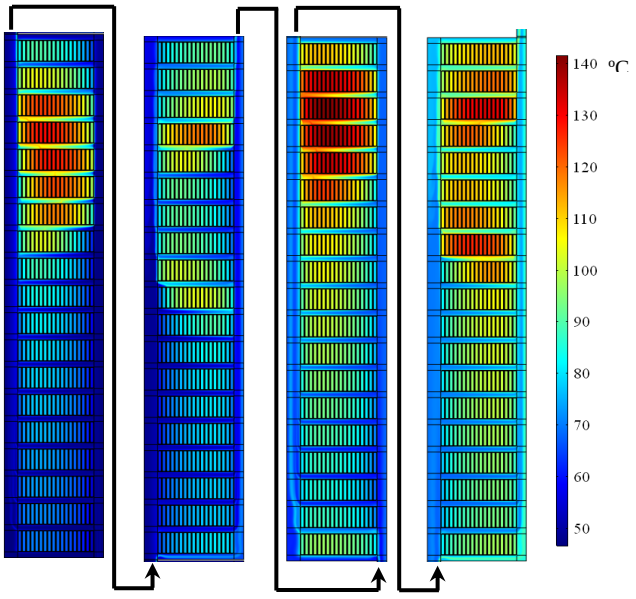

Fig. 4. Contours of the temperature distribution in the winding (Part 1 of pass 1 is excluded). (a) Pass 1 at the bottom of the winding. (b) Pass 2. (c) Pass 3. (d) Pass 4 at the top of the winding.

The temperature contour of this case study is shown in Fig. 4. It can be seen from Fig. 4 that localized overheating with hot-plumes as described in [13] exists in the upper half of each pass. The average of the velocity profile at the centre of each horizontal duct is shown in Fig. 5 where flow from the inner vertical duct to the outer vertical duct is regarded as positive and vice versa. The maximum temperature of each disc is shown in Fig. 6. As can be seen from Fig. 4, 5 and 6, the temperature distribution corresponds with the flow distribution. There is a strong coupling between fluid flow and heat transfer. In addition, a strong coupling between different passes exists due to hot-streak dynamics, as detailed in [13]. Reverse flow occurs in each pass of the winding model. The crossovers of the flow in Fig. 5 correspond to the local temperature peaks in Fig. 6. Obvious crossover regions can be identified in pass 2 and pass 4, resulting in two temperature peaks. In pass 1 and pass 3, the fluid is almost at rest in the crossover region resulting in one temperature peak. The hot-spot temperature, 141.6 ºC, appears in the upper portion of pass 3 in the flow crossover region. The hot-spot factor of this case study is 2.12. The *Re*, Gr/Re^2 and *Pr* determined at the average top and bottom oil temperature ($(T_{bo}+T_{to})/2$) are 195, 1.46 and 57, respectively.

It is worth noting that, for the same simulation conditions, studies in this paper and in [13] both find the occurrence of reverse flow, whereas [14] do not show the reverse flow. This is not due to the different numerical codes used as almost identical flow and temperature distribution results are obtained by the 3 papers for a one-pass model. The differences could be caused by the simulation strategies adopted in the 3 papers: this paper and [13] simulate the whole 4-pass winding in one model, while [14] adopts a pass-by-pass simulation strategy. The pass-by-pass strategy cuts off the effects of the downstream passes on the upstream passes, which is probably responsible for the "no show" of reverse flow in [14].

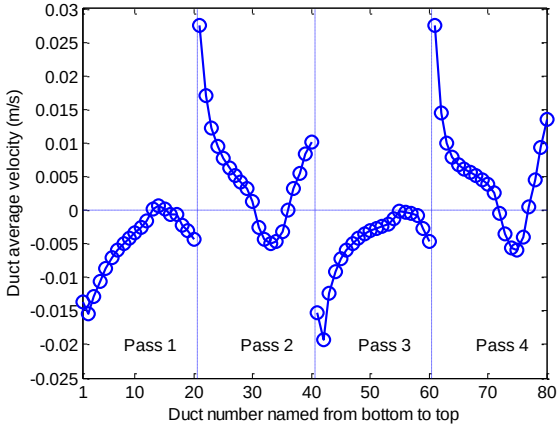

Fig. 5. Average oil velocity at the centre of each horizontal duct with power loss being 677 W/disc. Flow from inner vertical duct to outer vertical duct is regarded as positive and vice versa.

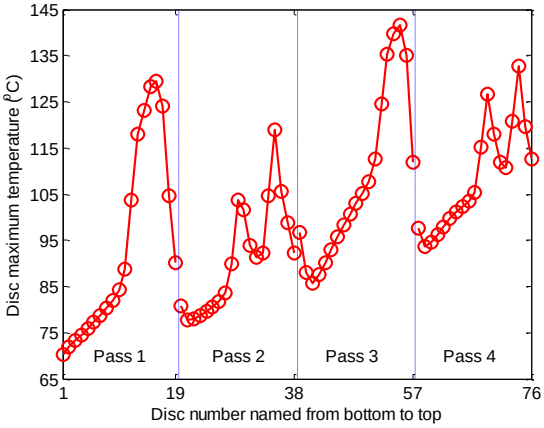

Fig. 6. Disc maximum temperature distribution with power loss being 677 W/disc.

VI. Parametric sweeps

It is shown in section III that oil flow distribution and disc temperature distribution is controlled by *Re*, Gr/Re^2 and *Pr*. To generalize the CFD results, parametric sweeps of Gr/Re^2 with fixed *Re* and *Pr* are performed. To achieve this, computational scenarios are created with changing gravitational acceleration, *g*, and fixed other parameters. Since these scenarios are purely artificial, only the dimensionless parameters, e.g. the oil volumetric flow fraction in each horizontal duct and the dimensionless disc maximum temperature in each disc will be practically meaningful. For the calculation of *Re*, Gr/Re^2 and *Pr*, average oil temperature at the top and bottom of the winding is used to determine oil properties.

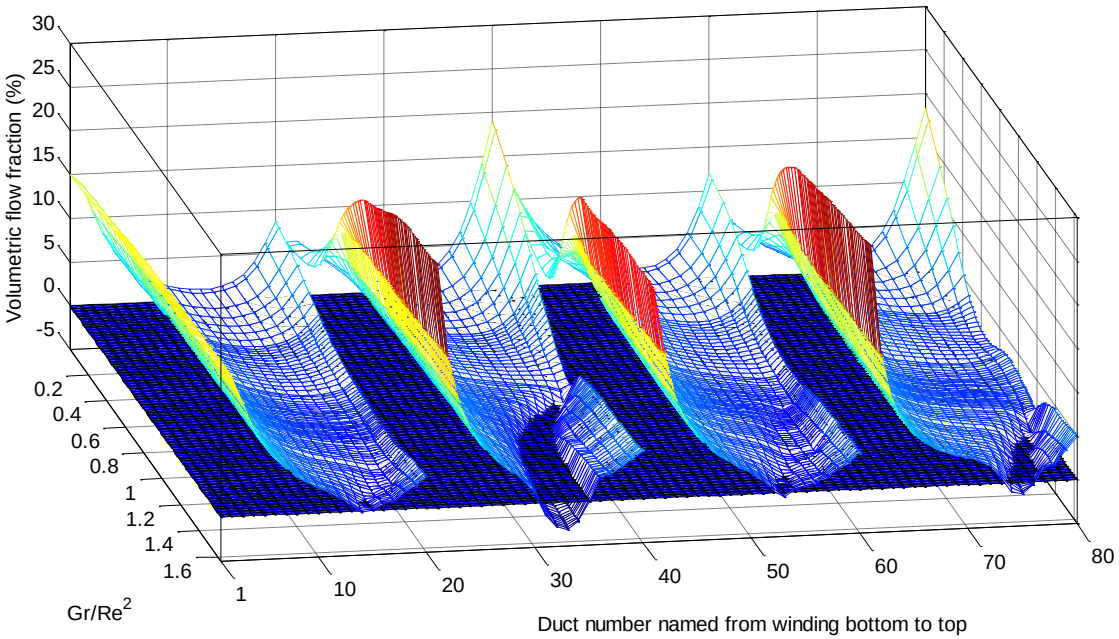

Fig. 7. Oil flow distribution variation with Gr/Re^2 in each horizontal duct with *Re* being 118. Negative flow fractions mean reverse flow.

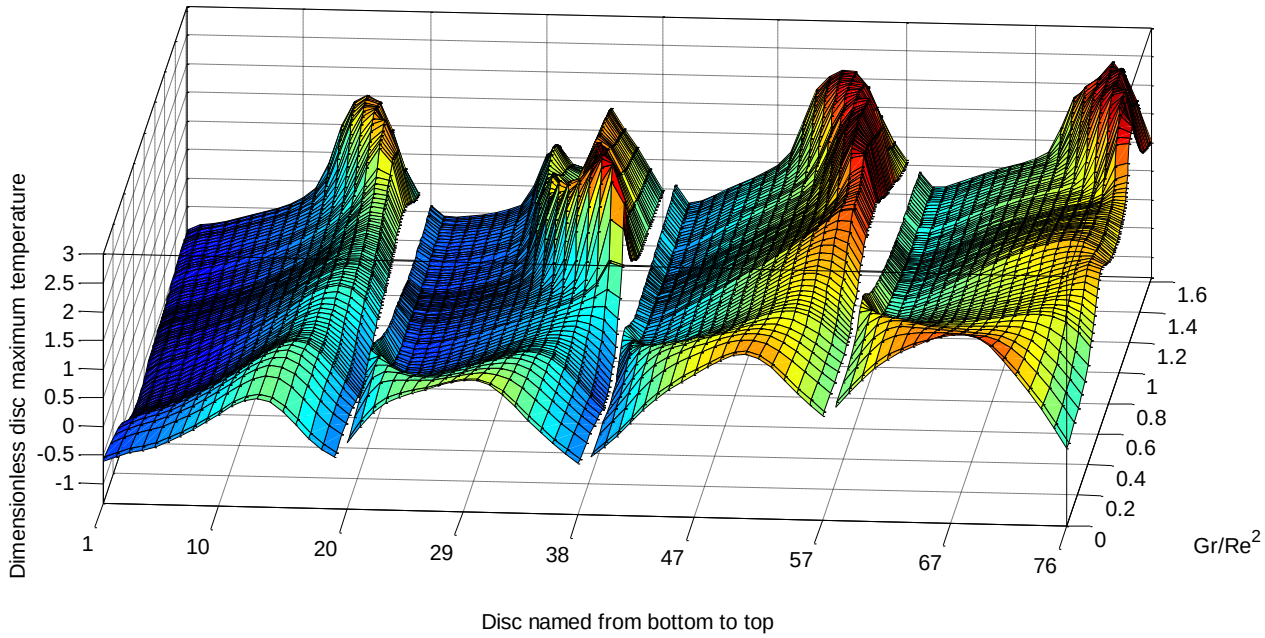

Fig. 8. Dimensionless disc maximum temperature variation with Gr/Re^2 on each disc with *Re* being 118.

When *Re* is fixed to be 118, the variation of oil flow distribution and dimensionless disc maximum temperature distribution with Gr/Re^2 is shown in Fig. 7 and Fig. 8 respectively. It can be seen from Fig. 7 that with the increase of Gr/Re^2 to 0.9, reverse flow occurs first at the top part of pass 2 (the penultimate duct). With a further increase of Gr/Re^2 more ducts at the top of pass 2 suffer from reverse flows and the region of reverse flow starts shifting to the middle part of pass 2 with top ducts recovering a normal flow direction and a higher flow rate. When Gr/Re^2 exceeds

1.2, other passes start to suffer revers flow. The region of reverse flow in pass 1 and pass 3 is not as obvious as that in pass 2 and pass 4 because the inlet vertical duct width in pass 1 and pass 3, which is the outer vertical duct width (6.4 mm), is smaller than that for pass 2 and pass 4, which is the inner vertical duct width (8.9 mm). A smaller vertical duct width brings a smaller Gr/Re^2 and therefore makes reverse flow less obvious and more difficult to happen. The dimensionless disc maximum temperature distribution in Fig. 8 corresponds to the flow distribution in Fig. 7.

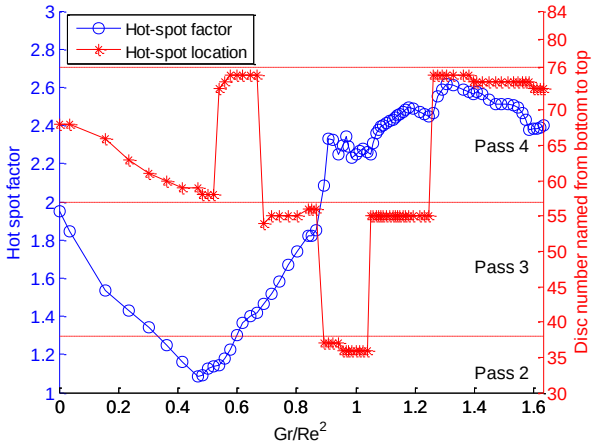

Fig. 9. Variation of hot-spot factor and the location of the hot-spot. (a) Variation of hot-spot factor with Gr/Re2. (b) Variation of hot-spot location with Gr/Re2.

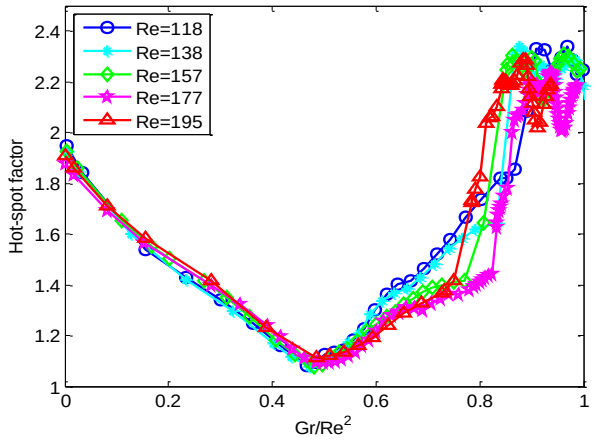

Fig. 10. Variation of hot-spot factor with *Re* and Gr/Re^2.

The maximum value of the dimensionless disc maximum temperature is actually the hot-spot factor, *H*. The variation of *H* with Gr/Re^2 can therefore be extract from Fig. 8, as shown in Fig. 9. As can be seen from Fig. 9 (left y-axis), initially with the increase of Gr/Re^2 from zero, *H* keeps decreasing and then it starts to increase. The first trough is achieved at Gr/Re^2 being approximately 0.5, where the effect of buoyancy force is balanced by the effect of inertial force and *H* is the minimum being approximately 1.1. When Gr/Re^2 is beyond 0.9, reverse flow starts to occur; *H* becomes a large value (>2) and it fluctuates due to the shifting of the location of the hot-spot. The shifting of the location of the hot-spot with Gr/Re^2 can be seen in Fig. 9 (right y-axis). It can be seen from Fig. 9 (right y-axis) that the hot-spot can appear at the top part of pass 2, pass 3 and pass 4, depending on the corresponding flow distribution.

Results of parametric sweeps for other *Re's*, which are typical to ON cooling modes, are shown in Fig. 10. It can be seen that for different *Re's* their first troughs of *H* coincide at Gr/Re^2 being approximately 0.5. When Gr/Re^2 exceeds 0.6, the variations of *H* start to diverge. For transformer thermal design and on-site operation, the lowest *H* is of great interest, while the divergent thermal behaviour at a large Gr/Re^2, which leads to a large *H*, is of less interest.

It is worth mentioning, for the parametric sweeps in Fig. 10 the effect of *Pr* is not shown. When the average oil temperature increases from 40 ºC to 80 ºC, *Pr* of the mineral oil investigated in this paper decreases from 108 to 43. Since a range of *Re* from 118 to 195 does not alter the location of the first trough of *H* and *Re* is more influential than *Pr* as shown in section 3, we can therefore conclude that in the practical range of *Pr*, its influence on the location of the first trough of *H* is negligible.

VII. Case Study in Optimal Operational Regime

The case study in section 5 shows that the LV winding is operated at a regime with Gr/Re^2 being 1.46 and the hot-spot factor being 2.12 where reverse flow occurs in each pass. In order to shift the operational regime to a quasi-optimal one, Gr/Re^2 needs to be reduced to the range between 0.4 and 0.6. This can be achieved by halving the power loss and at the same time keeping the total oil flow rate unchanged. It is proven experimentally in [18] that the total oil flow rate in an ON transformer is proportional to the square root of the total power loss in the winding and the square root of the height difference between the central point of the radiator and the central point of the winding. Therefore, the height difference needs to be doubled to keep the same total oil flow rate for the case with a halved power loss.

In the new case with halved power loss and unchanged other parameters the hot-spot temperature is 77.4 ºC with Gr/Re^2 being 0.6 and *H* being 1.13. The average velocity at the centre of each horizontal duct is shown in Fig. 11. It can be seen from Fig. 11 that no reverse flow occurs. The corresponding maximum temperature of each disc is shown in Fig. 12. Compared to the benchmark case, the new case gives a hot-spot temperature that is 64.2 ºC lower.

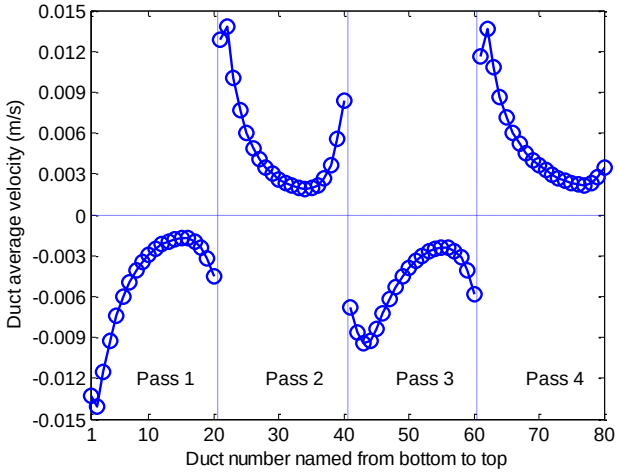

Fig. 11. Average oil velocity at the centre of each horizontal duct with power loss being 339 W/disc. Flow from inner vertical duct to outer vertical duct is regarded as positive and outer vertical duct to inner vertical duct as negative.

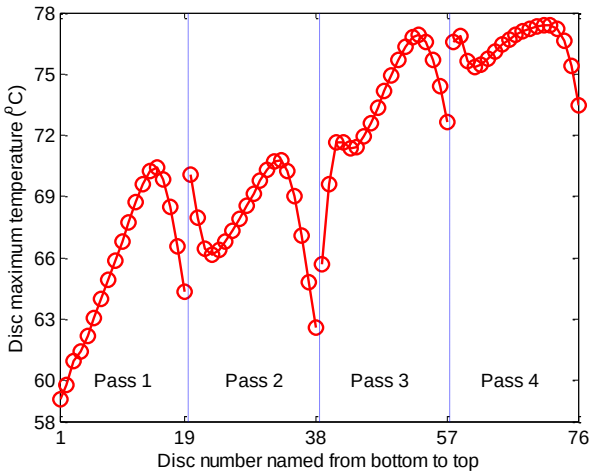

Fig. 12. Disc maximum temperature distribution with power loss being 339 W/disc.

VIII. Conclusion

Oil flow distribution and temperature distribution in disc-type ON transformer windings has been analysed using dimensional analysis with the Boussinesq approximation. For a fixed winding geometry with a fixed power loss distribution, in dimensionless senses, volumetric flow fraction in each horizontal cooling duct and the dimensionless disc temperature are functions of *Re*, Gr/Re^2 and *Pr*. Gr/Re^2 is a controlling parameter and *Re* is more influential than *Pr*.

A benchmark case study has been conducted which demonstrates the occurrence of reverse flow and hot-plumes. For the benchmark case, the hot-spot temperature is 141.6 ºC and *H* is 2.12.

CFD parametric sweeps of *Re* and Gr/Re^2 show that *H* decreases with increasing Gr/Re^2 from zero until Gr/Re^2 reaches approximately 0.5, where the effects of buoyancy force is balanced by the effects of inertial forces. Then the increase of Gr/Re^2 brings increasing *H*, forming the first trough of *H* against Gr/Re^2 where the minimum of *H* can be obtained. With a further increase of Gr/Re^2, reverse flow occurs and *H* starts to fluctuate with the increase of Gr/Re^2 due to the shifting of the hot-spot location. The effect of *Re* and *Pr* of the mineral oil investigated is found to be negligible on the location of the first trough of *H*. This invariable first trough of *H* against Gr/Re^2 makes optimization of the operational regime possible.

A new case study based on the benchmark case has been executed with Gr/Re^2 being shifted from 1.46 to 0.6. The new oil flow distribution and temperature distribution becomes much more preferable with hot-spot temperature being 77.4 ºC and *H* being 1.13.

Acknowledgement

The authors would like to express their gratitude to M&I Materials, National Grid, Scottish Power, Shell, TJ|H2b Analytical Services, UK Power Networks and Weidmann Electrical Technology AG for their financial and technical contributions to the Transformer Research Consortium at The University of Manchester.

References

[1] IEC, "Loading guide for oil-immersed power transformers," *IEC standard 60076-7*, 2005.

[2] IEEE, "IEEE Guide for Loading Mineral-Oil-Immersed Transformers and Step-Voltage Regulators," *IEEE standard C57.91*, 2011.

[3] IEC, "Temperature rise for liquid-immersed transformers," *IEC standard 60076-2*, 2011.

[4] P. Picher, F. Torriano, M. Chaaban, S. Gravel, C. Rajotte, B. Girard, "Optimization of transformer overload using advanced thermal modelling," in CIGRE Conference, Paris, France A2-305, 2010.

[5] A. J. Oliver, "Estimation of transformer winding temperatures and coolant flows using a general network method," *Proc. Inst. Elect. Eng.*, vol. 127, pp. 395-405, 1980.

[6] Z. R. Radakovic, and M. S. Sorgic, "Basics of detailed thermal-hydraulic model for thermal design of oil power transformers," *IEEE Transactions on Power Delivery*, vol. 25, no. 2, pp. 790-802, 2010.

[7] E. Rahimpour, M. Barati, and M. Schäfer, "An investigation of parameters affecting the temperature rise in windings with zigzag cooling flow path," *Applied thermal engineering*, vol. 27, no. 11, pp. 1923-1930, 2007.

[8] E. Kranenborg, C. Olsson, B. Samuelsson, L. Lundin, R. Missing, "Numerical study on mixed convection and thermal streaking in power transformer windings," in 5th European Thermal-Sciences Conference, The Netherlands, 2008.

[9] F. Torriano, M. Chaaban, and P. Picher, "Numerical study of parameters affecting the temperature distribution in a disc-type transformer winding," *Applied Thermal Engineering*, vol. 30, no. 14, pp. 2034-2044, 2010.

[10] W. Wu, Z. Wang, A. Revell, H. Iacovides, P. Jarman, "Computational fluid dynamics calibration for network modelling of transformer cooling oil flows-part I: heat transfer in oil ducts," *IET Electric Power Applications*, vol. 6, no. 1, pp. 19-27, 2012.

[11] W. Wu, Z. Wang, A. Revell, P. Jarman, "Computational fluid dynamics calibration for network modelling of transformer cooling oil flows-part II: pressure loss at junction nodes," *IET electric power applications*, vol. 6, no. 1, pp. 28-34, 2012.

[12] J. Coddé, W. Van der Veken, and M. Baelmans, "Assessment of a hydraulic network model for zig–zag cooled power transformer windings," *Applied Thermal Engineering*, vol. 80, pp. 220-228, 2015.

[13] A. Skillen, A. Revell, H. Iacovides, W. Wu, "Numerical prediction of local hot-spot phenomena in transformer windings," *Applied Thermal Engineering*, vol. 36, pp. 96-105, 2012.

[14] F. Torriano, P. Picher, and M. Chaaban, "Numerical investigation of 3D flow and thermal effects in a disc-type transformer winding," *Applied Thermal Engineering*, vol. 40, pp. 121-131, 2012.

[15] X. Zhang, Z. D. Wang, and Q. Liu, "Prediction of Pressure drop and flow distribution in disc type transformer windings under an OD cooling mode," *IEEE Transactions on Power Delivery*, vol. 32, no. 4, pp. 1655-1664, 2017.

[16] X. Zhang, Z. D. Wang, and Q. Liu, "Interpretation of Hot Spot Factor for Transformers in OD Cooling Modes," *IEEE Transactions on Power Delivery*, accepted, in press, 2017.

[17] T. L. Bergman, A. S. Lavine, F. P. Incropera, D. P. DeWitt, *Fundamentals of heat and mass transfer*: John Wiley & Sons, 2011.

[18] M. Yamaguchi, T. Kumasaka, Y. Inui, S. Ono, "The flow rate in a self-cooled transformer," *IEEE Transactions on Power Apparatus and Systems*, no. 3, pp. 956-963, 1981.

4.3 Paper 6

Numerical Investigation of Influence of Liquid Types on Flow Distribution and Temperature Distribution in Disc Type ON Transformers

Xiang Zhang, Zhongdong Wang, Qiang Liu Massimo Negro, Attila Gyore and Peter W.R. Smith

2017

The 19th International Conference on Dielectric Liquid (ICDL)

Accepted

Blank page

Numerical Investigation of Influence of Liquid Types on Flow Distribution and Temperature Distribution in Disc Type ON Transformers

Xiang Zhang[1], Zhongdong Wang[1], Qiang Liu[1]
[1]School of Electrical & Electronic Engineering
The University of Manchester
Manchester, UK
zhongdong.wang@manchester.ac.uk

Massimo Negro[2], Attila Gyore[3], Peter W.R. Smith[4]
[2]Weidmann Electrical Technology AG, Chiasso, Switzerland
[3]M&I Materials, Manchester, UK
[4]Shell Global Solutions, Manchester, UK

Abstract—**In this paper, dimensional analysis is adopted to study fluid flow distribution and temperature distribution in disc-type oil natural (ON) cooled transformer windings. Theoretical analysis on the thermal driving force and the pressure drop in the liquid circulation loop is also performed to determine the total liquid flow rate in the transformer. The thermal performance of three different liquids, a hydrocarbon mineral oil, a hydrocarbon gas-to-liquid (GTL) oil and a synthetic ester are investigated using computational fluid dynamics (CFD) simulations, based on the understanding from dimensional analysis and the flow rates determined from the theoretical analysis. It is found in the investigated conditions that the hydrocarbon mineral and GTL oil share similar thermal performance; the synthetic ester has a lower total flow rate due to its higher viscosity and therefore requires additional effort to improve its thermal performance.**

Keywords—CFD; dimensional alanalysis; disc-type winding; flow distribution; hot-spot temperature;hot-spot factor; ON transformer; ester; mineral oil; GTL oil

I. Introduction

Power transformers connect power systems of different voltage levels. The reliability of the transformer is of great importance to the reliability and safety of the power system. Apart from premature failure due to faults, transformer life expectancy is mainly dictated by the thermal ageing process of the insulation cellulose [1, 2]. The highest temperature in the winding, usually referred to as the hot-spot temperature, is of great interest to the transformer thermal designer and operator because it causes the severest thermal degradation of the insulation.

Generally, the cooling of the windings of power transformers relies on the circulation of the dielectric coolant fluid between the radiator and the winding. The liquid flow distribution in conjunction with power loss distribution determines the temperature distribution. The liquid flow and the heat transfer processes in the winding, are mainly investigated by using thermal-hydraulic network models and models that incorporate computational fluid dynamics (CFD). For oil directed (OD) cooling modes, liquid flow and heat transfer are weakly coupled. Therefore, the hydraulic system and the thermal system can be investigated separately [3-5]. For oil forced/natural (OF/ON) cooling modes, liquid flow and heat transfer are strongly coupled and therefore buoyancy force and hot-streak dynamics play vital roles in determining the fluid flow distribution and temperature distribution in the winding [6-8].

Other than traditional hydrocarbon mineral oil, alternative liquids like synthetic esters, natural esters and hydrocarbon gas-to-liquid (GTL) oils are increasingly being used as dielectric coolant for power transformers due to their properties and performance, and potential for reduced fire and environmental risks. The influence of different liquids on OD transformer flow and temperature distributions is shown in [9]. In this paper, fluid flow and temperature distributions in disc-type ON transformer windings are investigated theoretically, followed by numerical investigation of the influence of different liquids upon the fluid flow distribution and the temperature distribution.

II. Winding Geometry under Investigation

The winding under investigation is a LV winding of a 66 MVA 225/26.4 kV ONAN/ONAF transmission transformer [10]. This LV winding consists of 4 passes with pass 1 at the bottom being an anomaly, as shown in Fig. 1. There are 2 parts in pass 1. Part 1 is not representative of an ON transformer winding pass with 2 discs and three horizontal ducts. Part 2 is a typical ON winding pass and it is repeated to become the other 3 following passes with inlet alternating between the inner and outer vertical ducts to form a zigzag flow pattern. Since the geometry of the last 3 passes repeats part 2 of pass 1, the geometry of the whole winding is not illustrated in Fig. 1.

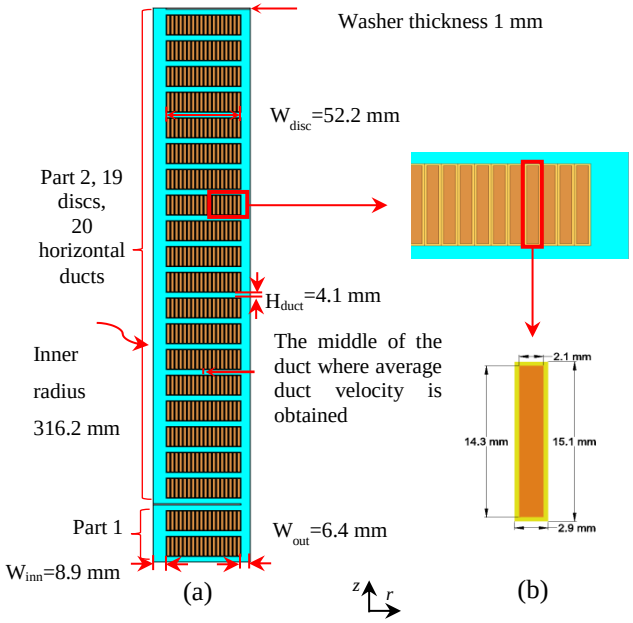

Fig. 1. Axisymmetric 2D geometry. (a) Winding geometry of pass 1at the bottom of the LV winding. (b) Geometric details of one strand.

III. Dimensional Analysis

Heat transfer in the winding involves conduction in the solid domain (copper and paper insulation) and convection in the fluid domain. The conduction is governed by Fourier's law

of conduction. The convection, which is the challenging part, is governed by three conservation laws, i.e. the conservations of mass, momentum and energy.

A. Boussinesq Approximation

According to the Boussinesq approximation all fluid properties are assumed constant except for density in the buoyancy force term. In cylindrical coordinates, the conservation equations of mass, momentum and energy for axisymmetric 2D flow can be expressed by (1), (2) and (3), respectively.

$$\frac{1}{r}\frac{\partial(\mathrm{r}u_r)}{\partial r}+\frac{\partial u_z}{\partial z}=0 \tag{1}$$

$$\begin{cases} \mathrm{u}_r\dfrac{\partial u_r}{\partial r}+\mathrm{u}_z\dfrac{\partial u_r}{\partial z}=-\dfrac{1}{\rho}\dfrac{\partial p}{\partial r}+\nu\left(\dfrac{\partial}{\partial r}\left(\dfrac{1}{r}\dfrac{\partial(\mathrm{r}u_r)}{\partial r}\right)+\dfrac{\partial^2 u_r}{\partial z^2}\right) \\ \mathrm{u}_r\dfrac{\partial u_z}{\partial r}+\mathrm{u}_z\dfrac{\partial u_z}{\partial z}=g\beta(T-T_{to})+\nu\left(\dfrac{1}{r}\dfrac{\partial}{\partial r}\left(\mathrm{r}\dfrac{\partial u_z}{\partial r}\right)+\dfrac{\partial^2 u_z}{\partial z^2}\right) \end{cases} \tag{2}$$

$$u_r\frac{\partial T}{\partial r}+u_z\frac{\partial T}{\partial z}=\frac{k}{\rho c_p}\left(\frac{1}{r}\frac{\partial}{\partial r}\left(\mathrm{r}\frac{\partial T}{\partial r}\right)+\frac{\partial^2 T}{\partial z^2}\right) \tag{3}$$

where r (m) is denoted for the radial coordinate, u_r (m/s)for velocity radial component, z (m) for axial coordinate, u_z (m/s) for velocity axial component, ρ (kg/m^3) for liquid density, p (Pa) for static pressure, ν (m^2/s) for kinematic viscosity, g (m/s^2) for gravitational acceleration, β (1/K) for volumetric thermal expansion coefficient, T (K) for liquid temperature, T_{to} (K) for liquid temperature at the top of the winding, k (W/(m·K)) for liquid thermal conductivity, c_p (J/(kg·K)) for liquid specific heat.

It is worth mentioning that the viscous dissipation term in the energy equation is neglected due to the small flow rates in transformer windings.

2. Dimensionless Forms

To transfer the governing equations to their dimensionless forms, the dimensionless independent variables are defined as:

$$r^*=\frac{r}{D_h} \quad \text{and} \quad z^*=\frac{z}{D_h} \tag{4}$$

$$u_r^*=\frac{u_r}{u_m} \quad \text{and} \quad u_z^*=\frac{u_z}{u_m} \tag{5}$$

$$p^*=\frac{p}{\rho u_m^2} \quad \text{and} \quad T^*=\frac{T-T_{to}}{T_{aw}-(\mathrm{T}_{to}+\mathrm{T}_{bo})/2}=\frac{T-T_{to}}{g_{ave}} \tag{6}$$

where D_h (m) is denoted for hydraulic diameter, defined as twice the inner vertical duct width (w_{inn}), u_m (m/s) for average liquid velocity at the inner vertical duct inlet, T_{aw} (K) for average winding temperature, T_{bo} (K) for winding bottom liquid temperature, g_{ave} (K) for the average temperature gradient between the winding and the average liquid temperature taken as the average of the winding top and bottom liquid temperatures.

Substituting (4), (5) and (6) into the governing equations (1), (2) and (3), and noticing that the reference parameters (D_h, T_{aw}, T_{to}, T_{bo}, u_m) are not functions of the coordinates, we have the dimensionless governing equations:

$$\frac{1}{r^*}\frac{\partial(\mathrm{r}^* u_r^*)}{\partial r^*}+\frac{\partial u_z^*}{\partial z^*}=0 \tag{7}$$

$$\begin{cases} \mathrm{u}_r^*\dfrac{\partial u_r^*}{\partial r^*}+\mathrm{u}_z^*\dfrac{\partial u_r^*}{\partial z^*}=-\dfrac{\partial p^*}{\partial r^*}+\dfrac{1}{\mathrm{Re}}\left(\dfrac{\partial}{\partial r^*}\left(\dfrac{1}{r^*}\dfrac{\partial(\mathrm{r}^* u_r^*)}{\partial r^*}\right)+\dfrac{\partial^2 u_r^*}{\partial z^{*2}}\right) \\ \mathrm{u}_r^*\dfrac{\partial u_z^*}{\partial r^*}+\mathrm{u}_z^*\dfrac{\partial u_z^*}{\partial z^*}=\dfrac{Gr}{\mathrm{Re}^2}T^*+\dfrac{1}{\mathrm{Re}}\left(\dfrac{1}{r^*}\dfrac{\partial}{\partial r^*}\left(\mathrm{r}^*\dfrac{\partial u_z^*}{\partial r^*}\right)+\dfrac{\partial^2 u_z^*}{\partial z^{*2}}\right) \end{cases} \tag{8}$$

$$u_r^*\frac{\partial T^*}{\partial r^*}+u_z^*\frac{\partial T^*}{\partial z^*}=\frac{1}{\mathrm{Re}\cdot\mathrm{Pr}}\left(\frac{1}{r^*}\frac{\partial}{\partial r^*}\left(\mathrm{r}^*\frac{\partial T^*}{\partial r^*}\right)+\frac{\partial^2 T^*}{\partial z^{*2}}\right) \tag{9}$$

where the definitions of *Re*, *Pr* and *Gr/Re*^{2} are shown below:

$$\mathrm{Re}=\frac{u_m D_h}{\nu} \tag{10}$$

$$\mathrm{Pr}=\frac{\mu c_p}{k} \tag{11}$$

$$\frac{Gr}{\mathrm{Re}^2}=\frac{g\beta(T_{aw}-(T_{to}+T_{bo})/2)D_h}{u_m^2} \tag{12}$$

where μ (Pa·s) stands for liquid dynamic viscosity.

C. Flow and temperature distribution in the fluid domain

For a fixed winding geometry with a fixed power loss distribution in dimensionless senses, both liquid flow distribution and temperature distribution are determined by the coefficients, *Re*, *Gr/Re*^{2} and *Pr* as shown in the dimensionless governing equations (7)-(9). *Pr* plays the same role as *Re* in (9). *Re* in conjunction with *Gr/Re*^{2} determines liquid flow distribution in (8). For ON cooling modes, flow and temperature are strongly coupled. Therefore, *Re* is more influential than *Pr* in determining flow and temperature distribution. *Gr/Re*^{2} is related to buoyancy force which is the main driving force of the flow. In conclusion, liquid flow distribution and temperature distribution are mainly controlled by *Re*, *Pr* and *Gr/Re*^{2}. Following the same argument as presented in [11], we can conclude that the hot-spot factor for ON cooling modes are mainly controlled by *Re*, *Pr* and *Gr/Re*^{2}.

IV. Determination of Total Liquid Flow Rate

For ON cooling modes, total liquid flow rate in the winding has a significant influence on the liquid flow distribution, and the temperature distribution. The total liquid flow rate is determined by the thermal driving force (p_T) and the pressure drop (p_D) over the whole circulation loop. A schematic illustration of the loop is shown in Fig. 2.

A. Thermal Driving Force

The thermal driving force can be expressed as:

$$p_T=\oint\rho\cdot\vec{g}d\vec{l} \tag{13}$$

Under the assumptions that heat transfer occurs only in the winding and the radiator, and temperatures rise linearly with elevation in the winding and the radiator, the thermal driving force in (13) can be approximated to be:

$$p_T=\rho_0\cdot g\cdot\beta\cdot\Delta T\cdot\Delta H \tag{14}$$

where ρ_0 (kg/m^3) is a reference density at 20 ºC, ΔT (K) is the liquid temperature gradient between the top and bottom of the winding, ΔH (m) is the height difference of the central points of the radiator and the winding.

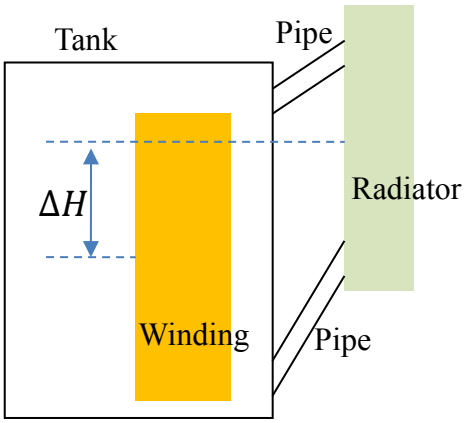

Fig. 2. Schematic illustration of the liquid circulation loop.

B. Pressure Drop in the Loop

The pressure drop in the loop is determined by the geometry, liquid properties and liquid flow rate. It is verified experimentally that for ON cooling modes, the so called minor pressure drops related to the change of flow direction is negligible, compared to the major pressure drop due to friction [7]. Therefore, the pressure drop over the loop can be expressed as:

$$p_D = \frac{C}{\mathrm{Re}}\frac{L'}{H'}\frac{\rho u_m^2}{2} \tag{15}$$

where C is a constant, L' (m) and H' (m) are the equivalent length and the equivalent diameter of the circulation loop.

C. Determination of Total Flow Rate

Applying energy conservation to the total liquid flow through the winding or the radiator, in steady state we have:

$$\Delta \mathrm{T} = \frac{P}{\dot{m}c_p} = \frac{P}{Au_m\rho c_p} \tag{16}$$

where P (W) is the total power loss in the winding or radiator, A is the cross sectional area of the winding inlet.

Combining (14), (15) and (16), we have:

$$u_m^2 = \frac{2\rho_0 g\beta H'^2}{\mu CL'A\rho c_p}\Delta H \cdot P \tag{17}$$

Notice that for a given liquid and a given winding geometry ρ_0, g, β, H', L', μ, C, A, ρ, c_p can all be treated as constant. Therefore the total liquid flow rate characterized by the winding inlet velocity u_m is proportional to the square root of the total power loss in the winding, and the square root of the central point height difference between the radiator and the winding. These square root relationships between u_m and P and ΔH are obtained experimentally in [7].

V. Influence of Liquid Types

For a fixed winding geometry (fixed geometric boundary conditions and fixed ΔH) with a fixed power loss distribution (fixed P), the total liquid flow rate is determined by the properties of the liquid as shown in (17). In (17), liquid-type related properties are ρ_o, μ, ρ and c_p. Three types of liquid are investigated in this paper. They are a traditional hydrocarbon mineral oil, a hydrocarbon gas-to-liquid (GTL) oil and a synthetic ester. The properties of these three liquids as functions of temperature are obtained from least-square curve fittings of the results provided by the manufacturers.

$$\begin{cases}
\rho_1 = -0.6568\times \mathrm{T}+1064\ [\mathrm{kg/m^3}] \\
\mu_1 = 7.863\times 10^{-5}\times \exp(632.0/(\mathrm{T}-176.0))\ [\mathrm{Pa\cdot s}] \\
c_{p1} = 3.950\times \mathrm{T}+560\ [\mathrm{J/(kg\cdot K)}] \\
\beta_1 = 7.778\times 10^{-4}\ [1/K] \\
\rho_2 = -0.6455\times \mathrm{T}+995.5\ [\mathrm{kg/m^3}] \\
\mu_2 = 6.133\times 10^{-5}\times \exp(749.8/(\mathrm{T}-157.4))\ [\mathrm{Pa\cdot s}] \\
c_{p2} = 4.449\times \mathrm{T}+871.7\ [\mathrm{J/(kg\cdot K)}] \\
\beta_2 = 8.273\times 10^{-4}\ [1/K] \\
\rho_3 = -0.7327\times \mathrm{T}+1185\ [\mathrm{kg/m^3}] \\
\mu_3 = 6.239\times 10^{-5}\times \exp(914.1/(\mathrm{T}-162.4))\ [\mathrm{Pa\cdot s}] \\
c_{p3} = 2.069\times \mathrm{T}+1287\ [\mathrm{J/(kg\cdot K)}] \\
\beta_3 = 7.790\times 10^{-4}\ [1/K]
\end{cases}$$

where the subscript 1 is for the mineral oil, 2 for the GTL, 3 for the synthetic ester, T for temperature in Kelvin.

When we choose the flow rate of mineral oil as a unit, and liquid temperature as 70 ºC to determine the properties (ρ_0 is determined at 20 ºC), according to (17), the volumetric flow rate for the mineral oil, the GTL oil and the synthetic ester is 1: 0.919: 0.581.

Computations have been performed by using commercial finite element method based software COMSOL Multiphysics in laminar model. To compare the thermal performance of the three liquids, the winding inlet temperature is fixed to be 46.7 ºC and the power loss of each disc is set to be 420 W, corresponding to a current density of 4 A/mm^2 at 85 ºC copper resistance. The flow rate of the mineral oil is the benchmark which corresponds to a winding inlet velocity of 0.053 m/s. The inlet velocities of the GTL oil and the synthetic ester are therefore 0.049 m/s and 0.031 m/s, respectively.

The average liquid velocity in the middle of each horizontal cooling duct and the maximum temperature of each disc are shown in Fig. 3 and Fig. 4 respectively. Since part 1 of pass 1 is not representative of an ON transformer winding pass, the flow and temperature results in this part is not included in this paper. The comparisons of some lumped parameters and hot-spot temperature for these three liquids are shown in Table 1.

It can be seen from Fig. 3 and Fig. 4 that both hydrocarbons, the mineral oil and the GTL oil, share similar flow and temperature distributions because they have similar Re, Pr and Gr/Re^2 as shown in Table 1. Although the mineral oil has a slightly higher total flow rate than the GTL oil, the temperature of the GTL oil is slightly lower than the mineral oil due to its higher thermal conductivity and higher specific heat (which arise from its lower density). The synthetic ester has a much lower flow rate than the other two liquids and therefore has lower velocities in most of the horizontal ducts and higher disc temperatures. The flow distribution and temperature distribution of the synthetic ester are very different from those of the mineral oil and the GTL oil because they have quite different Re, Pr and Gr/Re^2 as shown in Table 1. For the synthetic ester, the liquid at the top part of pass 4 is almost in stagnation, causing overheating at the top

of the winding. The uneven temperature distribution of the synthetic ester results in a larger hot-spot factor than the other two liquids. To improve the thermal performance of the synthetic ester, a higher total liquid flow rate is needed. According to (17), a feasible way to do this would be to increase the height difference between the centre line of the radiator and the centre line of the winding, ΔH.

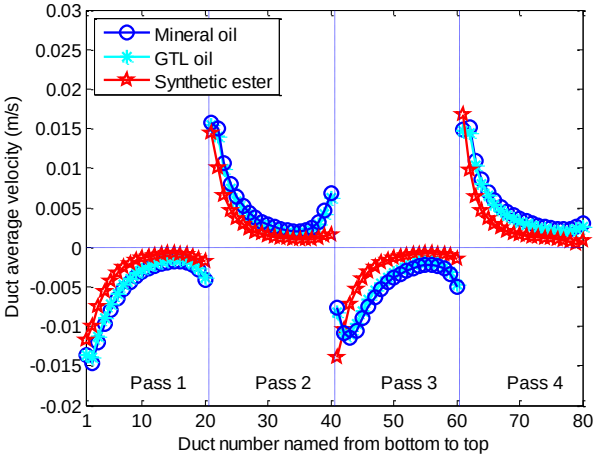

Fig. 3. Average liquid velocity in each horizontal cooling duct. Flow from outer vertical duct to inner vertical duct is set to be negative and vice versa.

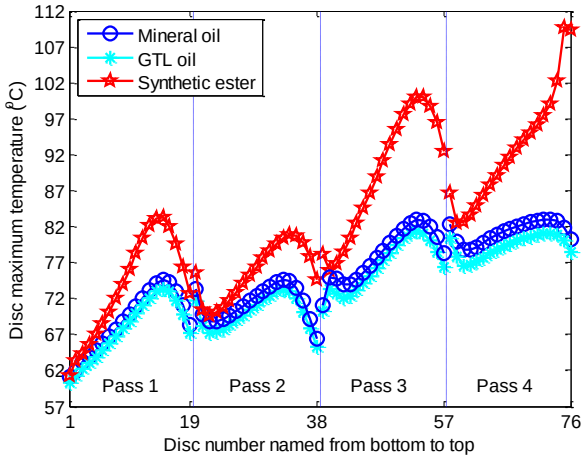

Fig. 4. Maximum temperature of each disc.

Table 1. Comparisons of lumped parameters.

	T_{aw} (°C)	T_{to} (°C)	T_{hs} (°C)	*Re*	*Pr*	Gr/Re^2	*H*
Mineral oil	70.4	67.4	83.0	169	68	0.65	1.17
GTL oil	69.1	66.1	81.4	143	80	0.72	1.20
Synthetic ester	76.9	78.6	109.6	42	172	2.06	2.17

where T_{aw} refers to average winding temperature, T_{to} refers to top oil temperature, T_{hs} refers to hot-spot temperature, H refers to hot-spot factor. *Re*, *Pr* and Gr/Re^2 are calculated based on oil properties at the average of winding top oil and winding bottom oil temperatures.

VI. Conclusion

Dimensional analysis on fluid flow and heat transfer in the winding has been performed for ON transformers. It is found that for a fixed winding geometry and a fixed power loss distribution in dimensionless senses the flow distribution and temperature distribution are governed by *Re*, *Pr* and Gr/Re^2.

Theoretical analysis of the thermal driving force and the pressure drop in the liquid circulation loop, shows that the total volumetric flow rate is proportional to the square root of the total power loss in the winding, and the square root of the height difference between the centre line of the radiator and the centre line of the winding, ΔH.

For different liquids, the ratios of total liquid flow rate are determined. CFD simulations of typical cases are performed. It is found that the hydrocarbon mineral oil gives similar thermal performance to the GTL oil in this evaluation. The synthetic ester on the other hand has quite different flow and temperature distribution due to the significant differences in *Re*, *Pr* and Gr/Re^2. The low liquid flow rate of the synthetic ester can cause local overheating in the winding. A feasible way to improve the thermal performance of the synthetic ester would be to increase ΔH.

Acknowledgment

The authors would like to express their gratitude to M&I Materials, National Grid, Scottish Power, Shell, TJ|H2b Analytical Services, UK Power Networks and Weidmann Electrical Technology AG for their financial and technical contributions to the Transformer Research Consortium at The University of Manchester.

References

[1] IEC, "Loading guide for oil-immersed power transformers," *IEC standard 60076-7*, 2005.

[2] IEEE, "IEEE Guide for Loading Mineral-Oil-Immersed Transformers and Step-Voltage Regulators," *IEEE standard C57.91*, 2011.

[3] X. Zhang, Z. D. Wang, and Q. Liu, "Prediction of Pressure drop and flow distribution in disc type transformer windings under an OD cooling mode," *IEEE Transactions on Power Delivery*, vol. DOI (identifier) 10.1109/TPWRD.2016.2557490, In press, 2016.

[4] X. Zhang, Z. D. Wang, Q. Liu, P. Jarman, A. Gyore, P. Dyer, "Investigation of Convective Heat Transfer Efficiency in the Horizontal Cooling Duct of a Disc Type Transformer Winding," in 19th International Symposium on High Voltage Engineering (ISH), Paper ID 280, Pilsen, Czech Republic, 2015.

[5] M. Nakadate, K. Toda, K. Sato, D. Biswas, C. Nakagawa, T. Yanari, "Gas cooling performance in disc winding of large-capacity gas-insulated transformer," *IEEE Transactions on Power Delivery*, vol. 11, no. 2, pp. 903-908, 1996.

[6] A. Skillen, A. Revell, H. Iacovides, W. Wu, "Numerical prediction of local hot-spot phenomena in transformer windings," *Applied Thermal Engineering*, vol. 36, pp. 96-105, 2012.

[7] M. Yamaguchi, T. Kumasaka, Y. Inui, S. Ono, "The flow rate in a self-cooled transformer," *IEEE Transactions on Power Apparatus and Systems*, no. 3, pp. 956-963, 1981.

[8] F. Torriano, M. Chaaban, and P. Picher, "Numerical study of parameters affecting the temperature distribution in a disc-type transformer winding," *Applied Thermal Engineering*, vol. 30, no. 14, pp. 2034-2044, 2010.

[9] X. Zhang, Z. D. Wang, Q. Liu, P. Jarman, A. Gyore, P. Dyer, "Numerical investigation of influence of coolant types on flow distribution and pressure drop in disc type transformer windings," in International Conference on Condition Monitoring and Diagnosis (CMD), 2016, Xi'an, P.R. China, 2016, pp. 52-55.

[10] P. Picher, F. Torriano, M. Chaaban, S. Gravel, C. Rajotte, B. Girard, "Optimization of transformer overload using advanced thermal modelling," in CIGRE Conference, Paris, France A2-305, 2010.

[11] X. Zhang, Z. D. Wang, and Q. Liu, "Interpretation of Hot Spot Factor for Transformers in OD Cooling Modes," IEEE transactions on Power Delivery, 2017, under review.

Chapter 5 Conclusions and Future Work

5.1 Conclusions

Transformer thermal modelling is of importance for transformer thermal design and operation. This PhD thesis is focused on the CFD thermal modelling of disc-type transformer windings in steady state. Dimensional analysis is widely adopted for its simplicity and provision of insight in fluid mechanics; therefore it is adopted in the thermal modelling to obtain more universally applicable results and principles than conducting CFD modelling for specific transformer designs.

In the transformer thermal modelling, CFD parametric sweeps are guided by dimensional analysis to cover all the practical ranges of the controlling parameters: winding geometric dimensions, liquid flow rate and liquid properties. Some experimental tests are implemented to verify the correlations for flow distribution and pressure drop obtained from the CFD parametric sweeps.

The work is split into two parts on OD cooling modes and ON cooling modes. These two cooling modes are differentiated by the effects of buoyancy forces in the fluid flow and heat transfer processes. For OD cooling modes, the effects of buoyancy forces are found to be negligible by both CFD simulations and experimental tests. For ON cooling modes, on the other hand, buoyancy forces and hot-streak dynamics are responsible for the liquid flow distribution and temperature distribution and therefore cannot be neglected. Detailed conclusions for OD and ON cooling modes are presented in the following subsections.

5.1.1 Conclusions on OD Cooling Modes

Liquid flow distribution in and pressure drop over the winding are important for transformer thermal design: Flow distribution has a direct impact on the cooling performance and a more uniform flow distribution is preferred to avoid localized overheating. Pressure drop over a winding in relation to the total liquid flow rate in

the winding determines oil split among windings connected hydraulically in parallel, e.g. LV winding and HV winding in the same phase.

For OD cooling modes, it is found that the flow distribution is not affected by the number of passes in the winding and the pressure drop over the winding is proportional to the number of passes in the winding. Therefore, In the CFD parametric sweeps, 3-pass winding models with 6 discs (7 horizontal ducts) per pass are used. The flow distribution in the third pass of the winding model and pressure drop over the 3-pass winding model are representative fluid flow and pressure drop results.

Dimensional analyses transform average oil velocity in each horizontal cooling duct and pressure drop over the winding to volumetric flow proportion in that duct and pressure drop coefficient over the winding, respectively. Both the flow proportion and the pressure drop coefficient are controlled by *Re* at the winding pass inlet and dimensionless geometric parameters, which are chosen in this PhD research as the winding geometric dimensions normalized against the vertical duct width. OD flow distributions feature the pattern of high flow rates in the pass top horizontal cooling ducts and low flow rates in the pass bottom horizontal cooling ducts, which is mainly related to the flow separation at the entrances of the bottom horizontal cooling ducts. **The higher *Re*, (i.e. the higher flow rate or the higher liquid temperature) the more uneven the flow distribution will be.** Among the dimensionless geometric parameters, the ratio of the horizontal duct height to vertical duct width, referred to as α, is the most influential one. **The smaller α is, the more uniform the flow distribution will be, at the cost of a higher pressure drop over the winding. Reverse flows at the bottom of the pass occur under the conditions of high *Re* or large α, and this phenomenon is observed by both CFD simulations and experimental tests by particle image velocimetry (PIV) measurements.** Therefore, for OD cooling modes, it is not necessarily the higher the total liquid flow rate the better the cooling performance. These qualitative conclusions are valid for the practical range of number of discs per pass (6-12) for OD transformers.

The quantitative correlations for flow proportion in each horizontal cooling duct and pressure drop coefficient over the winding with the governing dimensionless

groups—*Re* and dimensionless geometric parameters—are obtained from the CFD parametric sweep results using multi-layer curve fitting strategies. **The correlations for flow proportion and pressure drop coefficient of the tested winding models are satisfactorily verified by experimental tests, where the occurrences of reverse flow under certain conditions can be obtained from the flow correlation and ascertained by the PIV measurements**. These correlation equations can provide one with results that are as accurate as CFD modelling, while the computational effort required is even lower than network modelling. For OD cooling modes, a reverse flow occurs first at the bottom duct of a pass. Therefore, the flow proportion correlation for the bottom duct can be used to identify quantitatively the conditions for the occurrence of reverse flow. It is found that **the occurrence of the reverse flow is associated with the condition of high *Re* or high α**. To quantify the uniformity of flow distribution in the winding pass, a parameter called maldistribution factor is defined as the ratio of the maximum flow rate to the minimum flow rate in a pass. The variation of maldistribution with the controlling dimensionless parameters is quantified by using the flow proportion correlations derived. It is found that **the maldistribution factor increases monotonically with the increase of *Re* and the increase of α, which can provide guide to OD transformer design.**

The effects of three different liquids—a mineral oil, a GTL oil and a synthetic ester—on the flow distribution in and pressure drop over the winding, arisen from their different properties (k, c_p ρ, μ) and potentially different total flow rates, are investigated by using the correlations derived. It is found that **for OD cooling modes the synthetic ester, which is the most viscous of the three, is advantageous in terms of suppressing the occurrence of reverse flow and getting a relatively more uniform flow distribution at the cost of a larger pressure drop.**

The hot-spot factor, H, is interpreted as a dimensionless temperature at the hot-spot. It is found that **for a given winding geometry and a given power loss distribution, H is a function of *Re* and *Pr*. In addition, *Re* is found to be much more influential than *Pr* in controlling H.** Case studies on a three-pass winding model with uniform power loss distribution show that H stays quite constant in the region of *Re* between 200 and 700 and increases rapidly when *Re* exceeds 700 because of

the increasingly uneven flow distribution. For nonuniform power loss distribution scenarios, *H* increases linearly with the increase of the *Q* factor at the hot-spot and this linear relationship is coupled with the nonlinear relationship between *H* and *Re* and *Pr*. The effects of operational conditions—ambient temperature, loading level and total liquid flow rate—on *H* are investigated according to the correlations obtained between *H* and *Re* and *Pr*.

5.1.2 Conclusions on ON Cooling Modes

For ON cooling modes, dimensional analyses on fluid flow and heat transfer show that **for a given winding geometry and a given power loss distribution, the dimensionless flow distribution, temperature distribution and *H* are all controlled by *Re*, *Pr* and Gr/Re^2.** Gr/Re^2 is a dominant factor for flow and temperature distribution because it provides a measure of the ratio of buoyancy forces to inertial forces. In addition, *Re* is more influential than *Pr*.

For a 5-pass LV winding model with constant power loss distribution, it is found that *H* keeps decreasing when Gr/Re^2 increases from 0 to approximately 0.5 with minimum *H* being approximately 1.1, and then *H* increases with the increase of Gr/Re^2 until Gr/Re^2 reaches approximately 0.9. When Gr/Re^2 is larger than 0.9, reverse flows in horizontal cooling ducts at the top part of passes, opposite to that of OD conditions, start to occur, and the occurrence of reverse flow leads to a large *H* of approximately 2. With a further increase of Gr/Re^2, the region suffering from reverse flows shifts down to the middle part of the pass and results in the shift of the hot-spot and the fluctuation of *H*. In addition, the first trough of *H* at Gr/Re^2 being approximately 0.5 is observed for a wide range of *Re* which is typical for ON cooling modes. **This indicates that there is an optimal design and operational regime at Gr/Re^2 being approximately 0.5 for this winding, where the effects of buoyancy forces are balanced by the inertial forces and therefore the flow is the most uniform and *H* the smallest.**

For an ON transformer with a given winding geometry and a given power loss distribution, the effects of three different liquids—a mineral oil, a GTL oil and a synthetic ester—on the flow distribution and temperature distribution are also

investigated. First of all, the total liquid flow rates in the winding for the three different liquids are determined by assuming that heat transfer occurs only in the winding and the radiator, and temperature rises linearly with the height in both the winding and the radiator, and by neglecting the so called minor pressure losses due to the change of flow direction. A formula is established to correlate the total liquid flow rate to the controlling parameters: liquid properties (ρ, μ, k, c_p), the total power loss in the winding and the height difference between the centre point of the radiator and the centre point of the winding, ΔH. **It is found that for a fixed liquid type the total liquid flow rate is proportional to the square root of the total power loss in the winding and the square root of ΔH.**

CFD case studies of the three liquids are conducted to investigate the effects of different liquid types on the flow and temperature distributions based on the flow rates determined from the formula with a given flow rate of the mineral oil as a benchmark. The CFD results show that the mineral oil and the GTL oil share similar flow and temperature distributions, while the synthetic ester, which is the most viscous of the three, has the lowest total flow rate and a significant higher hot-spot temperature than the other two liquids due to the incipiency of a reverse flow at the penultimate ducts in winding passes.

5.2 **Future Work**

This PhD study has been focusing on CFD thermal modelling of disc-type transformer windings in steady state. Further experimental verification should be planned to further advance our understanding of transformer thermal design principles and so is to extend the dimensional analysis methodology to the dynamic thermal modelling research.

5.2.1 On Further Experimental Verification

Experimental verification of the dimensional analysis results on flow distribution in and pressure drop over disc-type transformer windings in OD cooling modes has been executed under isothermal flow conditions by a PhD student colleague in the same research group. In the experimental verification, the winding plates are made of

bare aluminium plates. This is acceptable for OD cooling modes. However, for accurately determining the temperature distribution, the effects of the paper insulation are not negligible. Furthermore, for ON cooling modes hot-streak dynamics, which play a vital role in determining flow and temperature distributions, are affected by the heat transfer in the winding plates. Therefore, modified winding model with paper wrapped and stranded winding plates are needed for the verification of the conclusions made in this PhD thesis on the hot-spot factor and flow and temperature distributions in ON cooling modes. Specific experimental verification plan is shown as follows:

1. Build up a disc-type winding model with winding plates consisting of paper wrapped strands to test the trend of H against increasing Re in OD cooling modes and to check the validity of the CFD predictions. With the use of a pump to control the total liquid flow rate in the winding, wide ranges of Re, Gr/Re^2 can be achieved for ON cooling modes and therefore the influence of these dimensionless controlling parameters on flow distribution, temperature distribution and H can be tested and compared with CFD predictions. The existence of the common first trough of H against Gr/Re^2, representing the optimal design and operational regime, can then be checked.

2. Build up a disc-type ON transformer model that can establish spontaneous flow (genuine ON flow regime) to test the relationship between the total liquid flow rate in the circulation loop and the total power injection in the winding and ΔH. In addition, the effects of different liquid types on the total liquid flow rate can also be tested and compared with theoretical predictions.

3. Dynamic thermal tests with the experimental models can be conducted to complement the theoretical work on dynamic thermal modelling to be implemented.

5.2.2 On Dynamic Thermal Modelling

Dynamic thermal modelling is of great practical importance because it can provide the transformer asset manager with real-time hot-spot temperature, which enables the

control of the loading level or to switch the cooling modes if more than one cooling mode is available. Furthermore, the loss of transformer insulation life during the operation can be calculated from the dynamic hot-spot temperature derived.

An accurate dynamic thermal model guarantees the quality of the guidance on transformer operation and transformer asset management. Dynamic CFD modelling can be performed to help calibrate the dynamic thermal model proposed in IEC 60076-7: 2005, loading guide for oil-immersed power transformers. The dynamic CFD model of a transformer should involve both the dynamic thermal model of the winding and the dynamic thermal model of the radiator. The thermal modelling of the radiator would be a challenge and the high computational demand to simulate a whole oil circulation loop in the transformer would also be a concern. Alternatively, a correlation could be adopted or developed to represent the thermal behaviour of the radiator.

In addition, the dynamic thermal model in IEC 60076-7: 2005 assumes H to be a constant [7]. With the new understanding of H as a function of Re, Pr and Gr/Re^2, modification of the dynamic thermal model, or, more precisely, H, in the IEC standard can be implemented.

Blank page

References

[1] D. J. Allan, "Power transformers-the second century," *Power Engineering Journal*, vol. 5, no. 1, pp. 5-14, 1991.

[2] M. Heathcote, *J & P transformer book*, Thirteenth ed.: Newnes, 2007.

[3] H. P. Moser, and V. Dahinden, "Transformerboard," 1979.

[4] CIGRE642, "Transformer Reliability Survey," 2015.

[5] J. Paul, H. Ruth, L. Walker, Q. Zhong, T. Ishak, Z.D. Wang, "Transformer life prediction using data from units removed from service and thermal modelling," 2010.

[6] C. Krause, "Power transformer insulation–history, technology and design," *IEEE Transactions on Dielectrics and Electrical Insulation*, vol. 19, no. 6, 2012.

[7] IEC, "Loading guide for oil-immersed power transformers," *IEC standard 60076-7*, 2005.

[8] IEEE, "IEEE Guide for Loading Mineral-Oil-Immersed Transformers and Step-Voltage Regulators," *IEEE standard C57.91*, 2011.

[9] P. Picher, F. Torriano, M. Chaaban, S. Gravel, C. Rajotte, B. Girard, "Optimization of transformer overload using advanced thermal modelling," in CIGRE Conference, Paris, France A2-305, 2010.

[10] M. Yamaguchi, T. Kumasaka, Y. Inui, S. Ono, "The flow rate in a self-cooled transformer," *IEEE Transactions on Power Apparatus and Systems*, no. 3, pp. 956-963, 1981.

[11] IEC, "Temperature rise for liquid-immersed transformers," *IEC standard 60076-2*, 2011.

[12] CIGRE659, "Transformer Thermal Modelling," 2016.

[13] CIGRE WG 12-09 Electra no. 161, "Experimental determination of power transformer hot-spot factor," 1995.

[14] W. CIGRE, "12.09 (Thermal Aspect of Transformers)," *A survey of facts and opinion on the maximum safe operating temperatures under emergency conditions, CIGRE*, vol. 25, 1995.

[15] M. Daghrah, Z.D. Wang, Q. Liu, D. Walker, Ch. Krause, G. Wilson, "Experimental investigation of hot spot factor for assessing hot spot temperature in transformers," in International Conference on Condition Monitoring and Diagnosis, Xi'an, P.R. China, pp. 948-951, 2016.

[16] Z. Radakovic, U. Radoman, and P. Kostic, "Decomposition of the Hot-Spot Factor," *IEEE Transactions on Power delivery*, vol. 30, pp. 403-411, 2015.

[17] D. Feng, Z. Wang, and P. Jarman, "Evaluation of Power Transformers' Effective Hot-Spot Factors by Thermal Modeling of Scrapped Units," *Power Delivery, IEEE Transactions on*, vol. 29, no. 5, pp. 2077-2085, 2014.

[18] A. J. Oliver, "Estimation of transformer winding temperatures and coolant flows using a general network method," *Proc. Inst. Elect. Eng.*, vol. 127, pp. 395-405, 1980.

[19] Z. R. Radakovic, and M. S. Sorgic, "Basics of detailed thermal-hydraulic model for thermal design of oil power transformers," *IEEE Transactions on Power Delivery*, vol. 25, no. 2, pp. 790-802, 2010.

[20] E. Rahimpour, M. Barati, and M. Schäfer, "An investigation of parameters affecting the temperature rise in windings with zigzag cooling flow path," *Applied thermal engineering*, vol. 27, no. 11, pp. 1923-1930, 2007.

[21] J. Zhang, and X. Li, "Oil cooling for disk-type transformer windings-part 1: theory and model development," *IEEE Transactions on Power Delivery,* vol. 21, no. 3, pp. 1318-1325, 2006.

[22] J. Zhang, and X. Li, "Coolant flow distribution and pressure loss in ONAN transformer windings. Part I: Theory and model development," *IEEE Transactions on Power Delivery,* vol. 19, no. 1, pp. 186-193, 2004.

[23] J. Zhang, and X. Li, "Coolant flow distribution and pressure loss in ONAN transformer windings. Part II: Optimization of design parameters," *IEEE Transactions on Power Delivery,* vol. 19, no. 1, pp. 194-199, 2004.

[24] J. Zhang, and X. Li, "Oil cooling for disk-type transformer windings-Part II: Parametric studies of design parameters," *IEEE Transactions on Power Delivery,* vol. 21, no. 3, pp. 1326-1332, 2006.

[25] E. Kranenborg, C. Olsson, B. Samuelsson, L. Lundin, R. Missing, "Numerical study on mixed convection and thermal streaking in power transformer windings," in 5th European Thermal-Sciences Conference, The Netherlands, 2008.

[26] A. Skillen, A. Revell, H. Iacovides, W. Wu, "Numerical prediction of local hot-spot phenomena in transformer windings," *Applied Thermal Engineering,* vol. 36, pp. 96-105, 2012.

[27] F. Torriano, M. Chaaban, and P. Picher, "Numerical study of parameters affecting the temperature distribution in a disc-type transformer winding," *Applied Thermal Engineering,* vol. 30, no. 14, pp. 2034-2044, 2010.

[28] F. Torriano, P. Picher, and M. Chaaban, "Numerical investigation of 3D flow and thermal effects in a disc-type transformer winding," *Applied Thermal Engineering,* vol. 40, pp. 121-131, 2012.

[29] J.-M. Mufuta, and E. Van den Bulck, "Modelling of the mixed convection in the windings of a disc-type power transformer," *Applied Thermal Engineering,* vol. 20, no. 5, pp. 417-437, 2000.

[30] D. K. Jamison, and J. R. Villemonte, "Junction losses in laminar and transitional flows," *Journal of the Hydraulics Division,* vol. 97, no. 7, pp. 1045-1063, 1971.

[31] W. Wu, Z. Wang, A. Revell, P. Jarman, "Computational fluid dynamics calibration for network modelling of transformer cooling oil flows-part II: pressure loss at junction nodes," *IET electric power applications,* vol. 6, no. 1, pp. 28-34, 2012.

[32] J. Coddé, W. Van der Veken, and M. Baelmans, "Assessment of a hydraulic network model for zig–zag cooled power transformer windings," *Applied Thermal Engineering,* vol. 80, pp. 220-228, 2015.

[33] H. Wong, *Handbook of essential formulae and data on heat transfer for engineers*: Longman London, 1977.

[34] W. M. Rohsenow, J. P. Hartnett, and E. N. Ganic, "Handbook of heat transfer applications," *New York, McGraw-Hill Book Co., 1985, 973 p. No individual items are abstracted in this volume.,* vol. 1, 1985.

[35] W. Wu, Z. Wang, A. Revell, H. Iacovides, P. Jarman, "Computational fluid dynamics calibration for network modelling of transformer cooling oil flows-part I: heat transfer in oil ducts," *IET Electric Power Applications,* vol. 6, no. 1, pp. 19-27, 2012.

[36] X. Zhang, Z. D. Wang, Q. Liu, P. Jarman, A. Gyore, P. Dyer, "Investigation of Convective Heat Transfer Efficiency in the Horizontal Cooling Duct of a

Disc Type Transformer Winding," in 19th International Symposium on High Voltage Engineering (ISH), Paper ID 280, Pilsen, Czech Republic, 2015.
[37] R. W. Fox, A. T. McDonald, and P. J. Pritchard, *Fluid Mechanics*, Eighth ed., New York: John Wiley & Sons, Inc., 2012.
[38] J. Holman, "Heat Transfer," McGraw-Hill Inc, 2002.
[39] COMSOL, "CFD Module User's Guide," 2013.
[40] J. Lee, S. Lee, J. Woo, I. Hwang, "CFD analyses and experiments of a winding with zig–zag cooling duct for a power transformer," in CIGRE Conference, Paris, France A2-310, 2010.
[41] W. Wu, "CFD calibrated thermal network modelling for oil-cooled power transformers," School of Electrical and Electronic Engineering, The University of Manchester, UK, 2011.
[42] H. Winter, "Contribution to the hydraulic branching problem," *Ing. Arch. 9 239e249 (in German),* 1955.
[43] K. J. Oh, and S. S. Ha, "Numerical calculation of turbulent natural convection in a cylindrical transformer enclosure," *Heat Transfer—Asian Research,* vol. 28, no. 6, pp. 429-441, 1999.
[44] T. L. Bergman, A. S. Lavine, F. P. Incropera, D. P. DeWitt, *Fundamentals of heat and mass transfer*: John Wiley & Sons, 2011.
[45] A. Weinläder, and S. Tenbohlen, "Thermal-hydraulic investigation of transformer windings by CFD-modelling and measurements."
[46] H. Campelo, M. Quintela, F. Torriano, P. Labbe, P. Picher, "Numerical thermofluid analysis of a power transformer disc-type winding," in Electrical Insulation Conference, Montreal, Qc, Canada, pp. 362-365, 2016.
[47] J. Zhang, X. Li, and M. Vance, "Experiments and modeling of heat transfer in oil transformer winding with zigzag cooling ducts," *Applied Thermal Engineering,* vol. 28, no. 1, pp. 36-48, 2008.
[48] A. Weinläder, W. Wu, S. Tenbohlen, Z.D. Wang, "Prediction of the oil flow distribution in oil-immersed transformer windings by network modelling and computational fluid dynamics," *IET electric power applications,* vol. 6, no. 2, pp. 82-90, 2012.
[49] J.-M. Mufuta, "Comparison of experimental values and numerical simulation on a set-up simulating the cross-section of a disc-type transformer," *International journal of thermal sciences,* vol. 38, no. 5, pp. 424-435, 1999.
[50] J.-M. Mufuta, and E. Van den Bulck, "Modelling of the mass flow distribution around an array of rectangular blocks in-line arranged and simulating the cross-section of a winding disc-type transformer," *Applied thermal engineering,* vol. 21, no. 7, pp. 731-749, 2001.
[51] P. Allen, O. Szpiro, and E. Campero, "Thermal analysis of power transformer windings," *Electric Machines and Electromechanics,* vol. 6, no. 1, pp. 1-11, 1981.
[52] M. Nakadate, K. Toda, K. Sato, D. Biswas, C. Nakagawa, T. Yanari, "Gas cooling performance in disc winding of large-capacity gas-insulated transformer," *IEEE Transactions on Power Delivery,* vol. 11, no. 2, pp. 903-908, 1996.
[53] J. Zhang, and X. Li, "Natural cooling oil flow in disk-type transformer windings with zigzag flow passages," International Journal of Transport Phenomena, vol. 7, no. 3, pp. 199-218, 2005.

Blank page

Appendix 1 Coefficients in Paper 1

Coefficient *d's* for pressure drop coefficient in equation (8) in paper 1 (d_{ijkl}, *i=1,2; j=1,2,3; k=1,2,3; l=1,2,3,4*).

d_{11kl}	$l=1$	$l=2$	$l=3$	$l=4$
$k=1$	-1.8042e-03	7.9181e-02	-1.4919e-01	4.4225e-01
$k=2$	-3.4610e-04	1.2707e-02	-1.3717e-01	2.0262e-01
$k=3$	-5.4244e-05	3.5012e-03	-7.8870e-02	4.9943e-01

d_{12kl}	$l=1$	$l=2$	$l=3$	$l=4$
$k=1$	2.7135e-04	-1.4335e-02	2.9232e-01	-5.5600e+00
$k=2$	9.1536e-05	-3.5931e-03	4.3912e-02	-9.3459e-02
$k=3$	2.8322e-05	-1.4633e-03	2.9159e-02	-2.2201e-01

d_{13kl}	$l=1$	$l=2$	$l=3$	$l=4$
$k=1$	-3.4971e-04	1.6457e-02	-2.9825e-01	2.5665e+00
$k=2$	1.1456e-04	-5.8513e-03	1.1396e-01	-2.7665e-01
$k=3$	3.4044e-05	-1.4200e-03	2.4393e-02	-1.9832e-01

d_{21kl}	$l=1$	$l=2$	$l=3$	$l=4$
$k=1$	-4.8523e-03	1.9217e-01	-2.5900e+00	1.2206e+01
$k=2$	-8.1541e-04	3.4546e-02	-4.6800e-01	1.6601e+00
$k=3$	4.0444e-04	-1.8817e-02	2.9219e-01	-1.4964e+00

d_{22kl}	$l=1$	$l=2$	$l=3$	$l=4$
$k=1$	5.9841e-04	-1.8270e-02	4.1821e-05	6.4343e+00
$k=2$	-2.1493e-04	1.0188e-02	-1.5817e-01	7.0123e-01
$k=3$	8.6712e-05	-5.0296e-03	8.3290e-02	-5.1667e-01

d_{23kl}	$l=1$	$l=2$	$l=3$	$l=4$
$k=1$	-7.8421e-05	-4.0686e-03	2.6807e-01	-3.7948e+00
$k=2$	-1.6041e-04	9.9204e-03	-1.8961e-01	8.9986e-01
$k=3$	-2.2668e-04	1.6188e-03	4.9217e-02	-5.4151e-01

Since there are too many coefficient *d's* for flow proportion in all the horizontal ducts in equation (9) in paper 1. Only the coefficient *d's* for flow in the bottom duct ($i = 1$) are displayed in this appendix (d_{1jkml}, *j=1,2,3,4; k=1,2,3,4;m=1,2,3,4; l=1,2,3,4*)

d_{111ml}	$l=1$	$l=2$	$l=3$	$l=4$
$m=1$	-1.1629e+00	4.1462e+01	-4.8129e+02	1.8528e+03
$m=2$	6.6298e+00	-2.3711e+02	2.7756e+03	-1.0778e+04
$m=3$	-1.0781e+01	3.9259e+02	-4.7207e+03	1.8689e+04
$m=4$	6.5080e+00	-2.4962e+02	3.1455e+03	-1.2250e+04

d_{112ml}	$l=1$	$l=2$	$l=3$	$l=4$
$m=1$	1.5932e+00	-5.6377e+01	6.4803e+02	-2.4739e+03
$m=2$	-9.0284e+00	3.2032e+02	-3.7128e+03	1.4321e+04
$m=3$	1.4491e+01	-5.2323e+02	6.2371e+03	-2.4664e+04
$m=4$	-8.4831e+00	3.2459e+02	-4.1038e+03	1.6231e+04

d_{113ml}	$l=1$	$l=2$	$l=3$	$l=4$
$m=1$	-6.9069e-01	2.4261e+01	-2.7603e+02	1.0435e+03
$m=2$	3.8855e+00	-1.3675e+02	1.5682e+03	-5.9967e+03
$m=3$	-6.1390e+00	2.1965e+02	-2.5912e+03	1.0208e+04
$m=4$	3.4554e+00	-1.3181e+02	1.6713e+03	-6.7307e+03

d_{114ml}	$l=1$	$l=2$	$l=3$	$l=4$
$m=1$	9.1970e-02	-3.2110e+00	3.6225e+01	-1.3582e+02
$m=2$	-5.1300e-01	1.7936e+01	-2.0386e+02	7.7385e+02
$m=3$	7.9671e-01	-2.8286e+01	3.3075e+02	-1.2986e+03
$m=4$	-4.2888e-01	1.6332e+01	-2.0791e+02	8.5302e+02

d_{121ml}	$l=1$	$l=2$	$l=3$	$l=4$
$m=1$	-1.4298e-01	5.0968e+00	-5.9163e+01	2.2725e+02
$m=2$	8.1536e-01	-2.9152e+01	3.4111e+02	-1.3203e+03
$m=3$	-1.3291e+00	4.8351e+01	-5.8017e+02	2.2839e+03
$m=4$	8.0453e-01	-3.0713e+01	3.8406e+02	-1.4779e+03

d_{122ml}	$l=1$	$l=2$	$l=3$	$l=4$

$m=1$	1.9570e-01	-6.9253e+00	7.9640e+01	-3.0358e+02
$m=2$	-1.1096e+00	3.9370e+01	-4.5638e+02	1.7561e+03
$m=3$	1.7868e+00	-6.4480e+01	7.6752e+02	-3.0198e+03
$m=4$	-1.0515e+00	4.0059e+01	-5.0273e+02	1.9636e+03

d_{123ml}	$l=1$	$l=2$	$l=3$	$l=4$
$m=1$	-8.4713e-02	2.9764e+00	-3.3897e+01	1.2807e+02
$m=2$	4.7696e-01	-1.6792e+01	1.9271e+02	-7.3586e+02
$m=3$	-7.5663e-01	2.7069e+01	-3.1917e+02	1.2523e+03
$m=4$	4.2963e-01	-1.6328e+01	2.0564e+02	-8.1805e+02

d_{124ml}	$l=1$	$l=2$	$l=3$	$l=4$
$m=1$	1.1264e-02	-3.9346e-01	4.4450e+00	-1.6672e+01
$m=2$	-6.2902e-02	2.2005e+00	-2.5042e+01	9.5025e+01
$m=3$	9.8151e-02	-3.4861e+00	4.0774e+01	-1.5964e+02
$m=4$	-5.3511e-02	2.0313e+00	-2.5702e+01	1.0423e+02

d_{131ml}	$l=1$	$l=2$	$l=3$	$l=4$
$m=1$	3.7502e-02	-1.3363e+00	1.5505e+01	-5.9351e+01
$m=2$	-2.1413e-01	7.6508e+00	-8.9420e+01	3.4446e+02
$m=3$	3.5035e-01	-1.2721e+01	1.5212e+02	-5.9404e+02
$m=4$	-2.1192e-01	8.0376e+00	-9.9491e+01	3.7720e+02

d_{132ml}	$l=1$	$l=2$	$l=3$	$l=4$
$m=1$	-5.1304e-02	1.8153e+00	-2.0879e+01	7.9375e+01
$m=2$	2.9135e-01	-1.0334e+01	1.1974e+02	-4.5887e+02
$m=3$	-4.7131e-01	1.6985e+01	-2.0164e+02	7.8746e+02
$m=4$	2.7795e-01	-1.0524e+01	1.3076e+02	-5.0278e+02

d_{133ml}	$l=1$	$l=2$	$l=3$	$l=4$
$m=1$	2.2180e-02	-7.7945e-01	8.8841e+00	-3.3511e+01
$m=2$	-1.2511e-01	4.4053e+00	-5.0572e+01	1.9256e+02
$m=3$	1.9958e-01	-7.1354e+00	8.4003e+01	-3.2755e+02
$m=4$	-1.1405e-01	4.3106e+00	-5.3779e+01	2.1052e+02

d_{134ml}	$l=1$	$l=2$	$l=3$	$l=4$

$m = 1$	-2.9459e-03	1.0294e-01	-1.1646e+00	4.3666e+00
$m = 2$	1.6485e-02	-5.7699e-01	6.5734e+00	-2.4906e+01
$m = 3$	-2.5891e-02	9.1958e-01	-1.0750e+01	4.1889e+01
$m = 4$	1.4278e-02	-5.3934e-01	6.7649e+00	-2.7012e+01

d_{141ml}	$l = 1$	$l = 2$	$l = 3$	$l = 4$
$m = 1$	7.3601e-01	-2.6241e+01	3.0464e+02	-1.1721e+03
$m = 2$	-4.1955e+00	1.5005e+02	-1.7565e+03	6.8144e+03
$m = 3$	6.8271e+00	-2.4858e+02	2.9875e+03	-1.1807e+04
$m = 4$	-4.1295e+00	1.5817e+02	-1.9882e+03	7.7109e+03

d_{142ml}	$l = 1$	$l = 2$	$l = 3$	$l = 4$
$m = 1$	-1.0078e+00	3.5667e+01	-4.1009e+02	1.5651e+03
$m = 2$	5.7114e+00	-2.0266e+02	2.3495e+03	-9.0569e+03
$m = 3$	-9.1759e+00	3.3132e+02	-3.9485e+03	1.5592e+04
$m = 4$	5.3872e+00	-2.0587e+02	2.5968e+03	-1.0227e+04

d_{143ml}	$l = 1$	$l = 2$	$l = 3$	$l = 4$
$m = 1$	4.3664e-01	-1.5340e+01	1.7460e+02	-6.6005e+02
$m = 2$	-2.4566e+00	8.6479e+01	-9.9211e+02	3.7928e+03
$m = 3$	3.8861e+00	-1.3906e+02	1.6407e+03	-6.4563e+03
$m = 4$	-2.1963e+00	8.3698e+01	-1.0591e+03	4.2482e+03

d_{144ml}	$l = 1$	$l = 2$	$l = 3$	$l = 4$
$m = 1$	-5.8106e-02	2.0291e+00	-2.2904e+01	8.5904e+01
$m = 2$	3.2417e-01	-1.1337e+01	1.2893e+02	-4.8947e+02
$m = 3$	-5.0417e-01	1.7905e+01	-2.0943e+02	8.2177e+02
$m = 4$	2.7287e-01	-1.0383e+01	1.3194e+02	-5.3918e+02

Appendix 2 Coefficients in Paper 2

Coefficient *d's* for pressure drop coefficient in equation (8) in paper 2 (d_{ijkl}, *i=1,2; j=1,2,3; k=1,2,3; l=1,2,3,4*).

d_{11kl}	$l=1$	$l=2$	$l=3$	$l=4$
$k=1$	-2.4208e-04	2.0470e-02	-9.6923e-02	9.4684e-01
$k=2$	-4.7388e-04	2.0306e-02	-2.9980e-01	1.1885e+00
$k=3$	2.2693e-04	-8.2269e-03	8.0954e-02	5.3877e-02

d_{12kl}	$l=1$	$l=2$	$l=3$	$l=4$
$k=1$	-7.9976e-04	3.0573e-02	-3.5235e-01	-3.2488e+00
$k=2$	1.1687e-04	-4.8559e-03	7.1584e-02	-2.9611e-01
$k=3$	-3.0106e-05	7.4727e-04	2.0851e-03	-1.7834e-01

d_{13kl}	$l=1$	$l=2$	$l=3$	$l=4$
$k=1$	3.2967e-04	-1.1183e-02	7.4633e-02	1.6906e+00
$k=2$	1.4510e-04	-6.1069e-03	1.0144e-01	-3.5391e-01
$k=3$	-4.4424e-05	1.1911e-03	-2.4302e-03	-1.8625e-01

d_{21kl}	$l=1$	$l=2$	$l=3$	$l=4$
$k=1$	-3.9098e-03	1.5410e-01	-2.1412e+00	1.1275e+01
$k=2$	-1.6319e-03	5.5234e-02	-6.0882e-01	1.9097e+00
$k=3$	1.3078e-03	-4.4513e-02	5.2351e-01	-2.2509e+00

d_{22kl}	$l=1$	$l=2$	$l=3$	$l=4$
$k=1$	-2.5982e-03	8.1721e-02	-8.8034e-01	8.2596e+00
$k=2$	-8.5303e-04	2.9390e-02	-3.3262e-01	1.2719e+00
$k=3$	6.5599e-04	-2.2464e-02	2.6193e-01	-1.1392e+00

d_{23kl}	$l=1$	$l=2$	$l=3$	$l=4$
$k=1$	1.8171e-03	-6.1696e-02	7.5417e-01	-4.9542e+00
$k=2$	-1.3631e-03	4.6713e-02	-5.2405e-01	1.9090e+00
$k=3$	1.0832e-03	-3.6788e-02	4.2461e-01	-1.7235e+00

Since there are too many coefficient *d's* for flow proportion in all the horizontal ducts in equation (7) in paper 2. Only the coefficient *d's* for flow in the bottom duct ($i = 1$) are displayed in this appendix (d_{1jkml}, *j=1,2,3,4; k=1,2,3,4;m=1,2,3,4; l=1,2,3,4*)

d_{111ml}	$l=1$	$l=2$	$l=3$	$l=4$
$m=1$	-4.5699e-01	1.5891e+01	-1.7950e+02	6.4458e+02
$m=2$	2.4632e+00	-8.8744e+01	1.0392e+03	-3.7764e+03
$m=3$	-4.2986e+00	1.5783e+02	-1.8533e+03	6.4637e+03
$m=4$	1.8797e+00	-6.7531e+01	7.5076e+02	-2.3151e+03

d_{112ml}	$l=1$	$l=2$	$l=3$	$l=4$
$m=1$	6.2817e-01	-2.1718e+01	2.4450e+02	-8.7870e+02
$m=2$	-3.3426e+00	1.1985e+02	-1.4037e+03	5.1416e+03
$m=3$	5.7841e+00	-2.1229e+02	2.5101e+03	-8.9080e+03
$m=4$	-2.5634e+00	9.2520e+01	-1.0431e+03	3.3068e+03

d_{113ml}	$l=1$	$l=2$	$l=3$	$l=4$
$m=1$	-2.7095e-01	9.3136e+00	-1.0453e+02	3.7670e+02
$m=2$	1.4244e+00	-5.0822e+01	5.9536e+02	-2.2032e+03
$m=3$	-2.4472e+00	8.9767e+01	-1.0692e+03	3.8764e+03
$m=4$	1.1055e+00	-4.0117e+01	4.5966e+02	-1.5117e+03

d_{114ml}	$l=1$	$l=2$	$l=3$	$l=4$
$m=1$	3.5752e-02	-1.2237e+00	1.3711e+01	-4.9614e+01
$m=2$	-1.8613e-01	6.6194e+00	-7.7653e+01	2.9046e+02
$m=3$	3.1869e-01	-1.1698e+01	1.4041e+02	-5.1948e+02
$m=4$	-1.4744e-01	5.3825e+00	-6.2636e+01	2.1342e+02

d_{121ml}	$l=1$	$l=2$	$l=3$	$l=4$
$m=1$	-6.7459e-02	2.3450e+00	-2.6442e+01	9.4652e+01
$m=2$	3.6205e-01	-1.3028e+01	1.5211e+02	-5.5020e+02
$m=3$	-6.2652e-01	2.2958e+01	-2.6846e+02	9.3010e+02
$m=4$	2.7259e-01	-9.7622e+00	1.0780e+02	-3.2783e+02

d_{122ml}	$l=1$	$l=2$	$l=3$	$l=4$

$m = 1$	9.2615e-02	-3.2014e+00	3.5984e+01	-1.2891e+02
$m = 2$	-4.9120e-01	1.7595e+01	-2.0549e+02	7.4914e+02
$m = 3$	8.4399e-01	-3.0919e+01	3.6412e+02	-1.2836e+03
$m = 4$	-3.7238e-01	1.3401e+01	-1.5014e+02	4.6974e+02

d_{123ml}	$l = 1$	$l = 2$	$l = 3$	$l = 4$
$m = 1$	-3.9930e-02	1.3725e+00	-1.5384e+01	5.5264e+01
$m = 2$	2.0944e-01	-7.4669e+00	8.7250e+01	-3.2137e+02
$m = 3$	-3.5777e-01	1.3102e+01	-1.5548e+02	5.6003e+02
$m = 4$	1.6102e-01	-5.8279e+00	6.6405e+01	-2.1581e+02

d_{124ml}	$l = 1$	$l = 2$	$l = 3$	$l = 4$
$m = 1$	5.2699e-03	-1.8041e-01	2.0190e+00	-7.2846e+00
$m = 2$	-2.7396e-02	9.7374e-01	-1.1397e+01	4.2440e+01
$m = 3$	4.6689e-02	-1.7114e+00	2.0468e+01	-7.5270e+01
$m = 4$	-2.1533e-02	7.8435e-01	-9.0826e+00	3.0635e+01

d_{131ml}	$l = 1$	$l = 2$	$l = 3$	$l = 4$
$m = 1$	2.0356e-02	-7.0755e-01	7.9633e+00	-2.8406e+01
$m = 2$	-1.0848e-01	3.8992e+00	-4.5368e+01	1.6323e+02
$m = 3$	1.8525e-01	-6.7730e+00	7.8804e+01	-2.7089e+02
$m = 4$	-7.9819e-02	2.8458e+00	-3.1117e+01	9.2828e+01

d_{132ml}	$l = 1$	$l = 2$	$l = 3$	$l = 4$
$m = 1$	-2.7903e-02	9.6450e-01	-1.0822e+01	3.8630e+01
$m = 2$	1.4715e-01	-5.2657e+00	6.1295e+01	-2.2221e+02
$m = 3$	-2.4998e-01	9.1382e+00	-1.0708e+02	3.7440e+02
$m = 4$	1.0935e-01	-3.9190e+00	4.3504e+01	-1.3361e+02

d_{133ml}	$l = 1$	$l = 2$	$l = 3$	$l = 4$
$m = 1$	1.2024e-02	-4.1337e-01	4.6260e+00	-1.6557e+01
$m = 2$	-6.2799e-02	2.2372e+00	-2.6060e+01	9.5443e+01
$m = 3$	1.0627e-01	-3.8840e+00	4.5872e+01	-1.6389e+02
$m = 4$	-4.7480e-02	1.7119e+00	-1.9340e+01	6.1741e+01

d_{134ml}	$l = 1$	$l = 2$	$l = 3$	$l = 4$

$m = 1$	-1.5874e-03	5.4362e-02	-6.0761e-01	2.1844e+00
$m = 2$	8.2266e-03	-2.9225e-01	3.4109e+00	-1.2632e+01
$m = 3$	-1.3911e-02	5.0898e-01	-6.0602e+00	2.2114e+01
$m = 4$	6.3779e-03	-2.3153e-01	2.6611e+00	-8.8380e+00

d_{141ml}	$l = 1$	$l = 2$	$l = 3$	$l = 4$
$m = 1$	3.1503e-01	-1.0952e+01	1.2362e+02	-4.4345e+02
$m = 2$	-1.6965e+00	6.1091e+01	-7.1468e+02	2.5932e+03
$m = 3$	2.9549e+00	-1.0842e+02	1.2715e+03	-4.4262e+03
$m = 4$	-1.2907e+00	4.6331e+01	-5.1424e+02	1.5806e+03

d_{142ml}	$l = 1$	$l = 2$	$l = 3$	$l = 4$
$m = 1$	-4.3287e-01	1.4962e+01	-1.6835e+02	6.0439e+02
$m = 2$	2.3019e+00	-8.2503e+01	9.6537e+02	-3.5309e+03
$m = 3$	-3.9768e+00	1.4586e+02	-1.7227e+03	6.1023e+03
$m = 4$	1.7605e+00	-6.3493e+01	7.1477e+02	-2.2589e+03

d_{143ml}	$l = 1$	$l = 2$	$l = 3$	$l = 4$
$m = 1$	1.8668e-01	-6.4162e+00	7.1975e+01	-2.5912e+02
$m = 2$	-9.8107e-01	3.4990e+01	-4.0956e+02	1.5135e+03
$m = 3$	1.6832e+00	-6.1707e+01	7.3422e+02	-2.6571e+03
$m = 4$	-7.5967e-01	2.7547e+01	-3.1523e+02	1.0339e+03

d_{144ml}	$l = 1$	$l = 2$	$l = 3$	$l = 4$
$m = 1$	-2.4635e-02	8.4314e-01	-9.4426e+00	3.4137e+01
$m = 2$	1.2823e-01	-4.5589e+00	5.3441e+01	-1.9962e+02
$m = 3$	-2.1931e-01	8.0461e+00	-9.6472e+01	3.5634e+02
$m = 4$	1.0137e-01	-3.6984e+00	4.2988e+01	-1.4605e+02

Appendix 3 Published Conference Paper on Heat Transfer Analysis in a Single Horizontal Cooling Duct

Investigation of Convective Heat Transfer Efficiency in the horizontal cooling duct of a Disc Type Transformer Winding

X. Zhang, Z.D. Wang, Q. Liu, P. Jarman, A. Gyore and P. Dyer

2015

The 19th International Symposium on High Voltage Engineering (ISH), Pilsen, Czech.

Published

Blank page

Investigation of Convective Heat Transfer Efficiency in the horizontal cooling duct of a Disc Type Transformer Winding

X. Zhang[1], Z.D. Wang[1*], Q. Liu[1], P. Jarman[2], A. Gyore[3], P. Dyer[4]
[1]University of Manchester, M13 9PL, UK
[2]National Grid, Warwick, CV34 6DA, UK
[3]M&I Materials, Manchester, M32 0ZD, UK
[4]UK Power Networks, Crawley, RH10 0FL, UK
*Email: < zhongdong.wang@manchester.ac.uk >

Abstract: Thermal ageing of the insulation cellulose is predicted to be one of the transformer failure mechanisms when considering the large population of ageing assets in the power network. Disc-type winding structure is widely used in power transformers. The thermal behaviour of the horizontal cooling ducts is critical to determining the temperature in the winding. Analytical and numerical analyses of the heat transfer process in the horizontal cooling duct are performed in this paper. It is shown that the Nusselt number (Nu) is a function of the dimensionless distance x^*, which is associated with duct geometry, flow condition, and coolant properties. The expressions for the Nu-x^* relationship from analytical analyses and computational fluid dynamics (CFD) simulations are slightly different due to the fact that variations of the coolant properties with temperature are taken into account only in the CFD simulations. Therefore, the CFD results are deemed more accurate. The CFD simulations reveal that the influence of gravity and duct inlet velocity profile over the Nu-x^* relationship at the duct outlet is negligible. Modification of the dimensionless distance x^* is recommended before its application to take into account the distortion of the duct inlet temperature profile due to the existence of eddy circulation at the duct inlet, and the cooling effect of the vertical duct near the horizontal duct outlet.

1 Introduction

The failure of a transformer, especially a power transformer incurs great economic loss. This is not only for the capital cost of the transformer itself, but also for the potential threat it may pose to the electrical power network that the transformer is connected in.

Failure mechanism of transformers is an extended subject of research [1]. One type of transformer failures is the result of cumulative ageing or deterioration of the solid insulation system. Thermal ageing or deterioration is predicted to be one of the dominating mechanisms of future transformer failure when considering the large population of ageing assets in the power network.

Heat generation in a transformer winding is due to resistive loss and eddy current loss. Heat dissipation in a liquid filled transformer winding is usually facilitated by oil circulation between the winding and the coolers/radiators. Heat generation and dissipation in a transformer winding can differ from point to point, resulting in the formation of non-uniform temperature distribution and therefore the existence of the hottest spot (hot-spot). The hot-spot temperature leads to the severest thermal ageing of the insulation cellulose and therefore determines the life expectancy of the transformer insulation system, which relies on its integrity. Therefore, the primary objective of transformer thermal design is to restrain the hot-spot temperature in steady state within a reasonable range for rated loading [2]. The thermal behaviour of the winding cooling system is critical to achieving this objective.

For high voltage power transformers, the windings would usually be wound into a disc-type form. In a disc-type winding, winding conductors/strands are wound into radial discs surrounding the winding base tube. As shown in Figure 1, strips of dovetail cross section are positioned between the discs and the winding base tube to form vertical cooling ducts. Spacers that can be interlocked with the strips are placed between winding discs to form horizontal cooling ducts. Usually, in order to facilitate oil flow in the horizontal cooling ducts, washers would be inserted at intervals in the winding so that the inner and outer vertical cooling ducts are closed off alternately. The winding segment between two adjacent washers is called a pass. Oil flow in passes is in a zig-zag pattern.

As shown in Figure 1, the width of the horizontal cooling duct is much larger than its height. The fluid flow and heat transfer processes in the ducts can therefore be reduced to a 2D approximation. Since the majority of heat transfer takes place in the horizontal cooling ducts. Thermal behaviour of a horizontal cooling duct is focused in this paper.

Particularly, the heat transfer coefficient at the end of the horizontal cooling duct will be investigated because it is the location where the hot-spot is supposed to be. The 2D horizontal cooling duct under investigation is shown schematically in Figure 2.

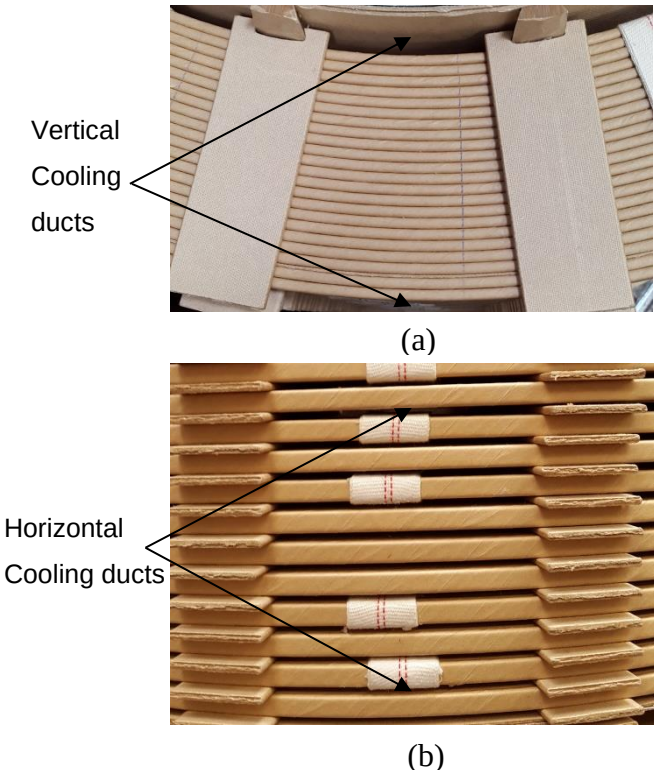

Figure 1. Disc-type winding geometry: (a) top view, (b) front view

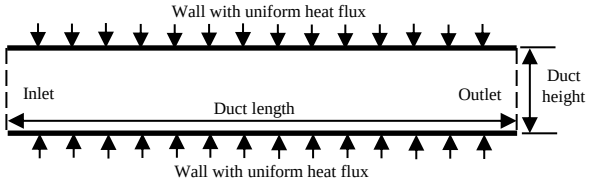

Figure 2: Schematic drawing of the 2D geometry of a horizontal cooling duct.

2 Analytical analyses of the heat transfer process

To analyse the heat transfer process in the horizontal cooling duct, the coolant motion analysis and the companion energy balance analysis have to be performed.

2.1 Motion analysis of hydrodynamically fully developed flow

The motion analysis of a hydrodynamically fully developed coolant flow is shown in Figure 3 [3]. Assumptions:

1. Laminar flow;
2. Constant material properties;
3. Steady state.

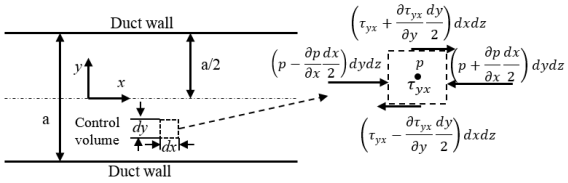

Figure 3: Motion analysis of the fluid flow in the horizontal cooling duct. The pressure and viscous force at the middle of the control volume is set to be p and τ_{yx}. τ_{yx} represents viscous force in y plate and directed in x direction.[3]

Applying force balance in the x direction, it follows that

$$\frac{\partial p}{\partial x} = \frac{\partial \tau_{yx}}{\partial y} \tag{12}$$

When the flow is hydrodynamically fully developed, the velocity profile in any section along the streamflow would be the same, so there is no viscous force difference present in the x direction, i.e. viscous force is only a function of y. If we apply force balance in y direction, it follows that pressure is only a function of x. Therefore, the only way to satisfy equation (1) is that both sides of the equation are the same constant.

$$\frac{dp}{dx} = \frac{d\tau_{yx}}{dy} = const \tag{13}$$

As transformer oil is a Newtonian fluid, viscous stress is expressed as

$$\tau_{yx} = \mu \frac{du}{dy} \tag{14}$$

where u is the velocity component in the x direction, μ is the dynamic viscosity.

Combining equation (2) and (3), integrating twice and applying boundary condition of $u(\pm a/2) = 0$ (no-slip boundary condition), one would have

$$u = \frac{a^2}{2\mu}\left(\frac{dp}{dx}\right)\left(\frac{y^2}{a^2} - \frac{1}{4}\right) \tag{15}$$

where a is the height of the duct, y is the distance away from the duct central line.

This is the parabolic velocity profile for fully developed flow. Substituting the velocity at the duct central line, $u_c = -\frac{a^2}{8\mu}\left(\frac{dp}{dx}\right)$, velocity expression would be

$$u = u_c\left(1 - \frac{4y^2}{a^2}\right) \tag{16}$$

2.2 Energy analysis of thermally fully developed flow

The energy analysis of thermally fully developed flow in the horizontal cooling duct is shown in Figure 4 [4].

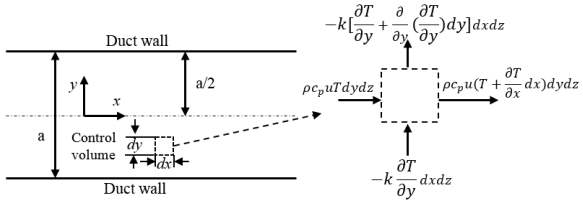

Figure 4: Energy analysis in the horizontal cooling duct. The temperature at the bottom left of the control volume is set to be *T*. [4]

Assumptions:

1. The flow is hydrodynamically fully developed laminar flow;
2. Constant material properties;
3. Negligible heat conduction in the *x* direction, i.e. $\partial T/\partial x \ll \partial T/\partial y$;
4. Negligible heat convection in the *y* direction, i.e. $v \ll u$; where v is the vertical velocity component and u is the horizontal velocity component.

In steady state, the energy balance in the control volume leads to the fact that the energy convected out in x direction is equal to the energy conducted in in y direction, that is

$$k\frac{\partial^2 T}{\partial y^2} = u\rho c_p \frac{\partial T}{\partial x} \tag{17}$$

For the case we are analysing, the heat flux at the duct wall is constant. Therefore the average temperature gradient along *x* direction would be constant. In addition, for thermally fully developed flow the temperature gradient in *x* direction at any position would also be constant.

The boundary conditions of equation (6) is

$$\begin{cases} \frac{\partial T}{\partial y}|_{y=0} = 0 \\ T|_{y=0} = T_c \end{cases}$$

where T_c is the duct central line temperature. When the flow is thermally fully developed, T_c would be a linear function of *x*.

For thermally fully developed flow, combining equation (5) and (6), integrating twice and applying the boundary conditions, one can obtain

$$T = \frac{u_c}{\alpha}\frac{\partial T}{\partial x}(\frac{y^2}{2} - \frac{y^4}{3a^2}) + \mathrm{T}_c \tag{18}$$

where $\alpha = \frac{k}{\rho c_p}$ is the thermal diffusivity of the fluid.

According to equation (7), the following equations are obtained

$$T_w = T|_{y=\pm a/2} = \frac{5a^2}{48}\frac{u_c}{\alpha}\frac{\partial T}{\partial x} + T_c \tag{19}$$

$$T_b = \frac{\int_0^{a/2}\rho c_p uTdy}{\int_0^{a/2}\rho c_p udy} = \frac{13a^2}{560}\frac{u_c}{\alpha}\frac{\partial T}{\partial x} + T_c \tag{20}$$

Where T_w is the temperature at the duct wall; T_b is fluid bulk temperature, i.e. the energy-averaged temperature.

At the wall of the duct, there is a stationary fluid layer because of the no-slip boundary condition. At this stationary layer heat transfer occurs via conduction. Combining Newton's law of cooling and Fourier's law of conduction, equation (10) emerges

$$q'' = h(\mathrm{T}_w - \mathrm{T}_b) = \mathrm{k}\frac{\partial T}{\partial y}|_{y=a/2} \tag{21}$$

Where *q"* is the heat flux at the wall, *h* is heat transfer coefficient.

According to equation (7), it follows that

$$\frac{\partial T}{\partial y}|_{y=a/2} = \frac{a}{3}\frac{u_c}{\alpha}\frac{\partial T}{\partial x} \tag{22}$$

Combining equation (8), (9), (10), and (11), one would have

$$h = \frac{70k}{17a} \tag{23}$$

When expressed in terms of the local Nusselt number (Nu), the result would be

$$Nu = \frac{hD_h}{k} = \frac{h2a}{k} = \frac{140}{17} \approx 8.235 \tag{24}$$

where D_h is the hydraulic diameter defined as $D_h = \frac{4A}{P}$ where *A* is the flow cross-sectional area and *P* is the wetted perimeter of the duct. For fluid flow in between parallel plate ducts, D_h is twice the height of the duct.

2.3 Real situation in the horizontal cooling duct

The Nusselt number would be a constant for hydrodynamically and thermally fully developed flow. However, for real situation in transformer horizontal cooling ducts, these conditions cannot always be fully met. In fact, oil flow in the horizontal cooling duct can be regarded as hydrodynamically developed and thermally developing flow [5]. In this flow regime, local

Nusselt number can be estimated by the following expressions [6]

$$Nu = \begin{cases} 1.490x^{*-1/3} & x^* \le 0.0002 \\ 1.490x^{*-1/3} - 0.4 & 0.0002 \le x^* \le 0.001 \\ 8.235 + 8.68(1000x^*)^{-0.506} e^{-164x^*} & x^* > 0.001 \end{cases} \quad (25)$$

where x^* is the dimensionless distance defined as

$$x^* = \frac{x}{D_h \operatorname{Re}_{D_h} \operatorname{Pr}} = \frac{xk}{D_h^2 \rho u_m c_p} \quad (26)$$

Where Re_{D_h} is the Reynolds number based on the hydraulic diameter; Pr is the Prandtl number; u_m is the average velocity in the duct.

It is worth noticing that when x^* is big enough the Nusselt number would be 8.235, which is the value for hydrodynamically and thermally fully developed flow condition as shown in section 2.2. In order to calculate duct wall temperature at its outlet, one needs to get the dimensionless distance x^* first. The Nusselt number at the duct outlet can be calculated according to equation (14), as is the heat transfer coefficient according to equation (13). Then the wall temperature at the duct outlet can be determined according to equation (10).

3 Numerical analyses of the heat transfer process

3.1 Simulation strategy

The Nusselt number obtained from analytical analyses in section 2 are based on assumptions like constant fluid properties and certain flow regime, etc. Therefore, the validity of these results needs to be checked by experimental tests or by accurate numerical calculations.

Computational fluid dynamics (CFD) simulations, which solve the governing equations directly with high accuracy and fine spatial resolution, are performed using commercial software COMSOL Multiphysics 5.0 to check and calibrate the results obtained in analytical analyses.

In the CFD simulations, fluid flow and heat transfer processes are fully coupled by associating fluid properties with temperature. The relationships between fluid properties and temperature are obtained from curve fitting of the measured data provided by the oil manufacturer. The relationships of density (ρ), thermal conductivity (k), specific heat (c_p), and dynamic viscosity (μ) with temperature for a mineral oil are as follows (in Kelvins):

$$\rho = -0.6511 \times T + 1066.9549$$

$$k = -7.5061 \times 10^{-5} \times T + 0.1537$$

$$c_p = 2.9029 \times T + 1165.4014$$

$$\mu = 5.9622 \times 10^{-5} \times \exp(707.6413/(T - 165.2016))$$

These functions are valid for temperature range of 293.15 K to 393.15 K (20 ^oC to 120 ^oC).

The simulation strategy is shown schematically in Figure 2. In the simulations, duct height, length, and heat flux on the wall can be varied, and duct inlet velocity and temperature can be prescribed as constants or with specific profiles. According to transformer design data [5, 7], the duct inlet velocity ranges from 0.01 m/s to 0.2 m/s with an interval of 0.01 m/s; inlet temperature ranges from 20 ^oC to 60 ^oC with an interval of 10 ^oC, heat flux on either wall ranges from 1500 W/m^2 to 6000 W/m^2 with an interval of 1500 W/m^2; duct length is set to be 150 mm with data extracted at 50 mm, 100 mm, and 150 mm; the height of the duct is chosen from 2 mm, 4 mm, 6 mm, and 8 mm. In total, there would be 4800 combinations. For each case, dimensionless distance x^* and the corresponding local Nusselt number can be extracted according to their definitions.

3.2 Influence of gravity

Before performing parametric sweeps, the influence of gravity over the *Nu*-*x** relationship was checked. In the simulations, the duct height is fixed to be 4 mm with other parameters changing in the range provided in section 3.1. Two scenarios, one with gravity and the other without, are simulated. The comparison of these two scenarios is shown in Figure 5.

As shown in Figure 5, the influence of gravity over *Nu*-*x** relationship in the horizontal cooling duct is negligible. This would be due to the fact that flow direction is perpendicular to the gravity direction.

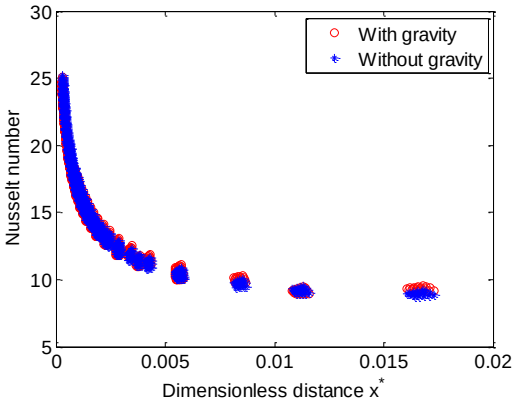

Figure 5: Comparison of the *Nu*-*x** relationship for scenarios with and without gravity.

3.3 Influence of duct inlet velocity profile

The influence of velocity profile at the duct inlet over the *Nu*-*x** relationship is investigated by prescribing constant velocities or parabolic velocity profiles at the duct inlet and keeping the flow rate

identical. In the simulations, the duct height is fixed to be 4 mm, and the other parameters (except for duct length) vary in the range provided in section 3.1. The Nusselt number and *x** values are extracted at different distances away from the duct inlet, which are 1 mm, 5 mm, 10 mm, and 20 mm. The comparisons for these two scenarios are shown in Figure 6. As shown in Figure 6, the influence of inlet velocity profile over the *Nu*-*x** relationship diminishes with the increasing distance away from the duct inlet. When the distance is 20 mm, the influence is hardly noticeable. This is due to the fact that oil possesses high Prandtl number, i.e. hydraulic boundary layer develops much faster than thermal boundary layer. Since horizontal duct length in a disc-type winding is usually larger than 50 mm. The influence of the duct inlet velocity profile over the *Nu*-*x** relationship at the duct outlet can therefore be neglected.

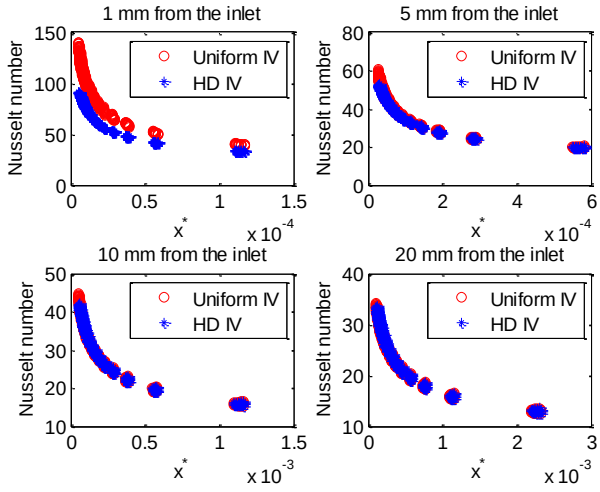

Figure 6: Comparison of the *Nu*-*x** relationship for uniform inlet velocity and fully developed inlet velocity profile. Each subplot shows the comparison at different distances away from the duct inlet. 'IV' stands for inlet velocity, 'HD' for hydrodynamically developed.

3.4 Comparison between analytical and numerical results

As indicated by section 3.2 and 3.3, the influence of gravity and duct inlet velocity profile over the *Nu*-*x** relationship at the duct outlet is negligible. Therefore, parametric sweep over parameters present in section 3.1 with uniform duct inlet velocity and uniform duct inlet temperature, disregarding gravity was performed. The *Nu*-*x** expressions from [6] and data points from CFD simulations are shown in Figure 7. The least square curve fitting of the simulated data points is divided into two parts with *x*=0.001* as a demarcation point. The curve fitting results are:

$$Nu = \begin{cases} 1.734x^{*-0.327} & x^* \le 0.001 \\ 8.577 + 9.350(1000x^*)^{-0.518} e^{-141x^*} & x^* > 0.001 \end{cases} \quad (27)$$

The maximum absolute deviation of the curve fitting from the data points for *x*<0.001* is 2.343, and 1.854 for *x*≥0.001*. The maximum absolute deviation of the expressions in [6] from the least square fitting curves is 3.360 located at the smallest *x** point.

It is noticed that when the flow is thermally fully developed, Nusselt number in equation (16) would be 8.577 which is slightly larger than the theoretical calculation value 8.235. This is because fluid properties are set to be temperature dependant in the CFD simulations. Higher temperature near the wall means lower viscosity there. Therefore, the actual developed velocity profile is distorted in such a way that velocity gradient at the duct wall gets larger and facilitates the convective heat transfer process in the duct, leading to a slightly larger Nusselt number. This is also the reason why simulated data points are above the curves from [6]. Since CFD simulations consider all the factors that may affect the heat transfer process, CFD results are deemed more accurate

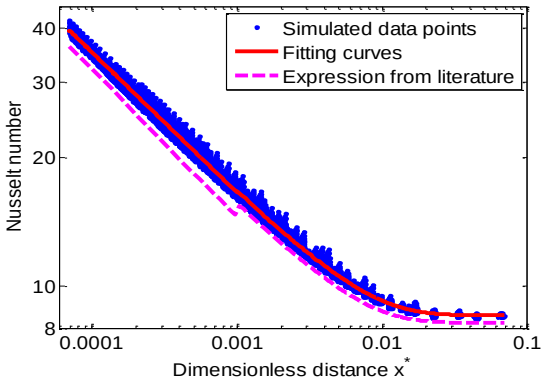

Figure 7: The *Nu*-*x** relationship from [6] and data points from CFD simulations with both axes being logarithmic. The curve fitting is divided into two parts with *x*=0.001* as a demarcation point.

4 discussion

The understanding of the *Nu*-*x** relationship is critical to conducting transformer thermal-hydraulic network modelling because the Nusselt number is used to describe the thermal behaviour of the horizontal cooling ducts in network model.

As shown from analytical and numerical analyses presented in section 2 and 3, local Nusselt number of a horizontal cooling duct can be expressed as a function of dimensionless distance x*, which is associated with the geometry of the duct (D_h , x), flow condition (u_m), and coolant properties ($\alpha = k/(\rho c_p)$), though there is a minor difference between analytical and numerical solutions. When the flow is hydrodynamically and thermally fully developed, the Nusselt number would be a constant. It is also shown that the effects of gravity and the inlet velocity profile over the *Nu*-*x** relationship at

the duct outlet are negligible. Therefore, it is concluded that temperature profile at the duct inlet is critical to determining the Nusselt number at the duct outlet. The distance x in equation (15) refers to the distance from the location of a uniform temperature profile to the destination location.

In reality, horizontal duct inlet temperature profile cannot always be regarded as uniform when considering the duct entrance eddy circulation that can arise at high flow rate [8]. The eddy circulation at the horizontal duct entrance disturbs the original duct inlet temperature profile which can be regarded as uniform. This disturbance effect lasts for a distance before it diminishes. Therefore, when calculating the Nusselt number at the duct outlet, the distance x used to calculate x^* in equation (15) should be smaller than the actual horizontal duct length.

In addition, due to the existence of vertical cooling duct at the end of the horizontal cooling duct, the highest temperature in the horizontal duct must shift upstream slightly. Therefore, the calculation of the Nusselt number at the hot-spot in the duct needs to be modified further.

5 Conclusion

Thermal behaviour of a horizontal cooling duct in a disc-type transformer winding was investigated analytically and numerically.

The Nusselt number in the horizontal duct is a function of dimensionless distance x^*. The expressions for Nu-x^* relationship obtained from literature and CFD simulations differ slightly due to the fact that coolant property variation with temperature is taken into account in CFD simulations. The simulation results are therefore deemed more accurate.

CFD simulations reveal that gravity and duct inlet velocity profile have negligible influence over the Nu-x^* relationship.

ACKNOWLEDGMENTS

The authors would like to express their gratitude to M&I Materials, National Grid, Scottish Power, Shell, TJ|H2b Analytical Services, UK Power Networks and Weidmann Electrical Technology for their financial and technical contributions to the Transformer Research Consortium at The University of Manchester.

REFERENCES

[1] M. Heathcote, *J & P transformer book*: Newnes, 2011.

[2] CIGRE Working Group A2.38, "Transformer thermal modelling, working version of the brochure," internal document.

[3] R. W. Fox, A. T. McDonald, and P. J. Pritchard, *Introduction to fluid mechanics*: John Wiley & Sons New York, 1998.

[4] J. P. Holman, *Heat transfer*: McGraw-Hill New York, 1986.

[5] W. Wu, Z. Wang, A. Revell *et al.*, "Computational fluid dynamics calibration for network modelling of transformer cooling oil flows-part I heat transfer in oil ducts," *IET Electric Power Applications,* vol. 6, no. 1, pp. 19-27, 2012.

[6] R. K. Shah, and A. L. London, *Laminar flow forced convection in ducts: a source book for compact heat exchanger analytical data*: Academic press, 1978.

[7] J. Zhang, and X. Li, "Coolant flow distribution and pressure loss in ONAN transformer windings. Part II: Optimization of design parameters," *IEEE Transactions on Power Delivery,* vol. 19, no. 1, pp. 194-199, 2004.

[8] A. Weinläder, W. Wu, S. Tenbohlen *et al.*, "Prediction of the oil flow distribution in oil-immersed transformer windings by network modelling and computational fluid dynamics," *IET electric power applications,* vol. 6, no. 2, pp. 82-90, 2012.

Appendix 4 List of Publications

Peer-reviewed Journal Papers:

1. **X. Zhang**, Z.D. Wang, and Q. Liu, "Prediction of Pressure Drop and Flow Distribution in Disc Type Transformer Windings under an OD Cooling Mode," *IEEE Transactions on Power Delivery*, vol. 32, no. 4, pp. 1655-1664, 2017.
2. **X. Zhang**, Z.D. Wang, and Q. Liu, "Interpretation of Hot Spot Factor for Transformers in OD Cooling Modes," *IEEE Transactions on Power Delivery*, In press, accepted on 25th May, 2017.
3. **X. Zhang**, M. Daghrah, Z.D. Wang, Q. Liu, P. Jarman, M. Negro, "Experimental Verification of Dimensional Analysis Results on Flow Distribution and Pressure Drop for Disc Type Windings in OD Cooling Modes," *IEEE Transactions on Power Delivery*, In press, accepted on 3rd August, 2017.
4. **X. Zhang**, Z.D. Wang, Q. Liu, P. Jarman, M. Negro "Numerical Investigation of Oil Flow Distribution and Temperature Distribution for ON Transformer Windings," *Applied Thermal Engineering*, under review.

International Conference Papers:

5. **X. Zhang**, Z.D. Wang, Q. Liu, P. Jarman, A. Gyore, and P. Dyer, "Investigation of Convective Heat Transfer Efficiency in the Horizontal Cooling Duct of a Disc Type Transformer Winding," in the 19th International Symposium on High Voltage Engineering (ISH), Paper ID 280, Pilsen, Czech Republic, 2015.
6. **X. Zhang**, Z.D. Wang, Q. Liu, P. Jarman, A. Gyore, and P. Dyer, "Numerical Investigation of Influence of Coolant Types on Flow Distribution and Pressure Drop in Disc Type Transformer Windings," in the International Conference on Condition Monitoring and Diagnosis (CMD), Xi'an, P.R. China, 2016.
7. **X. Zhang**, Z.D. Wang, Q. Liu, M. Negro, A. Gyore, and P. Smith, "Numerical Investigation of Influence of Liquid Types on Flow Distribution and Temperature Distribution in Disc Type ON Cooled Transformers," in International Conference on Dielectric Liquids (ICDL), Manchester, UK, 2017. Accepted.